Tribological Behaviour of Magnesium-Boron Carbide Metal Matrix Composites

Thesis submitted

By

Vikram Prabhakar Titarmare

Doctor of Philosophy

(Engineering)

Department of Mechanical Engineering

Faculty Council of Engineering & Technology

Jadavpur University, Kolkata, India

2025

This page is left intentionally blank

JADAVPUR UNIVERSITY

KOLKATA-700032, INDIA

INDEX NO. 290/21/E

1. **Title of thesis:**

   Tribological Behaviour of Magnesium-Boron Carbide Metal Matrix Composites

2. **Name, Designation & Institution of the Supervisor:**

   Prof. Prasanta Sahoo

   Professor, Department of Mechanical Engineering

   Jadavpur University, Kolkata-700032

3. **List of Publication (Referred Journals):**

   1. Titarmare, V.P., Banerjee, S. and Sahoo, P, 2026, Nanoindentation, scratch resistance and elevated temperature tribological behaviour of AZ31-B_4C composites. **ASME Journal of Tribology**, 148(2), 021403 (1-12). [**SCIE**]
   2. Titarmare, V., Banerjee, S. and Sahoo, P., 2024. Effect of sliding speed and sliding distance on wear behaviour of AZ31-B_4C composite. **Physica Scripta**, 99(8), 085016 (1-19). [**SCIE**]
   3. Titarmare, V., Banerjee, S. and Sahoo, P., 2024. Abrasive wear behaviour of AZ31-B_4C composites. **Tribology International**, 194, 109455 (1-14). [**SCIE**]
   4. Titarmare, V.P., Banerjee, S. and Sahoo, P., 2023. Dry sliding tribological behaviour of ultrasonic stir cast AZ31-B_4C composites. **Proc. Inst. Mech. Engrs, Part J: Journal of Engineering Tribology**, 237(4), pp.824-842. [**SCIE**]
   5. Titarmare, V.P., Banerjee, S. and Sahoo, P., 2023. Corrosion Characteristics of AZ31-B_4C Composites. **Trans Indian Inst Met.**,76, pp.2445–2461. [**SCIE**].
   6. Titarmare, V., Banerjee, S. and Sahoo, P., 2022. Fabrication and characterization of AZ31-B_4C composites. **Materials Today: Proceedings**, 59, pp.153-160. [**Scopus**]

4. **List of Patents**: Nil

5. List of Presentations in National / International Conference:

1. Titarmare, V.P., Banerjee, S. and Sahoo, P., 2024. Ultrasonic assisted stir casting synthesis and characterization of magnesium metal matrix composites. International Conference on Mechanical Engineering. January, 2024, Jadavpur University, Kolkata, India.
2. Titarmare, V.P.,2021. Development of magnesium-boron carbide (Mg-B_4C) metal matrix composites. National Conference on Sustainable Development and Circular Economy in Civil Engineering. December, 2021, Heritage Institute of Technology, Kolkata, India.
3. Titarmare, V.P., Banerjee, S. and Sahoo, P., 2021. Dry sliding tribological behaviour of AZ31-B_4C composites. International Tribology Research Symposium. December, 2021, SRM Institute of Sc. and Tech., Chennai, India.
4. Titarmare, V.P., Banerjee, S. and Sahoo, P.,2021. Corrosion Behaviour of AZ31-B_4C nanocomposites. TRIBOINDIA. December, 2021, Saintgits College of Engineering, Kottayam, Kerala, India.
5. Titarmare, V.P., Banerjee, S. and Sahoo, P.2021.Fabrication and characterization of AZ31-B_4C composites. International Conference on Recent Advances in Materials and Manufacturing. November, 2021, D.Y. Patil College of Engineering and Technology, Kolhapur, Maharashtra, India.

6. Book Chapter:

1. Titarmare, V.P., Banerjee, S. and Sahoo, P., 2025. Ultrasonic-assisted stir casting synthesis and characterization of magnesium metal matrix composites, pp.55-67, In: Sahoo, P., Barman, T.K. (eds) Advances in Materials, Manufacturing and Design. INCOM 2024. Lecture Notes in Mechanical Engineering. Springer, Singapore.

STATEMENT OF ORIGINALITY

I, **Vikram Prabhakar Titarmare** registered on 30.07.2021 do hereby declare that this thesis entitled **"Tribological Behaviour of Magnesium-Boron Carbide Metal Matrix Composites"** contains literature survey and original research work done by the undersigned candidate as part of Doctoral studies.

All information in this thesis have been obtained and presented in accordance with existing academic rules and ethical conduct. I declare that, as required by these rules and conduct, I have fully cited and referred all materials and results that are not original to this work.

I also declare that I have checked this thesis as per the "Policy on Anti Plagiarism, Jadavpur University, 2019", and the level of similarity as checked by iThenticate software is 6%.

Signature of Candidate: ……

Date: 09/09/2025

Certified by supervisor:

……..

(Prof. Prasanta Sahoo)

Dr. PRASANTA SAHOO
Professor
Department of Mechanical Engg.
JADAVPUR UNIVERSITY
KOLKATA - 700 032

Date: 09/09/2025

This page is left intentionally blank

CERTIFICATE FROM THE SUPERVISOR

This is to certify that the thesis entitled **"Tribological Behaviour of Magnesium -Boron Carbide Metal Matrix Composites** "submitted by **Shri. Vikram Prabhakar Titarmare**, who got his name registered on 30.07.2021 for the award of Ph.D. (Engineering) degree of Jadavpur University is absolutely based upon his work under the supervision of **Prof. Prasanta Sahoo** and that neither his thesis nor any part of the thesis has been submitted for any degree/diploma or any other academic award anywhere before.

Prasanta Sahoo

.....

Dr. PRASANTA SAHOO
Professor
Department of Mechanical Engg.
JADAVPUR UNIVERSITY
KOLKATA - 700 032

(Prof. Prasanta Sahoo)

Date: 09/09/2025

This page is left intentionally blank

ACKNOWLEDGEMENT

This thesis is the outcome of research work carried out at Jadavpur University over the last few years. During this period, I have worked as QIP-PhD research scholar in Machine Element Laboratory, in Department of Mechanical Engineering. I am gratefully acknowledging the AICTE QIP PhD scheme, Directorate of Higher and Technical Education, Mumbai and Government College of Engineering, Nagpur for all their valuable support. During this period, a number of people have supported me. It is my humble duty to convey my acknowledgement and express thanks to all who were directly or indirectly associated with this research work. Firstly, I would like to convey my heartfelt gratitude to my respected thesis supervisor, Prof. (Dr.) Prasanta Sahoo Sir for his erudite assistance, support and inspiration which was instrumental in the successful completion and submission of this thesis. His suggestion, advice and approach towards work & life is a lifetime lesson for me.

I take the opportunity to express my heartfelt adulation and gratitude to Dr. Sudip Banerjee, former research scholar for his insightful directions and continuous support and occasional humours which helped a lot during stressful work sessions. His presence and ambience of the laboratory colleagues, lighter fun filled moments and countless trips to the canteen for obligatory and quite often unnecessary ‘cup of tea/ coffee’ definitely provided a sense of solace and enjoyment in the toughest days. I sincerely acknowledge the support and encouragement offered to me by, Dr. Suman Kalyan Das sir, Dr. Tapan Kumar Barman sir and Dr. Anirban Mitra Sir. Above all, they provided me unflinching support in various ways. I will remain indebted to them for their advice and crucial comments about the work and life. It is a pleasure to acknowledge the support and help provided by Dr. Sanjib Acharyya sir.

I wish to further extend my thanks to other past and present members of Machine Elements Laboratory. Special thanks go to Dr. Debi Prasana Mohanty, Rakesh Bhadra, Dr. Tamonash Jana, Dr. Manik Barman and Dr. Palash Biswas for their continuous support. I also extend my thanks to the technicians allotted for SEM/FESEM/XRD laboratory of Jadavpur University, Metallurgy / Mechanical Department, IIEST Shibpur, S. N. Bose National Centre for Basic Sciences, VNIT Nagpur, NIT Durgapur and IIT Kharagpur for their contributions and support. I also acknowledge the support of my friends and faculties cum colleagues for their continuous encouragement and support.

Lastly, I thank my beloved family members (especially Aai, Baba, Brothers, My Wife, Son-Daughter and Family) for their patience and constant support without which this work couldn’t

have been completed. They are the ones for whom I am here. Definitely there are some persons whom I forget to mention, I am also acknowledging them.

Thank You.

Vikram Prabhakar Titarmare

Date: 09/09/2025

Abstract

This thesis evidences Magnesium-Boron Carbide Metal Matrix Composites as vital material for numerous tribological applications. Magnesium alloy (AZ31 Alloy) acts as matrix metal being one of the lightest structural materials. Magnesium alloy offers distinct advantages like ease of manufacturing, good machinability and lower latent heat of fusion. Consequently, AZ31 is considered as base matrix. Boron carbide (B_4C) submicron particle is chosen as reinforcement as it possesses excellent hardness (3500kg.mm^{-2}), high melting point (2450°C), good elastic modulus (460 GPa), excellent wear resistance even at elevated temperature, justifiable thermo-chemical stability and superior thermal expansion coefficient, good wettability and viable shock absorbing capability. AZ31-B_4C composites are fabricated through ultrasonic vibration assisted stir casting technique due to its ability of effective and uniform dispersion of submicron size particles in magnesium alloy melt. Later on, synthesized cast composites are observed under optical microscopy (OM) and scanning electron microscopy (SEM) along with energy dispersive x-ray analysis (EDAX) and X-ray diffraction (XRD) study. Furthermore, micro-hardness of all submicron-composites is also investigated along with base matrix alloy.

Tribological behaviour of matrix alloy and composites is examined at various operating conditions including varied load, speed, sliding distance at ambient as well as elevated temperature. Nanoindentation and scratch tests are also performed to estimate nano hardness, elastic modulus and scratch behaviour of developed composites. Subsequently, composites and base alloy are inspected in 3.5% NaCl solution to evaluate corrosion characteristics. In addition, both SEM micrographs and EDAX spectra are analysed for worn and corroded surfaces of alloy and composites. In brief, tribological behaviour, nanoindentation response and corrosion characteristics of AZ31-B_4C composites are investigated. Characterization results validate inclusion of submicron particles (B_4C) along with good interfacial bonding between matrix phase and reinforcement phase. Hard ceramic B_4C particles improve load bearing capacity of composites and results in enhanced tribological properties at all operating conditions. Nano-hardness and elastic modulus upgrade continuously with incorporation of B_4Cparticles. Corrosion behaviour of AZ31 alloy enhances due to incorporation of B_4C particles. Incorporation of 1 wt.% of boron carbide particles effectively strengthen corrosion behaviour of AZ31 alloy but additional incorporation may result in deleterious consequences. It is anticipated that the results dispensed in the thesis will be beneficial to both academic and industrial community.

This page is left intentionally blank

About the Author

The author, **Shri. Vikram Prabhakar Titarmare** was born in the district of Maharashtra in the year 1978. He is graduated in Mechanical Engineering (B.E.) in 2000 from Rashtrasant Tukdoji Maharaj Nagpur University (RTMNU). In 2007, he completed his Masters in Mechanical Engineering Design (M. Tech) degree from Rashtrasant Tukdoji Maharaj Nagpur University (RTMNU).

He has total industrial experience of about 9 years in different steel plant in Maharashtra which includes Sipta Steel Industry Ltd., Nanded, Bhushan steel Industry Ltd., Khopoli, and Lloyd's steel Industry Ltd. Wardha.

He got selected as an Assistant Professor in Mechanical Engineering, Government Engineering Colleges, Maharashtra Engineering Teachers Services, Group-A, Directorate of Technical Education through Maharashtra Public Service Commission on dated 20/10/2010. He has previously served as Assistant Professor in Mechanical Engineering Department, Government College of Engineering Chandrapur, Maharashtra from 01/01/2011 to 31/05/2018. He is presently working as an Assistant Professor in Mechanical Engineering Department, Government College of Engineering Nagpur, Maharashtra from 01/06/2018 to till date. He has a total teaching experience of about 15 years as an Assistant Professor in Mechanical Engineering Department till date. He was granted QIP-PhD fellowship from AICTE for pursuing research work at Jadavpur University, Kolkata for 3 years (2020-2023) with prior permission from Directorate of Higher and Technical Education, Mumbai. The present thesis is the outcome of the research study performed at Department of Mechanical Engineering, Jadavpur University, during this period.

This page is left intentionally blank

In presence of Indian spiritual perfect master

beloved 'Avatar Meher Baba'

To

My Parent, Teachers,

My Wife, Children, Brothers

and

family

This page is left intentionally blank

Table of Contents

This page is left intentionally blank

List of Figures

This page is left intentionally blank

List of Tables

This page is left intentionally blank

Chapter 1

Introduction and Literature Review

1.1 Magnesium Matrix Composites

Magnesium matrix composites have gained demand as multifunctional materials for a variety of applications mostly at the commercial level. Magnesium matrix composites have been investigated worldwide in recent years [Friedrich et al., 2006; Kainer and Mordike, 2000]. Magnesium matrix composites are preferred as structural material in transport / automobile industries owing to their light weight, good specific strength and stiffness properties. These factors are vital in design of weight saving components in automobile and aerospace applications. Other benefits of using magnesium matrix composite include manufacturing of energy efficient vehicles with control over emissions leading to cleaner transportation [Gupta and Ling, 2011, Lin et al., 2014]. Moreover, magnesium composites can be tailor made in specific applications as like other composites. Such a customized option is very limited in pure magnesium alloys.

In recent scenario, the transport sector consumes more than one fourth of the world's total energy and is responsible for about one third of total greenhouse gas emissions [Blawert et al., 2004; Kumar et al., 2021; Joost, 2012]. Such a trend can't be sustainable in the future owing to concerns over environmental issues and fossil fuel scarcity. As a result, transport sectors have focused mainly on lightweight, good strength materials for the automobile and aerospace industries [Lin et al., 2014; Joost, 2012]. Use of magnesium matrix composites in transport vehicles may reduce the legislative and environmental concerns to some extent. In aerospace industries, most typical objective is weight reduction which would aid to bring down operational cost by lowering fuel consumption. Magnesium matrix composites find applications in civil and military aircraft, electronic, sports as well as medical fields [Song et al., 2020; Kim and Do, 2008; Kulekci et al., 2008., Blawert et al., 2004]. Hence, many researchers, scientists and industries are in search of this advanced variety that will help to reduce the weight of the vehicles and harmful emissions along with customized option. Composites usually correlate properties of matrix phase and reinforcement. Accordingly, matrix and reinforcement materials need to be sensibly chosen in order to customize attributes of final application. Existing literature discloses that frequently used matrix materials are

aluminium (Al), copper (Cu), iron (Fe), titanium (Ti) and magnesium (Mg). In this regard, magnesium and magnesium alloys are most commonly utilized due to their light weight, lower weight to strength ratio, easy formability, good availability and stability at room temperature.

Magnesium and its alloys have density around 1.74-1.77 g/cm^3, which is very close to structural plastic (1.7g/cm^3) and quite lower compared to widely used metallic materials like steel (7.2 g/cc), aluminum (2.75 g/cc), and titanium (4.52 g/cc) respectively [Gupta and ling, 2011; Joost and Krajewski, 2017]. These values advocate that pure magnesium is around 33% lighter than Aluminium and 75% lighter compared to steel. Magnesium alloys have considerable advantage as a structural material too among existing alloys and is useful in applications like automobile, aerospace, electronics, orthopaedic and sports industries [Kulekci, 2008; Cole and Sherman, 1995; Kumar et al., 2015]. Additionally, magnesium alloys possess combination of distinct properties such as good castability, excellent manufacturability, machinability and recyclability [Mordike and Ebert, 2001; Song et al., 2020]. Moreover, magnesium being soft material can be machined 1.25 -1.5 times faster than aluminium resulting in considerable saving in power consumption. Lower latent heat of fusion is another attribute that helps to increase rate of solidification and eventually produce maximum numbers of castings per unit time. Hence, magnesium could produce up to 1.5 times more numbers of castings than aluminium [Mallick, 2020].

In the past, magnesium is extensively found applications in Volkswagen (VW) beetle after 1930, as used about 20 kg of magnesium in transmission housing and crankcase. Automobile manufacturers like Audi, VW, M. Benz, Kia Motors, Toyota, Jaguar, and Hyundai have replaced steel parts used in automobiles with magnesium and its alloys [Blawert et al., 2004; Gupta and Ling 2011; Joost and Krajewski, 2017]. Magnesium materials have been frequently utilized by manufacturers in gearbox housing (Audi), steering wheels (Toyota), fuel tank cover (M. Benz), seat frame & steering column housing (Hyundai / KIA). The KIA Motors achieved about 6 kg reduction in weight of seat frame just by using magnesium instead of steel. Magnesium has got application in aerospace where weight reduction is the most important objective to reduce emission and increase fuel efficiency. Reduction in weight of aerospace causes fuel-saving and reduce overall operating cost [Khan et al., 2025; Kainer and Mordike, 2000; Gupta and Seetharaman, 2017; Nie et al., 2021]**.**

Most commonly used magnesium alloys are AZ31 (Al-3%, Zn-1%), AZ61A (Al-6%, Zn-0.9%), AZ91 ((Al-9%, Zn-0.7%), AM50 & AM60 (Al-4.9-6.0%, Fe-0.005%, ZN-0.22

max) etc. It is found that AZ31 has a good combination of properties and is widely used in casting [Avedisian and Baker, 1999; Song et al., 2020]. However, magnesium alloy still has few bottlenecks like poor creep resistance, inferior abrasion resistance, poor tribological properties, high corrosion susceptibility, and low elastic modulus in the target applications [Gupta and Ling, 2011; Song et al., 2020]. In industrial applications, components may have frequent contact with other harder material during the process of energy transfer. Accordingly, life of component gets affected due to wear between interacting surfaces and resulting in an obvious consumption of energy [Banerjee et al., 2019a]. Thus, tribological aspects become a vital domain to be focused in order to justify magnesium alloy in industrial usage.

Existing literature suggests that these limitations of magnesium alloys can be overcome by successfully incorporating micron or sub-micron sized reinforcements. Properties of metal matrix composites are primarily dependent on the selection of reinforcement size, its type and amount, matrix material and fabrication technique utilised. Normally particulate reinforcement is preferred over whiskers and fibres owing to its economical aspect, ease of fabrication and isotropic properties. The particulate reinforcement utilised so far in magnesium matrix are oxides, carbides and nitrides. A review of existing literature reveals that SiC [Lan et al., 2004; Wang et al., 2014; Nie et al., 2011a], TiC [Contreras et al., 2004; Hasan and Gupta, 2002], WC [Banerjee et al., 2019c; Banerjee et al., 2020; Praveenkumar et al., 2020], Al_2O_3 [Khandelwal et al., 2017; Shanthi et al., 2010; Paramsothy et al., 2012], ZnO [Tun et al., 2012], BN [Sankaranarayanan et al., 2014; Kavimani et al., 2017; Kaviti et al., 2018], TiB_2 [Xiao et al., 2018], Y_2O_3 [Tun and Gupta, 2007] etc. have been utilized as reinforcement to enhance tribo-mechanical properties of Mg-based alloys.

Recent literatures reported that particle size is an important aspect to achieve desirable properties. Dey and Pandey (2015) reveals that reinforcement having lower particle size in nano scale helps to achieve better specific properties. Gopal et al. (2025) investigated the role of quantity and size of reinforcement on mechanical and tribological characteristics. It was observed that reinforcement having nano particle size possesses better result. Rudimentary properties like corrosion resistance, hardness, tribological properties, strength etc. improve noticeably with the incorporation of reinforcing phase. But property improvement of metal matrix composites occurs up to a certain threshold limit of reinforcement amount, after which properties tend to drop [Gupta and Ling, 2011]. Casati and Vedani (2014) reported that incorporation of sub-micron sized reinforcement around $\leq$ 2 wt.% is enough to provide noticeable improvement in properties like hardness, tensile strength, toughness etc. Hassan and

Gupta (2006) investigated the impact of incorporation of different length scale reinforcement and reported that composites with sub-micron or nano-scale reinforcement possess far better mechanical characteristics compared to micro-composites. Even fortification of micron reinforcements may have certain fabrication related issues like generation of voids, clustering, cracking of particles, and decreased ductility etc. [Hassan and Gupta, 2002]. Hence, composites having sub-micron sized reinforcements are favourable than micron sized reinforcements. Moreover, addition of ceramic particles like SiC, Al_2O_3, MWCNT, B_4C, ZnO, BN, ZrO_2, Y_2O_3, TiC, TiB_2 etc. are widely observed in literature to enhance mechanical properties, corrosion characteristics, tribological properties, and microstructural properties due to their high hardness, high melting point, good oxidation resistance, higher elastic modulus, noticeable shock observing capability etc. [Banerjee et al., 2019d, Casati and Vedani, 2014; Nie et al., 2011b]. Thus, judicious selection of matrix material, reinforcement and fabrication technique is a prerequisite in development of magnesium matrix composites.

1.2 Review of Magnesium Matrix Composites

1.2.1 Fabrication Methods

Development of metal matrix composites (MMCs) mainly depend on selection of three parameters: (a) matrix material, (b) reinforcement and (c) fabrication method [Kumar et al., 2021; Banijamali et al., 2022]. Moreover, development of MMCs through conventional casting process generally faces two main challenges: i) issues related to the homogeneous distribution of submicron or nano size particles due to their high surface-to-volume ratio or high viscosity of melt ii) attaining a strong interfacial bonding due to poor wettability of nano/submicron-sized ceramic particles. Magnesium (Mg) is very reactive at elevated temperature. Thus, its fabrication is carried out normally in an inert atmospheric condition to avoid oxidation with surrounding environment. The most challenging task is to synthesis the metal matrix nano composites due to higher surface area of submicron or nano particles. Literature on magnesium composites have shown that uniform distribution or appropriate wetting ability of ceramic particles in matrix is required to improve different properties. Accordingly, selection of appropriate synthesis process is essential to limit agglomeration of submicron-sized particles. So far various methods have been suggested by research fraternity for metal matrix composites. In this regard, widely utilized processes are powder metallurgy [Bharathi and Sampath Kumar, 2023], stir casting [Nirala et al., 2020; Kumar et al., 2019;

Kumar et al., 2022], disintegrated metal deposition (DMD) technique [Gupta et al., 2000], ultrasonic stir casting [Banerjee et al., 2021a] etc.

Different methods of fabrication have been identified and utilized over time to produce Mg-MMCs. The processing techniques utilized for composites are broadly classified as solid and liquid metallurgy methods. However, every fabrication method is having some advantages and limitations over other. Thus, with the outcome of variety of literature published till date, it is observed that the size of reinforcement, industrial scalability, ease of production and cost effectiveness specifically affect the selection of particular fabrication method. It is found that liquid metallurgy is generally preferred as commercially accepted technique and has the capability to fabricate large and complex designed product. Furthermore, the results of thermal expansion coefficient measurement signify that the dimensional stability of Mg-MMCs is significantly improved by liquid state processing over solid state processing [Bharathi and Sampath Kumar, 2023, Monish et al., 2023]. Accordingly, liquid metallurgy is normally preferred technique for nano composites [Idrisi and Mourad, 2019; Dieringa, 2018].

Liquid metallurgy processing includes stir casting, ultrasonic stir casting (USC) and disintegrated melt deposition (DMD) techniques. Stir casting is commonly utilized in liquid metallurgy technique to synthesize composite materials [Jutanaiman and Syahrial, 2020; Zhou et al., 2014; Hashim et al.,1999; Veeranjaneyulu et al., 2023]. It is considered as economical and simplest technique and is mainly suitable for development of particulate reinforced metal matrix composites. Stir casting allows the production of big sized, complex geometry products and suitable to carry out volume production [Mussatto et al., 2020]. Many researchers choose stir casting technique to assimilate metal oxides, nitrides and carbide micron size particles in magnesium matrix. But very few literatures are available to incorporate nano size particles in magnesium matrix considering stir cast route. In conventional stir casting, several factors need considerable attention: lacking ability to have uniform distribution of nano sized particulate reinforcement in matrix metal, wettability between to different materials, porosity in produced composites etc. Zhou and Xu (1997) have reported that mechanical stirring alone cannot solve the issue of poor wettability and recommended that it is essential to break the layer of gas surrounding the particles to improve wettability. Hashim et al. (1999) have mentioned that vortex development in mechanical stirring is essential for pouring slurry of particles into matrix melt due to pressure difference between the inner and outer surface of the melt which sucks the particles into liquid. But air-gas bubbles and other impurities are also get sucked with this

mechanism resulting in porosity and inclusions in the cast product. Jutanaiman and Syahrial (2020) have developed Mg-B_4C composite through stir casting and noticed porosity and agglomeration issue in fabricated Mg-4%B_4C composite under microscopic investigation. The tendency of cluster and porosity is likely to get increased with the inclusions of nano particles in magnesium matrix.

Above mentioned limitations in the fabrication of nano composites can be overcome in ultrasonic-assisted stir casting. This process avoids issues of non-uniform dispersion, porosity, wettability, and agglomeration in the fabricated casting. Recently, Banerjee et al. (2019d) synthesized nanocomposites by incorporation of WC (50 nm) as reinforcement in magnesium alloy. Ultrasonic assisted stir casting process shows considerable improvement in hardness and wear resistance due to uniform dispersion of nano particle in the matrix. Lan et al. (2004) have incorporated SiC nano particles in magnesium matrix through ultrasonic stir casting. It is confirmed that intense ultrasonic waves are sufficient in uniformly disbursing nano size SiC particles in the matrix alloy. However, small clusters (300 nm) are noticed in the developed composite. Similarly, Wang et al. (2003), Liu et al. (2014) and Sardar et al. (2017) have also utilised ultrasonic assisted stir casting technique for nanocomposite fabrications. Ultrasonic vibration or transient cavitation and acoustic streaming have been proved to be effective technique for uniform dispersion of nanoparticles. Ultrasonic process applies high frequency cyclic ultrasound waves through 'sonotrode', which results in generating alternate positive (collapse) and negative (expansion) pressure cycle in molten metal. The generated pressure cycle is sufficient in breaking the clusters of nanoparticles and is termed as 'acoustic cavitation'. The transient temperature at micro hotspots during ultrasonic treatment is also sufficient for improving wettability. Repeated acoustic cavitation effect helps in de-agglomerating or forming nanoparticles in the form of small clusters or individual particles. Similar observations are reported by Mohanty et al. (2020) and Nie et al. (2012). Idrisi and Mourad (2019) have examined the physical and mechanical characteristics of composites fabricated through both stir casting and ultrasonic stir casting route. Investigation of microstructure displayed that SiC micro particles were homogeneously dispersed with the use of ultrasonic probe. As a result, mechanical and physical properties (tensile and compressive strength, density and hardness) were improved significantly with USC process. Kumar and Thakur (2023) have utilised ultrasonic stir cast route to fabricate AZ91-Al_2O_3 composite and observed improved mechanical and wear performance. It is concluded that the incorporation of 1 wt.% alumina in AZ91 alloy through ultrasonic stir cast caused noticeable improvement in

impact toughness and ductility with reduction in porosity. Moreover, significant reduction in grain size was visible with ultra-sonication which resulted in grain refinement of composite. Thus, ultrasonic vibration aids in the destruction of dislocations and the manifestation of the recrystallization process.

Disintegrated melt deposition technique (DMD) is an expensive and complex process compared to other processing methods. DMD process utilizes benefit of conventional casting and spray forming. This process is invented in the National University of Singapore in 1994 [Gupta and Wong, 2015]. For fabrication of magnesium metal or alloy, the desired wt% of reinforced material and mg alloy are placed in graphite crucible. The materials are superheated to over 650℃ in resistance furnace under inert argon environment. After the temperature reached superheated range, the composite slurry is stirred with mechanical stirrer to facilitate the incorporation and uniform distribution of reinforcement material in the metallic matrix. The mechanical stirrer (rotated 450 rpm for 5 min) is coated with water-based zircon wash to avoid any Fe content in the composite melt slurry. The crucible has arrangement at bottom for pouring melt through the orifice placed at its base for releasing melt. The composite slurry is disintegrated by two jets of argon gas normal to stream of molten metal. The flow rate of Ar is maintained approx. 25 lit/min. Disintegrated composite melt gets deposited into metallic substrate placed at the base approx. 500 mm distance from the location or point [Nguyen et al., 2015; Shanti et al., 2010; Gupta et al., 2000]. Shanti et al. (2010) has fortified Al_2O_3 in magnesium alloy and fabrication is carried out under DMD route. Nguyen et al. (2015) fabricated AZ31B Magnesium matrix with Al_2O_3 through DMD process and reported equiaxed grains in developed composites along with good interfacial strength. Gupta and Seetharaman (2017) fabricated Mg-SiC through DMD and observed good distribution of SiC in magnesium matrix. Uniform distribution of reinforced particles directly improves mechanical properties of composites like ductility, tensile strength etc. Lim et al. (2005) synthesized mg with AL_2O_3 (50 nm) reinforcement through the DMD route. The mechanical and tribological properties of nano composites are improved due to the addition of nano-Al_2O_3. DMD process also improves mechanical and wear properties and the main advantage is that it allows wt. % of nanoparticle more than 2% which is not possible in other processes.

Solid metallurgy route of composite fabrication includes powder metallurgy (P/M) technique. It requires the proper size of matrix material and reinforcement powder to have a homogeneous composite without any agglomeration. Fabrication of composites through P/M includes preparation of powders from matrix material and reinforce phase. The next step

involves mixing or blending via ball mills to ensure good interfacial bonding between matrix and reinforced phase. In subsequent step, a blended powder is compacted in dies or mould to obtain the desired shape. Next step is sintering, a most critical step in P/M processing. During sintering, solid-state diffusion takes place, resulting in bonding of particles together. This leads to densification, eliminate pores and form solid or strong composites. Finally, post-processing (hot working or treatment) is scheduled to improve grain refinement and overall mechanical properties.

P/M route dependency is more on particle aspect ratio as its size and particle brittleness may create cracks during processing. Again, powder cost, handling of powders, lower fracture toughness, and ductility are some limitations of P/M [Majzoobi and Rahmani, 2020; Lim et al., 2003]. Refined microstructural features, superior strength are some advantages of solid processing [Yao and Chen, 2014]. Satish and Satish (2018) have prepared magnesium metal matrix composites using SiC and Al_2O_3 as reinforcement phase. Density improvement is noticed for all reinforced composites (5-15 wt.%) before and after sintering process. Similarly, composites produced are found to be good wear resistant material. Jiang et al. (2005) have fabricated magnesium metal matrix composites incorporating micron size B_4C particles in range from 10-30 vol.% via P/M technique. Improved hardness and wear resistance is detected for composites. Rajkumar et al. (2020) has fortified micro (5-10 wt.%) and nano (5-10 wt.%) B_4C separately through powder metallurgy technique. Increase in B_4C content in magnesium alloys, typically improves relative density, formability stress index parameter and workability in composites.

Friction stir processing is another solid-state material processing evolved from friction stir welding. Friction stir processing (FSP) has materialized as a particularly encouraging and efficient technique for fabricating metal matrix composites (MMC), mostly surface MMC. It holds the unique solid-state material flow and severe plastic deformation characteristics of the friction stir principle to uniformly distribute reinforcement particles within a metallic matrix. The basic theme is to incorporate reinforcing particles into a localized region of a metallic workpiece and then use the FSP tool to forcefully mix and distribute these particles within the softened matrix. FSP involves creating grooves on surface of cast work piece. The size of grooves depends upon required depth and weight percentage of reinforced phase. Powdered form (nano or micro size) reinforced particles are carefully introduced in generated grooves or holes. In next step, “pin-less” FSP pass is processed to pre-consolidate

the particles. FSP tool geometry is key for efficient materials flow and particle dispersion. The rotating FSP tool is pitched into the metallic workpiece, with pin extended into the workpiece and shoulder touching the surface. Thus, there occurs plastic deformation by pin and friction between contacting surfaces. This phenomenon generates local heat spots. This heat softens the matrix material to plastic or visco-plastic state well below its meting point. Once the material is completely plasticized, the tool is traversed horizontally along the groove or across the filled holes. As the tool traverses, the softened matrix flows vigorously around the rotating pin. Such intense stirring act mechanically mixes the pre-placed reinforcement particles into plasticized matrix. Overall, FSP represents a powerful and versatile solid-state route for manufacturing advanced MMCs, offering superior microstructural control and mechanical properties compared to many conventional techniques. However, process is complex and not economical compared to other liquid processing of MMC. Recently, Tomar et al. (2023) have utilised FSP to reinforce MoS_2 particles (13.6 wt.%) in AZ31 alloy. The FSP sample is processed at 1000, 2000 and 3000 rpm and tool traverse speed is kept as 70 mm/min. Wear resistance and hardness improvement is evaluated for all composite samples.

1.2.2 Mechanical Properties

The main aim of incorporating submicron and nano size reinforcement in magnesium matrix is to improve mechanical and tribological properties of composites. Typical mechanical properties include hardness, yield stress (YS), ultimate tensile strength (UTS), compressive strength and creep characteristics etc. Accordingly, researchers have incorporated different nano/micro particles (SiC, Al_2O_3, Y_2O_3, AIN, TiB_2, WC, CNT) in magnesium matrix. Meenashisundaram et al. (2015) have synthesized dense Mg-TiO_2 nano composite through disintegrated melt deposition technique with hot extrusion as end process. It reported around 47% reduction in grain size with the addition of 2.5 vol.% of nano size TiO_2. Furthermore, proof stress, ultimate tensile strength and fracture strain are improved by 37%, 9% and 31% respectively. Jutanaiman and Syahrial (2020) have developed Mg-B_4C composites through stir casting. B_4C is fortified in 2, 4, 6 and 8 vol. % in magnesium matrix. Magnesium composites with 8 vol.% B_4C show improved hardness of 72.8 HRH, reduced wear rate of 0.0023 mm^3 and better impact value of about 0.11 J/mm^2 than pure magnesium. Comparatively high density and low porosity is observed in composite. UTS and % elongation values are optimal for 8 vol.% B_4C. Meenashisundaram et al. (2014) developed Mg-TiB_2 nanocomposites which are prepared through DMD route. It is noticed that Mg-1.98 % TiB_2 nano-composite shows good room

temperature tensile property. While other mechanical properties such as yield strength (55%), UTS (16%), fracture strain (78 %), compressive strength (48%), ultimate compressive strength (11%) and fracture strain (10%) are improved compared to pure magnesium. Ponappa et al. (2013) introduced yttria (Y_2O_3-5μm) in AZ91D through stir casting process. Fortification of yttria particles improved hardness, Young's modulus and yield strength of pure magnesium and AZ91D alloy. Precipitate hardening, grain refinement and lower cracking tendency are the main reasons for improved mechanical properties.

Dalmis et al. (2016) have developed ZA27-Gr nano composites. Density values of nanocomposites decrease with increasing graphite rate while porosity ratio increases. Also, the ultimate tensile strength and Brinell hardness values decreased with increase in graphite content. Hasan and Gupta (2006) fortified submicron & nano size Al_2O_3 particulates in magnesium alloy through disintegrated melt deposition (DMD) processing route and reported improved hardness values as 64%, 47%, and 40% respectively for 50 nm, 300 nm and 1 μm sized Al_2O_3. Goh et al. (2007) studied physical and mechanical properties of Mg-1.0 vol.% MgO composite. There is an improvement in thermal stability, macro hardness, yield and tensile strengths, and modulus of the nano-composites relative to pure magnesium. Goh et al. (2008) fabricated Mg-1.3CNT through DMD process and noticed improved ductility and fatigue behaviour. Thakur et al. (2007) fortified nano SiC and CNT in magnesium alloy through powder metallurgy (P/M) route. It is noticed that the presence of silicon carbide particles led to a progressive reduction in coefficient of thermal expansion for a constant overall number of reinforcements. Similarly, improved micro-hardness, 0.2% YS and UTS values are noticed for Mg-SiC composites.

1.2.3 Tribological Behaviour

Tribology plays an important role in modern machinery involving sliding and rolling surfaces. All mechanical elements in an automobile such as brakes, clutches, bolts, nuts, driving wheels etc. utilize friction in very productive way. At the same time, wear is also considered to be productive in case of cutting, machining, shaving, and writing with pencil. In contrast, friction and wear considered to be unproductive in gears, engines, bearings, and seals. Friction and wear cause significant energy loss in machineries as well as replacement of spares. In that context, productivity of equipment decreases as well as monetary burden on industries yields. Accordingly, studies related to tribology is essential in order to prevent extra capital investment on maintenance or repairs, breakdowns and frequent replacement of spares in industries.

Researchers are finding ways to minimize friction and wear through new technologies in tribology. Now a days, researchers are involved in fabrication of variety of nano and submicron composites with the incorporation of different ceramic reinforcements in magnesium alloy. Similarly, research focus is to improve tribological properties at room temperature, elevated temperature, abrasive and corrosion environment. Also, evaluation of microhardness, nanoindentation characteristics and scratch resistance of produced composites is in active research focus. Based on these research opportunities, related literature is reviewed here.

Raghav et al. (2018) studied wear resistance of Mg-Co composites synthesized using ultra sonic associated stir casting. The coefficient of friction (COF) is found to reduce compared to pure magnesium and increase with increase in applied load. Mg-Co composites show significant decline in friction values with increase in sliding distance. Wear resistance gets improved with increase in wt. % of Co. Hardness improvement is around 30 % for Mg-25 wt.% Co compared to pure mgnesium. Similarly, Zhang et al. (2018) scrutinized wear characteristics of Mg-SiC composites and asserted that Mg- 15% SiC composite exhibits the twenty-three times lowest wear rate than pure magnesium alloy. Composite worn surfaces exhibit oxidation as a dominant wear mechanism. The produced oxide layer is quite stable due to presence of SiC particles in composites. Seenuvasaperumal et al. (2017) investigated tribo-mechanical behaviour of calcium hexaboride (CaB_6) reinforced Mg composite on a pin-on disk tribo meter at room temperature. Improved mechanical property and wear resistance is reported for the composite. Nguyen et al. (2015) examined wear mechanism of Mg-Al_2O_3 fabricated through DMD method. Composites exhibit better wear behaviour at high sliding speed and load than AZ31 alloy. The dominant wear mechanisms were abrasion with oxidative wear sporadically and delamination at sliding speeds of 1-3 m/s and loads of 10-30 N. Adhesion occurred at intermediate speeds of 5-7 m/s with similar load range. Mainly, adhesion occurred at high speeds and loads of 10-30 N range.

García-Rodríguez et al. (2017) have fabricated AZ91-SiC (5 and 10 %) composite through semisolid route. Alloys and composites are studied for dry sliding at 10-250 N load and sliding speeds of 0.1, 0.3, 0.5 and 1.0 m/s against steel disc counter body. AZ91 composites shows excellent wear resistance comparatively at low sliding speed up to 0.3 m/s and medium load range of 40-80 N. While wear rate enhanced at higher load range of 90-250 N for composite in spite of presence of SiC particles. Kaviti et al. (2018) investigated wear behaviour of Mg-BN composite fabricated through P/M technique followed by hot extrusion. Dry sliding tests are conducted at different sliding speed (0.6, 0.9 and 1.2 m/s) and loads (5,7 and 10 N) at

room temperature. Composite exhibits improved wear resistance till medium range of load and speed and lacks thereafter. Aatthisugan et al. (2023) fabricated magnesium composites (AZ91D-B_4C) and hybrid composites (AZ91D-B_4C-Gr) via stir casting method. Tribological and mechanical properties of produced composites were examined. It is reported that with the addition of B_4C, hardness and wear resistance improved while ultimate tensile strength declined. Under dry sliding test, wear loss increases with the rise in load for both alloy and composite. In brief, addition of B_4C strengthens material, resists plastic deformation and increases load bearing capacity.

Shanthi et al. (2011) had fabricated AZ31B-1.5Al_2O_3 & AZ31B-1.5 Al_2O_3-Ca. Wear test carried out at sliding velocities 1-10 m/s at load 10 N. Transition in wear mechanism is assessed from abrasion to adhesion with increase in sliding velocity. Aydin et al. (2018) fortified B_4C particles (10, 20 and 30%) in magnesium alloy through P/M. Significant increase in hardness and wear resistance was achieved by incorporating B_4C. Mg-30 wt.% B_4C composite possess the highest wear resistance for all loads (5, 10 and 20 N) at 64 mm/s and 500 m sliding distance. It is observed that abrasive and oxidative wear are dominated mechanisms for composite. Habibnejad–Korayem et al. (2010) fortified nano- Al_2O_3 (2 wt.% Al_2O_3,100 nm) in Mg and AZ31 alloy using ultra sonic stir casting route. Wear test conducted under stress 0.5, 1.0, 1.5 MPa at sliding speed 0.5 and 1.5 m/s at 2000 m sliding distance and at 12, 24 and 36 N load range. Composite materials show much lower wear rate mainly due to strength improvement with the addition of hard nano particles. Improved hardness, grain refinement, higher load bearing capacity are some contributions to the overall wear resistance.

Gopal et al. (2017) developed Mg-CRT-BN (CRT: 5, 10 and 15 wt.%) with BN particle (size 10, 30 and 50 μm) with 2 wt.% utilizing P/M. Increase in reinforcement content and particle size reduces the wear rate whereas the opposite trend is recorded for coefficient of friction. Lim et al. (2005) has investigated Mg-Al_2O_3 composite where wear rate shows decreasing trend up to sliding speed of 7 m/s and a reverse trend at 10 m/s. At low speeds up to 3 m/s, abrasion is the dominant wear mechanism. At high speed of 10 m/s, adhesion mechanism dominates along with the consequences of thermal softening and melting. Saravanan and Surappa (2000) have prepared Mg-30 vol.% SiC composite using melt stir technique. Fabricated composite exhibits a finer grain structure compared to unreinforced magnesium. Sliding test is carried out for sliding distance of 1.5 km with loads varying as 5, 10 and 50 N and at a sliding velocity 0.5 m/s. Sliding wear rate of the Mg-30 vol.% SiC_P composite is found to be less compared to pure magnesium. Wei et al. (2013) developed Mg-

SiC (20-40 μm) and Mg-MWCNT (40 nm dia. and 10-30 μm length) composite through P/M route. Vicker's hardness values of magnesium composites are found to be improved. Dry sliding test is conducted at 40 N load with sliding velocities of 0.5, 1.5, 3.5 m/s for a sliding distance of 5 km. Low specific wear rates at 3.5 m/s for magnesium composites are obtained which signifies the good wear resistance ability of MMC. Adhesion and delamination are the dominant wear mechanisms at 0.5-1.5 m/s, while adhesive wear dominates at 3.5 m/s. Banerjee et al. (2019a) conducted dry sliding test on AZ31-WC nanocomposite. Hardness values of composites enhanced with increased wt.% of WC. Wear resistance of fabricated composites show improvement with increasing amount of WC nanoparticles. COF values of composites depict decreasing trend with increase in load and speed.

Deng et al. (2010) utilised stir casting to synthesize AZ91-SiC (submicron and micron) bimodal size composite. Distribution of bimodal particles depends upon size on particle size. Micron size SiC particles mainly distribute at grain boundaries and submicron sizes distribute at grain boundaries as well as at interior of grains. Considerable improvement in mechanical properties occurs due to significant grain refinement of Mg alloy with incorporation of bimodal size SiC particles. Sharma et al. (2000) have synthesized AZ91-(1-5) % feldspar of size 30-50 μm through liquid metallurgy vortex method. It is observed that feldspar particle-reinforced composites exhibited reduced wear rate than the unreinforced alloy specimens. Wear rate gets decreased with increasing feldspar content. The wear rate of the composites as well as the matrix alloy increases with the rise in applied load. Abrasion and delamination wear mechanisms are detected respectively at low and high loads. Thakur and Dhindaw (2001) fabricated SiC reinforced Al/Mg composites through vacuum infiltration technique. Magnesium composites show better wettability compared to Al composites. Coating of SiC reinforcements with Ni and Cu generally leads to good quality interface characteristics in composite as both micro-hardness and wear properties are improved.

Lim et al. (2003) synthesized Mg-SiC composite through powder metallurgy route. Composites exhibit slightly superior wear resistance under the lower load, but the influence of the SiC particulate reinforcements on wear resistance are not as conclusive under the higher load. The suggested useful range for Mg-SiC composites appears to be limited to loads and speeds below 30 N and 5.0 m/s, respectively. Mondal and Kumar (2009) have synthesized AE42-Saffil Fibre-SiC composite through squeeze casting. The test is conducted at sliding velocity of 0.837 m/s and 10-40 N load for sliding distance of 2.5 km. Wear rate of the alloy is found to be 71% higher than saffil composite at 10 N. Wear rate progressively decreased

with the partial replacement of saffil short fibre with SiC particles. Liang et al. (2014) studied sliding wear of AZ31Mg alloy at applied load range of 5-360 N and sliding speed range of 0.1-0.4 m/s. At high sliding speeds, transition from mild to severe wear occurred. Oxidation, abrasion and delamination in the mild wear regime whereas thermal softening and melting in severe wear regimes are identified as mechanism of wear. Zhang et al. (2009) fabricated AZ91-0.8Ce-Al_2O_3-Gr hybrid composite through squeeze-infiltration technique. It is noticed that with increasing graphite content, the micro-hardness of the composites decreases but the wear resistance increases. The graphite which works as lubricant during dry sliding process decreases the wear loss. At low load, the wear mechanism of the composite is mainly abrasive wear and oxidation wear. At high load, the wear mechanism of composites changes to delamination wear.

Prabhu et al. (2016) studied AZ81 reinforced with synthetic graphite/activated charcoal. Tensile strength and ductility increase with increasing carbon content. Wear tests are conducted at speed 5.37 m/s and load 20-30 N. Wear rate decreases with the increase of carbon content in the alloy. The activated charcoal with 0.98 wt.% C is found to be a better grain refiner in improving tensile behaviour and wear resistance. Wear surface morphology depicts abrasive and delamination wear mechanisms. These mechanisms are responsible for the wear loss in the AZ 81 alloy. Qi (2006) fabricated AZ91-(5-20) wt.% Gr and noticed that the wear loss and coefficient of friction are decreased to low level. Wear rate increases quite slowly under a certain range of load and fiction coefficient reaches the minimum especially for the composite with graphite particle content. A continuous black lubricating film forms progressively on the worn surface along sliding, which effectively limits the direct interaction between the composite tribo surface and the counterpart, and remarkably delays the transition from mild wear to severe wear for magnesium alloy composite.

Thirugnanasambandham et al. (2019) studied the influence of load and sliding speed on dry sliding wear behaviour of Mg-Al_2O_3 (50 nm) nanocomposite. Dry sliding tests were carried out for fixed sliding distance at varying loads and speeds. It is observed that the wear rate gets increased with load and decreased with increasing wt. % Al_2O_3 in nano composites. Thirugnanasambandham et al. (2021) fabricated Mg-SiC nanocomposite and investigated tribological behaviour at different loads and sliding speeds. It is revealed that Mg-SiC nano composite exhibits superior wear resistance at almost all ranges of sliding conditions. Ravichandran et al. (2022) developed Mg-B_4C composite through powder metallurgy route. It

has been reported that Mg-B_4C composite possesses excellent hardness, tribological properties and compressive strength. Narayanasamy et al. (2018) prepared a magnesium composite by reinforcing TiC particles (size: 25-35 μm) through powder metallurgy technique. Superior microhardness, low wear loss and higher coefficient of friction were observed for Mg-TiC composite.

Selvam et al. (2014) studied wear behaviour of Mg-ZnO nanocomposite produced through P/M route. The wear rate and friction coefficient variation were analysed at different loads (5, 7.5, 10 N) and sliding velocities (0.6, 0.9, 1.2 m/s) at room temperature. Wear rate was found to increase with load and sliding velocities. COF decreased with the increased sliding velocity for a particular sliding distance. Zafari et al. (2012) examined wear behaviour of AZ91D alloy under varying loads of 5, 20 and 40 N at varying temperature from 25 to 300ºC with a sliding speed of 0.4 m/s and for a fixed sliding distance of 1 km. The investigation of worn surfaces depicts abrasive wear at 25ºC and 40 N load. The wear loss increases with rise in temperature. At 20 N and 100ºC, wear rate gets decreased about 58%. With further increase in temperature to 250ºC, wear of alloy increases due to softening and dissolution of β-$Mg_{17}Al_{12}$. Wang et al. (2010) investigated wear behaviour of AZ91D alloy at temperature of 25-200ºC. Load of 25 N is observed as a critical value, below which the wear resistance of alloy increases even though temperature is increased. Recently, Sunu Surendran and Gnanavelbabu (2022) have examined tribological properties of AZ91D alloy and its composites fortified with Ti-based reinforcements. Superior tribological performance is observed for composites at elevated temperature. Plastic deformation followed by delamination, oxidation and thermal softening are identified as dominant wear mechanisms at elevated temperature.

Banerjee et al. (2019c) investigated wear behaviour of AZ31-WC composites at elevated temperature. Wear and friction behaviour gets significantly enhanced with addition of WC particles in Mg alloy. At 20 N and 200ºC, wear rate and COF decreased about 75% and 15% respectively with respect to the base alloy. Formation of harder surface layer due to nano-hard particles incorporation resulted in delay in thermal softening effect. Das et al. (2010) investigated AZ31 alloy at 5 N load at 400 ºC and sliding speed of 0.01 m/s. It is reported that surface grains are re-crystallized and coarse grains are observed below the recrystallization zone. Labib et al. (2016) studied elevated temperature behaviour for Mg-SiC composites with 5, 10 and 15 vol.% of SiC. Wear behaviour is investigated at 5-60 N, sliding speed of 0.4 m/s and temperature varying between 25-200ºC. At higher temperatures of 100, 150 and 200°C, a

significant lower wear rate was observed for the composites compared to the pure magnesium. Increase in the normal load resulted in a transition from mild to severe wear at all wear temperatures. Below the transition load, oxidation was the dominant wear mechanism, while above that severe plastic deformation and adhesion contributed majorly to wear. Gnanavelbabu et al. (2022) have investigated AZ91D alloy reinforced with different ceramic particles (TiB_2, TiC and TiN). Wear test is conducted at temperature range of 50-200ºC, sliding speed of 0.25 -1 m/s and normal load of 10-50 N. It is found that wear rate and friction values are significantly reduced for composites. It is inferred that presence of hard particles can cause localized deformation and resist plastic yielding.

Moheimani et al. (2022) have prepared AZ31-B_4C composite through stir casting and observed higher wear under high load irrespective of sliding speeds. Adaveesh et al. (2017) investigated the wear behaviour of stir cast ZA43-B_4C composite. Influence of applied load and sliding distance on wear behaviour of composites is investigated for a sliding distance varying up to 6 km at a constant speed. The wear resistance is effectively increased with the fortification of B_4C particulate reinforcement. The wear rate typically shows increasing trend with reference to increasing sliding distance. Rahmani and Majzoobi (2019) have fortified B_4C particles in Mg matrix through compaction method and examined the effect of compaction loading rate on wear characteristics of Mg-MMC. It was reported that wear resistance was enhanced around 70% and coefficient of friction (COF) was reduced around 43% compared to base alloy. Oge et al. (2019) have incorporated varying amount of B_4C particles in AZ91 matrix through powder metallurgy and hot pressing. It was reported that AZ91-10B_4C possessed lowest wear volume and COF.

1.2.4 Corrosion Behaviour

Material selection for any component depends on various factors like strength, corrosion resistance etc. Strength and stiffness furnish requisite functions and safety. Higher strength to weight ratio helps to achieve higher payload while durability is dependent on corrosion characteristics. Being lightweight structural material, magnesium alloys extend distinctive and unique properties. Magnesium offers excellent machinability, noticeable damping capability, better stiffness and good castability. Consequently, magnesium materials are drawing attention of scientific community. In automotive and aerospace industry, magnesium alloys are found to be a possible potential replacement of aluminium due to low density.

Still, application of magnesium is hindered owing to high corrosion rate of magnesium alloys. Basically, magnesium alloys are highly susceptive to galvanic corrosion which disturbs the steadiness of the set-up [Esmaily et al., 2017]. Accordingly, researchers are trying to improve the corrosion behaviour of magnesium alloys by either incorporating ceramic based reinforcements or using high purity alloying components. Use of high purity alloying element may enhance corrosion behaviour of magnesium. But that much enhancement is inadequate to resolve galvanic corrosion related issues of magnesium alloys. Accordingly, researchers have incorporated different ceramic-based particles (Al_2O_3, Y_2O_3, ZnO, TiC, SiC, CNT, WC etc.) in magnesium matrix and examined the effect of fortified particles on corrosion behaviour of Mg matrix. However, literature reveals that scientific community have different observations regarding corrosion behaviour of Mg-MMCs. Researchers also observed that Mg-MMCs do not follow any particular trend.

Raghav et al. (2018) investigated corrosion behaviour of Mg-Co composites (5,10, 15, 25 Vol.%) in 5 % NaCl solution for 1 hour. Potentiometric polarization analysis indicates that Mg-25Co composite exhibit better corrosion resistance compared to magnesium alloy. Banerjee et al. (2019b) studied AZ31-nWC (0-2 wt.%) in 3.5% NaCl solution. Effect of amount of WC particles and roughness of composite surface was examined through potentiodynamic polarisation test. It was identified that Mg-0.5 wt. %WC is the most corrosion resistant one followed by AZ31 alloy.

Endo et al. (2008) studied corrosion behaviour of AZ91-(0-5wt.%) MWCNT, in wet condition and salt water (3 wt.% NaCl, 293 K). A drastically improved anticorrosive characteristic of magnesium composites is observed with the introduction of MWCNTs. Falcon et al. (2011) analyses corrosion behaviour of AZ91E reinforced with TiC particles in 3.5% NaCl through electrochemical technique. It is observed that composites exhibit better corrosion resistance compared to unreinforced alloy. The tendency to suffer from pitting corrosion is higher in base alloy than composites. Zhang et al. (2015) studied corrosion characteristics of AM60-Al_2O_3 in 3.5wt.% NaCl medium. Effect of Al_2O_3 volume fraction on corrosion behaviour is examined. No evidence of galvanic corrosion is revealed for composite surface. Bakkar and Neubert (2007) investigated corrosion behaviour of magnesium matrix composites in NaCl solution through electrochemical potentiostat set up. Comparable corrosion resistance is observed for pure alloy and composites. The corrosion potential didn't show increased trend with the addition of Al_2O_3 fibres. It reported the absence of galvanic and

interfacial corrosion due to presence of Al_2O_3 fibres. This phenomenon indicates the improved corrosion resistance for magnesium matrix composites. Hihara et al. (1993) investigated Mg-SiC and ZE41A- SiC in nitrate, sulphate and chlorine solution. High galvanic corrosion rates were noticed in the presence of oxygen. It was also observed that magnesium composites exhibit better corrosion resistance than pure magnesium. Lei et al. (2012) studied corrosion behaviour of AZ91-(0.1, 1, 5) MWCNT in 3.5% NaCl. A good dispersion of MWCNTs leads to even higher corrosion rates on the composite surface. Chan et al. (1997) studied corrosion behaviour of AZ91C-20 % Al_2O_3 in 3.5% NaCl. Investigation indicated that in alkaline solution containing chloride ions, the presence of $A1_2O_3$ short fibres in the alloy did not drastically alter the corrosion behaviour, but significantly reduced its corrosion resistance. Corrosion current density value reached three times higher than that of matrix alloy. Zucchi et al., (2004) studied corrosion behaviour of AZ80A-SiC and ZK60A-20SiC, in 0.1N Na_2SO_4, 1N Na_2SO_4 and NaCl solution respectively. The corrosion resistance of SiC_p/AZ80A MMC was slightly lower than that of ZK60A/ 20% SiC_p in 0.1 N and 1 N Na_2SO_4 solutions. The corrosion voltage of both MMCs increased about tenfold by increasing the sulphate concentration from 0.1 N to 1 N. Chloride solutions were much more corrosive toward both MMCs, but the influence of the anion concentration was not so evident. Impedance spectra revealed the difficulty in formation of protective magnesium hydroxide. Funatsu et al. (2013) studied corrosion characteristics of AZ61B-CNT (heat treated at 823 K) for 10h in salt water. Salt water immersion test indicated that the corrosion rate of AZ61B-CNT composite materials was reduced to less than 30% with the reduction in heat treatment temperature. Gobara et al. (2015) studied corrosion behaviour of AZ91-TiC-Ti_2AlC-TiB_2 in 3.5% NaCl solution. EIS and potentiodynamic polarization results indicated that the reinforcing particles significantly improve the corrosion resistance of the reinforced alloy in 3.5% NaCl solution. Hamid et al. (2011) studied AM50-5/10 ZrO_2 in 5% NaCl. The presence of ZrO_2 decreases the corrosion rate of AM50.

Mindivan et al. (2014) developed Mg-CNT composites and revealed that the addition of CNT content possesses detrimental effect on corrosion performance. Tiwari et al. (2007) examined corrosion characteristics of Mg-SiC composites in NaCl solution and yielded that composite shows higher corrosion rate compared to base alloy. Turan et al. (2017) investigated effect of incorporating graphite particles in magnesium matrix on corrosion characteristics. It is observed that corrosion behaviour of composites was negatively affected with increase in graphite content. Nunez- Lopez et al. (1995) examined corrosion rate of ZC71-12%SiC_p

composite. It is reported that composites possess three times higher corrosion rate than that of matrix alloy due to formation of less protective corrosion layers.

Nunez -Lopez et al. (1996) studied corrosion performance of high purity Mg-SiC metal matrix composites and noticed absence of micro galvanic corrosion in the vicinity of SiC particles. Ma et al. (2014) fabricated β-TCP-MgCa composite material for biodegradable bone implant using suction casting route. Compressive strength of about 1000-fold higher than that of MgCa bulk alloys is reported. The corrosion potential of the composite is found to be higher than that of bulk alloy. Thus, β-TCP-MgCa composite exhibits superior corrosion resistance than MgCa bulk alloy. Pardo et al. (2008) carried out study on Mg-Al-Zn alloy and inferred that corrosion severity is mainly caused by formation of corrosion layer of $Mg(OH)_2$. It is also noticed that fine β-$Mg_{17}Al_{12}$ network and enhancement of amount of Al limits the progression of the corrosion attack. Toptan et al. (2016) examined corrosion properties in 9 g/L NaCl for Ti-B_4C composites mainly for orthopaedic implants. Corrosion tests conducted are electrochemical impedance spectroscopy and potentiodynamic polarisation under open circuit potential. Incorporation of B_4C particles (16-53 micron) in titanium (Ti) shows comparatively lower affinity to corrosion than pure matrix phase. Ti and its alloys are usually utilised in dental and orthopaedic implants due to its corrosion resistance characteristics. With the addition of B_4C in Ti alloys, the composite shows improvement in tribo-corrosion behaviour.

Lv et al. (2022) incorporated submicron SiC particles (0.5, 1 and 2 vol.%) in magnesium alloy (AZ91) through ultrasonic assisted semi solid stir cast route. Corrosion test is performed on magnesium composites by employing electrochemical impedance and potentiodynamic polarisation techniques. It is reported that addition of traces of SiC (0.5 vol. %) notably increases the corrosion resistance of AZ91 alloy due to presence of lamellar (α+β) phase. Most specifically, $Mg_{17}Al_{12}$ phase acts as a barrier for corrosion in lamellar form. Further, increase in SiC considerably reduces corrosion resistance due to development of $Mg_{17}Al_{12}$ phase in globular form. Pardo et al (2009) conducted corrosion test of SiC reinforced magnesium composites and reported increase of corrosion rate of the composite with incorporation of SiC that promotes cracking and spalling of the corrosion layer.

1.2.5 Nanoindentation and Scratch Resistance

Nanoindentation is an indispensable tool for research and development of MMCs. It moves beyond average bulk properties to provide localized, nanoscale insights into the mechanical behaviour of the matrix, reinforcement, and their interfaces, enabling a deeper

understanding of strengthening mechanisms and tailoring of MMCs for diverse, high-performance applications. Accordingly, nanoindentation is carried out to understand behaviour of different materials.

Recently, Banerjee et al. (2021a) have carried out nanoindentation study for AZ31-WC-Gr hybrid composites. The mechanical behaviour is determined for both base alloy and nanocomposites. It is concluded that AZ31-2WC-1Gr exhibits better mechanical properties. Further addition of Gr content slightly deteriorates the mechanical properties. Similarly, Balikai et al. (2022) conducted nanoindentation test on AZ91D-Si_3N_4 composites. Four different compositions were prepared with varying range of Si_3N_4 wt.% (2.5-10%). Load displacement plot obtained for composites is slightly irregular, due to structural changes and varying strength of composites. The varying strength or structural changes are resulted with the addition Si_3N_4 wt.%. It is concluded that the improved elastic modulus and nano hardness is obtained for composites due to contribution of Si_3N_4 wt.%. Haghshenas et al. (2020) carried out work on magnesium-samarium oxide nanocomposites. Nanohardness and elastic modulus increase with the increase in wt.% of samarium oxide reinforcement. Ghasemi et al. (2018) also conducted nanoindentation analysis of Mg-SiC nanocomposites synthesized through mechanical milling. Mg-SiC nanocomposites resulted a lower load-displacement linked to higher resistance to the indenter. Evaluated values of nanohardness and elastic modulus of nanocomposites are improved remarkably due to addition of SiC nanoparticles. Thus, reinforced particles produce improved strengthening capacity of the Mg matrix. He et al. (2015) have investigated nanohardness and elastic modulus of different thermoelectric materials using nanoindentation technique with indentation depth of 1000 nm.

Scratch investigation is a practical methodology for assessment of process parameters in dry machining. It is notable that there has been a recent boost in bio medical fields for magnesium alloys. Scaffolds and implants made of magnesium alloy have proved to be biocompatible. Such bio devices are prone to surface wear due to biological entities in the body. Thus, to analyse mechanical behaviour of materials, knowledge of scratch resistance is essential to justify life span of bio devices in human bodies [Zhao et al., 2009; Aronson, 1995; Li and Zheng, 2013; Nautiyal et al., 2016]. Sinha et al. (2006) studied the effect of submicron SiC and SiC+Ti particulate addition in Mg matrix on scratch behaviour. The tests confirm the increase in scratch hardness of Mg composites. With the increase in wt.% of SiC and SiC+Ti particulates, the scratch hardness and elastic modulus increase monotonically. COF values also increase for composites and enhances with the increase in wt.% of reinforcement compared to

base Mg alloy. Banerjee et al. (2019d) have investigated scratch resistance of Mg-WC nano composites. The scratch volume of Mg-WC nano composites decreases with the increase in wt.% of WC. COF values for composites remain almost constant but show increasing trend with wt.% of WC. Worn surface morphology reveals mostly abrasive mechanism during scratch deformation.

1.3 Scope of Present Work

In the current study, boron carbide (B_4C) particles are fortified in AZ31 magnesium alloy through ultrasonic stir casting process. Metallographic tests of fabricated composites are conducted to identify homogeneous distribution of B_4C particulates, grain size refinement, overall microstructure stability and agglomeration if any. Tribological studies are performed at both room temperature and elevated temperatures for varying sliding parameters using pin-on-disc tribometer. Similarly, abrasive wear tests are also conducted under varying grit size and sliding distance. Corrosion behaviour of composites and AZ31 alloy is studied through potentiodynamic polarization tests and electrochemical impedance spectroscopy. Finally, nanoindentation testing is performed to evaluate nanohardness and elastic modulus. Moreover, scratch resistance behaviour is evaluated using dedicated scratch tester for ramp loading.

1.4 Structure of Present Thesis

The present thesis consists of 9 chapters. Chapter 1 introduces magnesium-based metal matrix composites and reports literature survey of magnesium matrix composites. Chapter 2 focuses on fabrication methods and characterization of fabricated composites. This chapter deals with results of density evaluation, microhardness tests and overall characterizations. Chapter 3 mainly concentrates on detailed results of dry sliding behaviour of fabricated composites at room temperature under varying sliding parameters like sliding load, speed and distance etc. Chapter 4 provides in-depth analysis of the effect of higher sliding speeds and distances on tribological performances of the composite. Chapter 5 includes results of abrasive behaviour of prepared composites for varying abrasive grit size and track distance. Elevated temperature sliding behaviour of composites is discussed in Chapter 6 and results are presented for varying temperatures, loads and speeds. Chapter 7 is devoted to corrosion behaviour of composites. Both potentiodynamic polarisation and electrochemical impedance spectroscopy are utilised to investigate corrosion characteristics. Chapter 8 reports

nanoindentation behaviour and scratch resistance characteristics of AZ31-B_4C composites. Finally, Chapter 9 concludes the present work and discusses the future scope of work.

1.5 Summary

This chapter has presented the general discussion on magnesium-based metal matrix composites. It explains the dominance and requirement of magnesium matrix composites in different weight sensitive applications. The chapter focuses on the type of matrix materials, the effect of ceramic reinforcement and the importance of fabrication techniques in the preparation of magnesium matrix composites. It includes literatures based on different magnesium alloys, variety of ceramic reinforcements and different fabrication routes for magnesium matrix composites utilized till date. Review pertaining to mechanical properties, tribological behaviour, corrosion characteristics, nanoindentation and scratch characteristics of magnesium matrix composites are mainly assessed. Finally, the objective of the present work and structure of thesis is presented.

Chapter 2

Preparation and Characterization

2.1 Selection of Base Alloy and Reinforcement

It is well established in literature that the characteristics of composites mainly depend on matrix material, reinforcing phase and synthesis technique. Accordingly, selection of matrix phase, reinforced phase and fabrication technique is of prime importance for composite preparation. In this study, magnesium alloy (AZ31), a category of Mg-Al-Zn alloy, is employed as base alloy. AZ31 alloy is typically selected owing to its lighter density (1.74 g/cc), formability at different working temperatures, adequate specific strength, good castability and excellent dimensional stability [Gupta and Ling, 2011, Dey and Pandey, 2015]. AZ31 has comparable compressive strength (180 MPa), good tensile strength (220 MPa), sufficient elongation (15%), good shear strength (160 MPa) and significant hardness. AZ31 alloy characteristics involve good room temperature strength and ductility, corrosion resistance, excellent weldability, good thermal and electrical conductivity. Chemical composition of AZ31 alloy is shown in Table 2.1.

Boron carbide (B_4C) in 99% pure form with average size of 500 nm is utilized as reinforcement particles. B_4C nano ceramic particles is purchased from Hongwu International Group, China in powdered form with product code k-520. Chemical composition of B_4C is shown in Table 2.2. Submicron sized boron carbide particles are utilized in this study as a ceramic reinforcement in AZ31 alloy. B_4C is mainly chosen here due to its non-reactivity with molten AZ31 alloy, moderate density (2.52 g/CC), excellent hardness (3500 $kg.mm^{-2}$), good elastic modulus (460 GPa), high melting point up to 2450°C, excellent wear resistance, good wettability and high thermo-chemical stability. It has good interfacial bonding and flexural strength with Mg alloy. Boron carbide has got rhombohedral structure and consists of a covalently bonded distorted $B_{11}C$ icosahedra with linear chain of C-B-C atoms. Such a peculiar structure creates a series of appreciable properties like high melting point, light density, high hardness and low thermal expansion coefficient [Thevenot, 1990; Zhang et al., 2021]. Thus, B_4C acts as a suitable particulate ceramic reinforcement in the production of MMCs. Boron carbide also acts as elevated temp semiconductor and can be exploited in making novel electronics applications [Domnich et al., 2011]. Few researchers have fortified B_4C in

magnesium matrix and observed enhanced mechanical, microstructural and tribological properties [Aatthisugan et al., 2017; Aydin et al., 2018; Jutanaiman and Syahrial, 2020].

Table 2.1 Chemical composition of AZ31 alloy

Element	**Al**	**Zn**	**Mn**	**Fe**	**Si**	**Mg**
Wt.%	3.1-3.3	1.1-1.3	0.28	0.004-0.005	0.08-.10	Balance

Table 2.2 Chemical composition of boron carbide powder

Product	**Boron carbide (B_4C) Powder**
Crystal Structure	Rhombohedral
Purity	99 percentage
Average Particle Size	500 nm
Color	Grey
Composition of B_4C	B-77.48 % and C-21.52%

However, tribological literatures related to B_4C particles reinforcement in magnesium matrix are very few. Detailed tribological investigations of AZ31-B_4C composites are thus planned in the present study. It attempts to fulfil the literature gap by performing tribological studies at different experimental conditions.

2.2 Selection of Fabrication Method

It is well documented in literature that particle size and composition as well as fabrication process affects the mechanical and tribological properties of Mg-MMCs. Successfully utilized technique for fabrication of Mg based sub-micron composites is ultrasonic stir casting due to its effectiveness in particle distribution and handling wettability issue. In the current research, the submicron B_4C/AZ31 composites are produced by ultrasonic vibration assisted stir casting technique (USC). Figures 2.1 and 2.2 illustrate the schematic and pictorial view of the USC set up respectively. The fabrication unit has different special attachments like mechanical stirrer, particle preheating unit, die heating set up, bottom pouring hole and inert gas supply arrangement. This special type of furnace has stainless steel crucible where weighted amount of AZ31 ingot is placed and heated at 750°C. A thermocouple is inserted inside the furnace to observe the temperature. At the same time, selected wt.% of B_4C particles are preheated at 300° C in preheating furnace in order to exhibit sufficient wettability with

magnesium alloy by removing moisture. After certain time, a sudden drop is noticed in the melt temperature. Drop in temperature indicates that ingot gets melted.

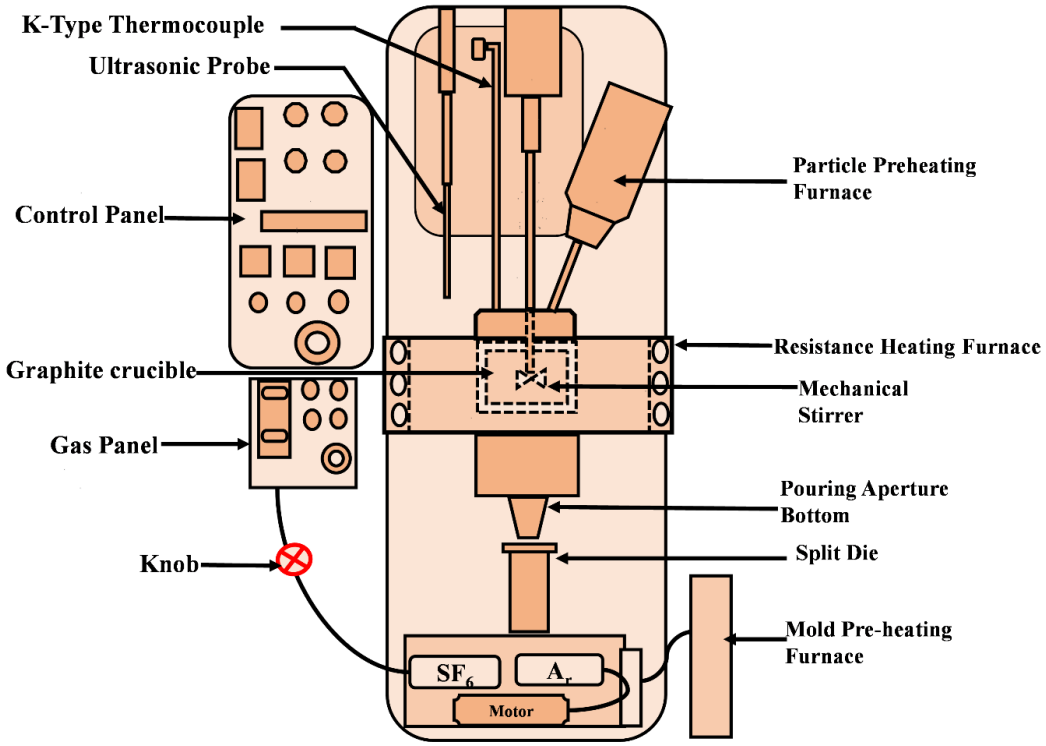

Figure 2.1: Schematic of ultrasonic assisted stir cast furnace

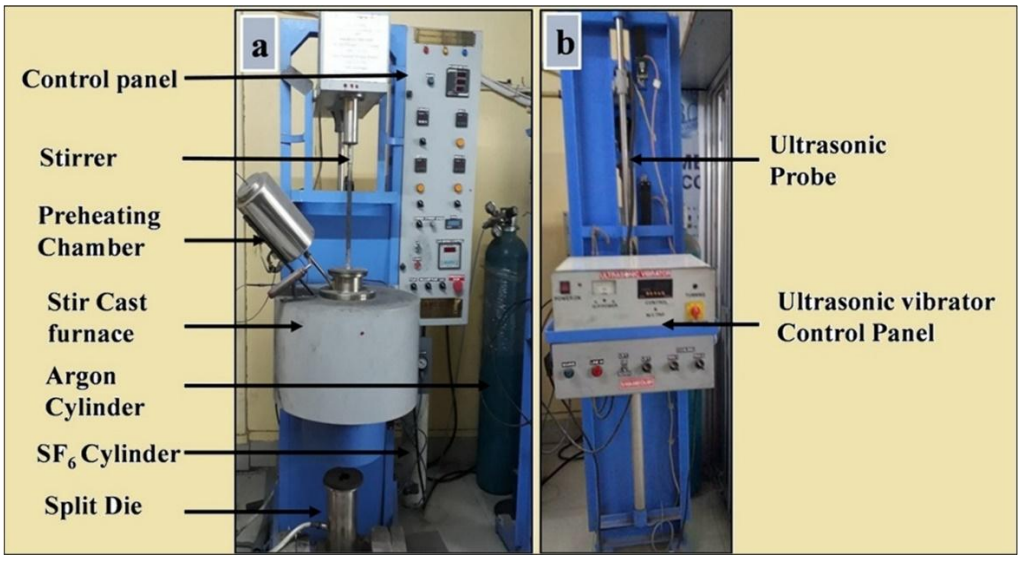

Figure 2.2: Pictorial view of a) stir cast furnace b) ultrasonic transducer (Probe)

Initially, the ranges of stirring speed and time are selected from available literature [Dey and Pandey, 2015, Banerjee et al., 2019a]. Afterwards, hit and trial method is followed to get the

optimal condition of speed and time. In hit and trial method, different set of experiments were performed and microstructural characterizations were done to find particle distribution along with microstructural integrity. Based on those studies, the optimal condition of stirring speed and time has been selected in this study. Thus stirrer rotation is maintained in molten AZ31 alloy inside furnace at 500 rpm for 4-6 minutes so as to form vortex. Preheated particles are then continuously injected into the vortex. Then, the speed of stirrer is increased to 600 rpm and continued for about 8 minutes to uniformly distribute particles in the molten AZ31 alloy.

After that, mechanical stirrer is removed and ultrasonic 'sonotrode' is inserted in the resistance heating furnace. This ultrasonic 'sonotrode' is inserted up to 2/3rd depth of molten alloy to transfer the ultrasonic cavitation for 3-5 minutes at 20 kHz frequency in the melt. By this time, a metallic split type die is preheated to 300°C. The melt is then poured into metallic die through a bottom opening switch of the furnace under strict vacuum condition (10^{-2} mbar). The molten slurry in metallic die is then allowed to solidify by natural convection in air. The solidified cylindrical cast of size Φ 50 mm x 150 mm length is then removed by disengagement of the split die. The entire process is carried out in inert atmosphere by supplying Argon-SF6 in 9:1 ratio. The process is repeated for fabrication of composites with varying amount of reinforcements. Wt.% of B_4C is varied as 0.5, 1.0, 1.5 and 2.0. The cylindrical cast samples of composites and base alloy are then machined into required dimension for executing metallurgical and mechanical characterisation. The experimental parameters are mentioned in Table 2.3.

Table 2.3 Experimental parameters of ultrasonic assisted stir cast unit

Unit	**Specifications**
Mechanical stirrer	Stainless steel
Blade angle	45°
Ultrasonic frequency	20 kHz
Vibration period	3-5 mins
Furnace temperature	750° C
Die dimensions	Ø 50 mm ×300 mm (Split type)
Particle preheating temperature	300° C
Die preheating temperature	300° C
Mechanical stirring time	8-10 min

2.3 Metallographic Tests

2.3.1 Sample Preparation

Microstructural characterization of any material is of immense importance as material properties highly rely on microstructure. Before conducting characterization, sample preparation is required. At first, the as-cast bars are parted and sequence of operations like shaping, turning, grinding and polishing are done to get required dimensions. All samples are cleaned before and after test using acetone to avoid any introduction of foreign particles on sample surface. AZ31 alloy and AZ31-B_4C composite specimens are prepared as cylindrical pins (Φ 6 mm x 30 mm) and square pieces (15 x 15 x 10 mm^3). The square samples are utilised to measure hardness and density. Again, these samples are used for characterisation studies of composites (AZ31- B_4C) and base alloy (AZ31). Pictorial view of AZ31-1.0B_4C ingot and samples is shown in Figure 2.3. Cylindrical pin samples are utilised for tribological studies to discussed in latter chapters.

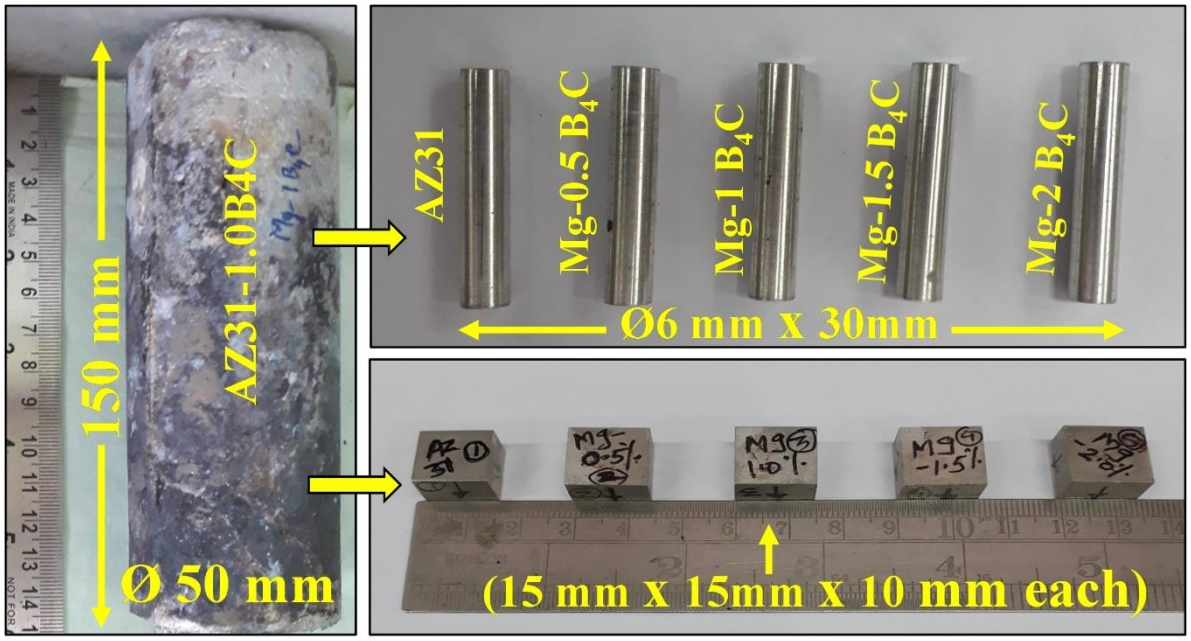

Figure 2.3: Pictorial view of samples

2.3.2 Optical Microscopy and Scanning Electron Microscopy

Microstructural characterization is done by utilizing optical microscope (Leica Model: DM2700M) and Scanning electron microscope (FESEM Version 5.09, Carl Zeiss microscope Ltd., United Kingdom). The pictorial view of optical microscope (OM) and field emission scanning electron microscope (FESEM) is shown in Figure 2.4. Compositional

analyses of samples are carried out through energy dispersive X-ray analysis, EDAX (Make: AMETEK, Model: Element, United States of America). The characterisation process mainly examines B_4C particle distribution in the matrix alloy, different phases in the fabricated alloy and composites and accordingly grain structure refinement in the composites. Before characterisation, all samples are polished by SiC emery paper of different grades. Prepared specimens are finally polished by using diamond paste (1μ) on velvet cloth. The surfaces of these samples are finally etched using acetic acid solution (90 ml acetic acid and 10 ml H_2O) as etchant for 3-4 sec.

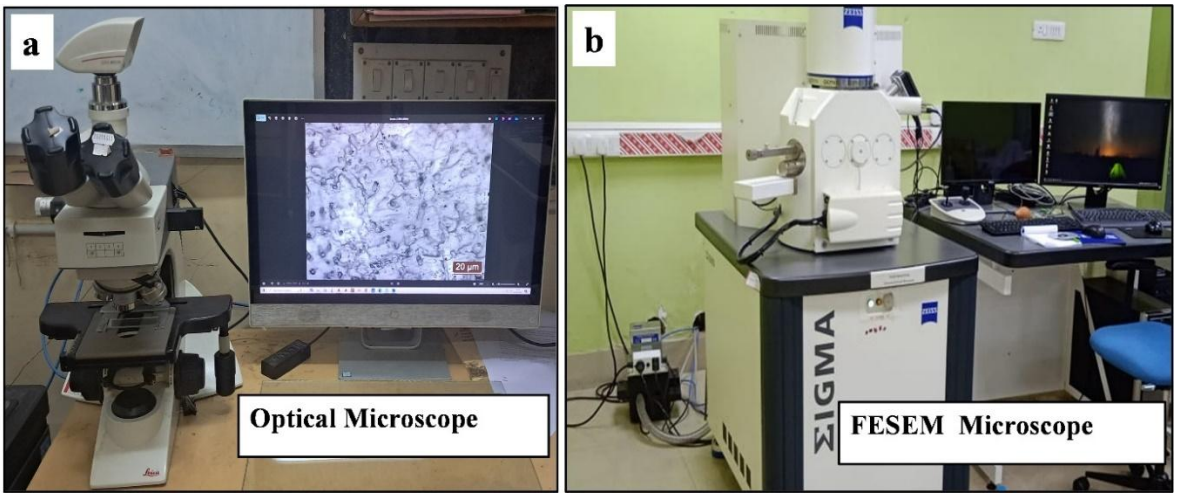

Figure 2.4: Pictorial view of a) optical microscope (OM) b) field emission scanning electron microscope (FESEM)

Optical micrograph (OM) helps to examine microstructure while field emission scanning electron microscope (FESEM) provides a clear view of particle distribution in matrix metal. The optical micrographs of AZ31 alloy and AZ31-B_4C submicron composites are shown in Figure 2.5. Typically, no noticeable defects are observed in the fabricated composite surfaces. However, unavoidable minimal agglomeration was found at the grain boundaries of Mg alloy due to high surface area of submicron particles. Figure 2.5 depicts that microstructure of all samples typically contains α-Mg phases and plate like β-$Mg_{17}Al_{12}$ phases. Excellent interfacial bonding is revealed within matrix and reinforced phase. Presence of β-phase is well acknowledged in microstructures of all AZ31-B_4C composites resulting in restricted grain growth. Ceramic B_4C reinforcement nucleates at grain boundaries and blocks the dislocation movement.

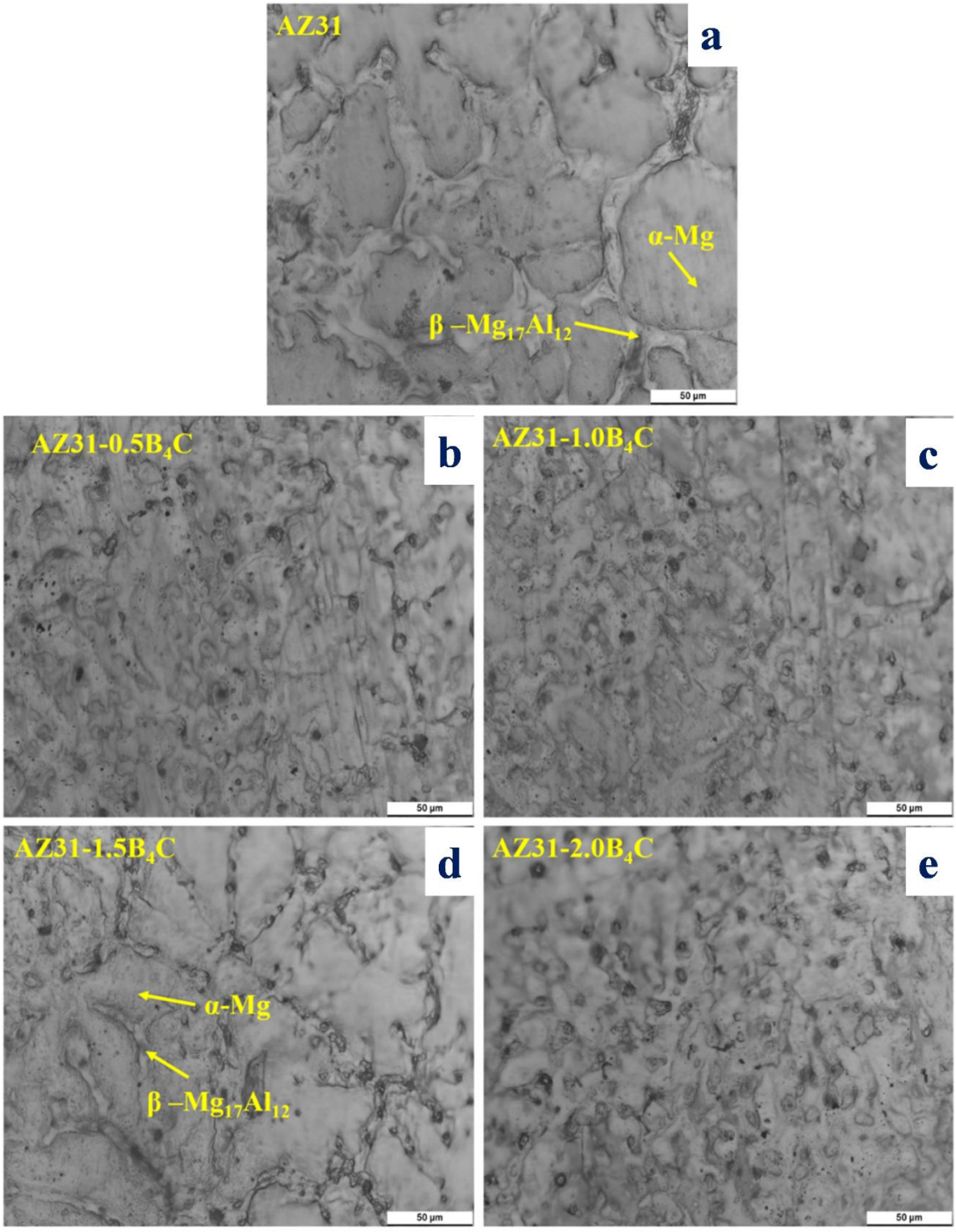

Figure 2.5: Optical micrographs of base alloy and composite variants

These effects of pinning exhibit grain refinement in composites with the addition of hard and non-deformable B_4C particles. It is also observed that the pinning effect is

significantly more in submicron composites having higher content of B_4C particulates. FESEM micrograph of boron carbide is presented in Figure. 2.6. FESEM micrograph of boron carbide nanoparticles approximately justifies the average particle size to be 500 nm.

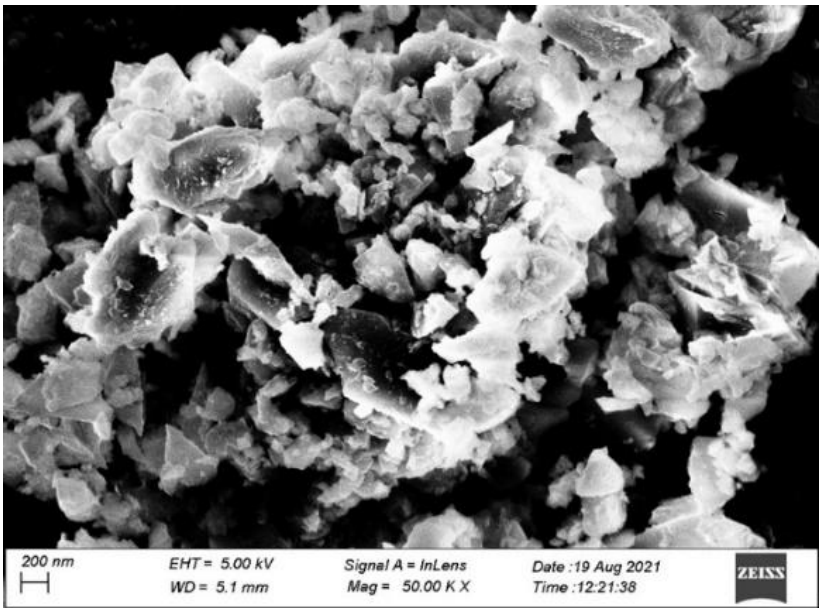

Figure 2.6: FESEM image of boron carbide

The morphology of AZ31 alloy and AZ31-B_4C submicron composites are scrutinized under FESEM and depicted in Figure 2.7. Accordingly, FESEM image of bulk Mg alloy fabricated through USC shows mainly α-Mg phases and β-$Mg_{17}Al_{12}$ phases present in grains and grain boundary respectively. Phase α-Mg is soft one while intermetallic compound, i.e., β-phase is comparatively harder phase at room temperature. Base alloy shows peculiar α-Mg equiaxed grain structure while β-phase settles surrounding soft phase in grain boundaries. The morphology is depicted in ascending order of wt. %. of B_4C.

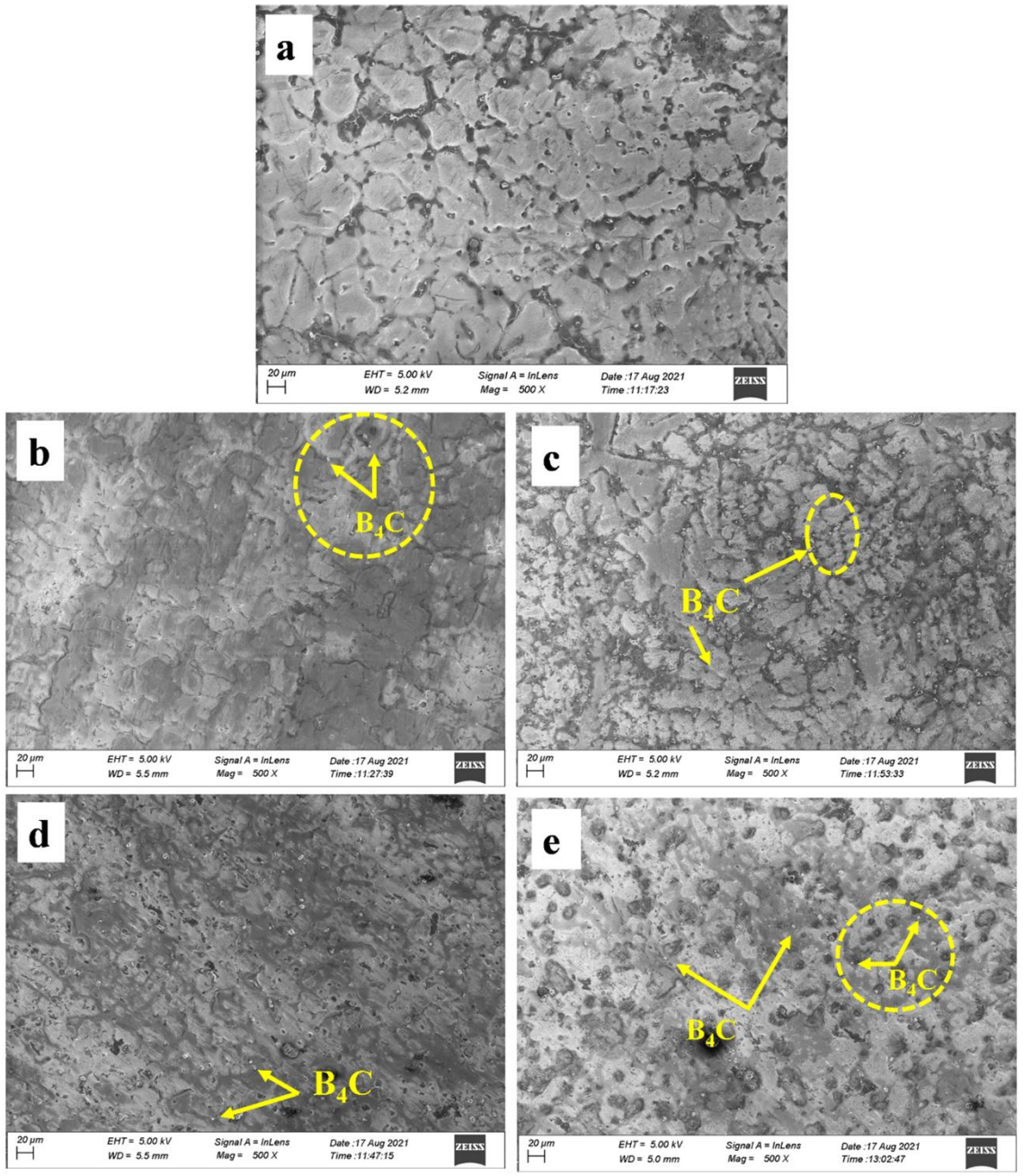

Figure 2.7: FESEM Image a) AZ31 alloy, b) AZ31-0.5B_4C c) AZ31-1.0 B_4C d) AZ31-1.5 B_4C e) AZ31-2.0 B_4C

Figure 2.7 depicts that incorporation of B_4C doesn't show any considerable defect on surface of composites indicating that reinforcements are homogeneously distributed throughout the matrix and presence of B_4C particles increases with increase in incorporated amount of B_4C. Hence, FESEM micrograph justifies the successful incorporation of B_4C particles in AZ31 matrix. The additions of B_4C particles have restricted grain growth of composites and its refinement clearly enhances with the increase in wt. % of B_4C particles. As

such, no noticeable agglomeration is identified in FESEM images which justify that homogeneous distribution of B_4C has taken place during fabrication. Composites fabricated through ultrasonic assisted stir casting method have avoided noticeable cluster formation.

2.3.3 Energy Dispersive X-ray and X-Ray Diffraction Analysis

Furthermore, typical composition analysis should be performed to confirm the presence of B_4C particles and successful fabrication of AZ31-B_4C composites. Energy dispersive X-ray analysis (EDAX) spectra are specifically used to evaluate compositional details of samples. Accordingly, EDAX spectra of AZ31 alloy and AZ31-B_4C are shown in Figure 2.8.

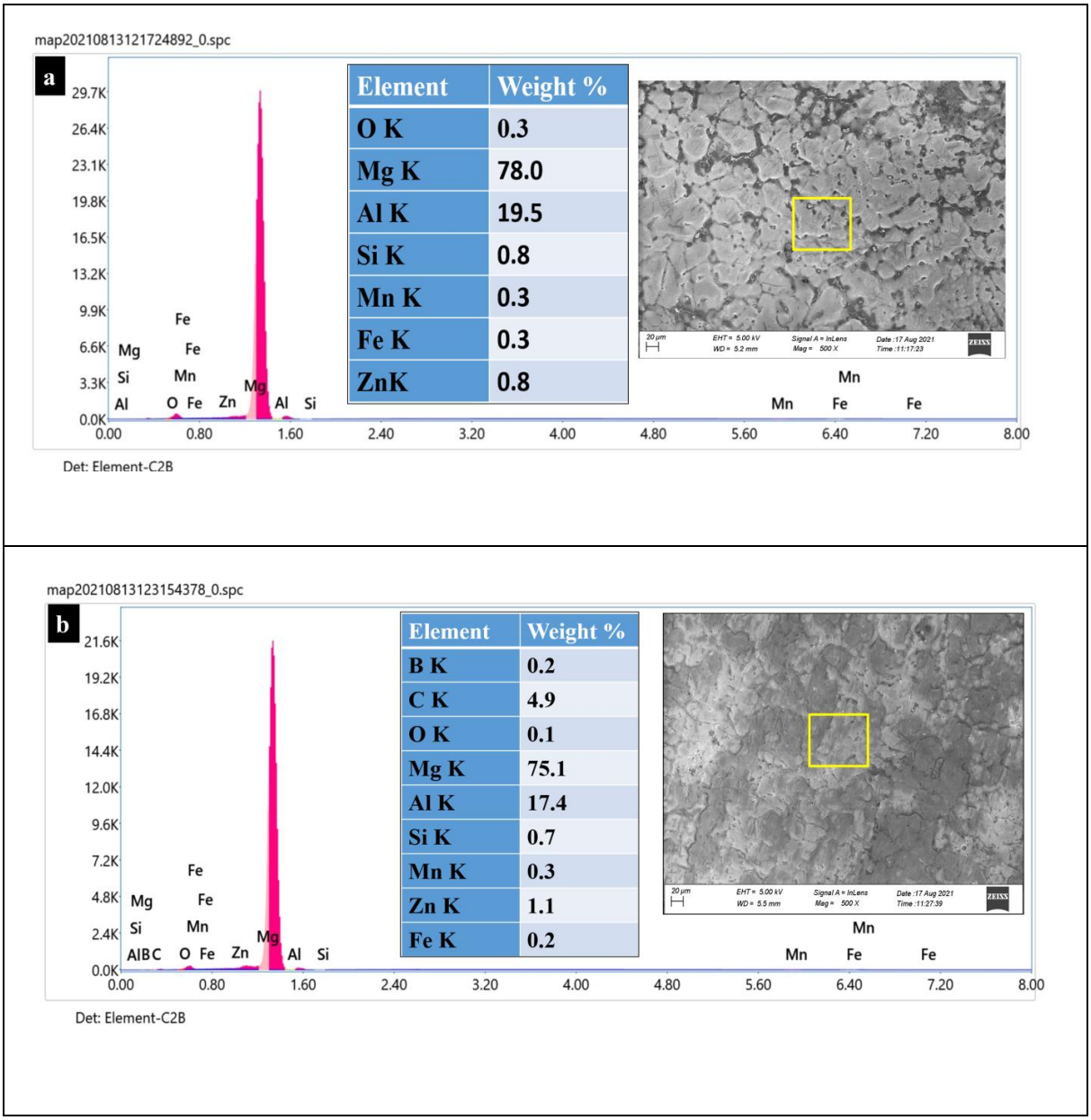

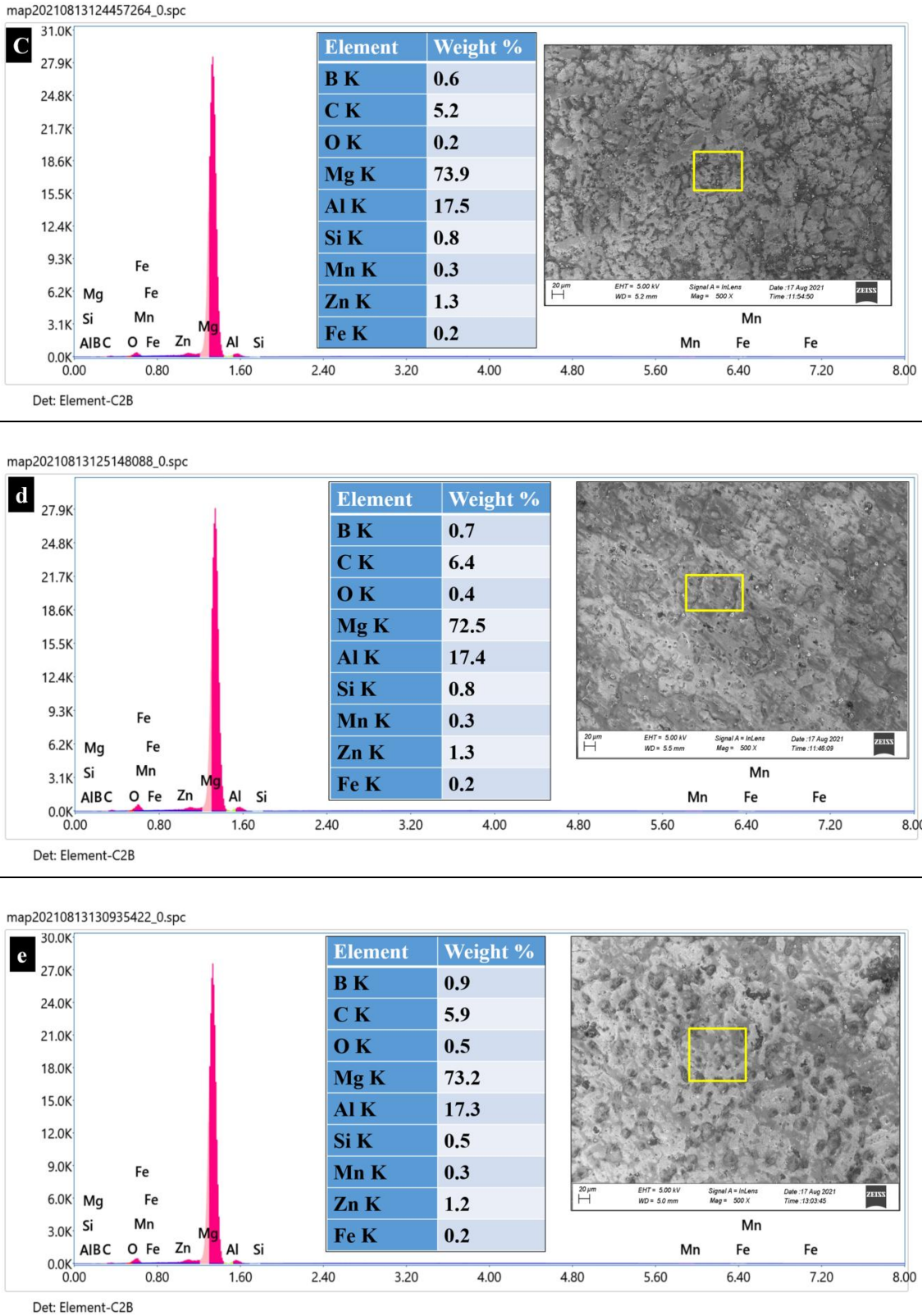

Figure 2.8: EDAX spectra a) AZ31 alloy, b) AZ31-0.5B_4C c) AZ31-1.0B_4C d) AZ31-1.5B_4C e) AZ31-2.0 B_4C

EDAX spectra of all samples are presented. EDAX spectra of composite samples depict presence of Mg, Al, Zn, O, C and B. Typically, EDAX spectra of all tested samples suggest that basic elements of AZ31 are present in all samples. EDAX spectra of AZ31-B_4C composites shows presence of Boron (B) along with all other elements of base alloy. Similarly, it is depicted that boron weight percentage gets increased with increase in wt.% of B_4C. These findings justify incorporation of B_4C in AZ31 matrix. However, accurate wt. % of all constituents do not match with EDAX spectra because of sub-micron level particle size and small amount (wt. %) of particles. Even, a very small area of sample is scanned. Furthermore, elemental mapping of composites is done to affirm the homogeneous distribution and formation of AZ31-B_4C composites. EDAX spectra and elemental mapping of B_4C particles is depicted in Figure 2.9. The wt.% of Boron and Carbon are individually depicted in EDAX spectra and mapping too.

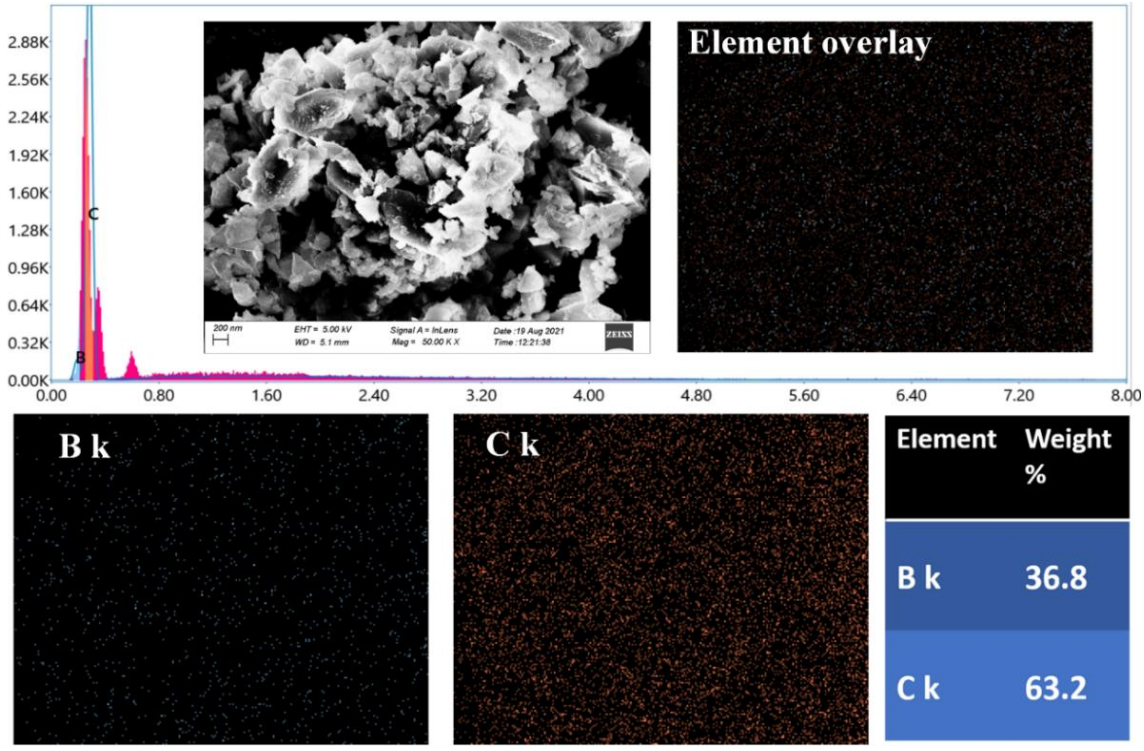

Figure 2.9: EDAX spectra and elemental mapping of boron carbide

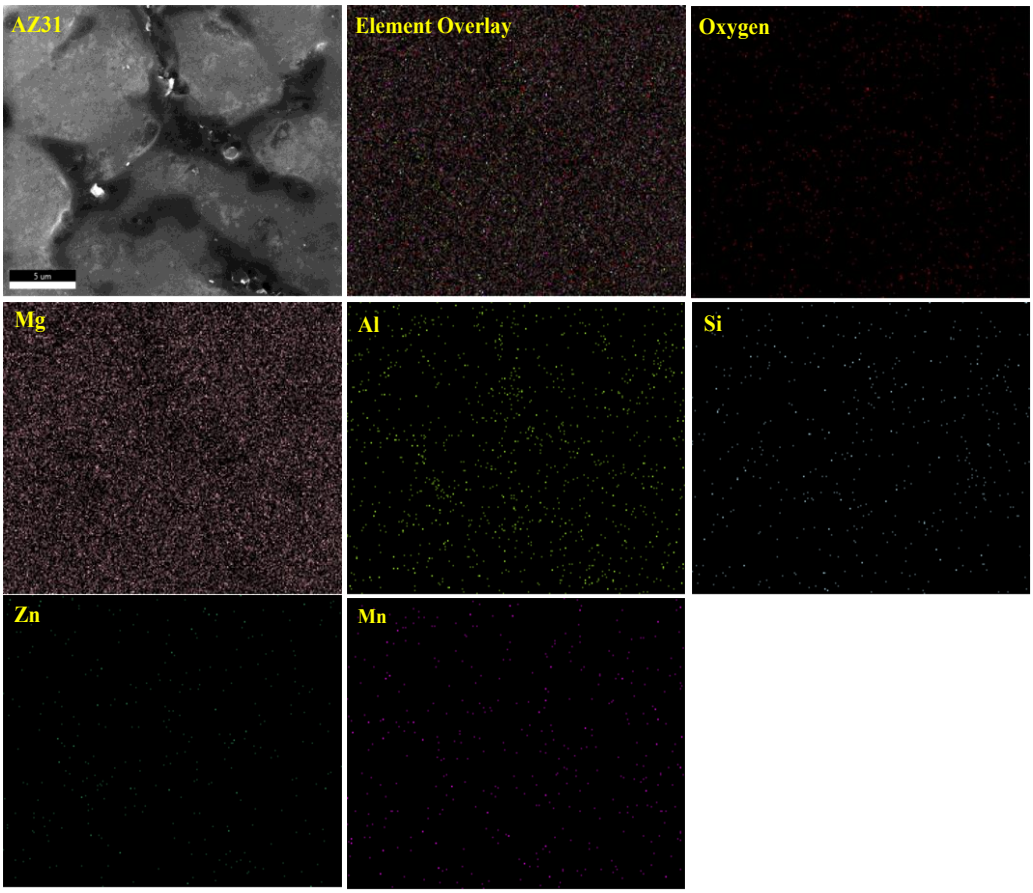

Figure 2.10: Elemental mapping of AZ31alloy

Elemental mapping of AZ31 alloy and AZ31-1.5B_4C composite are presented in Figures 2.10 and 2.11 respectively. Elemental mapping spectra clearly disclose that all related elements are well distributed in the alloy and composites. SEM micrograph, EDX spectra and lastly elemental mapping confirms successful development of composites. Thus, all composites exhibited good interfacial bonding between matrix and reinforcement phase. Similarly, results of point EDAX of AZ31-1.5B_4C is presented in Figure 2.12. Point EDAX spectra is done at few locations. Almost similar results are obtained for all selected locations. Figure 2.12 discloses that the wt.% of B and C are around 26.8% and 38.5% respectively at selected point. Thus, presence of boron carbide particles is revealed under EDAX analysis. X-ray diffractometer (machine) is shown in Figure 2.13(a). X-Ray diffraction (XRD) plots are obtained at scanning rate of 0.02º/min for 2-Theta degree values from 10º to 100º (boron carbide) and 5º to 80º (base alloy and composite). XRD analysis of boron carbide (B_4C) particle is provided in Figure 2.13(b). It represents major intensity peaks at 19.65°, 21.90°, 23.35° 31.90°, 34.75° and 37.65°. However, small scattered peaks are not considered.

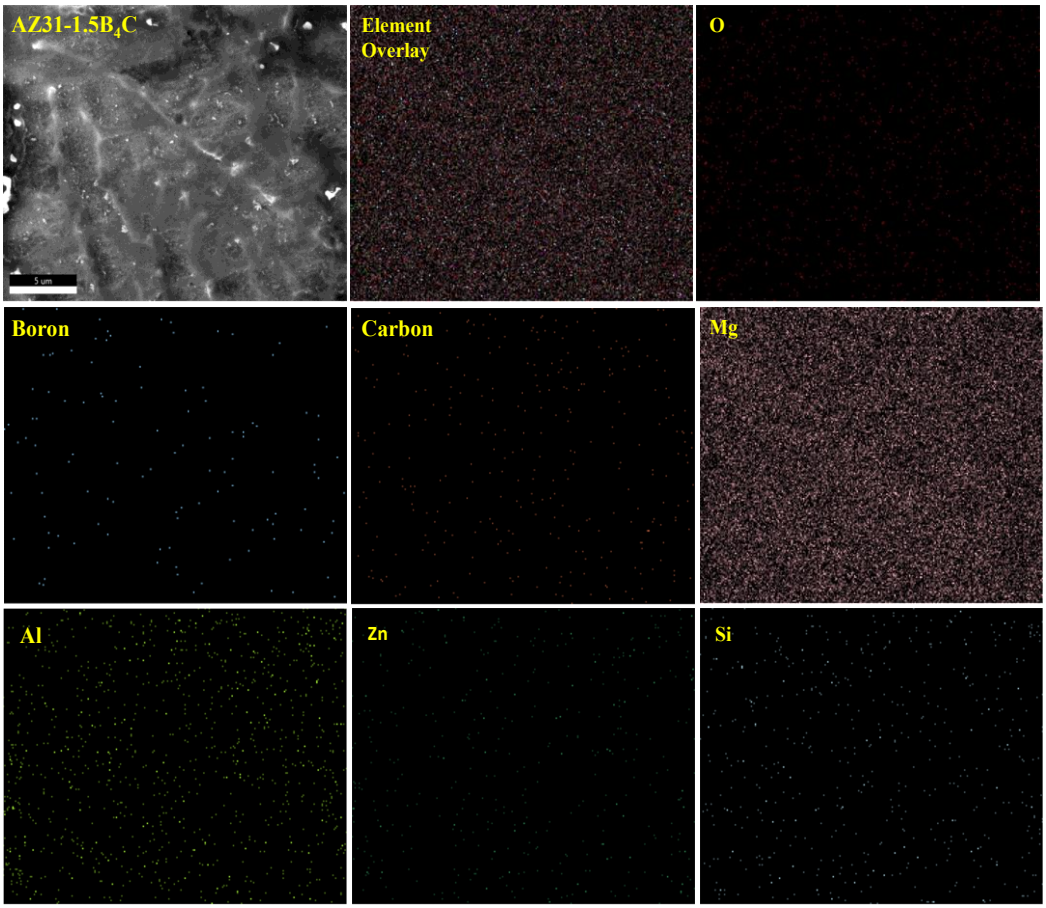

Figure 2.11: Elemental mapping of AZ31-1.5B_4C composite

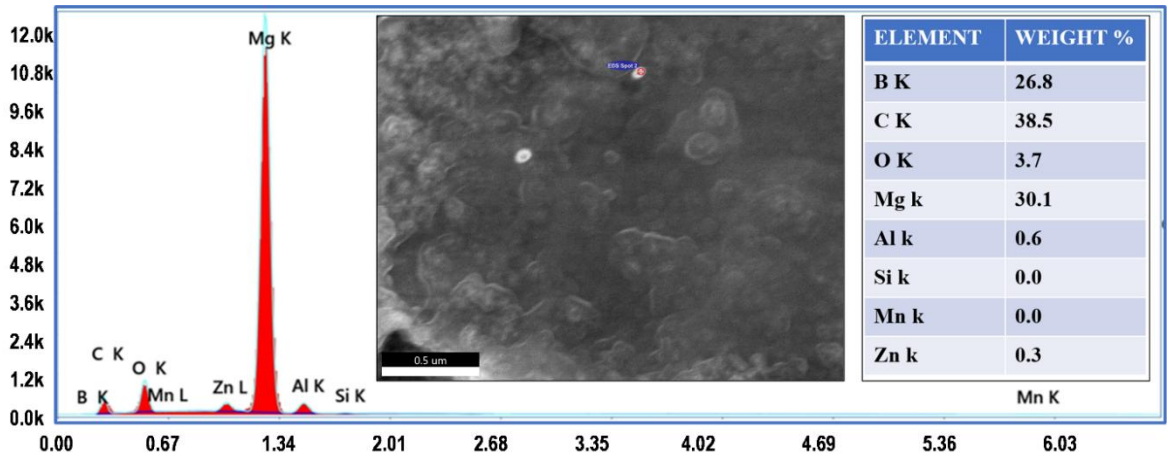

ELEMENT	WEIGHT %
B K	26.8
C K	38.5
O K	3.7
Mg k	30.1
Al k	0.6
Si k	0.0
Mn k	0.0
Zn k	0.3

Figure 2.12 Point EDAX spectra of AZ31-1.5B_4C composite

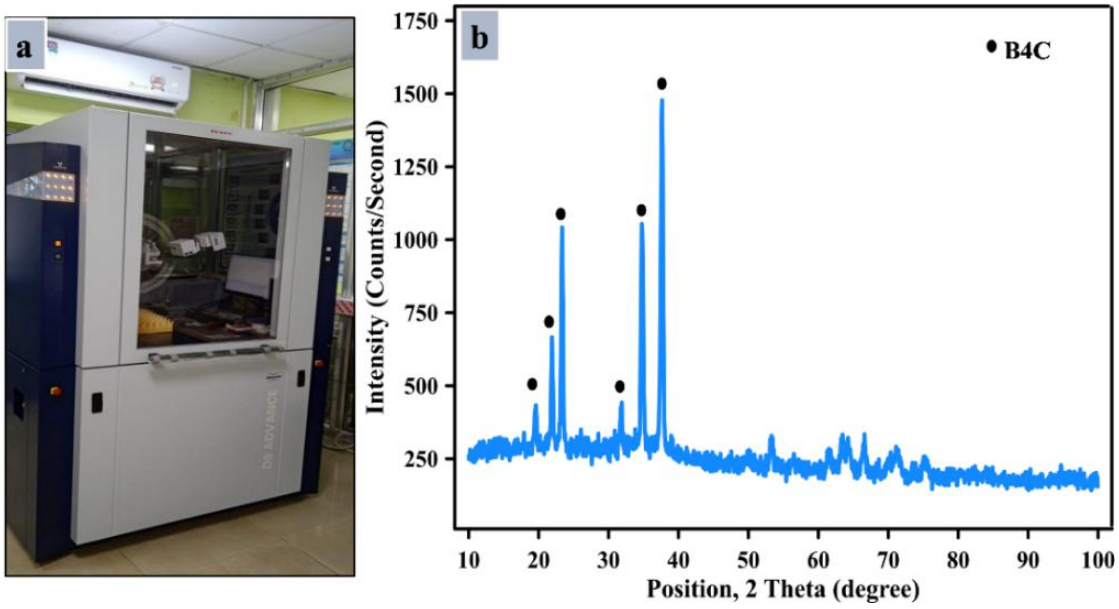

Figure 2.13: a) Pictorial view of X-ray diffractometer b) XRD spectra of boron carbide

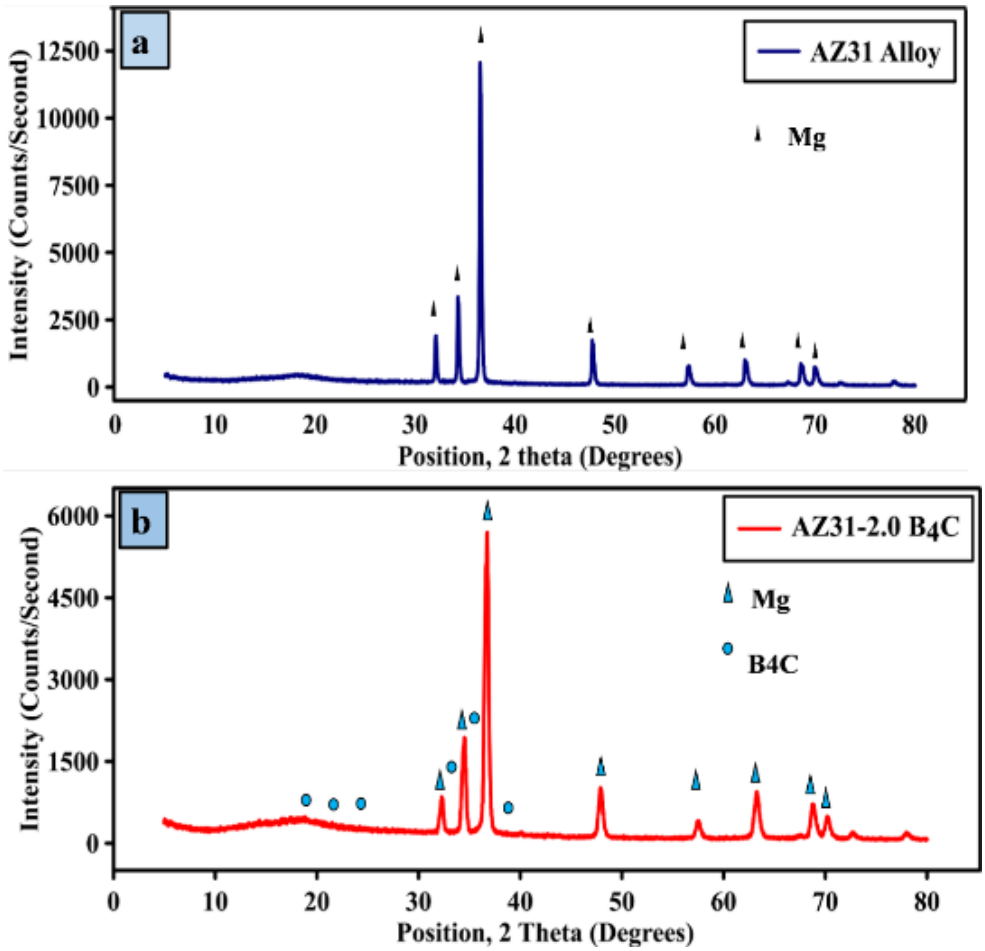

Figure 2.14: XRD spectra of a) AZ31 alloy and b) AZ31-2.0 B_4C composite

XRD spectra of AZ31 and AZ31- 2.0B_4C are presented in Figure 2.14(a, b). Peaks of Mg alloy (AZ31) is revealed at 2θ values of 32.30º, 34.53º, 36.10º, 36.75º 47.93º, 57.46º, 63.17º and 68.75º. In case of AZ31- 2.0B_4C composites, XRD pattern has not clearly represented B_4C peaks. This may be either due to incorporation of low-density submicron B_4C particles or relatively lower wt. % of boron carbide particles (<=2 wt.%) in composites [Sankaranarayanan et al., 2014; Banerjee et al., 2021b; Guleryuz et al., 2012]. However, analysis conducted through crystallographic (Search-Match version 2) 'Match-3' software, displays presence of B_4C peaks for 2 thetas at 19.60º, 21.85° 23.67º, 32.08°, 34.72º, 37.79º etc. XRD analysis is represented by JCPDS card number 1-1141(Mg alloy) and 1-1163 (composite) respectively. While 'Match 3' software analysis report represented Mg composite with entry number 96-901-3056/57/58.

2.3.4 Density and Hardness Measurement

Samples after cast usually possess defects (blow holes, subsurface cracks etc.) due to inadequate optimum processing conditions and may lack requisite compatibility. In order to justify the expected soundness of composites and base alloy, density and porosity tests are carried out initially. Fabricated cast bars are machined to produce samples of 15 x15 x10 mm^3 as shown in Figure 2.3 and are utilized for density and porosity measurement. Density of all composites is measured experimentally by Archimedes principle. Mass of each composite sample is measured through sensitive electronic balance (Afcoset ER-182A). Volume of samples comes out to be approx. 2.25 cm^3. The experimental density is then calculated utilizing mass to volume relation. The theoretical density of magnesium alloy (AZ31) and boron carbide is considered as 1.77 g/cc and 2.52 g/cc respectively. Applying the rule of mixture, theoretical density is determined Rule of mixture: $\boldsymbol{\rho}_c = \boldsymbol{\rho}_m w_m + \boldsymbol{\rho}_r w_r$. Symbols $\boldsymbol{\rho}$ and w denote density and weight fraction of phases involved, subscripts c, m and r indicate composite, matrix and reinforced phase respectively. Experimental and theoretical densities are used to calculate the porosity of fabricated samples using the following formulae:

$$\%\text{Porosity} = \frac{\text{Theoretical Density - Experimental Density}}{\text{Theoretical Density}} \text{ x } 100 \qquad (2.1)$$

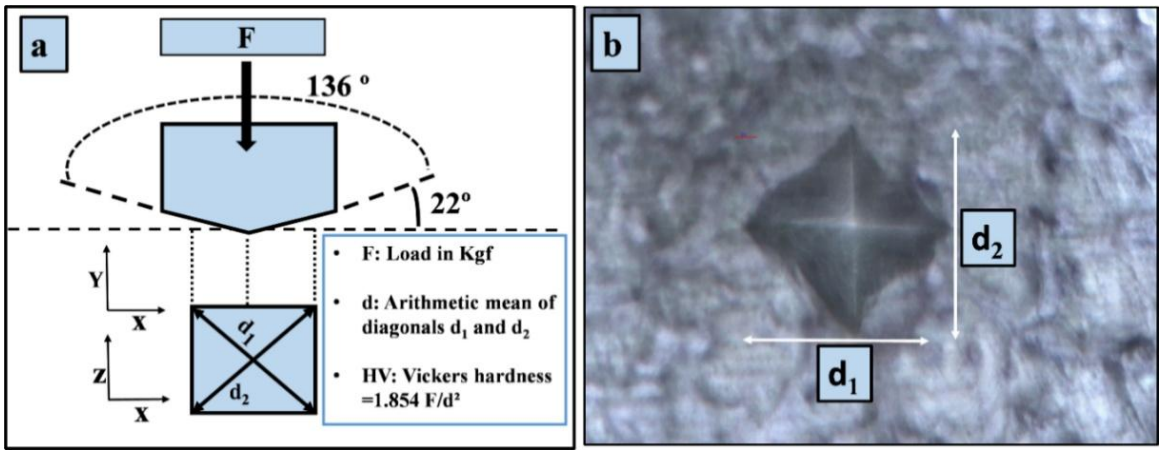

Figure 2.15: a) Schematic of hardness measurement b) Microscopic view of indentation marks

Hardness measurement is done using Vickers micro-hardness tester (UHL, Technische Mikroskopie). ASTM standard E384-99 is used to measure hardness with a diamond indenter using 50 gm load for fixed dwell time of 10 s. The hardness tester is well equipped with a digital camera and dedicated computer. The micro hardness indentation is taken at five different locations on the samples. The indentation marks are carefully analysed to estimate micro hardness of composites (AZ31-B_4C) and base alloy. Microhardness values are computed from indentation marks and microscopic view of indentation mark is shown in Figure 2.15. Table 2.4 lists the values of density, porosity and microhardness for AZ31 alloy and composites. The variation of density and microhardness are shown with the help of bar chart in Figure 2.16.

Table 2.4: Density, Porosity and Microhardness values

Samples	**Material**	**Density (g/cc)**	**Porosity (%)**	**Microhardness ($HV_{0.5}$)**
1	AZ31 Alloy	1.7483	1.129	58.3±3
2	AZ31-0.5 B_4C	1.7558	1.183	63.0±5
3	AZ31-1.0 B_4C	1.7586	1.238	69.6±3
4	AZ31-1.5 B_4C	1.7602	1.291	79.4±5
5	AZ31-2.0 B_4C	1.7664	1.411	90.3±6

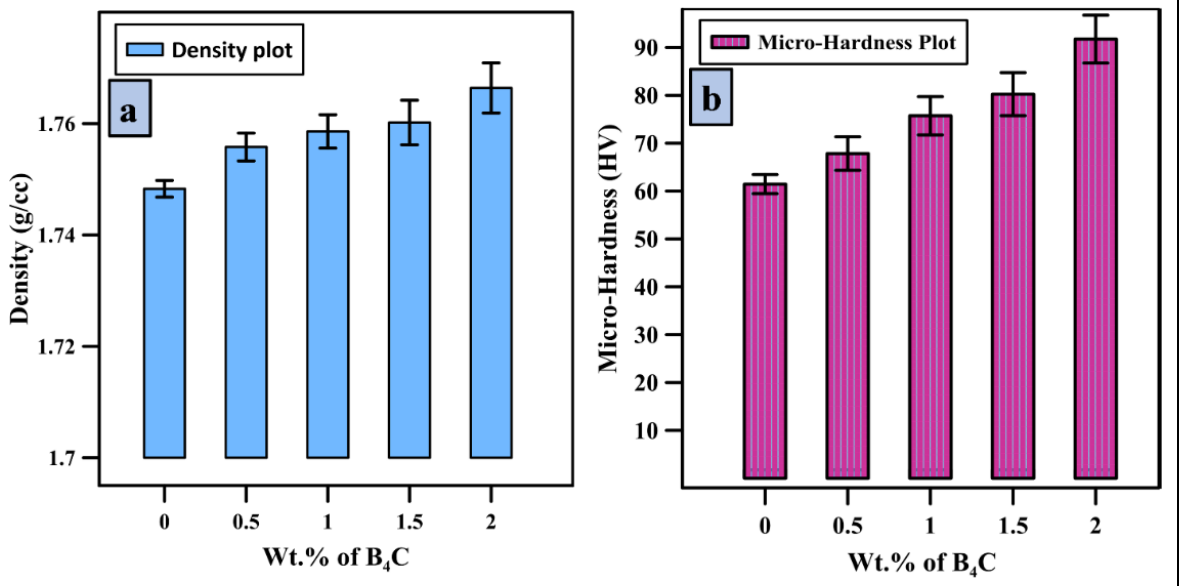

Figure 2.16: a) Density plot, b) Micro-hardness plot

Density plot depicted in Figure 2.16 (a) shows increasing trend with increase in wt. % of B_4C particles. Addition of B_4C particles in magnesium alloy has noticeably increased the density of composites. Similar results were already reported in literature [Aydin et al., 2018; Sankaranarayanan et al., 2014; Aatthisugan et al., 2017]. The porosity values are evaluated as 1.129%, 1.183%, 1.238%, 1.291% and 1.411% for AZ31, AZ31-0.5B_4C, AZ31-1.0B_4C, AZ31-1.5B_4C, and AZ31-2B_4C respectively as mentioned in Table 2.4. Figure 2.16 (b) discloses that composite possesses significantly higher hardness than unreinforced alloy. It is also found that microhardness gets improved with increase in wt.% of B_4C particles. The improvement in hardness is due to incorporation of submicron sized B_4C particles and its uniform dispersion in AZ31 alloy. Ceramic based B_4C particles are contributing mainly in strengthening the bond between base alloy and reinforcement. Incorporation of B_4C particles also hinders the dislocation movement which in turn increases the hardness of composites Similar results are also reported by other researchers [Sankaranarayanan et al., 2014, Nguyen et al., 2015; Majzoobi and Rahmani, 2020; Aydin et al., 2018]. Atthisugan et al. (2017) have investigated the effect of addition of micron sized B_4C in AZ91D and observed enhancement in density values (0.59%-1.18%) for composites. It was reported that B_4C particles blocks the dislocation fraction and thereby increases the mechanical properties of Mg matrix. Similar trend for hardness and density plot is also suggested in the study of Banerjee et al. (2019a) while incorporating WC reinforcement in AZ31 matrix.

2.4 Summary

This chapter exclusively provided the detailed insight about the preparation of AZ31-B_4C composite and its mechanical and microstructural characterization. AZ31 alloy exhibits coarse grain structure compared to the composite variants. Thus, composite exhibits superior mechanical properties with the reinforcement of B_4C particles in AZ31 alloy. The microstructure depicts good interfacial bonding between AZ31 alloy and B_4C particles. No significant cluster formation was observed in SEM images of composites due to small wt.% of B_4C in AZ31 alloy. The microhardness values are measured for base alloy and composites and a typical linear trend with increase in wt.% of B_4C is observed. Density of composite specimens increase as expected with the increase in wt.% of B_4C. Minimal porosity is observed with or without addition of the respective wt.% of B_4C in AZ31 alloy during fabrication.

Chapter 3

Dry Sliding Tribological Behaviour

3.1 Introduction

The present chapter deals with the tribological behaviour of AZ31-B_4C composites synthesized through ultrasonic vibration associated stir casting route. B_4C particles with varying weight percentage (0.5-2.0 wt.%) are reinforced in magnesium alloy to produce the composites. The present research focuses on evaluating tribological behaviour of Mg-B_4C composites at dry conditions at room temperature. The wear and friction characteristics are experimentally studied for AZ31 alloy and B_4C reinforced composites. Tribological study is vital in most mechanical engineering applications such as in bearings, engine parts and gears etc. Wear is a dominant problem which disturb surface finish or fine tolerances and cause complete failure of industrial components. Hence, wear and friction characteristics are important domain to be focused, as it directly affects the durability of machine component.

In the previous chapter, utilization of optical microscope (OM), field scanning electron microscope (FESEM) and energy dispersive X-ray analysis (EDAX) is already discussed in order to thoroughly characterize fabricated AZ31 alloy and AZ31-B_4C composites. Initial characterization illustrates the presence of boron carbide (B_4C) and its effect on the grain refinement of composites. Vicker's micro hardness test is already conducted to determine the hardness of all materials. It is found that, AZ31-B_4C composites exhibit better hardness compared to AZ31 magnesium alloy. Micro-hardness improvement justifies uniform dispersion of B_4C particles in magnesium alloy. Extensive review of available literature reveals that tribological investigation on AZ31-B_4C composite using ultrasonic treatment assisted casting is scanty [Banerjee et al., 2021c]. The present research focuses on developing Mg composites reinforced with sub-micron B_4C particulates using ultrasonic vibration associated stir casting process and evaluating tribological behavior of AZ31-B_4C composites at dry sliding conditions. The wear and friction characteristics are experimentally studied for AZ31 alloy and B_4C reinforced composites. Attempt is also made to identify the dominant wear mechanism of AZ31-B_4C composites and AZ31 alloy tested at different loading and sliding conditions. Accordingly, characterisation of worn-out surface is done by utilizing SEM micrograph and EDAX pattern.

3.2 Experimental Details

Pin-on disc tribometer (DUCOM, India) is utilised to carry out tribological tests following ASTM G-99-05 at room temperature. Pictorial view of the tribometer is shown in Figure 3.1. Pin specimen of diameter Φ6 mm and length 30 mm is mounted perpendicular to counter face steel disk (EN-8, 58-62 HRC). Tribo-tests are conducted at four different loads from (10N, 20N, 30N and 40N) and speeds (0.1 m/s, 0.2 m/s, 0.3 m/s and 0.4 m/s). These ranges are chosen based on capacity of tribometer and geometry of specimen [Banerjee et al., 2021c; Srinivasan et al., 2012]. The tribo tests are done at 40 mm track diameter and sliding time of 10 min duration.

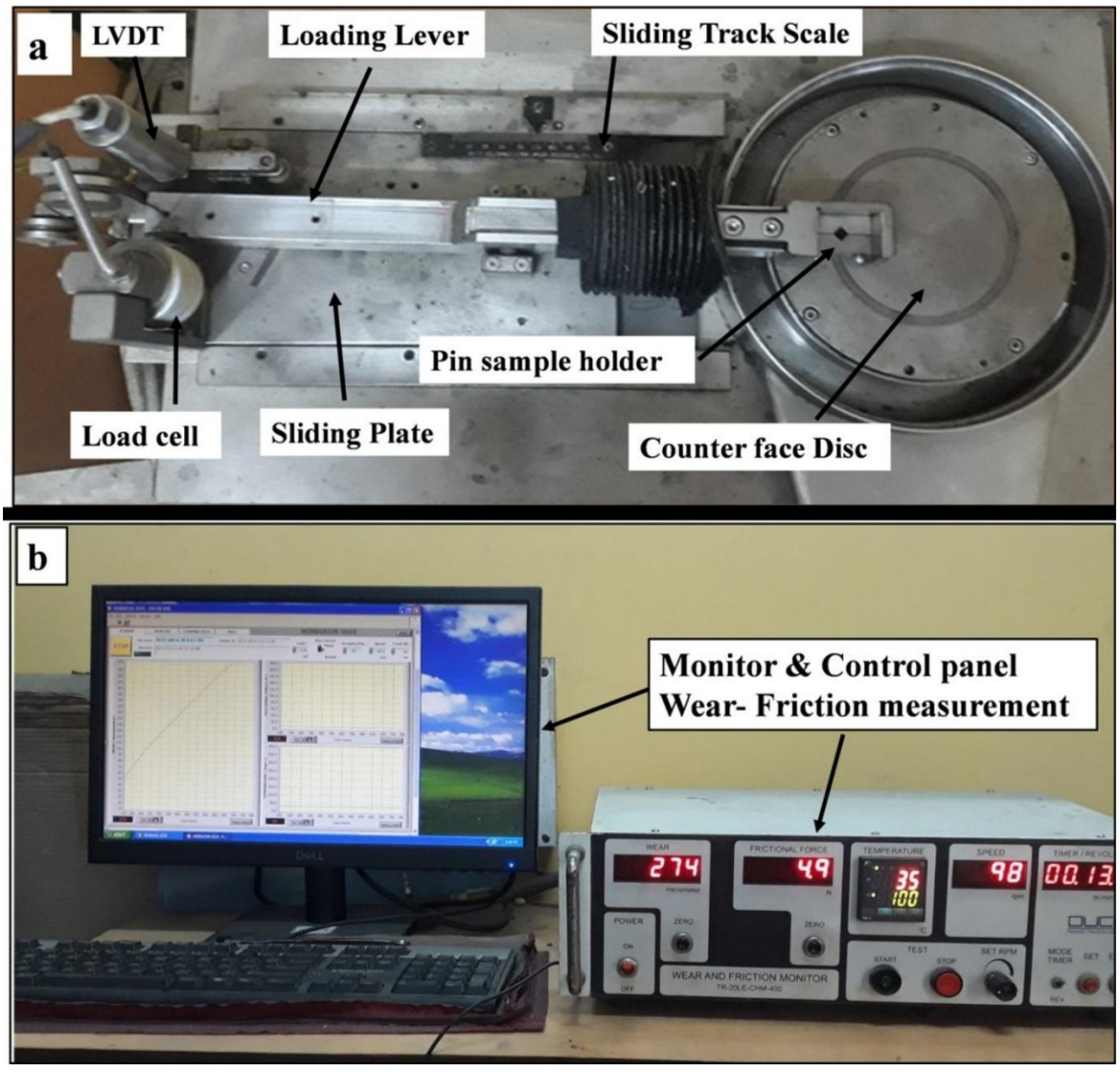

Figure 3.1: Pictorial view of a) pin-on-disc tribo-tester b) monitor and control panel for wear-friction measurement

The pin-on-disk tribo-tester is attached to dedicated computer and electronic measurement system for controlling duration of all experiments. The electronic control panel cum measurement system displays wear and friction parameters which are used to determine wear rate and coefficient of friction. The pin-on disk tribo-tester is first mounted with pin specimen in a pin post attached to the lever parallel to the horizontal plane of pin-on disk tribo-tester and required weights are mounted on loading pan. The beam type load cell acts as force sensor for measuring frictional force. The capacity of the load cell is 1000 kgf and the reading of frictional force is displayed directly. After the test is over, mass loss is measured with reference to initial and final weight in a dedicated digital weight balance machine with high accuracy. The wear rate is determined based on obtained mass loss and sliding distance. The worn surface analysis is done using SEM images and EDAX spectra to find out the dominated wear morphology at varying load and speed.

3.3 Result and Discussion

3.3.1 Wear Behaviour

In this study, wear behaviour of developed materials is examined under varying loads (10N - 40N) and varying speeds (0.1m/s - 0.4m/s). Typically, base alloy and composites behave differently at same operating conditions. Contribution of load on typical wear behaviour of AZ31 and AZ31-B_4C composites are presented in Figure 3.2(a). Figure 3.2(a) discloses that AZ31-B_4C composites possess better wear performance than AZ31 alloy. For AZ31- B_4C composites, wear rate increases linearly with increase in applied load. However, slope of wear rate of AZ31 is quite steeper compared to all composites. Additionally, slope of wear rate of composites gets milder with increase in wt.% of B_4C particles. AZ31-B_4C composites having higher wt.% of B_4C particles exhibits lower wear rate for experimental range at applied load 10N-40 N. Thus, Typical values of micro hardness can be directly correlated with wear rate. As it is already mentioned that microhardness values of AZ31-B_4C composites enhanced linearly with increase in wt. % of B_4C. This result is related to the findings of Archard's wear law [Archard, 1953; 1957].

Typically, fortification of hard B_4C particulates in softer AZ31 matrix helps to enhance load bearing capacity in AZ31-B_4C composites which in turn trap the dislocations and amplify the work hardening ability of fabricated composites. This phenomenon of ceramic based hard particles helps to possess positive wear behaviour. At lower load range of 10-20 N, contact pressure between sample surface and counter disc is less compared to that of higher

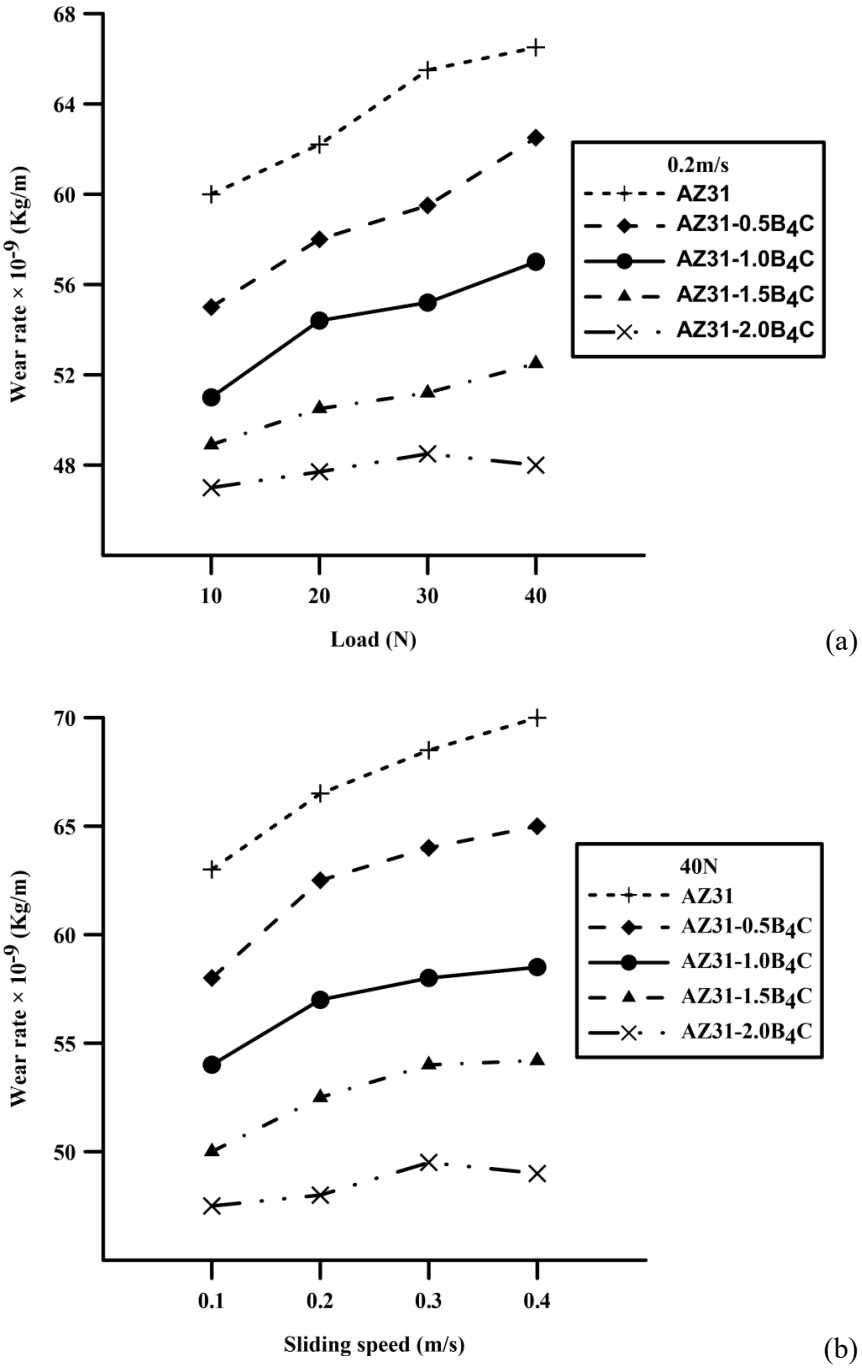

Figure 3.2: Variation of wear rate for AZ31 alloy and composites a) load and b) sliding speed

loads range of 30N-40N. Additionally, friction heating helps to generate oxidized wear debris which fill the contact surface and generate a positive tribo-layer between sample surface and counter face. As a result, wear rate gets decreased. However, with enhancement in load, contact pressure enhances and high temperature generates in between contact interfaces of pin sample and counter disc. High temperature causes plastic deformation and thermal softening, which

results in a high wear rate [Srinivasan et al., 2012; García-Rodríguez et al., 2017; Banerjee et al., 2019c; Guleryuz et al., 2013]. In case of AZ31 alloy, this thermal softening produces severe wear. However, AZ31-B_4C composites can resist hard penetration of counter face asperities and thermal effect due to presence of ceramic particles. High surface area of B_4C particles and strong interfacial bonding between Mg matrix and ceramic reinforcement helps to counter the thermal effect and penetration even at higher load. Accordingly, AZ31-B_4C composites yield better wear resistance compared to AZ31 alloy. Moreover, the load bearing capacity enhances and thermal effect can also be delayed with increase in wt. % of B_4C. As a result, AZ31 - $2B_4C$ exhibits best wear resistance among tested materials within experimental range.

It is well established in current literature that sliding speed is an important parameter to control wear behaviour of any material. Hence, judicious investigation on wear behaviour w.r.to sliding speed is highly solicited. Accordingly, typical effects of sliding speeds (0.1m/s-0.4m/s) at 20N load on wear behaviour of AZ31 and AZ31-B_4C composites are presented in Figure 3.2(b). It is evident that AZ31 shows highest wear rate among all samples and wear rate reduces continuously with enhancement in wt.% of B_4C particles. Figure 3.2 (b) also exhibits that wear rates of AZ31 alloy and AZ31-B_4C composites enhance continuously with increase in sliding speed. For base alloy, slope of increment of wear rate is steeper and that slope decreases continuously with increase in wt.% of B_4C particles. It is observed in Figure 3.2 (b) that AZ31-$2B_4C$ possesses moderate slope. AZ31-$2B_4C$ composite possesses highest wear resistance among all tested samples. Usually, duration of asperity contact between sample surface and counter-face is higher at low-speed range (0.1m/s-0.2m/s). At higher speed range (0.3m/s-0.4m/s), duration for asperity-to-asperity contact is less and oxide layer formation becomes easier due to frictional heating. These oxide layers protect the sample surface from counter-face asperities. Consequently, wear plots of all samples exhibit steeper increasing trend at low speed. Similar trend is also observed in literature [Banerjee et al., 2019a; Banerjee et al., 2019b]. The interfacial bonding of AZ31 alloy is weaker to withstand ploughing of counter-face asperities. With incorporation of B_4C particles, load carrying capacity increases and effective contact area between softer matrix and counter-face decreases.

Even protection of oxidative layer is also present. Combined effect of load carrying ability, protection of oxidative layer and lesser contact area help to achieve better wear resistance for composites compared to base alloy. Consequently, moderate slope of wear rate with respect to sliding speed is observed for composites. Similar trend is also reported in literature [Banerjee et al., 2019a; Nie et al., 2011a; Nie et al., 2011b; Aydin et al., 2015].

3.3.2 Friction Behaviour

Effect of process parameters (load and sliding speed) on coefficient of friction (COF) of AZ31 and composites are depicted in Figure 3.3. It is obvious from Figure 3.3(a) that all

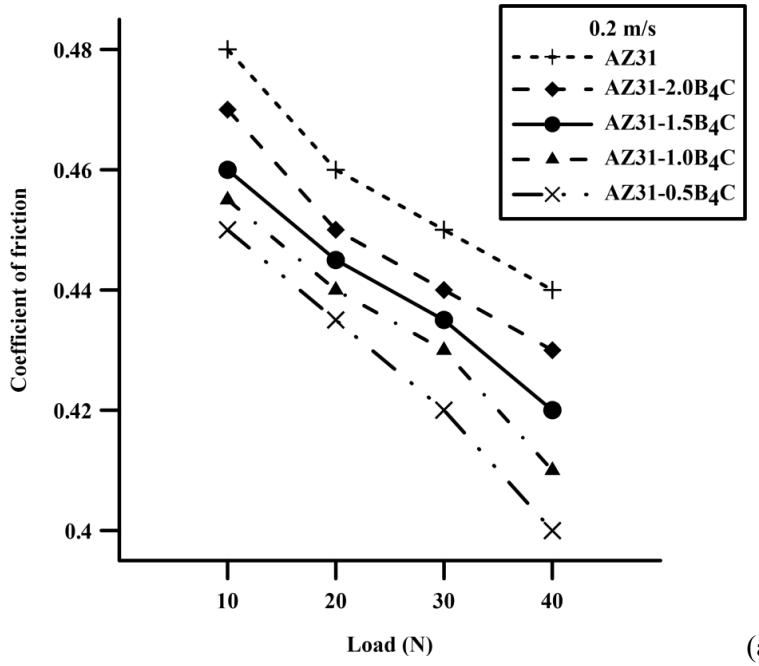

(a)

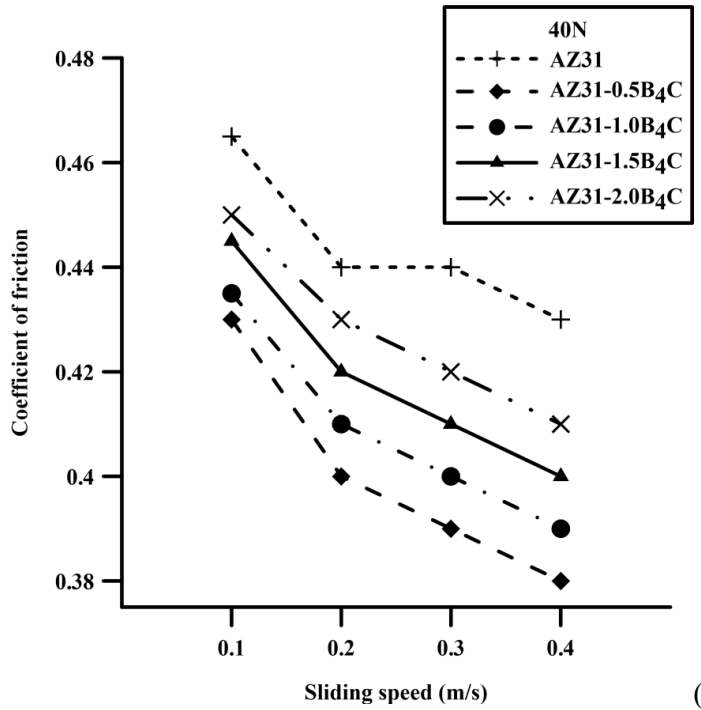

(b)

Figure 3.3: Variation of coefficient of friction for AZ31 alloy and composites a) load and b) sliding speed

developed AZ31-B_4C composites yields far better friction behavior than AZ31 alloy. It is found that COF values increased continuously with increase in wt.% of B_4C among composites. Similar findings are also noticed in literature by incorporating WC, Al_2O_3 and BN particulates in Mg matrix [Banerjee et al., 2019b, Kaviti et al., 2018, Nguyen et al., 2015]. Figure 3.3(b) depicts effect of sliding speed on COF of AZ31 and AZ31-B_4C composites. It is evident from Figure 3.3(a) and Figure 3.3(b) that COF decreased reasonably with continuous increase in sliding speed and load. Typically, flash temperature comes into play when either sliding speed or load is enhanced. Flash temperature is produced due to frictional heating between sliding interfaces. As a result, typical oxide tribo layer forms in between in between sample surface and counter-face resulting generation of lubricating effect. However, Overheating may occur with further enhancement in load and speed value. Accordingly, sample surface becomes weak resulting easy shearing of sample surface. Even sign of plastic flow in whole contact surface becomes prominent because of melting and thermal softening [Shanti et al., 2011, Lim et al., 2003; Banerjee et al. 2019a, Banerjee et al. 2019b]. Consequently, COF possesses detrimental effect with enhancement of speed and load for AZ31-B_4C composites. Similar observations are reported in literature [Banerjee et al., 2019b; Lim et al., 2003; Kaviti et al., 2019; Prakash et al., 2016, Arora et al., 2013; Selvam et al., 2014; Moheimani et al., 2022]. Effect of sliding distance on COF is depicted in Figure 3.4 for a load of 40 N and sliding speed of 0.4 m/s. AZ31 alloy shows highest COF value compared to all composites. However, moderate change in COF with respect to sliding distance for all samples.

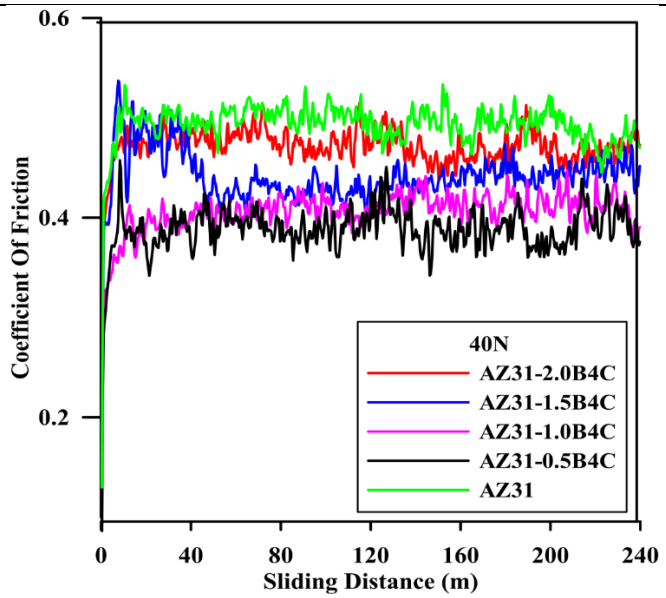

Figure 3.4: Variation of coefficient of friction with respect to sliding distance for base alloy and composites

3.3.3 Wear Mechanism

To justify the wear characteristics of AZ31 alloy and AZ31-B_4C composites, intensive studies of wear morphology are essential. It was observed that wear rate is getting affected due to variation in wt.% of B_4C, load and speed. Thus, samples surfaces are needed to

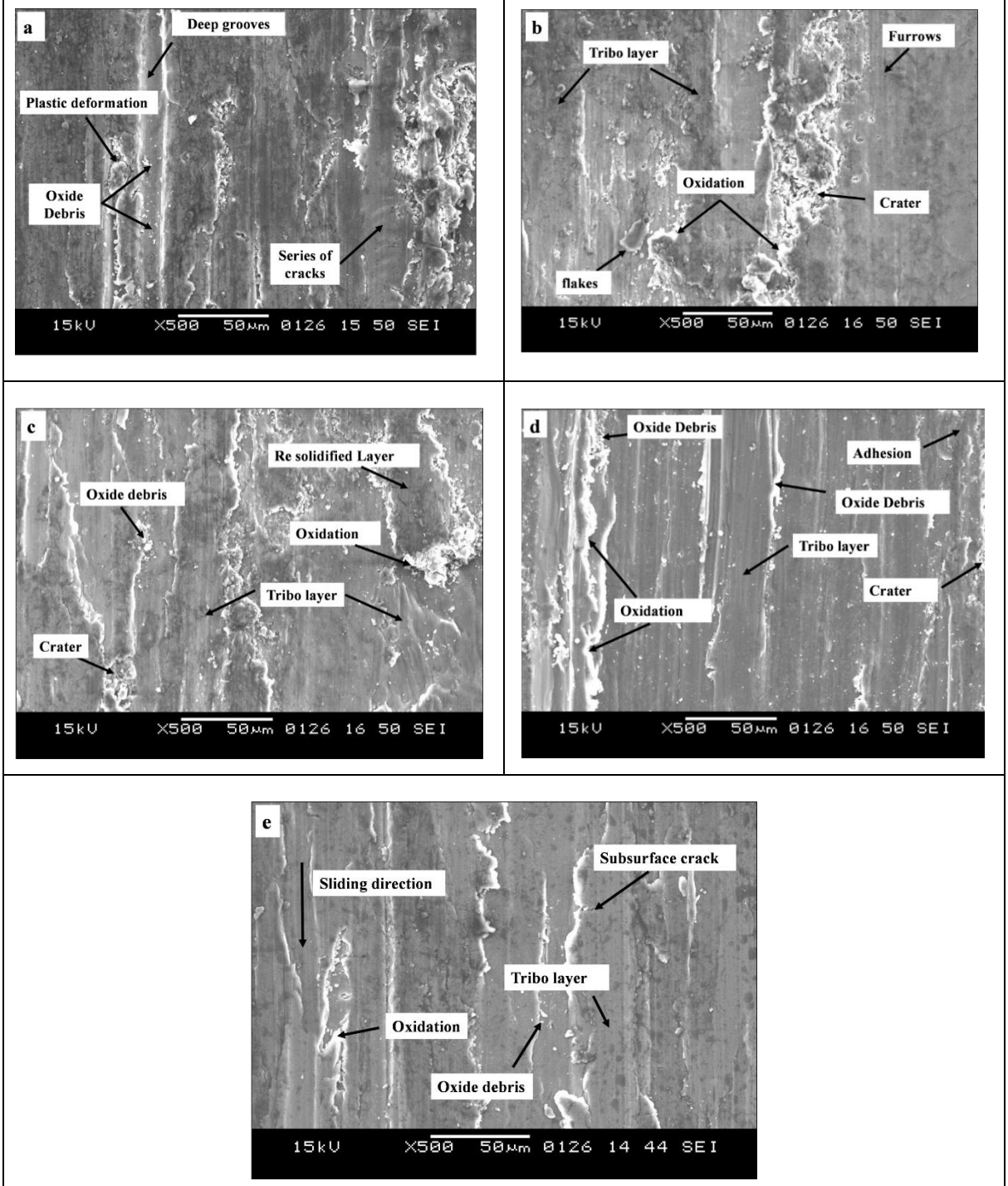

Figure 3.5: Worn surface morphology a) AZ31 b) AZ31-0.5 B_4C c) AZ31-1.0 B_4C d) AZ31-1.5 B_4C e) AZ31-2.0 B_4C at 40 N and 0.4 m/s

be examined under SEM and EDAX to investigate possible wear morphology at different experimental conditions. The SEM images of worn surfaces of AZ31 and AZ31-B_4C composites tested at 40N and 0.4m/s sliding speed are shown in Figure 3.5(a-e). Figure 3.5 helps to understand the role of wt.% of B_4C particles on wear mechanisms. It is quite evident from figure 3.5 that different types and degrees of wear have happened in AZ31 and AZ31-B_4C composites. Figure 3.5(a) depicts the SEM micrograph of worn surface of AZ31 alloy. Abrasive groove parallel to sliding direction and sign of ploughing is visible in worn surface. Figure 3.5(b) depicts the SEM micrograph of worn surface of AZ31-0.5B4C composite.

Comparatively smoother surface having series of parallel grooves are visible in Figure 3.5(b). Sign of oxidation and re-solidified layers are also distinct in the worn surface of AZ31-0.5B_4C composite. Additionally, some sheet like delaminated flakes, sign of craters is also visible. Hence, abrasion, oxidation and delamination are main wear mechanisms. Figure 3.5 (b-e) illustrate that worn surface is getting smoother with continuous enhancement in wt.% of B_4C particles. Deep grooves and sign of delamination are gently replaced by sign of oxidation, plastic deformation and re-solidified layers which clearly yield that abrasion and delamination are transformed into adhesion and oxidation. Typically, this trend is mainly because of enhancement in grain boundary density and ductility of developed composites [Banerjee et al., 2019; Nguyen et al., 2015]. It is well known that ductile materials generally adhere to the surface plastically instead of deforming completely. On the other hand, high interfacial energy is usually generated due to high grain boundary which makes the material adhesive in nature [Banerjee et al., 2019a,b].

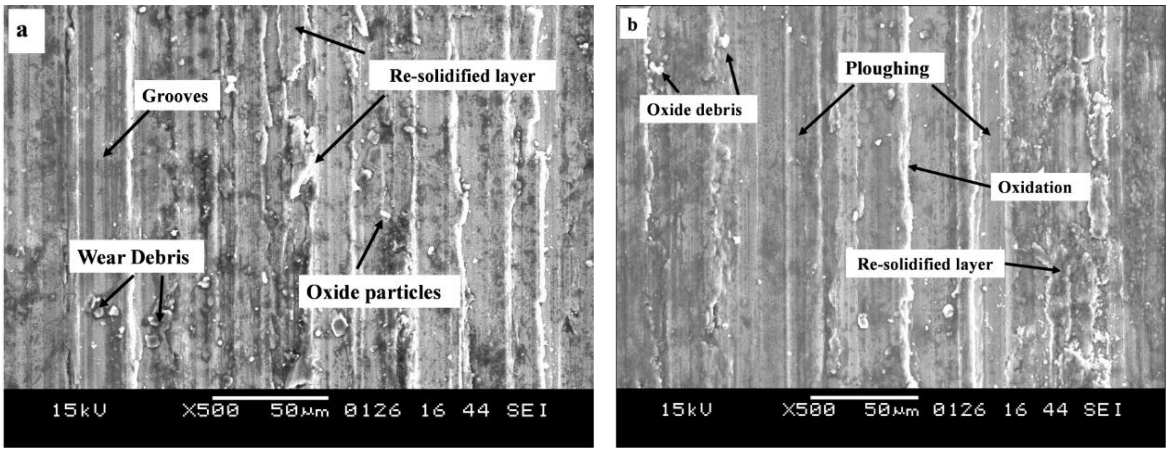

Figure 3.6: Worn surface of AZ31-2B_4C composite tested at (a) 20N load and 0.4 m/s sliding speed (b) 40N load and 0.2 m/s sliding speed

In Figures 3.5(b-e), sign of oxidized debris is prominent and amount of fractured oxidized debris has increased with increase in wt.% of B_4C. Increase in amount of oxidized debris suggests that oxidized tribo-layer has generated in among sample surface and counter-face. This tribo-layer protects the sample surface and results in lower wear rate for composites than base matrix. Figure 3.6(a) shows worn surface of AZ31-2B_4C composite analysed at 20N load and 0.4m/s sliding speed. Figure depicts the contribution of load on worn surface. It is observed that the sample surface is majorly filled with parallel abrasive grooves. Oxide debris is present on sample surface. Micro-cracks and cracks are also visible in SEM micrographs.

Hence, it can be said that abrasion and oxidation are main wear mechanisms for this experimental condition. Figure 3.6(b) shows the worn surface of AZ31-2B_4C composite tested at 40N load and 0.2m/s sliding speed. It depicts the role of sliding speed on worn surface. Abrasive grooves, sign of ploughing and oxide debris are mainly present in the sample surface. Welded debris are also present in some sections. Hence, it can be concluded that abrasion and oxidation are main wear mechanisms at low-speed conditions. Figure 3.7 represents EDAX spectra of worn surfaces of AZ31 and AZ31-B_4C composites analyzed at 40 N load and 0.4 m/s sliding speed. EDAX spectra of worn surfaces of AZ31-2B_4C tested at 20 N load and 0.4 m/s sliding and 40 N load and 0.2 m/s sling speed are shown in Figure 3.8(a) and 3.8(b) respectively. Corresponding SEM micrographs and table containing wt.% of elements are also incorporated in the EDAX spectra.

In each EDAX spectra, presence of noticeable oxygen peaks is distinct. Presence of noticeable oxygen peaks confirms that oxidation has taken considerable role in controlling wear behavior. Typically, presence of oxygen yields formation of oxide layer in between sample and counter face. These layers protect the sample surface from penetration of counter face asperity. Intensity of that oxide layer helps to understand about the level of protection. However, it is also observed in Figure 3.8(a) and 3.8(b) that percentage of oxygen is increasing continuously with increase in wt.% of B4C and maximum amount of oxygen is present for AZ31-2B_4C composite Careful observation of EDAX spectra also reveals significant presence of Fe and its amount enhances with increase in wt.% of B_4C and it again depends upon operating parameters (such as speed and load). Presence of Fe yields that mechanically mixed layer (MML) is formed and this MML helps to protect the sample surface from getting worn out [Prakash et al., 2016; Arora et al., 2013]. Accordingly, AZ31-2B_4C possesses least wear rate as the oxide layer and MML protect the sample surface. This result is in line with the observations reported in

literature [Banerjee et al., 2019a, Selvam et al., 2014; Suh, 1977; Sharma et al., 2000; Lim et al., 2005].

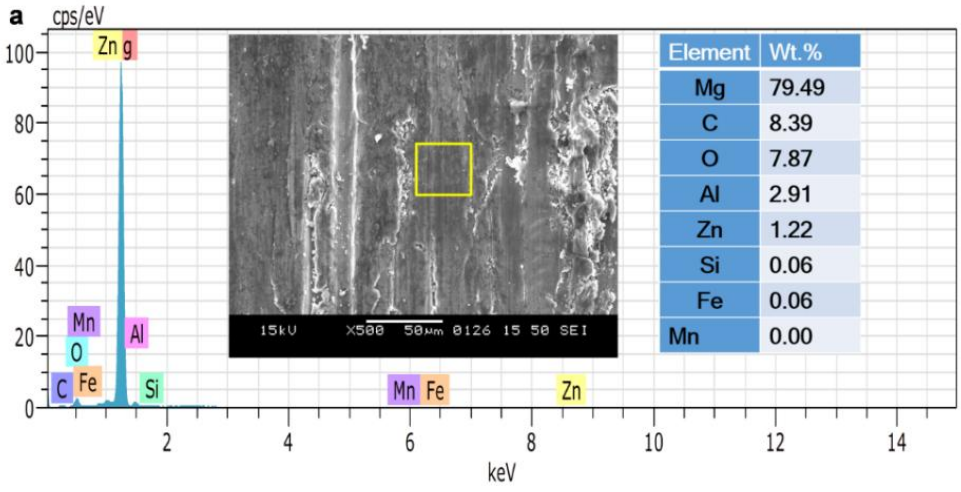

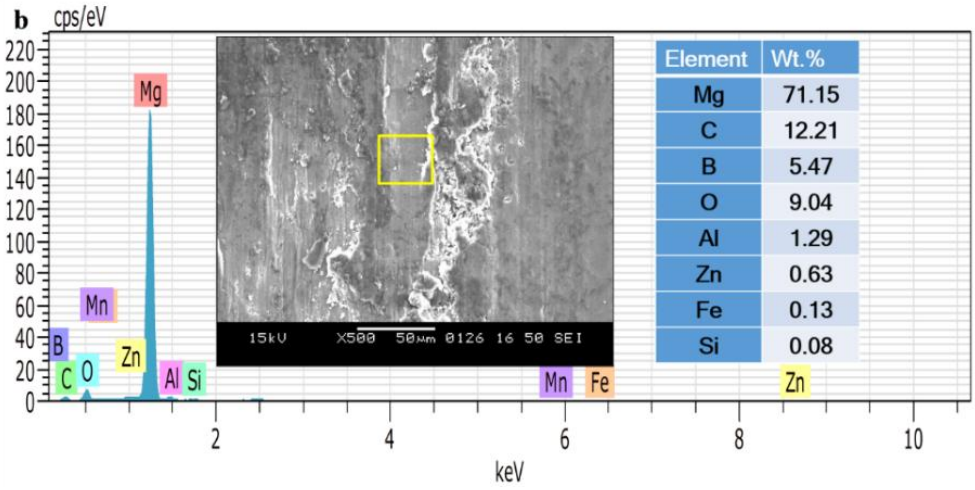

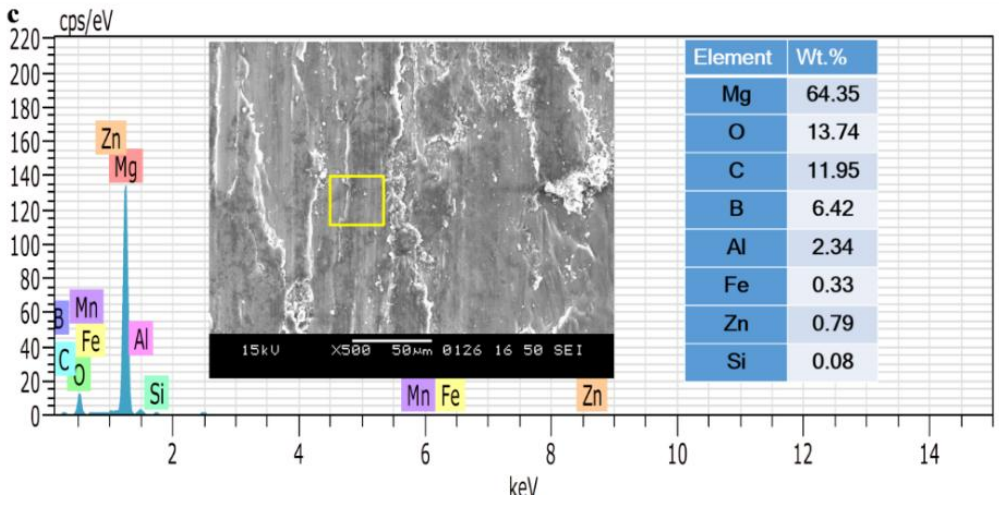

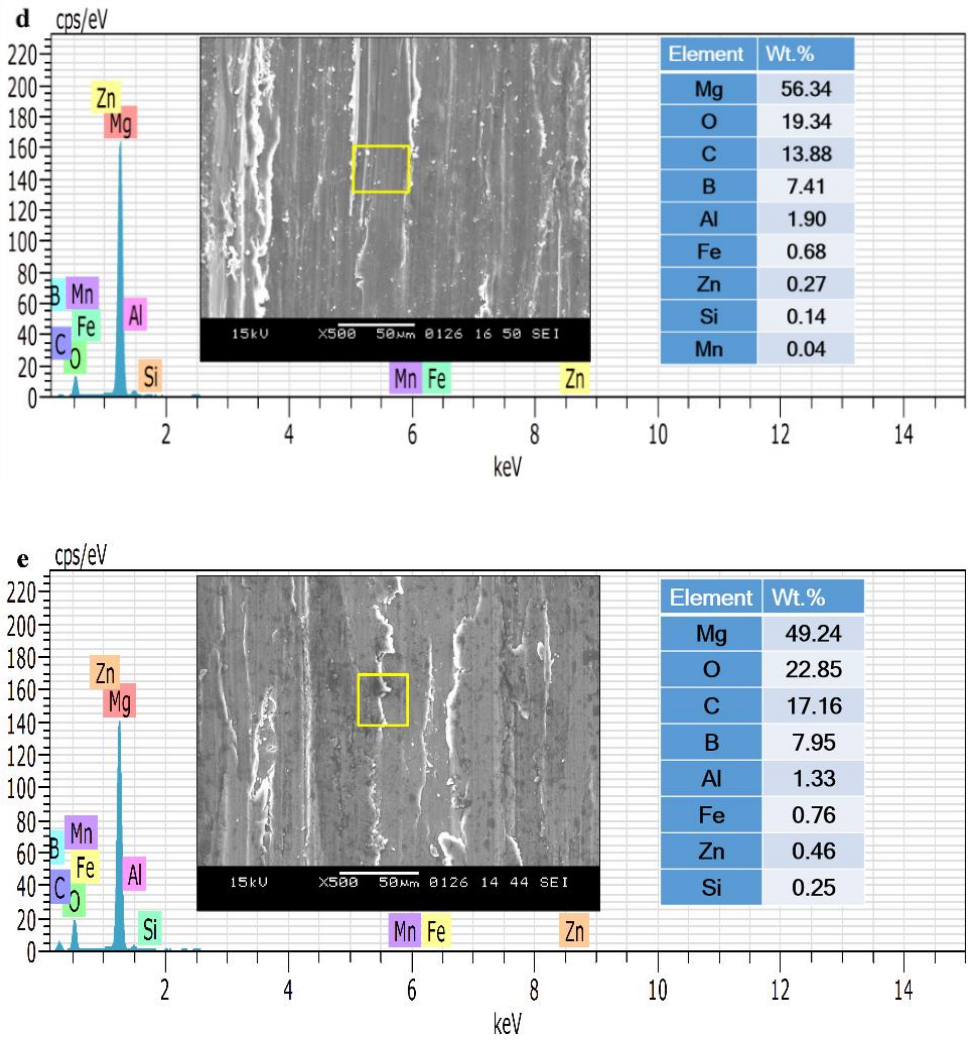

Figure 3.7: EDAX spectra of worn Surfaces a) AZ31 b) AZ31-0.5 B_4C c) AZ31-1.0 B_4C d) AZ31-1.5 B_4C e) AZ31-2.0 B_4C at 40N and 0.4 m/s

3.4 Summary

Dry sliding tribological behavior is also carried out in a pin-on-disc tribotester at varying loads and sliding speeds. Wear resistance of AZ31-B_4C composites enhances due to addition of B_4C ceramic particles in AZ31 alloy. Wear resistance of AZ31-B_4C composites enhances continuously with increase in wt.% of B_4C particles. For AZ31- B_4C composites, wear rate increases linearly with increase in applied load. However, slope of wear rate of AZ31 is quite steeper compared to all composites. Wear rate of AZ31 and AZ31- B_4Ccomposites increases continuously with increase in sliding speed. For base alloy, slope of increment of wear rate is steeper and that slope decreases continuously with increase in wt.% of B_4C particles. AZ31-B_4C composites yield far better friction behavior than AZ31 alloy but COF

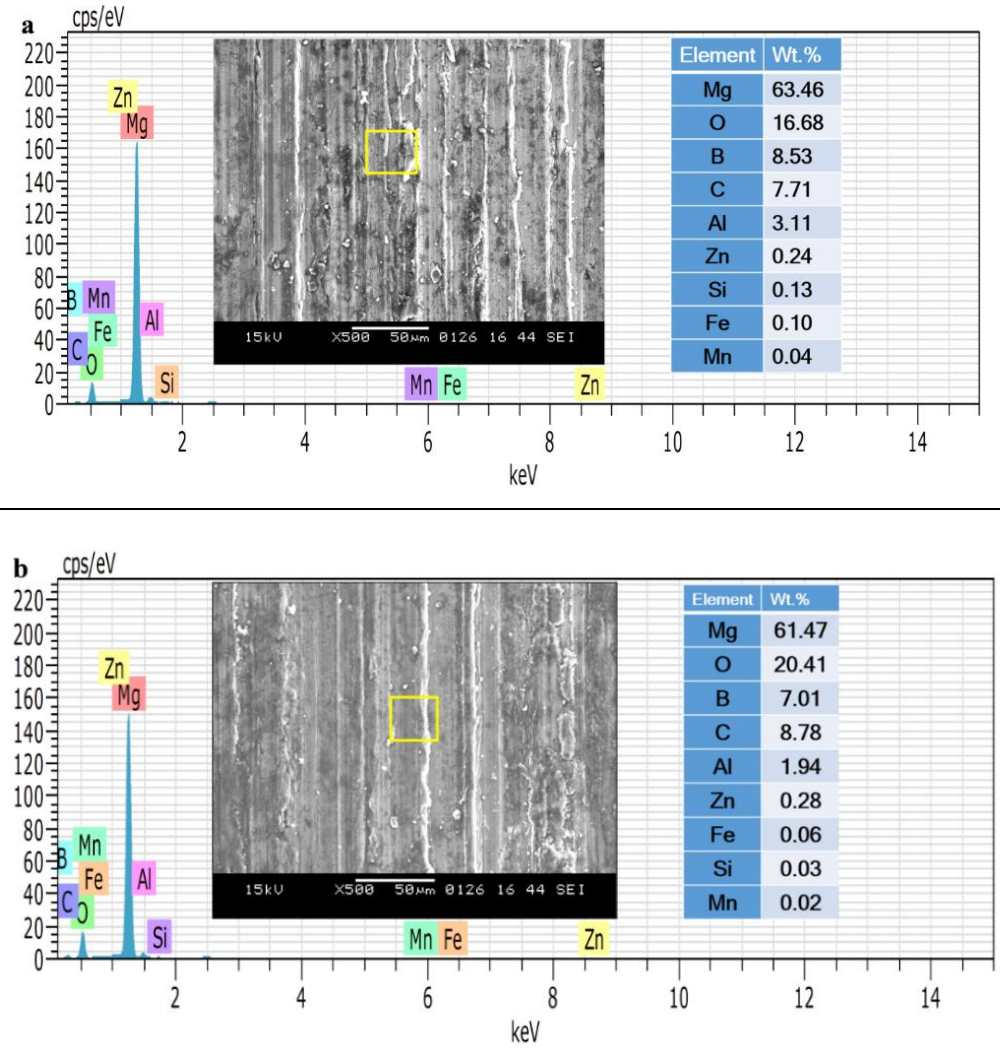

Figure 3.8: EDAX spectra of worn surfaces of AZ31-2B_4C tested at (a) 20N load and 0.4m/s, (b) 40N load and 0.2m/s

values increased continuously with increase in wt. % of B_4C among composites. Abrasion, plastic deformation and delamination are main wear mechanisms for AZ31 alloy while oxidation is the dominant wear morphology for AZ31-B_4C composites.

Chapter 4

Dry Sliding Behaviour At Higher Speeds and Distances

4.1 Introduction

The safe operation of mechanical components at high speeds is critical in advanced engineering applications. The friction and wear behaviour of the composite has been studied in the earlier chapter at low sliding speeds and loads. Speed is the most influential parameter for the kinetic energy of systems and has notable impact on many processes. The ranges of such processes include charging speed-dependent battery life, plasticity of materials and recrystallization processes [Eder et al., 2022]. Sliding velocity has an impact on friction and contacting interface behaviour. Moreover, sliding velocity is a crucial parameter where interacting surfaces have complex geometry, along with other factors like material pairing, applied stresses, environment, etc. According to Coulomb law of friction, kinetic friction is independent of velocity. This rule shows divergence.at high sliding speed. There are a few aspects that contribute to such divergence. Lot of metals gain strength with increased strain rates, leading to a smaller actual area of contact and reduced friction. Conversely, high sliding speeds could cause the interface temperature of the frictional contact to rise, which would lower the material's shear strength or possibly lead to localised melting [Molinari et al., 1999; Lim et al., 1989]. Moreover, tribological studies are normally required for components in continuous sliding contact for a prolonged time duration. Engine components have lower contact stresses and their wear depends mostly on sliding speed, sliding distance, and sliding time [Adaveesh et al.,2017; Shen et al.,2022]. However, there are fewer tribological investigations at higher range of sliding distances and speeds for magnesium composites. Thus, the present chapter is focused on investigating the wear and friction behaviour of AZ31-B_4C composite at higher sliding speeds and distances. This investigation is restricted to a single variety of composite, namely, AZ31-1.5B_4C and a comparison is made with the behaviour of base alloy AZ31.

For the present tribological investigation, sliding speeds and sliding distance are considered in the range of 0.25-1.25 m/s and 300-3000 m respectively in order to cover different ranges of load-speed (FV) factors typically considered in design of high speed machine components. Accordingly, the assessed minimum sliding duration is 6.67 minutes, and the maximum sliding duration is 40 minutes respectively for 0.25 m/s and 1.25 m/s.

4.2 Experimental Details

The same pin-on-disc tribometer ((DUCOM, India) as described in the previous chapter is used to measure friction and wear of base alloy and composite samples following ASTM (G-99-05) standard at room temperature. The same pin geometry is used here. The specific difference is that the ranges sliding speeds and distances are significantly higher. Pin specimens (Φ6 mm x 30 mm) are mounted normally to the counter disc (EN-8, 58-62 HRC). Tribo-tests are carried out on pin samples under two different conditions:

(a) Varying sliding speeds where speed varies from 0.25 to 1.25 m/s at varying load-speed (FV) factors (5-25 N-m/s) over a fixed sliding distance of 500 m and at 20 N load. Sliding duration is evaluated as 6.67 min to 33.33 min respectively.

(b) Varying sliding distances at different load-speed (FV) factors, speed variation of 0.25-1.25 m/s for sliding distances from 300-3000 m and sliding duration is estimated to be between 10 and 40 min.

The FV factors are selected based on prior literature, the capacity of the tribometer and the geometry of the specimen [Banerjee et al., 2021a; Wang et al., 2003; Shinde and Sahoo, 2022]. The tribo-tests are thus performed at 100 mm track diameter for varying sliding durations ranging from 6.67 minutes to 40 min over a fixed load of 20 N. The worn surface analysis is done using FESEM and EDAX spectra to find out the dominated wear mechanisms at different sliding speeds and distances for fixed applied load.

4.3 Wear and Friction Behaviour

4.3.1 Effect of Sliding Speed Variation

Wear rate of base alloy and composite are examined for five different sliding speeds (0.25-1.25 m/s) keeping sliding distance as 500 m and load as 20N. Figure 4.1(a) demonstrates the wear behaviour of AZ31 alloy and AZ31-1.5 B_4C composite for range of sliding speed at constant sliding distance of 500 m and fixed load of 20 N. Typically, both alloy and composite proclaimed similar wear rate trends with varying sliding speed. Initially, a moderate decrease in wear rate is noticed up to a transition speed of 0.5 m/s for both alloy and composite. On the contrary, a significant increase in wear rate is illustrated after that transition speed and maintained up to 1.25 m/s. AZ31-1.5B_4C composite reveals a considerably lower wear rate almost at all sliding speeds compared to base alloy.

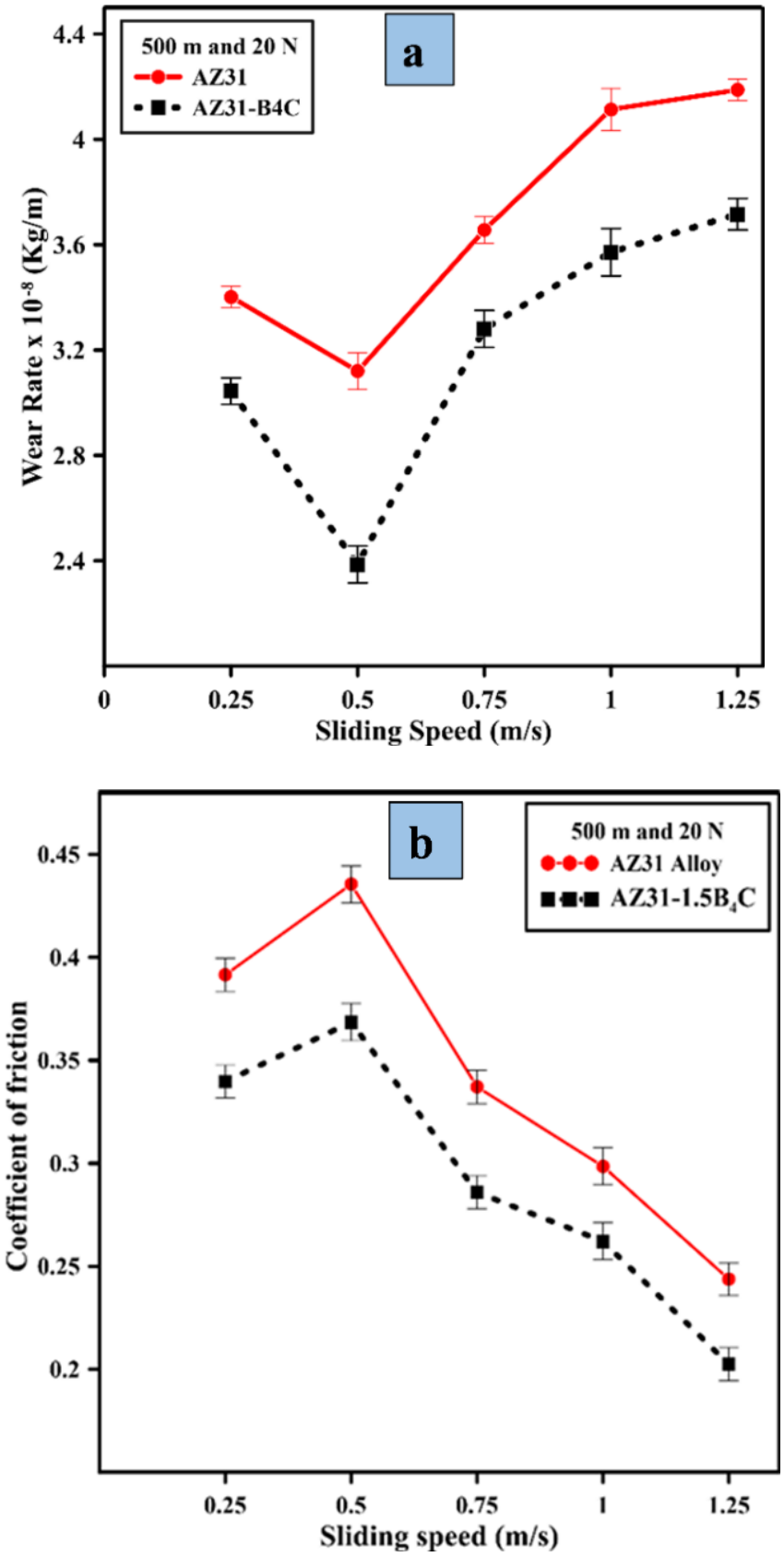

Figure 4.1: a) Wear rate versus sliding speed b) Coefficient of friction versus sliding speed

The improved wear resistance could be due to an increase in the hardness of the composite. It is also worth noting that the composite possesses better wear behavior during the speed range of 0.75-1.25 m/s. It may be because of high work hardening capacity and enhanced thermal stability provided by ceramic based B_4C particles. Shen et al. (2022) have identified a similar trend for AZ31-SiC nanocomposites at 0.5 m/s and 20 N and noticed improved wear behavior for composites. Moreover, Habibnejad-Korayem et al. (2010) put forth the illustration between the work-hardening effect and net flow stress. Work hardening capacity of composites is observed between 0.5-1.0 MPa. Accordingly, specific wear rate of AZ31-Al_2O_3 nanocomposites was found to be decreased at 0.5 m/s and 20 N load. Al_2O_3 and $Mg_{12}Al_{17}$ effectively act as a barrier to restrict subsurface deformation.

Subramanian et al. (1991) observed different phenomenon acting at a time for composites at higher speed. At higher speed, strain rate increased leading towards enhanced flow strength of sliding surface. Enhanced flow strength typically helps to deplete actual contact area which results in reduced wear rate for composites. Similar results are present in literature [Moheimani et al., 2022; Subramanian et. al., 1991; Shinde and Sahoo et al., 2022]. Moheimani et al. (2022) have discovered that composite samples exhibit more strain hardening during later-stage of sliding than they do at the beginning. A delay in the transition to the delamination wear mechanism is also observed for composite material. Thus, the competing effects of work or strain hardening and temperature rise were suggested in literature. It was mentioned that, up to a critical speed, the strain rate effectively predominates the temperature effect, after which the temperature effect dominates. As a result, beyond the critical speed of 0.5 m/s, a notable increase in the wear rate of the composite and base alloy is displayed in Figure 4.1(a).

Figure 4.1(b) demonstrates friction behaviour of AZ31 alloy and AZ31-1.5 B_4C composite for range of sliding speed at constant sliding distance of 500 m and fixed load of 20 N. It shows a decreasing trend of COF with increase in sliding speed for base alloy and composite after a transition speed. COF initially increased till 0.5 m/s sliding speed. However, composite sample possesses lower COF compared to base alloy. At lower speed (0.25-0.5 m/s), both materials offer higher resistance resulting in increase in COF. Above that critical velocity, frictional heating induces a temperature potential between the contact surfaces. Accordingly, the pin sample at high sliding speed conditions offers less resistance during sliding over the counter face due to frictional heating. Frictional heating generates oxidized debris and possesses thermal softening of contact surface, leading towards reduced frictional resistance. Thus, COF shows a decreasing trend with an increase in speed. The composite pin offer

comparatively lower COF may be due to the better load-bearing capacity of B4C particles or minimal contact point over the steel counter face. Moreover, lubricating effect provided by sub-micron B4C particles also helps to reduce COF of composite sample compared to base alloy.

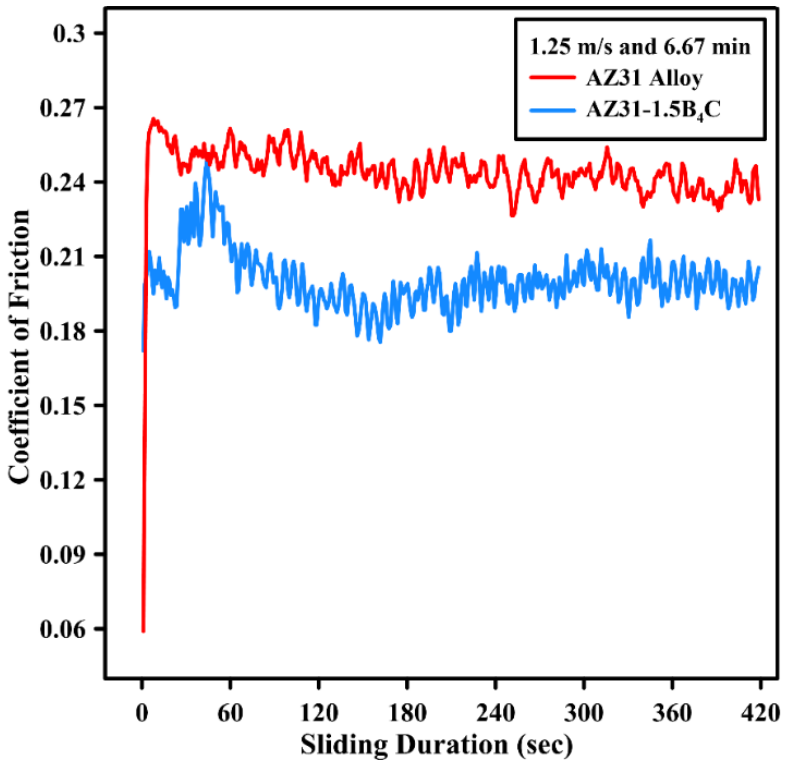

Figure 4.2: Friction profile at 1.25 m/s and 500 m for AZ31 alloy and AZ31-1.5B_4C

Similar observations are present in literature [Lan et al., 2004; Shen et al., 2022; Habibnejad-Korayem et al., 2010]. Zhang et al. (2022) have also observed lower COF values with incorporation of B4C particles in magnesium matrix composite. The real time friction profile at varying sliding durations for both the samples at 1.25 m/s sliding speed and 500 m sliding distance is depicted in Figure 4.2. The decrease in friction in the composite is attributed to the presence of hard ceramic based B_4C particles.

4.3.2 Effect of Varying Sliding Distance at 0.5 m/s

Previously, it was observed that wear rate possessed minimum and maximum value at sliding speed of 0.5 m/s and 1.25 m/s respectively. Hence these two speeds are considered to investigate the effect on tribological characteristics of developed alloy and composite by

varying sliding distance. In the current study, maximum sliding duration is taken as 40 min which generate different sliding distances. Consequently, both cases are presented separately. Figure 4.3(a) presents the effect of sliding distance (300 m – 1200 m) on wear rate for sliding speed of 0.5 m/s keeping load as constant at 20N. Figure 4.3(a) depicts that AZ31 alloy possesses considerably higher wear rate compared to AZ31-1.5 B_4C composite. However, wear rate of both samples initially decreases (up to 600m) with increase in sliding distance, afterwards, wear rate tends to increase with further increase in sliding distance. At initial stage of sliding, significant metal to metal contact exists which results in higher wear rate. However, further sliding produces oxidized wear debris which helps to produce lubricating tribo-layer as well as mechanically mixed layer (MML). These tribo-layer and MML reduces metal to metal contact and exhibits reduced wear rate. This phenomenon exists till a transition limit. After which, due to repetitive loading, action of oxidative layer nullifies as rate of removal of protective layer surpasses rate of formation and metal to metal contact increases again. As a result, increment in wear rate is observed for both samples. However, the wear rate for composite is considerably lower compared to the base alloy. This is mainly due to the presence of ceramic (B_4C) particles which delayed possible plastic deformation and thermal softening of the composite even during higher runs [Aatthisugan et al., 2023; Nguyen et al., 2015; Paider et al., 2021]. Similar findings were suggested by Rahmani and Majzoobi (2019) for Mg-B_4C composites.

Figure 4.3(b) represents the variation of coefficient of friction (COF) with the sliding distance at a speed of 0.5 m/s. Mostly, an equivalent trend is identified for AZ31 and AZ31-1.5B_4C. COF trend reveals significant improvement in friction behaviour for AZ31-1.5B_4C than base alloy with the increasing sliding distance at 0.5 m/s at 20N. An obvious decrease in COF with increased sliding distance was noticed for both base alloy and composites. This is attributed to frictional heating between contact asperities over longer sliding durations. However, for an initial sliding distance of 300 m, there may be more metallic contact and results in moderate increase in COF. After sliding distance of 600 m, sharp decrease in COF is observed. Such phenomenon occurred owing to frictional heating between counter-faces, resulting into the formation of a tribo-oxide layer. Exhibited oxide layer produces better protection for the composite material. Additionally, B_4C particles provide better stability to the tribo layer due to their inherent strength and high hardness even at high temperatures. Thus, composite depicts better friction behavior than base alloy. Similar trends are also noticed in previous literatures [Zhang et al., 2022; Behnamian et al., 2022].

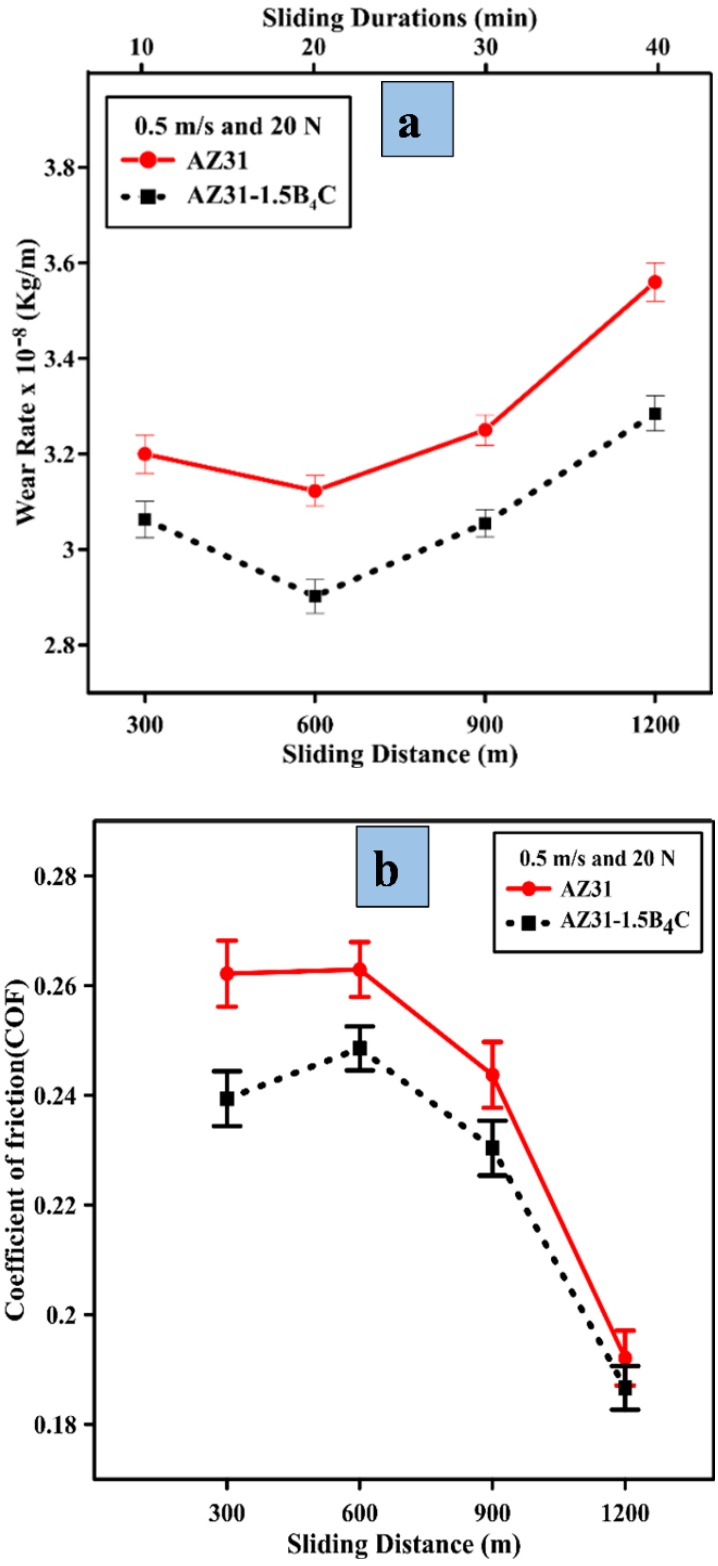

Figure 4.3: a) Wear rate versus sliding distance at 0.5 m/s b) Coefficient of friction versus sliding distance at 0.5 m/s

4.3.3 Effect of Varying Sliding Distance at 1.25 m/s

Figure 4.4(a) depicts the wear behaviour of AZ31 alloy and AZ31-B_4C composite with the respect to varying sliding distances ranges from 750 m to 3000 m at 1.25 m/s sliding speed and 20N load. Figure also discloses that wear rate trend of both AZ31 alloy and AZ31-B_4C increases linearly with increased sliding distances. The increased wear rate at 750 m for both alloy and composite are mainly associated with metallic contact between sliding interfaces. However, the lowest wear rate at 750 m may be correlated to a reduced sliding duration of 20 min between the asperities. Sliding at 1.25 m/s and 40 min gradually increases the wear rate for sliding distances up to 3000 m. Such an increase in wear rate is caused by temperature rise between sliding interfaces due to prolonged sliding. This phenomenon causes thermal softening or plastic deformation of the pin sample resulting in easy sharing of the slip plane of the material [Zhang et al., 2022; Lim et al., 2003; Zhang et al., 2018]. However, it is observed that AZ31 alloy possesses higher wear rate compared to AZ31-B_4C composites for all experimental conditions in current study. Greater wear resistance of composite sample may be attributed to strong interfacial bonding between matrix and reinforcement developed due to uniformly dispersed sub-micron sized B_4C particles. Almost 15% improvement in wear resistance is observed for whole sliding distance only due to fortification of B_4C particles. The incorporation of B_4C particles in AZ31 alloy effectively increased the load-bearing capacity and thermal stability of the matrix even at the highest FV ratio of 25 N-m/s. Guleryuz et al. (2013) reported increased wear rate with the increasing sliding distance for Mg-B_4C composites. Moreover, Mg-B_4C discloses significant wear resistance compared to the base alloy. Similarly, investigations are presented in earlier literatures [Adaveesh et al., 2017].

Figure 4.4(b) depicts friction behaviour with respect to varying sliding distance and durations at sliding speed of 1.25 m/s and load 20N. COF is decreased continuously with increase in sliding distance for both AZ31 alloy and AZ31-B_4C composite. However, AZ31-B_4C results better friction behavior compared to AZ31 alloy. Typical reduction in COF with increased sliding distance may be because of formation of typical oxide layer due to increased frictional heating between the counter face and pin surface of the sample. In addition to this, repeated sliding for long periods may cause overheating and eventually softening of the pin surface against the counter face. This phenomenon may cause easy shearing of the sample surface or even plastic flow in some cases. Accordingly, the decline COF trend is illustrated by the increased sliding distance and durations. Similar trend is observed in literature. AZ31-1.5B_4C composite shows improved friction behavior than AZ31 alloy due to reduced contact

area between the contacting asperities with the presence of B_4C particles along with the lubricating effect provided by reinforcement.

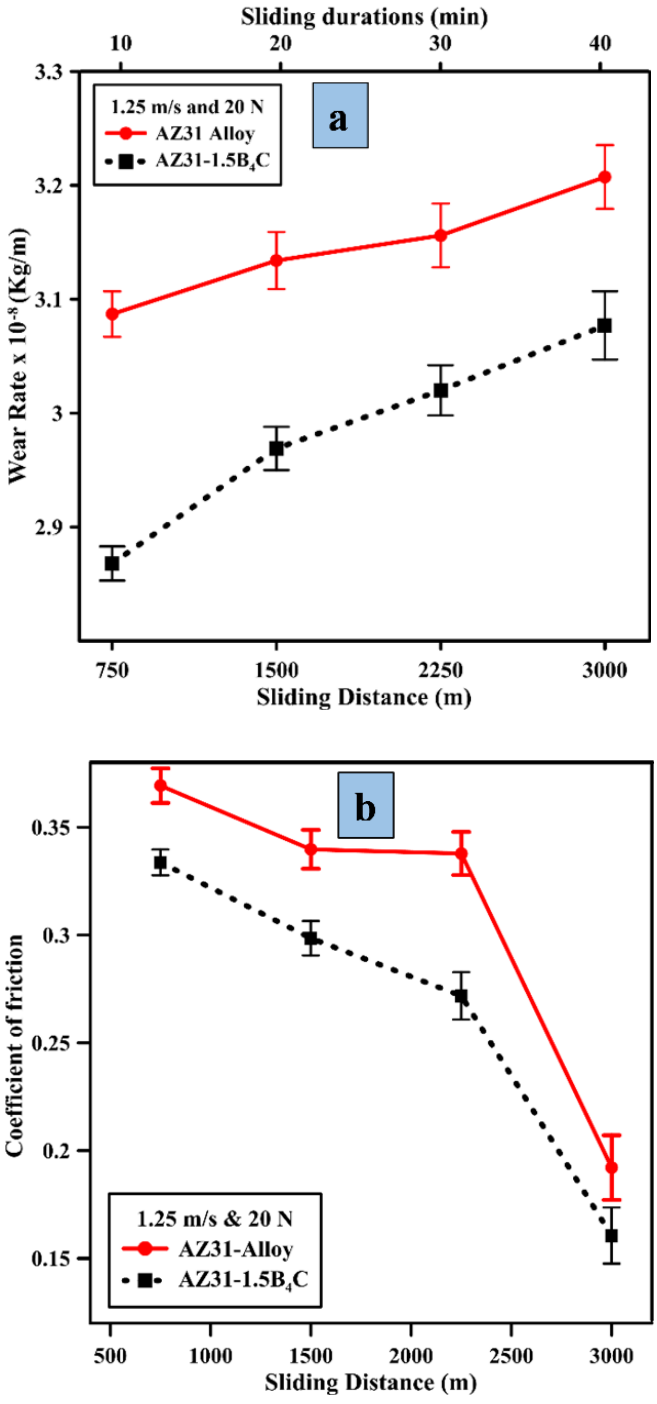

Figure 4.4: a) Wear rate versus sliding distance at 1.25 m/s b) Coefficient of friction versus sliding distance at 1.25 m/s

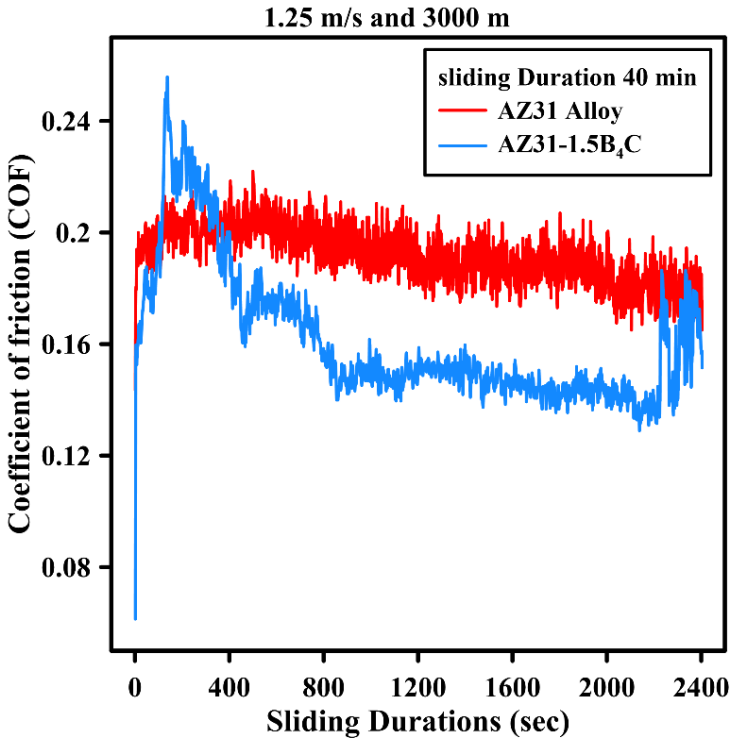

Figure 4.5: Friction profile at 1.25 m/s and 3000 m for AZ31 alloy and AZ31-1.5B_4C

Figure 4.5 depicts friction profile for base alloy and composites. The composite exhibits considerably lower COF than AZ31 alloy for 1.25 m/s at a sliding distance of 3000 m. The COF for composite shows significant variation for initial sliding durations of 1000 sec and finally gets stable up to 2400 sec (40 min). However, AZ31 alloy shows higher COF compared to composite at a sliding speed of 1.25 m/s over a sliding distance of 3000 m. Prolonged sliding (40 min) induces overheating heating due to temperature rise between sliding interfaces. This causes softening of both AZ31 alloy and AZ31-1.5B_4C pin surface which resulted into decreased COF.

4.4 Worn Surface Morphology

4.4.1 Effect of Sliding Speed on Wear Morphology

For disclosing wear morphology, worn surfaces are scrutinized under FESEM and EDAX. FESEM micrographs worn-out surfaces of AZ31 and AZ31-1.5 B_4C pin samples are represented in Figure 4.6(a-d). FESEM and EDAX spectra are illustrated to investigate the possible wear morphology at varying sliding speeds (0.5 m/s and 1.25 m/s) for constant normal load (20N) and sliding distance (500 m).

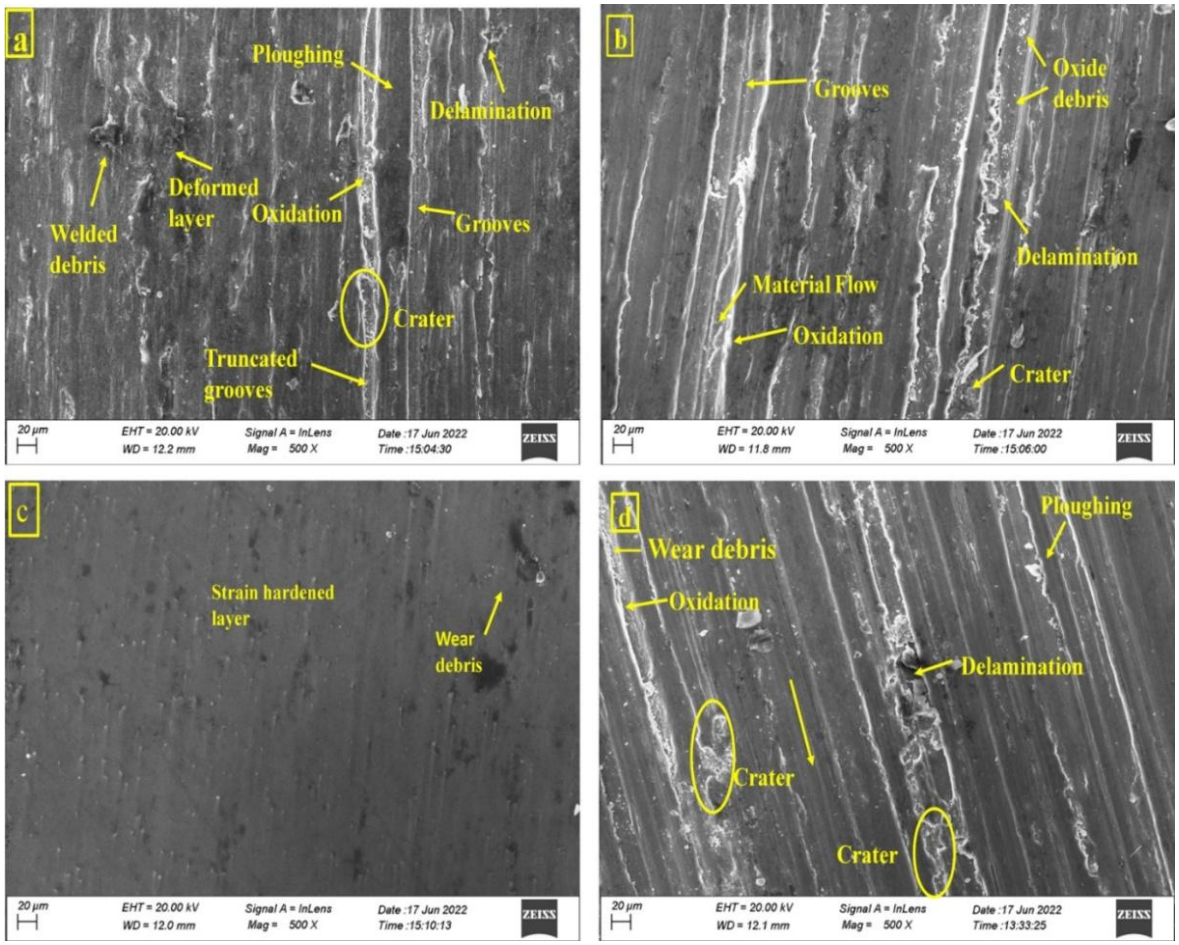

Figure 4.6: Worn surface Morphology (a, b) AZ31 alloy at 0.5 m/s and 1.25 m/s, (c, d) AZ31-1.5B_4C at 0.5 m/s and 1.25 m/s

The surface morphology of base alloy at 0.5m/s in Figure 4.6(a) shows features of oxidation, abrasive grooves, craters and mild delamination along the direction of sliding. Typically, grooves are formed by hard counter asperities of the steel disc counter-face. Thus, it resulted in wear by the removal of small fragments of soft magnesium matrix material from the pin surface. Little displacement of material along the sides of grooves indicates that the abrasion took place basically through ploughing. The already fragmented wear debris during abrasions or micro-cutting also carries iron particles of steel discs into the interfaces due to the transfer and back transfer of materials. As the sliding progresses for a longer time (16.66 min), impounded wear debris or particles got oxidized and pulverized into tiny sizes. These wear debris fill out the shallow grooves or cavities over the worn surface in the form of craters. Thus, adhesive and oxidative wear mechanisms were found to be dominated along with abrasive mechanisms. However, direct metal-to-metal contact could not be fully avoided just with the presence of oxide layers. Hence, traces of mild delamination and plastic deformation in the

form of welded, detached debris and deformed layers found over the pin subsurface. The present examinations are in accordance with earlier investigations, which suggest the occurrence of an abrasive wear mechanism at lower and intermediate speeds [Selvam et al., 2014; Arora et al., 2013].

However, sliding at a high speed of 1.25 m/s took 6.67 min to overcome the distance of 500 m, the alloy sample depicts the mode of abrasion, oxidation, and delamination mechanism individually or in combination (mixed wear mode). With the increase in speed, the flash temperature of pin surface gets increased which results in greater ductility of a sample. Accordingly, the softened pin undergoes increased loss of material. Frictional heating between sliding interfaces may facilitate the formation of oxidized areas over the worn surfaces. The worn surface morphology of AZ31-B_4C at 0.5m/s sliding speed for 16.66 min is mentioned in Figure 4.6(c) and looks featureless compared to AZ31 alloy. Only trace of strain hardened layer and wear debris is visible. This may be due to the thermal stability and load-bearing capability of hard ceramic B_4C particles along with strain hardening of the composite pin at critical speed (0.5m/s). Such consequences offer strong resistance to the counter face. It is observed that the presence of B_4C delayed the transition to delamination wear. Atthisugan et al. (2023) and Rahmani and Majzoobi (2019) have noticed similar results. Worn surface morphology depicted for AZ31 and composite pin sample at 1.25 m/s, involves the presence of ploughing, traces of oxidative, adhesive and delamination wear as presented in Figure 4.6(b, d). However, the composite pin sample appears to be smooth compared to base alloy. The presence of B_4C particles improved the thermal stability of the composite pin sample and avoids further damage to the pin surface. It can be justified from the worn surface that the dominant mechanism at the mentioned range of speeds involves abrasive and oxidative wear mechanism with traces of adhesion (craters) and delamination. A similar agreement is put forth by earlier researchers [Zhang et al., 2022; Moheimani et al., 2022; Nguyen et al., 2015; Behnamian et al., 2022].

Figure 4.7(a)-(d) depicts EDAX spectra for base alloy and composites at speeds of 0.5 m/s and 1.25 m/s at 20 N load for a fixed sliding distance of 500 m. EDAX spectra of base alloy shows Mg, Al, Zn, Fe, Si, Mn and O. Significant amount of oxygen (O) in the EDAX spectra indicates the dominance of oxidative wear due to increased sliding duration (17 min) at

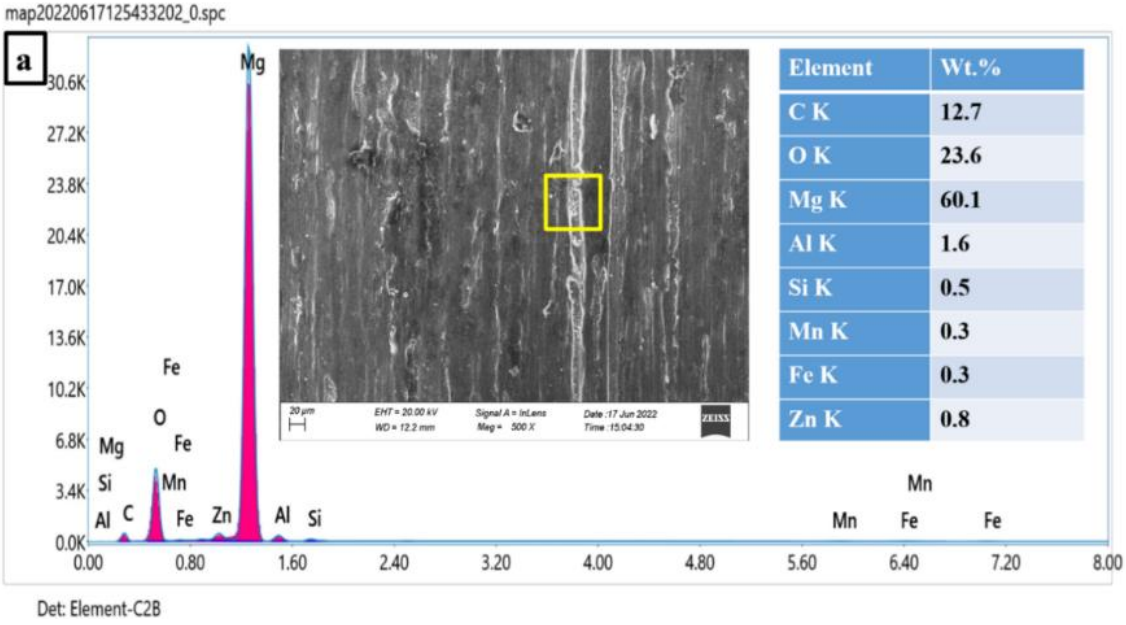

Element	Wt.%
C K	12.7
O K	23.6
Mg K	60.1
Al K	1.6
Si K	0.5
Mn K	0.3
Fe K	0.3
Zn K	0.8

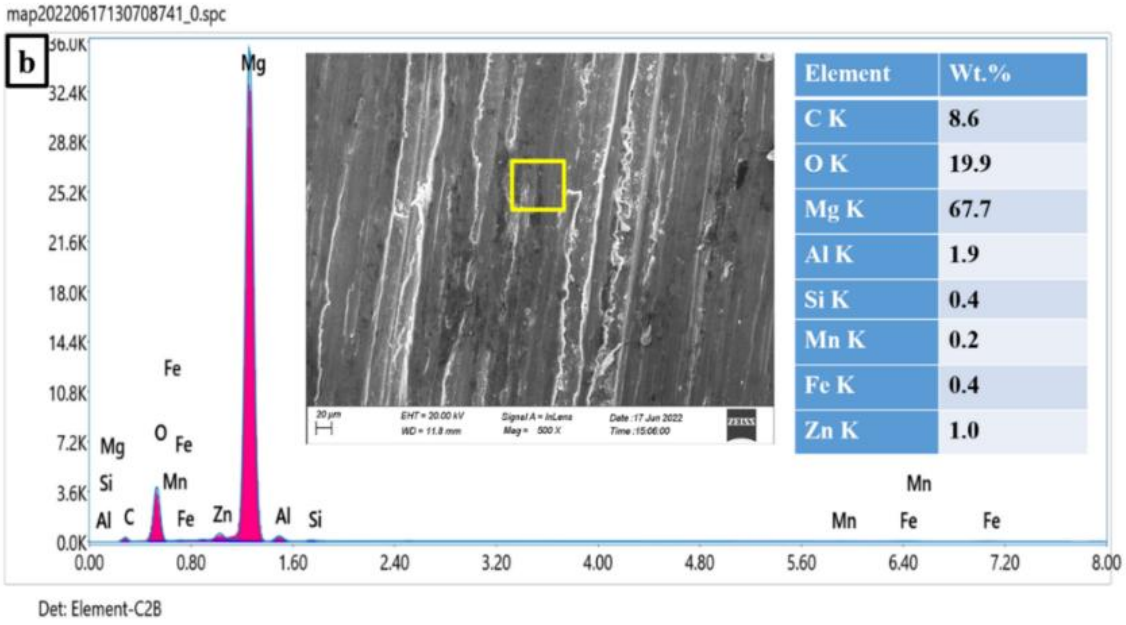

Element	Wt.%
C K	8.6
O K	19.9
Mg K	67.7
Al K	1.9
Si K	0.4
Mn K	0.2
Fe K	0.4
Zn K	1.0

Figure 4.7 *Continued*

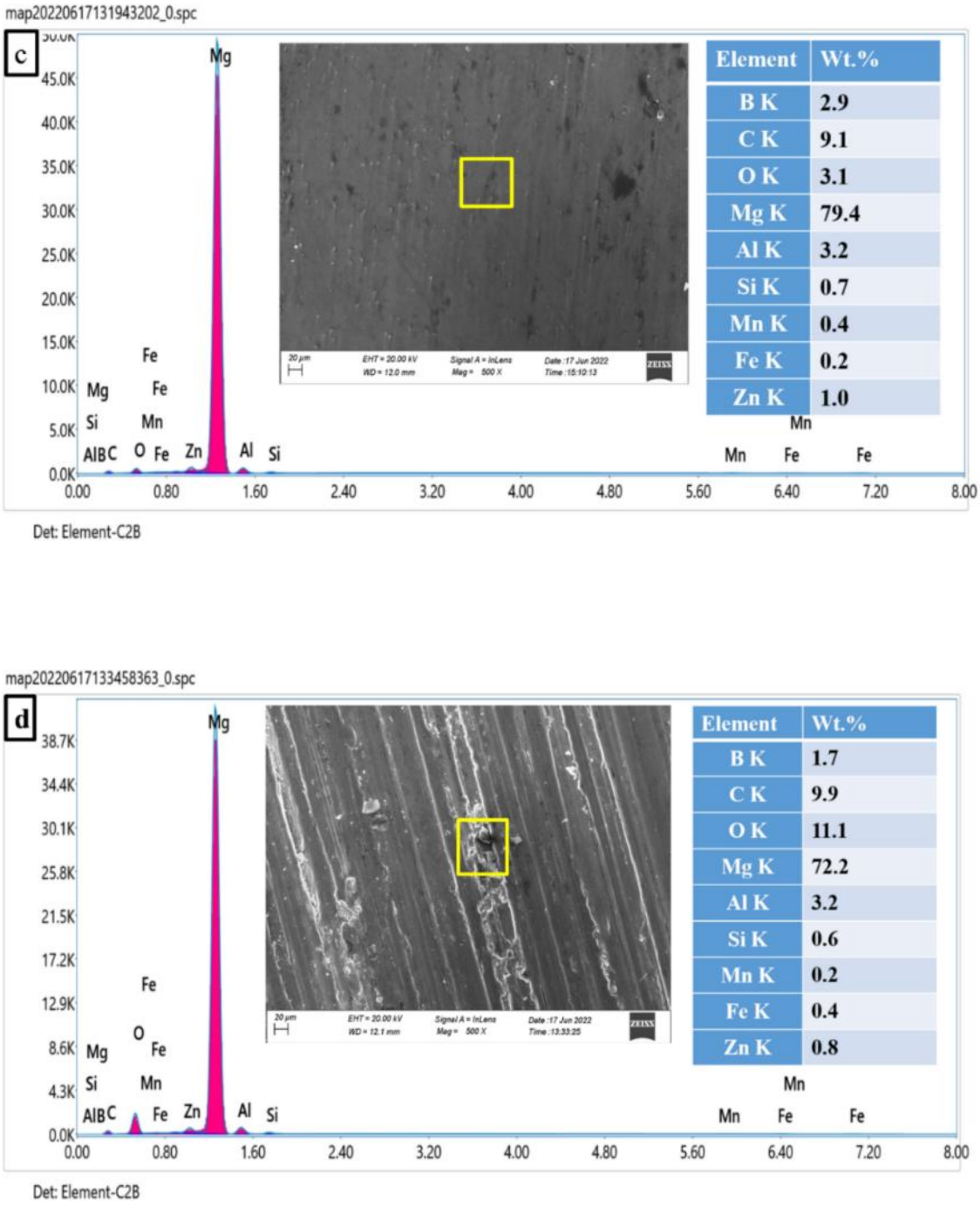

Figure 4.7: EDAX spectra: (a, b) AZ31 alloy at 0.5 m/s and 1.25 m/s, (c, d) AZ31-1.5B_4C at 0.5 m/s and 1.25 m/s

0.5 m/s. The formation of oxide layer (MgO) is justifiable from the worn-out surface and EDAX spectra of the base alloy. It is found that the formation of an oxide layer dominates the process of its removal, resulting in less loss of material and eventually lower wear rate. At a higher sliding speed (1.25 m/s) with the same operating condition displays similar elements in the EDAX spectra. The sliding between interacting surfaces lasts only for approx. 7 min, indicating the formation oxide layer. The amount of oxygen (O) got reduced may be due to the removal or fracture of the oxide layer. At this condition, the rate for formation of the oxide layer got reduced and the scope of transition to metallic wear may have occurred, resulting in an increased wear rate at a higher speed due to delamination. Such agreements are also presented by other researchers in prior literature [Moheimani et al., 2022; Shen et al., 2022; Habibnejad-Korayem et al., 2010]. Thus, the dominant wear mechanism is abrasion, oxidation along with delamination.

Figure 4.7(c) depicts the EDAX spectra for AZ31-1.5B_4C which presents similar elements to base alloy, except boron and carbon. The presence of boron and carbon is detected in EDAX spectra which represents B_4C inclusion in AZ31 alloy. The presence of hard boron particles in the composite reduces the area of contact at sliding interfaces. With the increased speed at 1.25 m/s (for 40 min), a significant amount of oxygen (O) is depicted in EDAX spectra (Figure 4.7(d)). Thus, the existence of oxidative wear can be depicted in EDAX spectra in Figure 4.7(d). The presence of B_4C particles provides extra resistance to wear that may occur due to adhesion and delamination. Because of the presence of Fe in EDAX, it is assumed that hard B_4C particles commence cutting on the counter face material. Accordingly, B_4C effectively delays the mode of adhesive and delamination wear compared to the base alloy. Presence of B_4C particles distributes the stresses equally and resists the wear by avoiding particle free region on the entire periphery of the pin surface. This result is in line with observations in available literature.

4.4.2 Effect of Sliding Distances on Wear Morphology

Figure 4.8(a)-(d) depicts wear morphology of base alloy and composites at 0.5 m/s over sliding distances of 300 m and 1200m. Wear morphology shows extensive grooves over the surface of pin samples of AZ31 and AZ31-1.5B_4C along the sliding direction, indicating wear caused mainly via abrasion. Moreover, base alloy and composite surfaces show the presence of wear debris, traces of oxide layer and delaminated areas typically on all sliding distances at 0.5m/s. Figure 4.8(a, b) reveal the worn morphology of AZ31 alloy and composite

at 0.5 m/s at 300 m under the load of 20N. Both SEM images exhibit abrasive grooves parallel to the sliding direction. The grooves are mainly produced via hard counterface that has ploughed into the soft matrix of the pin sample. However, for composite the wider ploughing marks are evident, indicating that hard counterface loses its cutting ability to protrude into the composite matrix. Moreover, Oxide layer is revealed over both base alloy and composite, but the composite worn surface is more wear-resistant in relation to unreinforced alloy. Again, mild delamination was also noticed over the surface of both unreinforced alloy and composites due to the detachment of flakes perpendicular to the sliding direction. Re-solidified layers are also depicted indicating the detachment in the form of layers. Thus, abrasive wear is mostly a dominant wear mechanism at 0.5 m/s under intermediate load and lower sliding distance. Similar findings are reported in literature [Chinthamani et al., 2020; Paider et al., 2021].

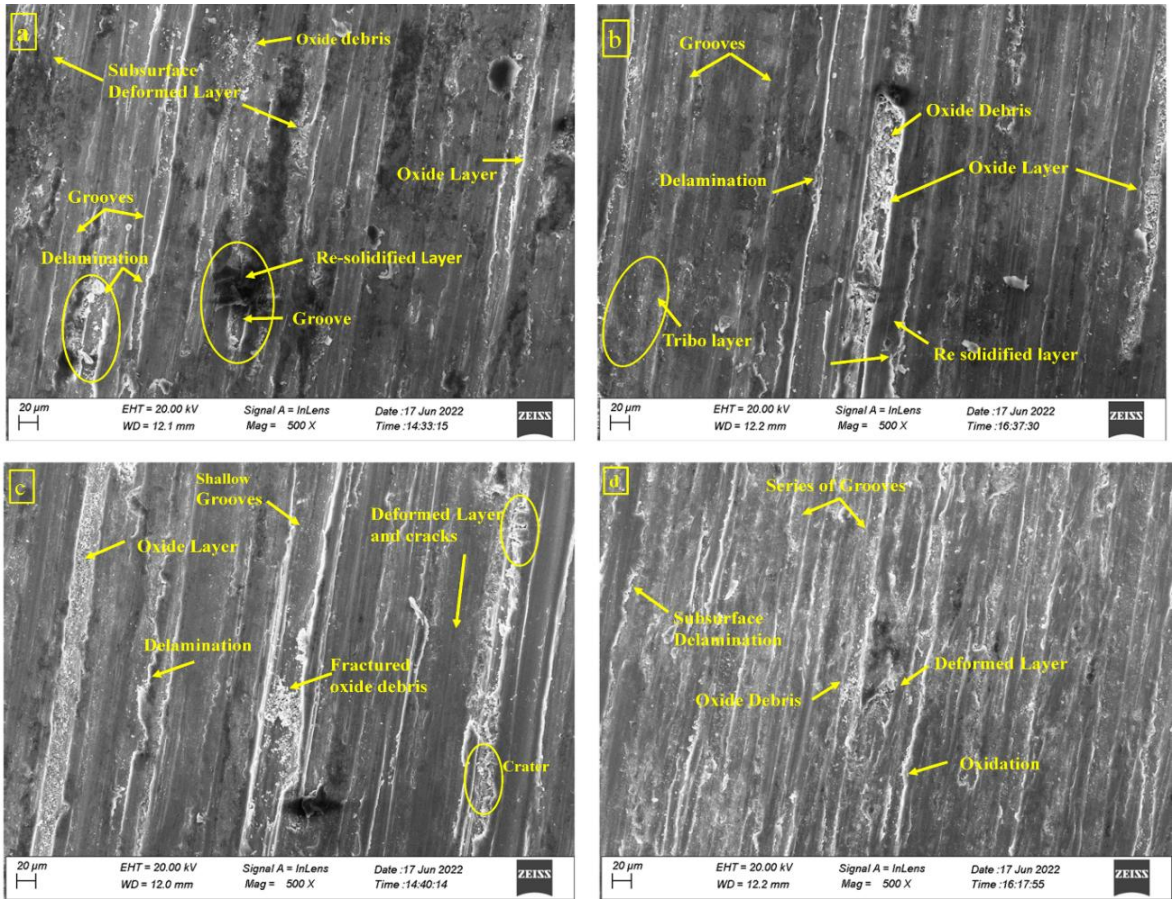

Figure 4.8: Worn surface morphology: (a, b) AZ31 alloy at 300 m and 1200 m, (c, d) AZ31-1.5B_4C at 300 m and 1200 m

Figure 4.8(c, d) depicts worn surfaces of AZ31 alloy and AZ31-1.5 B_4C respectively at 0.5 m/s sliding speed and 1200 m sliding distance for 40 min. With repeated and continuous sliding for 40 min up to 1200 m may induce frictional heating between the contacting interfaces. Frictional heating may cause (i) a sudden increase in temperature between interfaces and (ii) rapid growth of oxide film between the contacting surfaces. During the initial run, wear morphology exhibited oxidation along with abrasions on both alloy and composites. Consequently, progressive sliding for more time may result in the rupture of the oxide layer. Eventually, the oxide film formed over the worn surfaces may get fractured under applied stresses, attributed to fracture of the typical tribo-layer, which exhibits metallic contact and eventually enhances wear rate. However, the tribo layer formed on the surface of the composite consists of fractured B_4C and Fe particles which may provide extra stability to tribo layer. Consequently, improved surface morphology is observed for composites. Similar phenomenon was identified by earlier researchers [Arora et al., 2013; Sankaranarayanan et al., 2015; Shinde and Sahoo, 2022].

Figure 4.9(a)-(d) depicts EDAX spectra of the worn-out surface of AZ31 alloy and AZ31-1.5B_4C at 0.5 m/s for a sliding distance of 300 m to 1200 m at a normal load of 20 N. AZ31 alloy displays chemical compositions of various elements as mentioned in the earlier section with slightly varied proportion. The increased amount of Fe and O indicates the dominance of abrasive wear and oxidative wear. The wear debris found on the worn-out surface also indicates of the presence of MgO. Furthermore, as the sliding continued for a longer duration (40 min or 1200 m), it may cause the removal of oxide fragments. The fragmented oxide debris in powdered form can be noticed in the worn-out surface at multiple locations under SEM. With progressive sliding, oxide debris fills out the abrasive grooves and improves wear resistance by preventing metallic contact [Lim et al., 2003; Srinivasan at al., 2012]. EDAX spectra of AZ31-1.5 B_4C tested at sliding speed of 0.5m/s and sliding distances of 300 m and 1200 m for sliding duration of 10 min and 40 min are presented in Figure 4.9c and 4.9d respectively. Examination as mentioned for the base alloy is applied to the composite pin sample.

The presence of B_4C can be depicted in both EDAX spectra mentioned in Figure 4.9 (c) and (d). The increased amount of Fe and O was noticed over the worn surface of composite sample. In comparison to base alloy, a relatively increased amount of Fe on the surface of the composite is attributed to abrading of the steel counter-face by B_4C particles. However, the

abrading of the counter-face is relatively less severe in the case of submicron particles compared to micro-particles [Lim et al., 2003; Srinivasan at al., 2012]. EDAX spectra for a distance of 1200 m at a speed of 0.5 m/s show more amount of Fe. The presence of iron and oxygen indicates typical features of abrasive and oxidative wear. For longer durations,

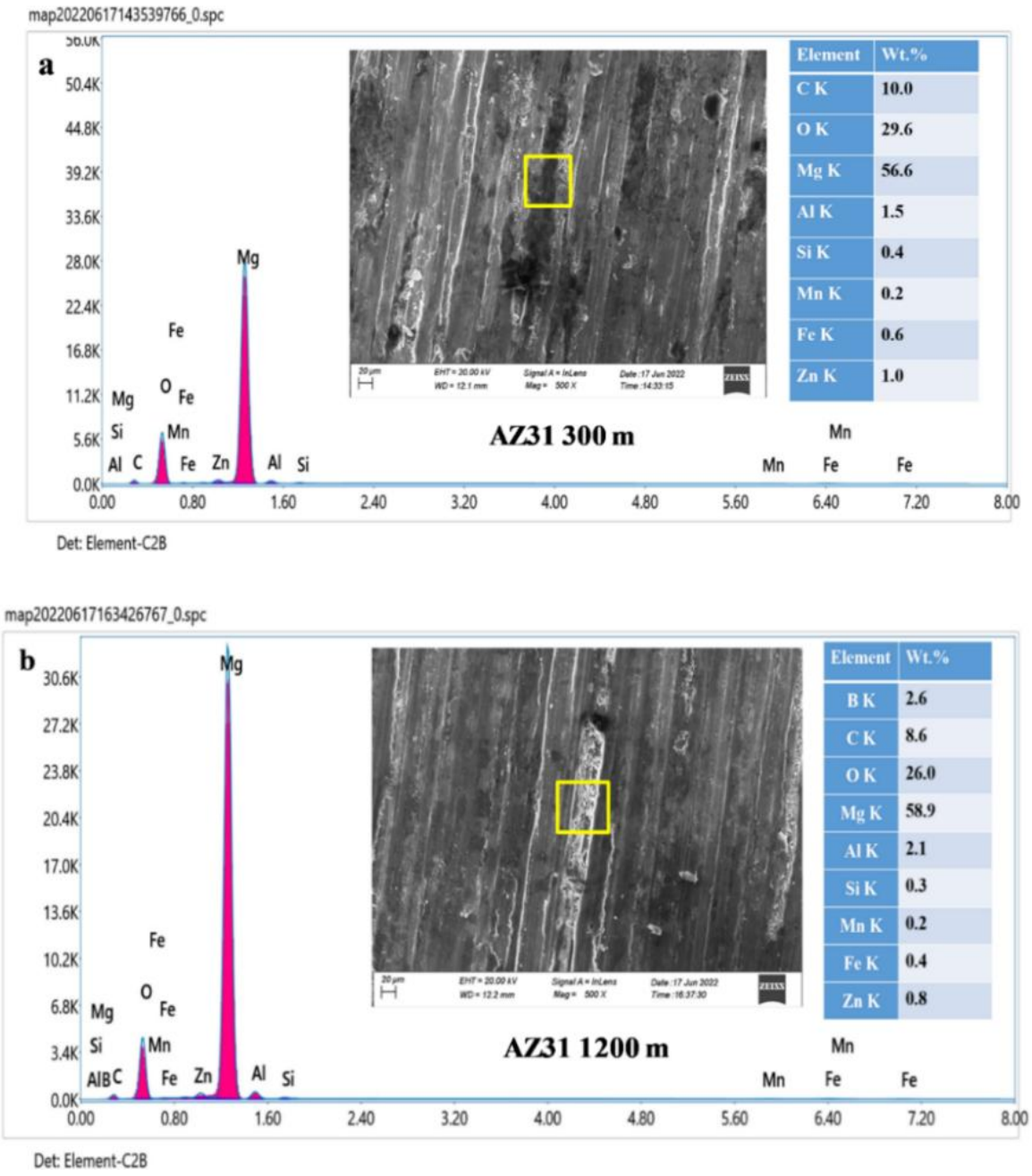

Figure 4.9 *Continued*

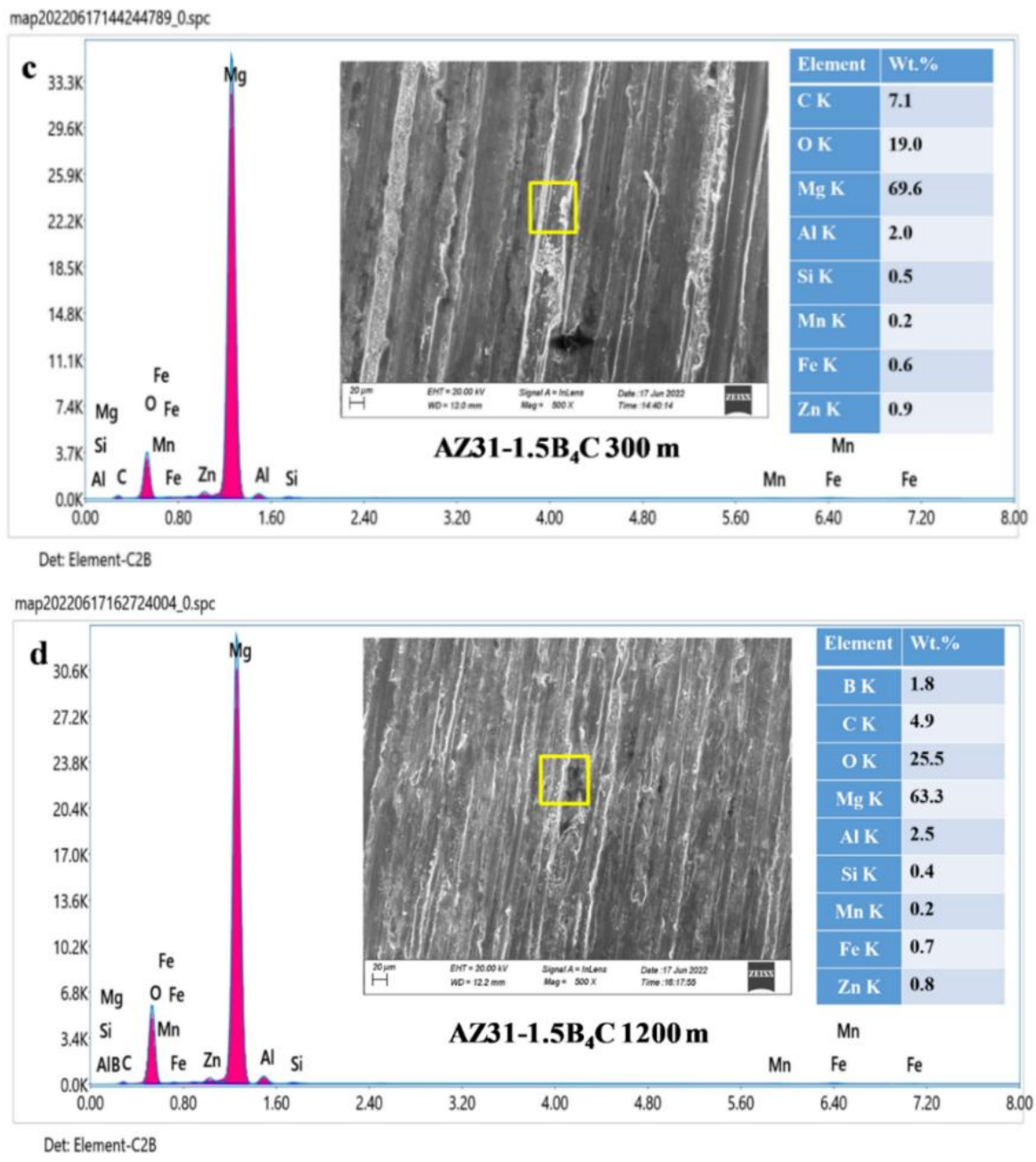

Figure 4.9: EDAX spectra: (a, b) AZ31 alloy at 300 m and 1200 m, (c, d) AZ31-1.5B_4C at 300 m and 1200 m

transferred iron particles get oxidized and mixed with wear debris and fractured B_4C particles. All these particles may get compacted in the abrasive grooves and cavities so form due to repeated sliding and may result in generation of MML [Srinivasan at al., 2012].

4.5 Summary

The present chapter presents the in-depth investigation of tribological behaviour at varying sliding distances and speeds for ranges of load-speed (FV) factor. The wear rate of AZ31-1.5B_4C composite is significantly improved compared to AZ31 alloy at all ranges of sliding velocities at a fixed sliding distance (500 m) and load (20 N). Moreover, the wear rate depicts a typical increasing trend after a transition limit with the increased sliding velocity for both AZ31 alloy and AZ31-1.5B_4C composite due to increased frictional heating between sliding interfaces. The wear rate illustrated for AZ31 alloy and AZ31-1.5B_4C depicts an increasing trend for varying sliding distances of 300 m -1200 m and 750 m - 3000 m respectively for sliding velocities of 0.5 m/s & 1.25 m/s. AZ31-1.5B_4C composite material represents improved wear resistance at all sliding distances over AZ31 alloy. The influence of sliding velocity and sliding distance brings a notable change in the wear behavior of both AZ31 alloy and AZ31-1.5B_4C. Furthermore, it is also confirmed that composite exhibits superior friction behavior for all experimental conditions. Worn surface morphology detected abrasion, oxidation, adhesion and delamination as dominant wear mechanisms with respect to experimental parameters. However, the composite surface appears to be relatively smooth and surely exhibit better wear behavior at all ranges of operating conditions.

Chapter 5

Abrasive Sliding Tribological Behaviour

5.1 Introduction

Scrutiny of literature reveals that tribological characteristics of Mg-MMCs are majorly examined either in dry sliding condition or elevated temperature conditions. But it is well acknowledged that 63% of total wear is caused by abrasive conditions. Recently, Banerjee et al. (2020) scrutinized the abrasive wear behaviour of AZ31 and AZ31-WC composites for different abrasive grit size and sliding distance. It was reported that wear resistance was enhanced around 56% by incorporating only 2wt.% of WC particles in AZ31 matrix. Similarly, several other researchers [Kaviti et al., 2018; Zhang et al., 2018; Labib et al., 2016; Nguyen et al., 2015] have fortified different ceramic-based particles like BN, SiC, B_4C, Al_2O_3 etc. in magnesium matrix and examined dry sliding wear characteristics.

In the context of tribological applications like cylinder heads, piston, power train, housings etc., investigation of abrasive wear behaviour is of equal importance as these applications involve typical contact with foreign particulates. Thus, it is quite obvious that detail examinations of abrasive wear behaviour of magnesium matrix composite are essential to establish them as necessary replacement of conventional materials. Extensive study of available literature clearly reveals that study on abrasive wear behaviour of magnesium matrix composite is scanty. To overcome this literature gap, the present chapter concentrates on examination of abrasive wear behaviour of AZ31-B_4C composites synthesised through ultrasonic treatment associated stir casting technique. Effects of varying wt.% of B_4C, sliding distance and abrasive grit size on wear and friction characteristics are thoroughly investigated. Furthermore, worn surfaces are also examined under SEM and EDAX to ascertain the possible wear morphology.

5.2 Experimental Details

The abrasive wear tests are performed on pin-on-disk type tribotester (DUCOM, TR-20LECHM-400) at ambient temperature. Tests are carried out for all four variants of the composite and the base alloy. Abrasive papers of required grit size are attached on counter-surface of tribotester during experimentation. The EN31 steel disc (60 HRC, Φ160 mm and 8 mm thick) is used as counter face. Initially, pin samples (Φ6 mm x 30 mm length) are properly

wiped with acetone to remove foreign particles. Afterwards wiped samples are fastened at the stationary attachment, perpendicularly on the counter-disc. Schematic diagram of tribotester is presented in Figure 5.1. In current study, experiments are performed on different SiC abrasive grit papers (400, 600 and 800 grit). The wear testes are conducted at varying track diameter (40, 50 and 60 mm) and constant speed of 100 rpm for 5 min duration. The varying track diameter justifies variations in sliding distance. In present investigation, sliding distance is represented by track diameter (TD). A dead weight of 30 N is placed on loading pan for each experiment.

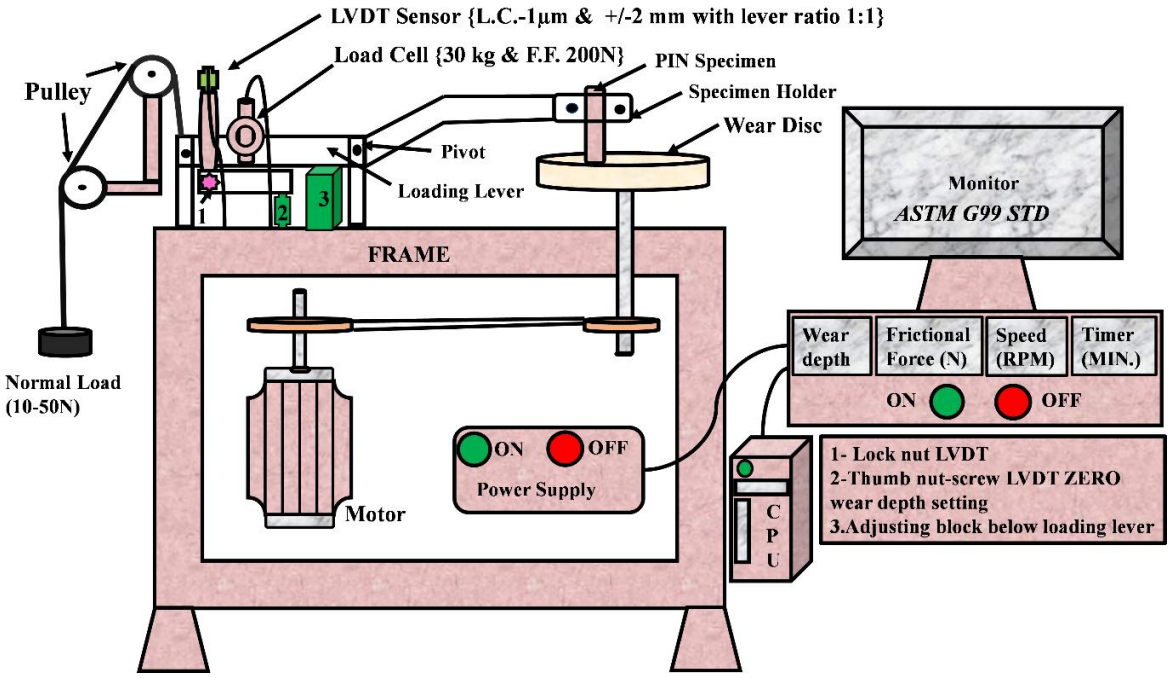

Figure 5.1: Schematic of pin-on-disc test rig

The wear values of samples are evaluated based on initial and final weight of pin measured via digital weighing balance (Afcoset, accuracy ±0.001 mg). The controller unit helps to analyze experimental parameters. In this investigation, wear depth of samples is evaluated from the following relations.

$$Weight\ loss\ of\ pin\ sample\ (\Delta W) = W_{initial} - W_{final} \tag{5.1}$$

Where, *W*=Weight of Pin samples at initial and final conditions.

Specific wear rate (W_{sp}) is expressed as,

$$W_{sp} = \frac{\Delta W}{L\,S} \tag{5.2}$$

Where, *L*= Applied load (N) and *S*= Sliding distance (m).

Wear Coefficient (K) is given as,

$$K = \frac{\Delta W\ H}{\rho L\ S} \tag{5.3}$$

Where, H = Micro-hardness of Pin sample and ρ=Density of Pin sample (g/cc).

Wear depth (W_d) is calculated as,

$$W_d = \frac{K\ L\ S}{AH} \tag{5.4}$$

Where, A= Cross sectional area of Pin sample.

5.3 Results and Discussion

5.3.1 Abrasive Wear Behaviour

In the current investigation, experiments are carried on different grit (400, 600 and 800 grit) SiC abrasive papers and considering three different sliding distances. For experimentation, track diameters (TD) are varied (40, 50 and 60 mm) to compute sliding distances keeping the sliding speed constant at 100 rpm and experiments are continued for 5 minutes. Figure 5.2 shows the effect of incorporation of amount of B_4C particles on wear rate of base alloy and composite samples for different track diameters under 800 grit abrasive paper. It is quite clear from Figure 5.2 that the wear rate of AZ31 alloy (base matrix) is maximum for selected range of sliding distances. Figure 5.2 also yields decreasing trend of wear rate with increase in amount of B_4C particles. AZ31-2B_4C possesses highest wear resistance among developed composites. Typically, good interfacial bonding of matrix and reinforcement interface enhances basic mechanical properties like hardness which results in increased load carrying capacity compared to base alloy. Accordingly wear resistance enhances with increasing amount of B_4C particulates. It is quite obvious from literature that hardness and wear rate possess inverse relation. In present investigation, AZ31-2B_4C is found to have highest hardness while AZ31 shows minimum hardness. Usually, penetration of counter asperity is dependent on applied load, speed, sliding distance, hardness and other factors. In base alloy, major load due to sliding is on matrix phase whereas the same for composite is governed by B_4C particles. Similar phenomenon is also observed in literature [Banerjee et al., 2020; Canakci, 2011].

Due to the enhanced load carrying capacity of composites, amount of worn-out material is less for composites compared to AZ31 alloy. Figure 5.2 also discloses that wear rate of all the developed materials increases with increase in sliding distance. For increased sliding distance, typical contact time of mating surfaces increases resulting generation of intensified

heat. This heat leads the sample surface towards thermal softening. As a result, material removal from sample surface becomes easier. In AZ31 alloy effect of this phenomenon is more compared to composites. In composites, presence of B_4C particles helps to minimize this thermal effect to a certain extent. Consequently, composites exhibit better wear resistance at all experimental conditions.

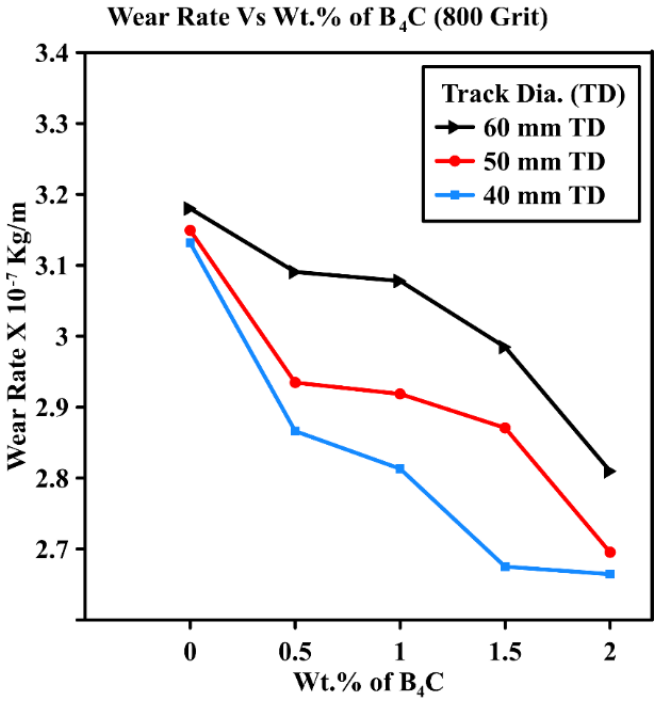

Figure 5.2: Wear rate versus wt.% of B_4C at varying sliding distance (TD)

Effect of variation of abrasive grit size (AGS) on wear rate of AZ31 alloy and AZ31-B_4C composites for 60mm TD is shown in Figure 5.3. Figure 5.3 depicts that initially wear rates of base alloy and composites decreases sharply coarse abrasive grit and then follow moderate trend for fine grit. Coarse grit to fine grit size varies from AGS 400 to 800. Basically, enhancement in number of grit size suggests the appearance of smoother surface (i.e., lesser grit size means presence of coarse asperity which penetrates faster and deeper). Thus, material removal should be more for 400 grit (coarse) compares to 600 or 800 grit (fine). As a result, steeper slope is observed in the initial range (400-600) of abrasive grits. In base alloy, matrix phase directly come across the counter-asperity (SiC grit) which easily penetrate the matrix phase resulting easy material removal. On the other hand, for composite samples, counter-asperities come across the reinforced B_4C particles which protect the matrix phase by preventing direct contact. Additionally, the bonding of matrix-reinforcement interface and higher microhardness of MMC safeguard the pin surface from the penetration of abrasive grits.

These effects enhance with increase in wt.% of B_4C. Accordingly, MMC possess lesser wear rate compared to base alloy and wear rate decreases with increase in wt.% of B_4C. This result is in line with literature [Kulekci et al., 2008].

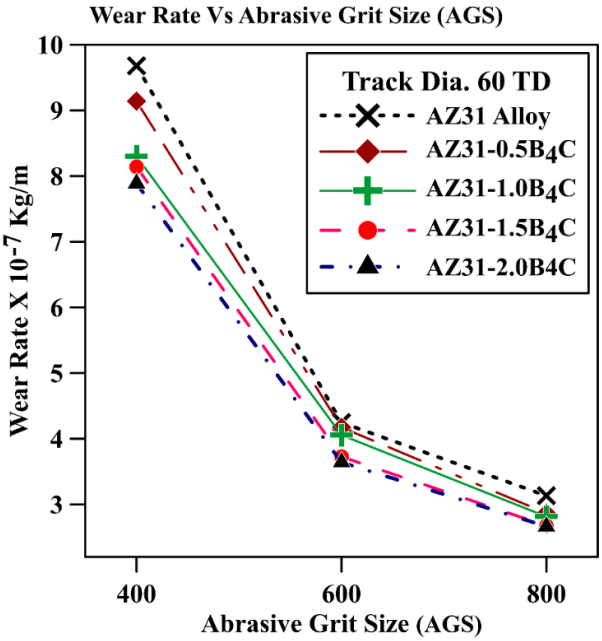

Figure 5.3: Wear rate versus abrasive grit size (AGS) for base alloy and composites

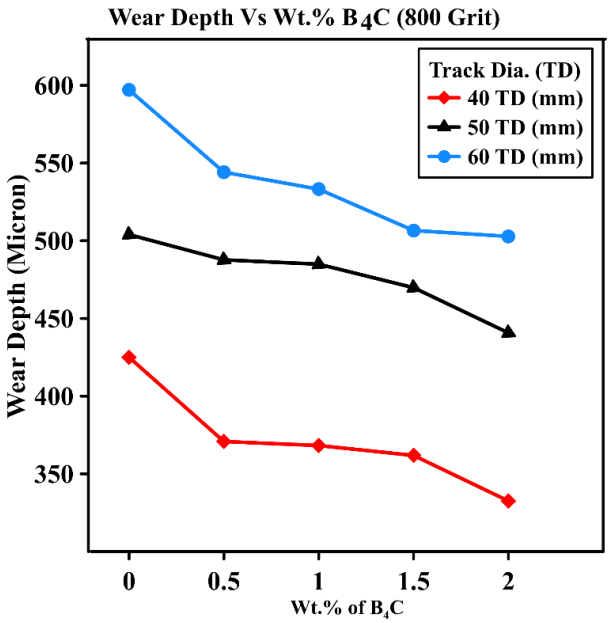

Figure 5.4: Wear depth versus wt.% of B_4C at varying sliding distance (TD)

Figure 5.4 shows the role of varying wt.% of B_4C on wear depth for different track diameter tested under 800 grit SiC abrasive paper. In current study, wear depth is calculated by considering equation (5.4). Figure 5.4 depicts that wear depth of AZ31 alloy is maximum for all experimental conditions and wear depth decreases simultaneously with increase in amount of B_4C. However, value of wear depth increases with increase in track diameter. Occurrence of this phenomenon is mainly due to homogeneous distribution of B_4C particles in AZ31 matrix. Strong interfacial bond between matrix and reinforcement helps to enhance hardness and load bearing capacity of AZ31-B_4C composites.

5.3.2 Friction Behaviour

Friction behaviour of AZ31 alloy and AZ31-B_4C composites in abrasive sliding are depicted in Figure 5.5. Figure 5.5 discloses the variation of COF w.r.to different wt.% of B_4C particles for different sliding distance under 800 AGS counter-body. It is clearly observed that COF possesses detrimental trend with increase in amount of B_4C particles in AZ31 matrix. Additionally, it is also found that COF increases with increase in sliding distance. Similar observations are also reported in literature for other composites [Oge et al., 2019; Meher et al., 2019; Banerjee et al., 2020]. In case of composites, abrasive asperities of counter-body will come in contact with reinforced B_4C particles during sliding. Composites also possess higher hardness compared to base alloy. Consequently, contact area in between composites and counter-surface will be lesser than that of base matrix. As a result, COF decreases.

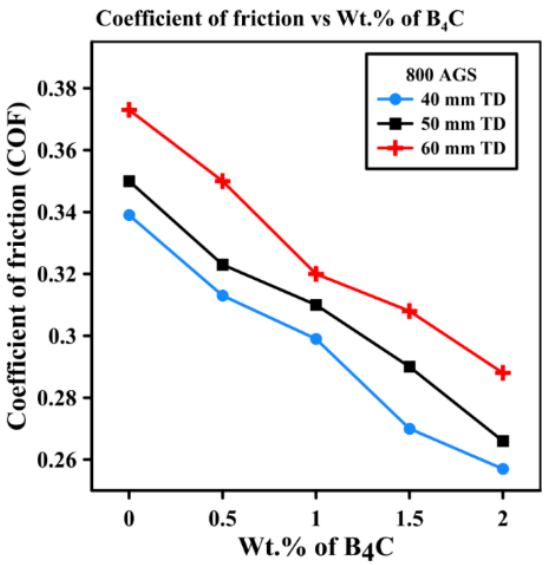

Figure 5.5: COF versus wt.% of B_4C particles for different sliding distance

In the contrary, increased sliding distance leads to more time of contact which initiates formation of local hot-spots due to the action of frictional heating. Due to frictional heating, shearing as well as bulk softening of pin surface may occur quite easily. Thermal softening leads towards easy penetration of counter asperity and increased area of contact between sample and counter-face [Kulekci et al., 2008]. As a result, value of COF shows incremental trend.

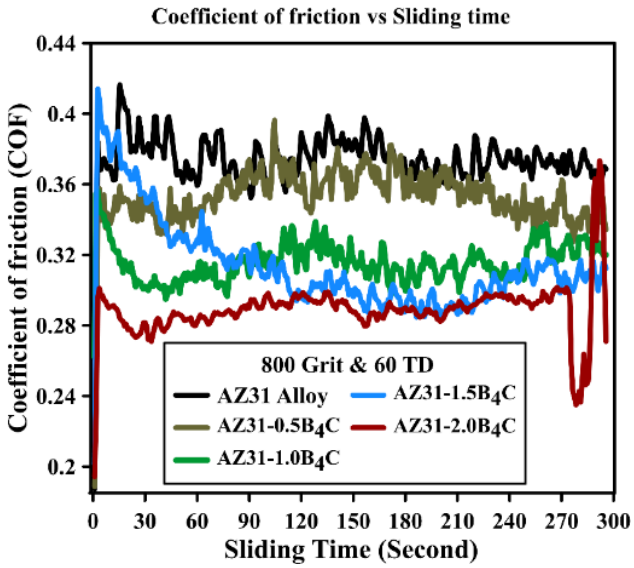

Figure 5.6: Fluctuations of COF versus time for all synthesized materials

Fluctuations of COF w.r.to time are presented in Figure 5.6 for all synthesized materials tested at 800 AGS and 50 mm TD. In Figure 5.6, moderate increment in COF is observed w.r.to time for all samples whereas COF possesses continuous decreasing trend with increase in amount of B_4C. Basically, effect of frictional heating enhances with increase in duration of contact which in turn enhances the thermal softening effect on surface of AZ31 alloy. Consequently, COF value enhances. On the other hand, presence of B_4C particles in MMC subsidizes the thermal effect and reduces the fluctuation of COF.

Figure 5.7 presents the role of AGS on COF of AZ31 and AZ31-B_4C composites for 60 mm TD. Figure 4.7 discloses that COF decreases moderately with increase in abrasive grit size. Here higher AGS refers finer abrasive surface. Moreover, COF value decreases continuously with increase in wt.% of B4C. Typical interaction of coarse particles with material surface produces greater friction force compared to the force generated by interaction of finer particles and material surface.

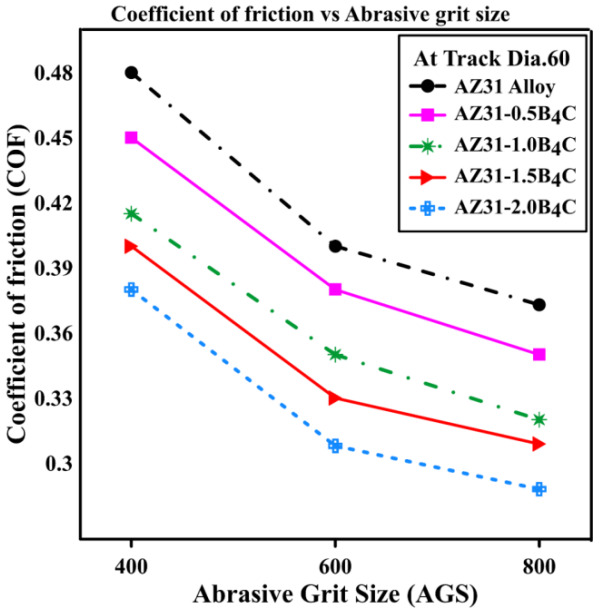

Figure 5.7: Variation of COF versus abrasive grit size for AZ31 and AZ31-B_4C composites

5.3.3 Wear Mechanism

Wear and friction behavior of AZ31 alloy and AZ31-B_4C composites clearly suggests the presence of different wear mechanisms during abrasive wear tests. In addition, different tribolayer may have formed and tribomechanical reactions may have occurred during experimentations. Hence further investigations are required on worn surfaces to understand the effect of wt.% of B_4C, AGS and sliding distance on surface morphology and protective tribolayer formation. Therefore, worn surfaces of samples are scrutinized with the help of SEM images and EDAX spectra. Effect of wt.% of B_4C particles on wear morphology of speciments experimented under 800 grit abrasive counter-surface and 60 mm TD is depicted in Figure 5.8. It is quite clear from Figure 5.8 that concentration and nature of wear for base metal and AZ31-B_4C composites are completely different. Figure 5.8(a) shows the SEM image of base alloy. Sign of grooves, ploughing, plastic deformation, delamination, press-in particle and craters are visible in SEM image. Basic nature of base matrix is softer which allows the harder counter-asperity to remove material quite easily either by ageing or by ploughing. As a result, different types of grooves (shallow or deep) are observed in the SEM micrograph. Furthermore, craters, press-in particles and sign of delamination are also found because of repetitive loading. In SEM micrograph, adhesion is also distinct which suggests the presence of adhesive wear. Additionally, craters and torn grooves are present along the sliding direction. These are sign of

delamination wear. Thus, it can be said that typical wear mechanisms behind wear of base matrix are abrasion, adhesion and delamination. Similar phenomenon is reported in literature [Kulekci et al., 2008; Banerjee et al., 2020].

Figure 5.8(b) and (c) depict SEM micrographs of worn surfaces of AZ31-1B_4C and AZ31-2B_4C composites respectively. In Figure 5.8(b), abrasive groove, sign of oxidation and delamination are clearly visible. However, presence of grooves are shallower due to the presence of B_4C particles. Welded debris are also present in the micrograph. Hence it can be said that along with abrasion and delamination, oxidation has also happened during experimentation for AZ31-1B_4C composite. Figure 5.8(c) discloses the presence of ploughing and spalled over oxidized debris along with small amount of welded debris. In this case, intensity of ploughing is quite lesser compared to the micrographs of base matrix and AZ31-1B_4C. Consequently it can be said that, higher wt.% of B_4C as well as higher hardness of composites have resulted in reduced penetration depth. Presence of small amount of welded debris suggests that B_4C particles have successfully reduced the effect of heat. However, abrasion along with oxidation is found to be as dominant wear morphology of AZ31-2B_4C composite. Moreover, it is of immense importance to investigate the effect of abrasive grits on wear morphology. Consequently, worn surface of AZ31-2B_4C sample tested at 60 mm TD and 400 grit SiC paper is thoroughly examined. Figure 5.9 presents the FESEM micrograph of above mentioned condition. Figure 5.9 and 5.8(c) are compared to distinguish the function of abrasive grits. Figure 5.8(c) represents the FESEM micrograph of AZ31-2B_4C sample tested at 800 grit at 60 mm TD and Figure 5.9(a) depicts the FESEM image AZ31-2B_4C samples tested at 400 grit and 60 mm TD. Figure 5.9(a) contains more number of deep abrasive grooves, delamination patch and rows of furrows. Typical presence of deeper grooves and rows of furrows in sample surface are mainly because of rubbing with coarser counter particles. Rubbing of coarser particles with sample surface generates more heat which in turns generate welded debris which also make the surface uneven. Presence of welded debris and rows of furrows also justify the existence of adhesive wear. Additionally, repeated loading creates the traces of delamination. Hence, it can be observed that abrasion as well as delamination and adhesion are dominant wear mechanism in this case. Moreover, effect of varying track diameter on wear morphology should also be examined. Figure 5.9(b) shows the FESEM image of worn surface of AZ31-2B_4C sample tested at 800 grit and 40 mm TD.

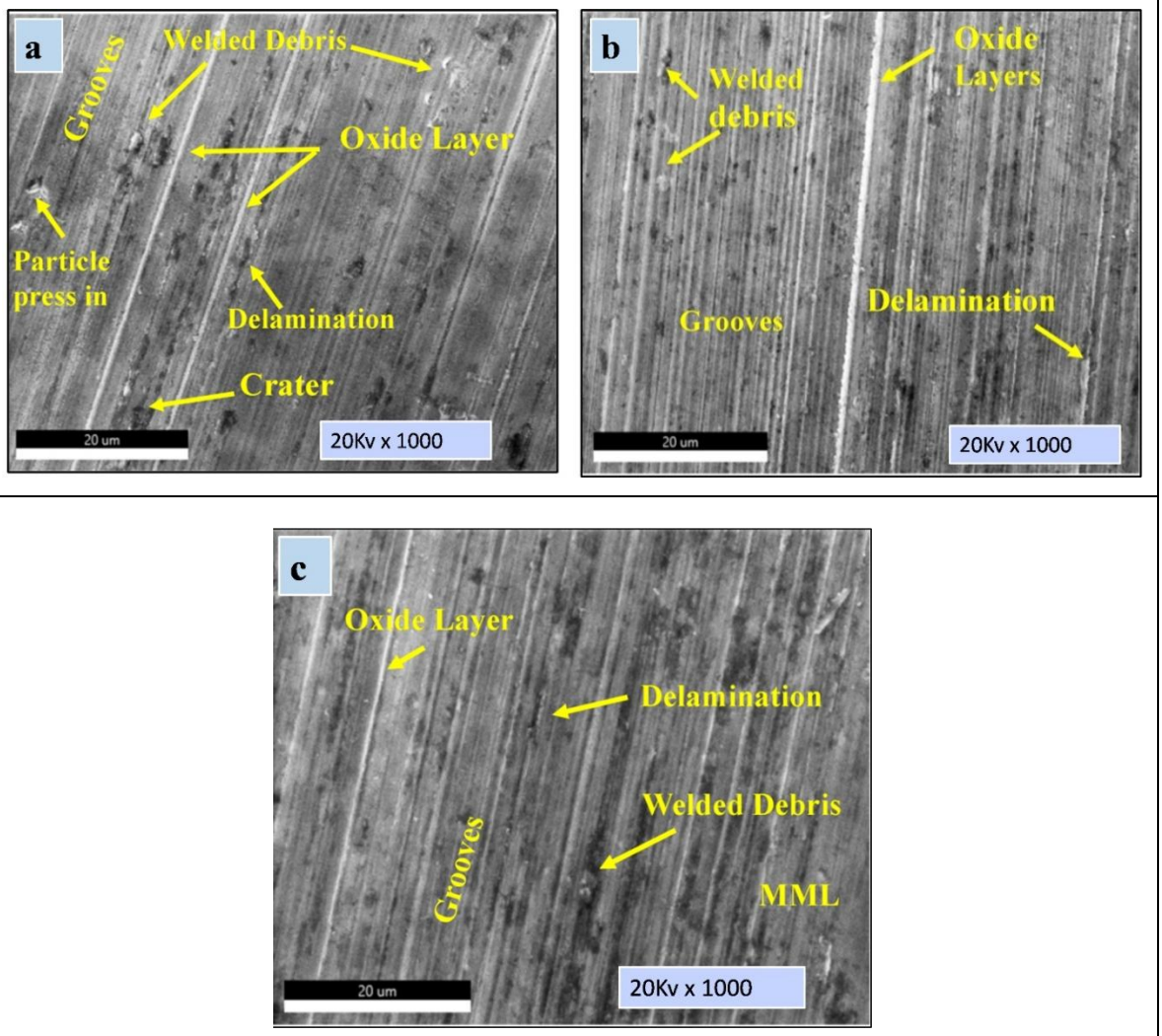

Figure 5.8: FESEM micrograph of worn surface of (a) AZ31, (b) AZ31-1B_4C and (c) AZ31-2B_4C for 800 grit abrasive counter-surface and 60 mm TD

Comparision between Figure 5.8(c) and Figure 5.9(b) helps to distinguish the function of TD. Figure 5.8(c) represents the FESEM micrograph of AZ31-2B_4C sample tested at 60 mm TD keeping all other experimental conditions same. Figure 5.9(b) clearly shows lesser grooves and more oxidized debris compared to the sample tested at 60 mm keeping all other conditions same. For the sample tested at 40 mm TD, the duration of contact is less compared to the sample tested at 60 mm TD. As a result chances of repeatitive loading is lesser resulting in less surface damage. Along with SEM micrograph, EDAX spectra need to be examined to evaluate composition details of worn-out surface during abrasive sliding. Accordingly, EDAX spectra of worn-out surfaces are presented in Figure 5.10.

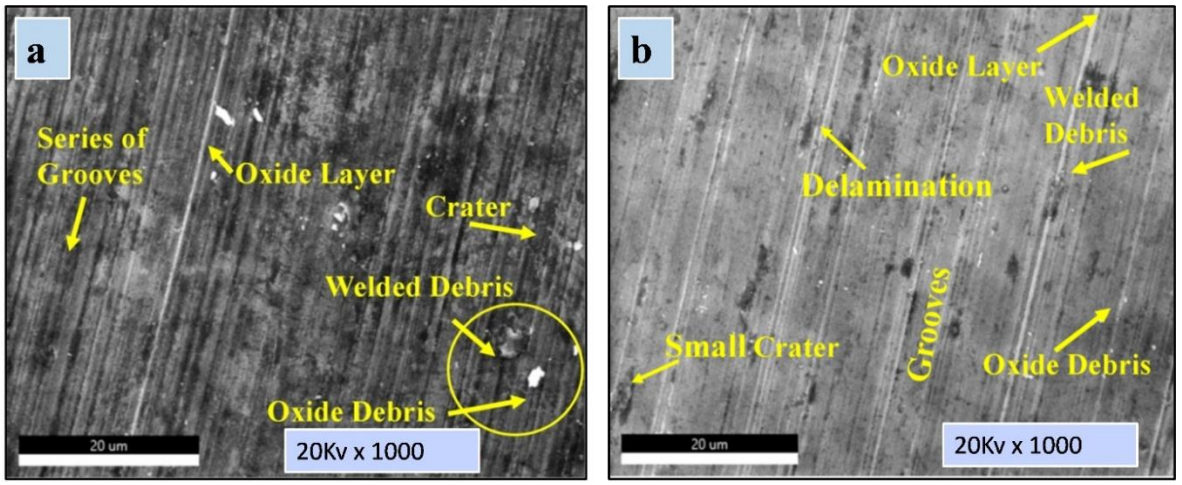

Figure 5.9: FESEM micrograph of worn surface of AZ31-2B_4C sample (a) 400 grit and 60 mm TD (b) 800 grit and 40 mm TD

The compositional analyses are carried out for base alloy, AZ31-1B_4C and AZ31-2B_4C composites tested with 800 grits SiC paper at 60 mm TD, 30N load and 0.3 m/s sliding speed. Figure 5.10(a) depicts the EDAX spectra of AZ31 alloy. In Figure 5.10(a), all the base elements of base matrix are present but wt.% of Si is comparatively higher which indicates transfer of ruptured particles from SiC emery paper. During sliding on abrasive SiC emery paper, SiC particles ruptures and may have increased the wt.% of Si. Typically, these fractured hard Si particles also left some scars over the worn surface during sliding. The continual sliding over abrasive surface cause frictional heating between interfaces which results in thermal softening of pin surface. The softened pin easily got penetrated by counter asperity and thus plastically deformed easily. However, EDAX spectra of AZ31-1B_4C and AZ31-2B_4C composites in Figure 5.10 (b) and (c) discloses significant reduction in wt. % of Si compared to AZ31 alloy which results in protection to pin surface from abrasive particles. Moreover, presence of protruding boron particles also restricts contact area between soft Mg matrix and abrasive particles. Accordingly, relatively less wear than base alloys is justified. The EDAX spectra of composite samples also depicts strong oxygen peak which indicates the generation of protective oxide tribo-layer over the worn-out surface. These layers are typically formed due to thermal heating between counter-face and pin surface during repeated sliding and loading. Thus, composite pin samples show relatively better wear behaviour at all experimental conditions than base alloy.

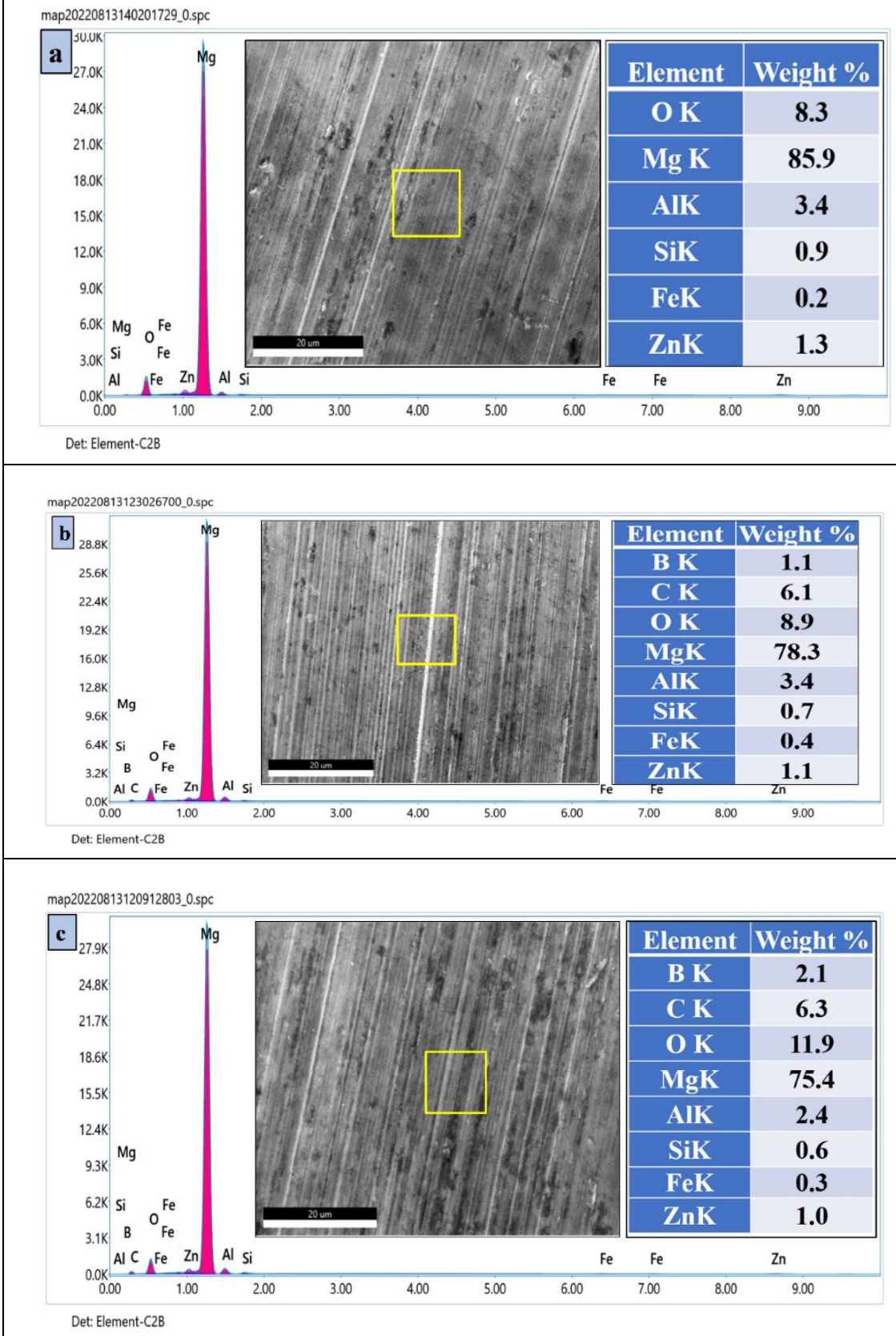

Figure 5.10: EDAX spectra of worn-out surfaces of (a) AZ31 alloy, (b) AZ31-1B_4C (c) AZ31-2B_4C composites tested with 800 grits SiC paper at 60 mm TD

5.4 Summary

A pin-on-disc tribo-tester is utilised to investigate abrasive wear characteristics of base matrix and AZ31-B_4C composites. Experimentations are performed under different grit (400, 600 and 800 grit) SiC emery paper and for different track diameters (40, 50 and 60mm). The composites possess better abrasive wear characteristic than base Mg alloy due to addition of B_4C particles. Wear rate values of AZ31 alloy is about 1.3-1.5 times more than AZ31-2.0B_4C. Accordingly, submicron composite offers better wear resistance at all experimental conditions. The increase in sliding distance enhances wear rate for all materials. However, composite material shows better load bearing capacity than base alloy even at higher sliding distance. Coarser grit abrasive paper removes material easily from pin surface resulting in higher wear rate compared to fine grit for base alloy and composites. Fine abrasive grade (800 AGS) illustrates lower wear rate compared to coarse grit SiC paper for all experimental conditions. Friction behaviour of composite material is significantly enhanced due to incorporation of B_4C particles in AZ31 alloy. COF values decreased with the increase in wt. % of B_4C. Worn surface morphology of AZ31 alloy depicts series of grooves, press in particles, furrows, crater and plastic deformation over the range of tested conditions. Wear mechanisms of AZ31 are found to be abrasion, adhesion and plastic deformation while abrasion, mild delamination and oxidation are dominant for composites.

Chapter 6

Tribological Behaviour At Elevated Temperatures

6.1 Introduction

Metal matrix composites have gained prominence as critical material in terms of trade as well as technology. Metal matrix composites offer higher strength, enhanced wear resistance, fracture toughness, stiffness and withstand elevated temperature. As a result, utilization of MMC has gained wide acceptance in transportation industries like automobile, railways and aerospace etc. [Guan et al., 2022; Bharathi et al., 2023]. Nowadays, magnesium (Mg), titanium (Ti), aluminum (Al) and nickel (Ni) alloys are widely used as matrix material because of their specific applications in aircraft, missiles, automotive and electronics applications. In this context, magnesium based composites have emerged as better alternative. Nowadays, magnesium composites are quickly displacing aluminium and other metals as a structural material in automotive and transportation industries owing to their elevated stiffness, specific strength etc. [Miracle et al., 2005; Nirala et al.,2020].

With the addition of suitable ceramic reinforcement particles, Mg composites are produced as a unique aspirant for wear–friction applications even in strident environments like in dry friction clutch, brake disc applications etc. Thus, improving properties of magnesium matrix composites in addition to their outstanding light weight feature can make them a possible choice for challenging tribological applications [Behnamian et al., 2022]. Main efficacy of wear resistant material depends on intrinsic and extrinsic parameters. Intrinsic parameters include type of material, microstructure and counterpart material. While extrinsic parameters are difficult to replace as they depend on equipment design. It includes applied load, wear environment, sliding speed and distance, wear environment including high temperature applications. Accordingly, investigation of elevated temperature tribological behaviour of magnesium matrix composites having thermally stable reinforcement is also a matter of inquisitiveness for researchers. However, magnesium and its alloys have notable restrictions when utilised in elevated-temperature applications. Such restrictions are primarily originated from the material's elemental properties, including its low melting point and susceptibility to creep. Due to this, magnesium is inappropriate in applications requiring long-term structural soundness (integrity) in elevated-temperature environment. Thus, the current investigation tries

to remit the mentioned research gap through examining the tribological performance of AZ31-B_4C composites at elevated temperatures.

6.2 Experimental Details

The elevated temperature dry sliding tests are performed on a pin-on-disc type tribotester (DUCOM, TR-20-M56) as per ASTM-G99-05. The test set up is shown in Figure 6.1. Pin samples (Φ6 mm x 30 mm length) are used against EN31 alloy steel disc (60 HRC, 8 mm thick and Φ160 mm) that act as counter material. It has induction heater (beryllium copper coil of 15 kVA heating capacity) for heating the counter-disc during experimentation. Noncontact type pyrometer (maximum capacity 975±1ºC) is oriented to record temperature of counter disc. Figure 6.1(a) presents tribotester view and Figure 6.1(b) depicts pin material flow (approx. at 300º C) on the wear track diameter. The pin samples are sequentially mounted perpendicularly and brought in conformal surface contact against the counter face. Force of friction is evaluated utilizing button type load cell.

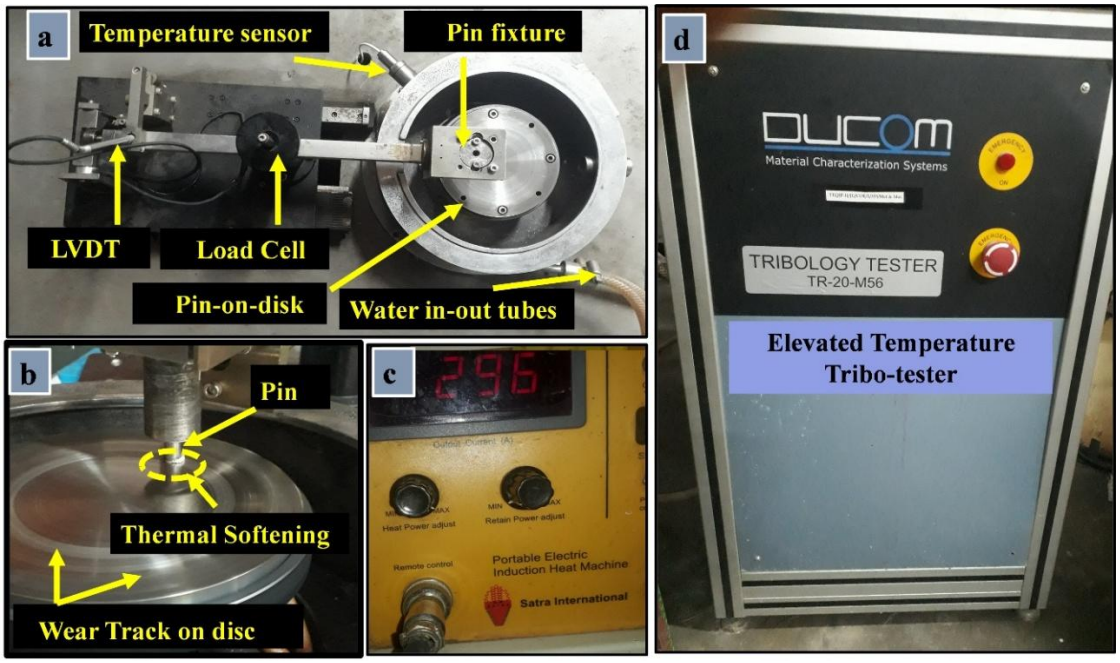

Figure 6.1: Pictorial view of (a) pin-on disc tribo-tester (top view) (b) wear track diameter and thermal softening of pin sample at elevated temp 300º C (c) temperature indicator (d) front view of elevated temperature pin-on disk

Experiments are performed for different loads (20-40 N) and constant velocity (0.4 m/s). The tribotester relates to computerized interface which helps to obtain the wear and friction characteristics. Wear rate is calculated by wear loss method and COF is directly recorded in the system. Worn surfaces of samples after scratch tests and elevated temperature tribological tests are analysed by employing Field emission scanning electron microscope (Carl Zeiss, Model: Sigma, Smart SEM).

6.3 Result and Discussion

6.3.1 Wear Behaviour

The wear rate of AZ31-B_4C MMC and AZ31 alloy under varying temperatures (50-250°C) and varying load (20N-40N) of wear testing are reported in Figure 6.2. Figure 6.2(a) depicts the wear rate variation at fixed load of 40 N as a function of temperature. It is noticed that rate of wear of AZ31 alloy and AZ31-0.5B_4C composite rise continuously with the elevated temperature at constant load. However, wear behaviour of other composite materials does not possess significant change up to a transition temperature. That specific transition temperature for AZ31-1B_4C is 100°C whereas the same for AZ31-1.5B_4C and AZ31-2B_4C is 200°C. However, Figure 6.2(a) discloses that as-cast composites exhibit better wear behaviour compared to AZ31 alloy at all testing environments and rate of wear decreases with rise in quantity of B_4C particles. Typical enhancement in wear resistance of composites is elementally due to enhanced microhardness. This is also in compliance with Archard's wear law [Archard, 1953]. For AZ31 alloy, the inter-dendritic secondary β-phase (β-$Mg_{17}Al_{12}$) possesses poor strength at high temperature and results in quick plastic deformation. Subsequently, AZ31 shows continuous increment in wear rate w.r.to increased temperature. Gokalp and Incesu (2023) reported that hot hardness of Mg-alloy deteriorates significantly with increased temperature which hinders generation of protective tribo-layer. As a result, wear resistance decreases continuously with increased temperature. The same mechanism is not adhered for composite materials. Moreover, trends of composite samples are completely different from base alloy, which may be due to the capability of composites to retain hot hardness up to a transition temperature and ability of composite samples to generate stable tribo-layer in the contact surface. Similar phenomenon is observed in literature [Sunu surendran and Gnanavelbabu, 2021; Gokalp and Incesu, 2023; Labib et al.,2016]. Most of mentioned literatures identified the lower rate of wear of composite correlated to pure alloy at elevated temperature. It was further

mentioned that improved hardness and strength levels of composites could cause more constrained flow of matrix and resist plastic deformation of matrix.

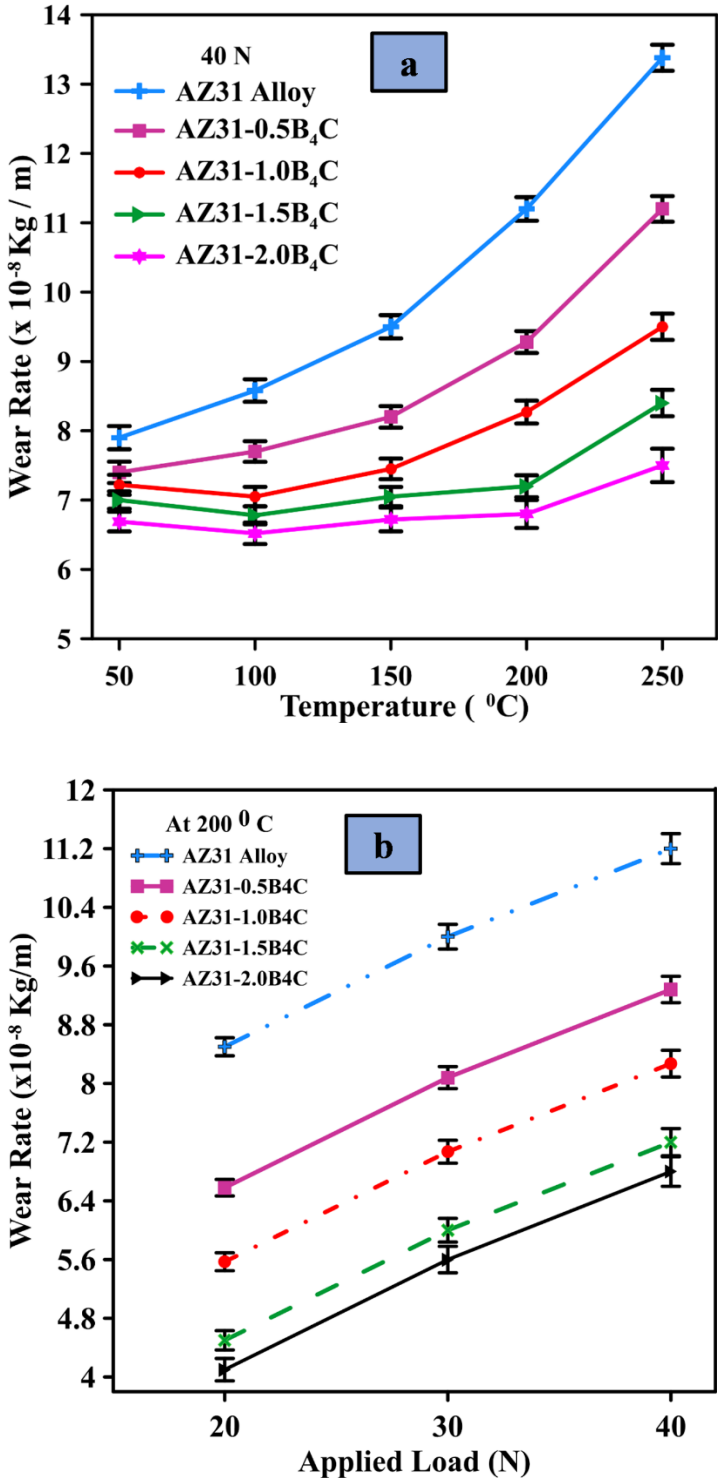

Figure 6.2: (a) Wear rate versus temperature (b) Wear rate versus applied load

Figure 6.2(b) represent the tribological behaviour of AZ31-B_4C composites and AZ31 alloy under varying loads (20N-40N) at elevated temperature of 200^0 C. Wear rate shows linear increment with the increase in applied load for all materials. Highest wear rate is depicted at 40 N whilst lowest wear rate at 20 N for all materials. Moreover, AZ31 alloy exhibit highest wear rate and AZ31-2.0B_4C possesses lowest wear rate at all experimental conditions. Furthermore, it is identified that all composite material exhibits improved resistance to wear compared to monolithic alloy. Increment of wear rate expeditiously with rise in enforced load advocates that a transition in nature of wear (mild to severe) happens. However, this transition is more prominent for base matrix while this transition diminishes due to incorporation of B_4C particles. Similar trend is reported in other literature [Labib et al., 2016; Gokalp and Incesu, 2023]. Typically, presence of B_4C particles in AZ31 matrix effectively restricts the deformation and improves hot hardness which in turn enhances wear resistance. Thus, all composites show comparatively lower wear rate than AZ31 alloy.

6.3.2 Friction Behaviour

Figure 6.3(a) illustrates the correlation between temperature and friction coefficient (COF) of AZ31 matrix and AZ31-B_4C composites. Friction characteristics are reported at 40 N load against varying temperatures (50-250^0C). It is observed from Figure 6.3(a) that COF shows modest decreasing trend as compared to increasing temperatures for both AZ31 alloy and MMCs. However, composite material shows improved friction behaviour compared to base alloy at all conditions. Similar observation is also present in literature [Surendran and Gnanavelbabu, 2021; Mansouri et al., 2022]. This reduction of COF may be attributed to generation of stable tribo-oxide layer due to frictional heating in between contacting surfaces. At high temperature and load, generated heat energy at the interfaces amidst sliding softens the pin surface, making local shearing of the asperity contact at the interface simpler. Consequently, thermal softening decreases friction at the contact surface. Gokalp and Incesu (2023) have detected similar tribological behaviour of magnesium-based materials at elevated temperature.

Figure 6.3(b) depicts the variation of COF w.r.to applied load at elevated temperature of 200^0C. It is depicted that COF decreases continuously with increasing load. However, the gradient of AZ31 alloy is slightly different from composites. For AZ31 alloy, gradient of COF line is sharp throughout the loading region while the same for composites are sub-divided into two regions. The gradient of line between 20N-30N is steeper while the same for 30N-40N is moderate. In low load region (20N-30N), effect of friction heating is lower, and condition of contact surface is better which provides more resistance resulting in steeper slope. On the other

hand, in high load region (30N-40N), thermal softening becomes conspicuous which reduces the friction resistance in between contact surfaces. As a result, counter asperities can easily invade the sample surface. Consequently, COF becomes lower. Similar phenomenon is reported in literature by Banerjee et al. (2019c) for AZ31-WC nanocomposites.

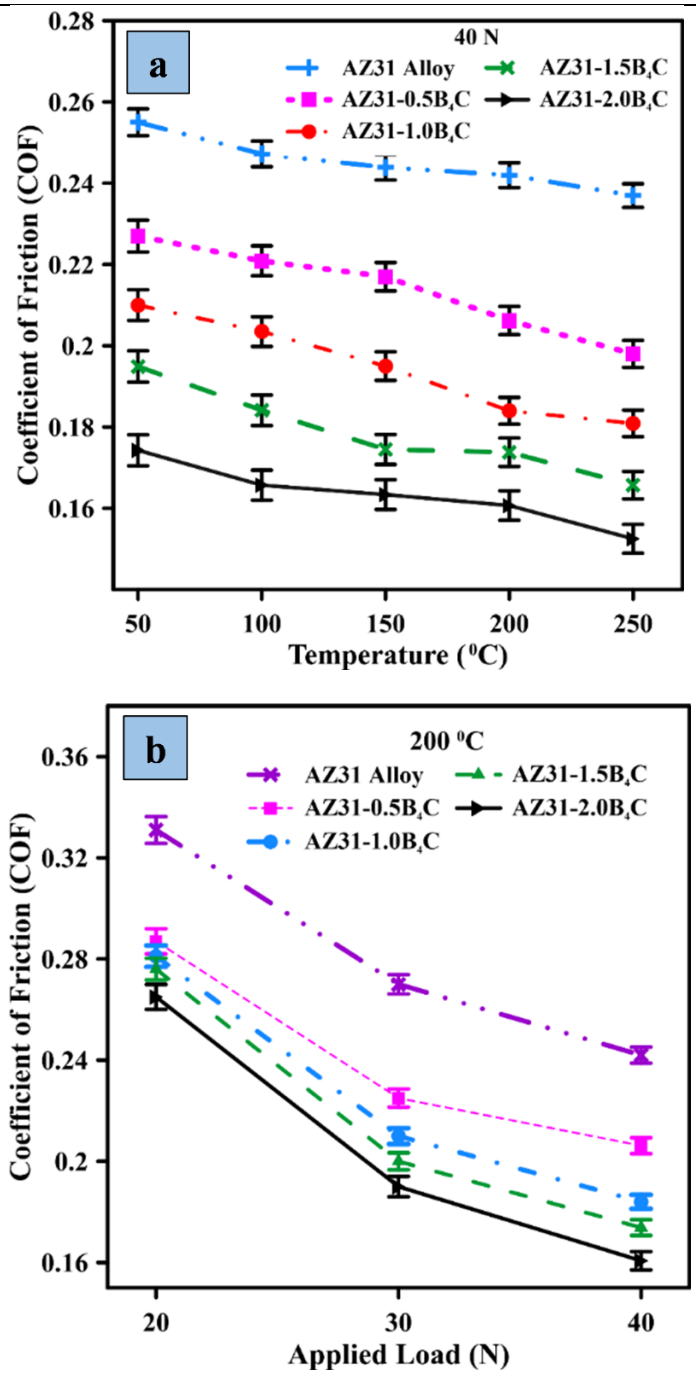

Figure 6.3: (a) Coefficient of friction versus temperature (^{0}C) (b) Coefficient of friction versus applied load (N)

6.3.3 Wear Mechanism

It is obvious from wear and friction behaviour that samples have encountered different wear mechanism during experimentation under different conditions. To examine those probable wear mechanisms, samples are investigated under FESEM. Figure 6.4 depicts the wear track of AZ31-2B_4C composite experimented under different temperatures (50-250^{0}C) at 40N load. Worn surface morphology at 50^0 Cin Figure 6.4(a) depicts series of abrasive grooves which indicates ploughing as dominant mechanism at lower temperature. Along with abrasive wear, oxidative and delaminated wear are identified over worn-out surface. Worn out oxide debris over the surface signifies the domination of oxidative and abrasive wear. Sign of delamination in the wear track is typically because of combined eventualities of temperature and high load. Moreover, presence of oxidized debris on wear track suggests the existence of oxide tribo-layer in between pin surface and counter-body. Similar phenomenon is observed by Banerjee et al. (2019c) and Zafari et al. (2014). At 100^{0}C (Figure 6.4(b)), moderately smoother surface and work hardened layers are observed.

Presence of work hardened layer justifies the prevention of sample surface from major change in wear rate as this tribo-layer protects the pin surface. In wear track of sample tested at 150°C in Figure 6.4(c), depicts flow of material, crack initiation and sign of delamination. Flow of material suggests the happening of thermal softening of sample surface. Further sliding carried out at 200°C as mentioned in Figure 6.4(d), shows lips of flow of material, heavy delamination and deformed layers. Such mechanism happens mostly due to delamination and thermal softening of pin against counter face under high load (40 N). Moreover, sliding at 250°C in Figure 6.4(e) results in severe deformation, heavy delamination, typical adhesive craters and furrows. Thus, AZ31-2B_4C composite pin losses its strength and resistance at elevated temperature. All materials including composites experienced severe wear because of temperature rising further. The β -phase of the alloy may lose strength critically and generate plastic deformity in the base alloy after 100^{0}C. Accordingly, grain boundary sliding may have happened in between 100-250^{0}C, which notably reduce material strength [Labib et al., 2016; Banerjee et al., 2019c; Gnanavelbabu et al., 2022].

Worn surface morphology of AZ31 alloy and AZ31-2.0B_4C at constant temperature (200^{0}C) and varying load (20N and 30N) is presented in Figure 6.5. It illustrates the effect of applying load on as-cast material at elevated temperature. Worn surface of AZ31 alloy at 20N load, depicted in Figure 6.5(a) possesses sign of ploughing, craters, delaminated crack and traces of oxide debris. Worn surface of AZ31 alloy reveals delamination and abrasion as

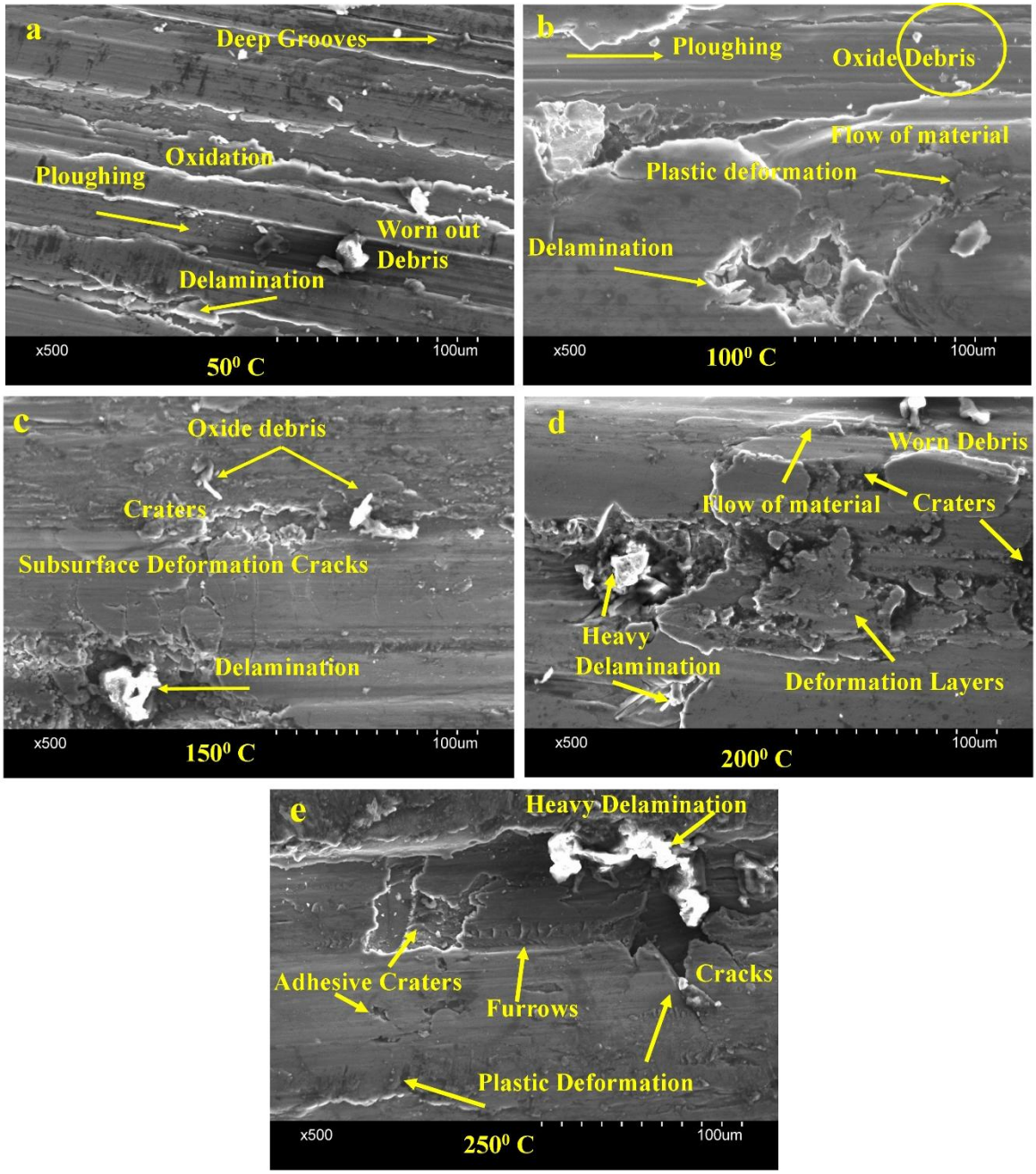

Figure 6.4: Worn surface morphology at 40 N of AZ31-2.0B_4C a) 50^0C b) 100^0C c) 150^0C d) 200^0C e) 250^0C

primary wear mechanisms, whereas worn surface of AZ31-2.0B_4C in Figure 6.5(b) mainly consists of sign of oxidation and ploughing. However, intensity of ploughing in composite sample is to a lesser degree compared to AZ31 alloy. Hence, for composites, oxidation is the primary wear mechanism for composite sample at elevated temperature and low load. With the

increase in load to 30N, worn surfaces of AZ31alloy in Figure 6.5(c) represents sever delamination, presence of furrows (adhesive patches) and cracks. Worn surface reveals that mode of wear has shifted to from mild to severe wear at 30N compared to 20N. Conversely, worn surface of AZ31-2.0B_4C in Figure 6.5(d) is mainly covered with signs of oxidation and mechanically mixed layer. Additionally, it is also found that the wear surface of AZ31-2.0B_4C is less damaged compared to base alloy. Typically, composite samples possess much higher hardness and better load carrying capacity correlated to base alloy. Thus, composite sample shows lower wear than base alloy. Archard's wear law agrees with this finding [Archard, 1953]. Additionally, the presence of compacted mechanical mixed layer (MML) in composite helps in protecting the pin surface. Mansouri et al. (2022) have shown that MML noticeably affect the contact conditions and rates of wear. This may be attributed to increased hardness and stiffness of MML in comparison to the substrate.

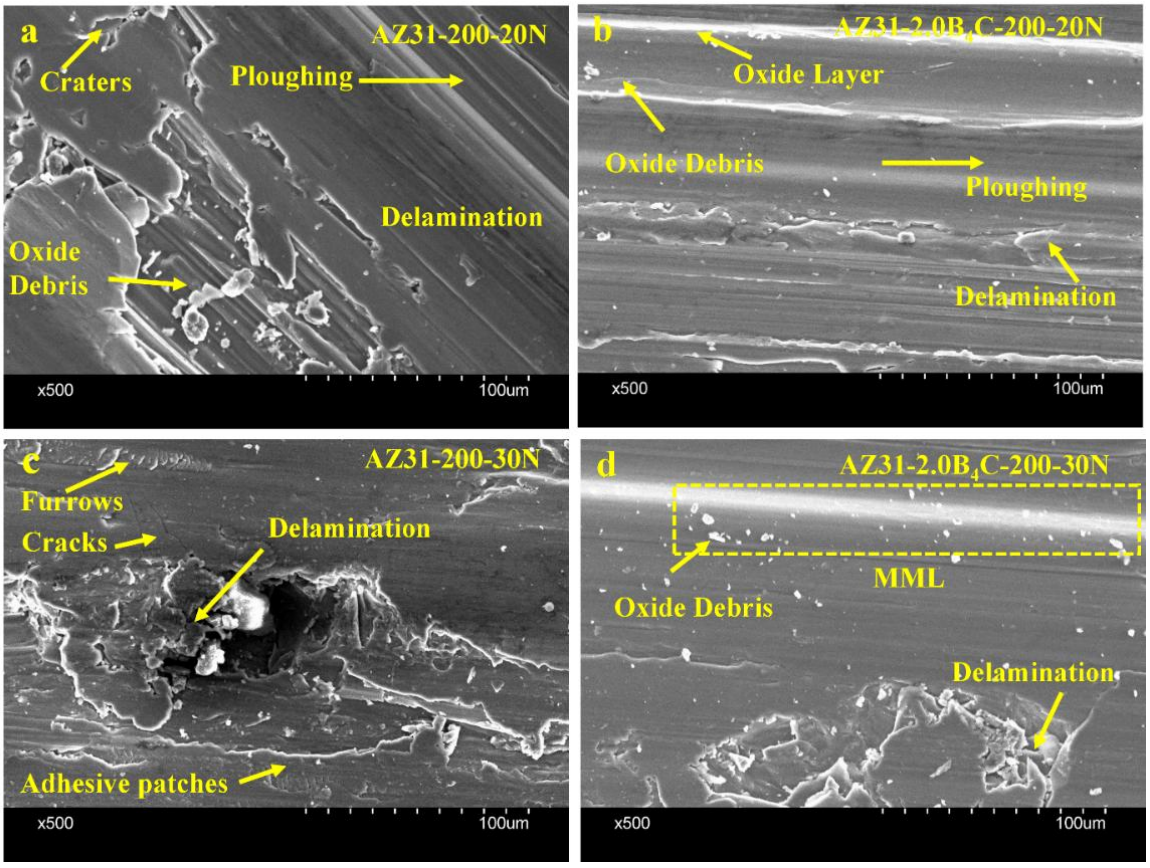

Figure 6.5: Worn surface morphology tested at 200^0C and varying load: a) AZ31 alloy at 20 N b) AZ31-2.0B_4C at 20 N c) AZ31 alloy at 30 N d) AZ31-2.0B_4C at 30 N

6.4 Summary

In the current chapter, elevated temperature behaviour of AZ31-B_4C composite is investigated. Scrutiny of elevated temperature wear behaviour of AZ31-B_4C is of immense importance to recognise its usage in different practical applications. AZ31-B_4C composites are fabricated through ultrasonic vibration assisted stir casting process by reinforcing varying amount of boron carbide (0.5-2 wt. %) in AZ31 alloy. AZ31 alloy possesses around two times more wear rate than AZ31-2B_4C at high temperature zone. Enhancement in applied load results in higher rate of wear for all samples. Although, composite samples show enhanced wear resistance at all testing conditions mainly due to presence of oxide and mechanical mixed layer. This layer effectively increases the load bearing capacity of magnesium matrix due to presence of B_4C ceramic reinforced phase. COF also reduces with elevation in temperature and reinforcement amount for all experimental conditions.

Chapter 7

Corrosion Behaviour

7.1 Introduction

In this chapter, influence of boron carbide (B_4C) particles on the corrosion behaviour of magnesium metal matrix composite is examined. As mentioned earlier, AZ31- B_4C composites are fabricated through ultrasonic vibration assisted stir casting process by reinforcing varying amount of boron carbide (0.5-2 wt. %) in AZ31 alloy. Electrochemical corrosion tests are carried out on AZ31-B_4C composites in 3.5 % NaCl solution. Corrosion morphology of the samples is scrutinized under SEM and EDAX.

Extensive scrutiny of literature as presented in Chapter 1 reveals that Mg-MMCs do not follow any particular trend so far as corrosion characteristics are concerned. Esmaily et al. (2016) fabricated AZ91-SiC composites by rheocasting technique and reported that AZ91-SiC MMCs are more susceptible to corrosion than monolithic alloy due to interfacial reaction in MMC, impurity in SiC particles and lesser degree of protective character of β-$Mg_{17}Al_{12}$. On the other hand, Ganguly et al. (2020) reinforced SiC nano particles in magnesium alloy (AZ91D) through squeeze casting and reported that AZ91D-2SiC possesses better corrosion resistance than magnesium base alloy in NaCl solution. Recently, Banerjee et al. (2021a) investigated corrosion characteristics of AZ31-WC-Gr nanocomposites and reported that AZ31-2WC-Gr possesses better corrosion resistance compared to base alloy. Existing literature reveals the corrosion characteristics of Mg based MMCs decide the acceptability of the material for varied applications involving corrosive environments. However, research on corrosion characteristics of Mg-B_4C is not unfolded yet. Thus, the present chapter tries to scrutinize the corrosion characteristics of AZ31-B_4C composites which are synthesized through ultrasonic vibration associated stir casting technique. In this study, corrosion characteristics of AZ31-B_4C composites are evaluated in 3.5% NaCl solution. Corrosion characteristics are examined by performing electrochemical impedance spectroscopy (EIS) and potentiodynamic polarization tests. After corrosion tests, transition of corrosion morphology of corroded samples is also examined using SEM and EDS spectra.

7.2 Experimental Details

Corrosion performance of AZ31 alloy and AZ31-B_4C composites are examined in 3.5% NaCl solution (electrolytic solution) at room temperature. The experiments are carried out using three electrodes with a potentiostat (Gill AC, ACM Instruments, UK). Potentiostat set up used to determine the corrosion performance of all samples through potentiodynamic polarization (PP) test and electro-chemical impedance spectroscopy (EIS). Magnesium alloy and composite samples of specific size (10 mm x 15 mm x 15 mm) act as working electrode,

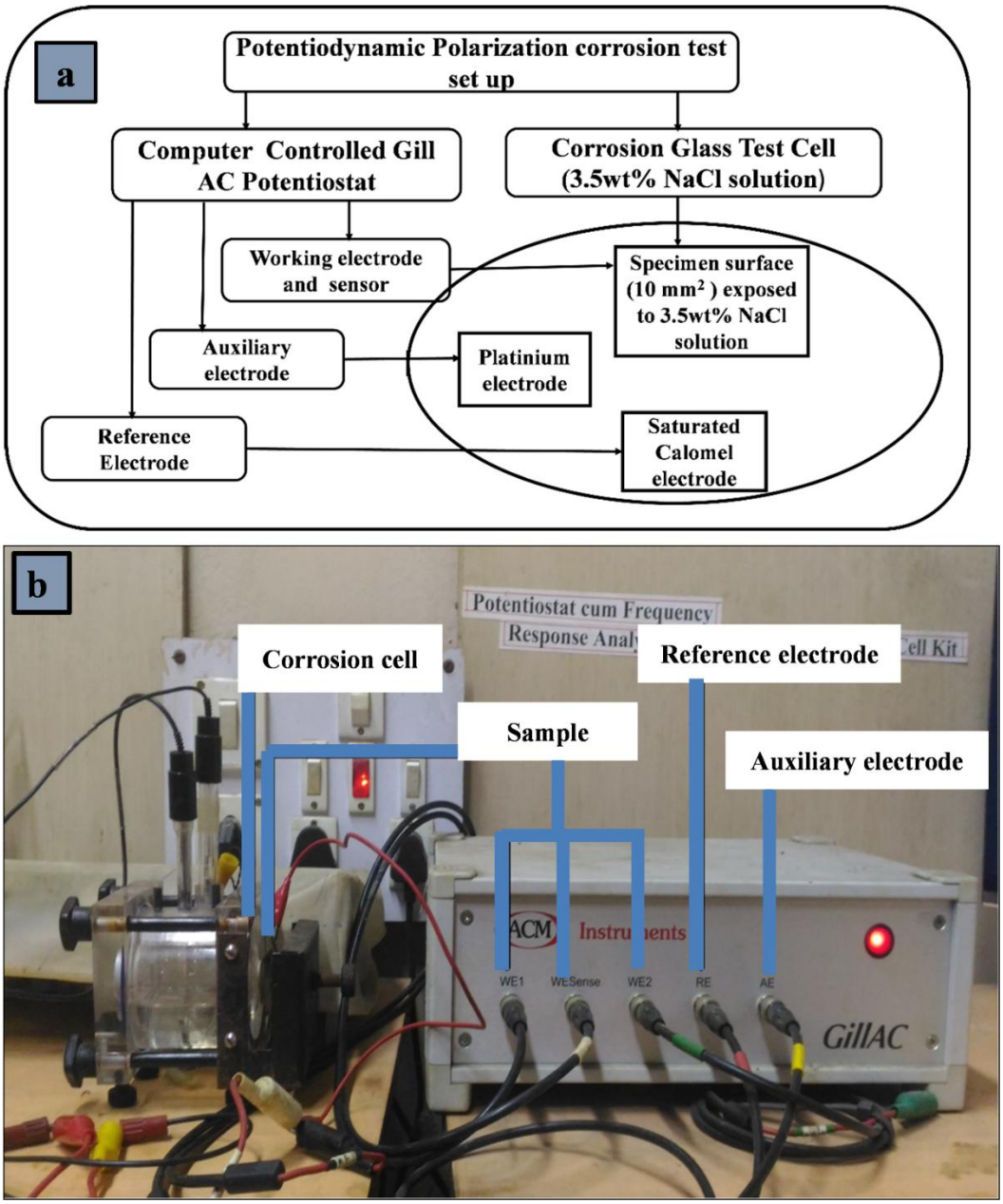

Figure 7.1: (a) Flowchart of corrosion test, (b) Pictorial view of corrosion set up

saturated calomel electrode as reference electrode as reference electrode and platinum electrode as auxiliary electrode. All electrical connections are made ready with a potentiostat. Flow chart of the experimental procedure and pictorial view of corrosion test rig is presented in Figure 7.1. A dedicated Gill AC software installed computer is interfaced with potentiostat to record all experimental data. Stable potential is typically obtained through calomel electrode and auxiliary electrode provides alternant path to connect applied current. These electrodes are placed in an electrolyte-filled glass cylinder and a 10 mm^2 area of the sample is in contact with the electrolyte solution. Afterwards, the system is kept in that condition for 15 min to get stabled and settled down the OCP (open circuit potential). The interfaced computer controls, the potentiostat and scrutinizes obtained curves with the help of installed Gill software. Potentiostat helps to obtain output curves such as Tafel plot and Nyquist plot. Extrapolations of anodic as well as cathodic parts of Tafel plot generate values of output parameters [corrosion potential (E_{corr}) and current density (I_{corr})]. Corrosion tests are controlled between two potential +250 mv and -250 mv and scan rate of 1 mV/s in both directions. Similarly, EIS results generate detailed data of corrosion characteristic of examined samples by providing values of different parameters.

7.3 Result and Discussion

7.3.1 Corrosion Test

Corrosion test includes two studies: (1) Potentiodynamic Polarization study (PP) and (2) Electrochemical Impedance Spectroscopy study (EIS), explained in subsequent sections. PP test performed to determine corrosion behaviour of material in corrosive environment. It establishes a relation between corrosion potential (E_{corr}) and corrosion current density (I_{corr}) for each material. This graphical relation developed is known as polarization curve or Tafel plot. Tafel plot actually controls the sweeping voltage and measures the resulting current. The current behaviour provides the insight into the electrochemical process happening on the surface of materials. Similarly, EIS study is dynamic and non-destructive technique to assess corrosion rate and corrosion mechanism. EIS actually compute impedance (opposite to current) of electrochemical system. In this study, gill ac voltage is applied to samples in electrolyte (3.5% NaCl) solution. Current trend is estimated across the range of frequencies from mHz to KHz. All results are graphically interpreted in the form of Nyquist plot.

7.3.1.1 Potentiodynamic Polarization Study

Evaluation of corrosion behaviour is very important to understand the durability of any material. In this study corrosion behaviour of AZ31-B_4C composites are evaluated by conducting potentiodynamic polarization study, i.e., Tafel plot and EIS study, i.e., Nyquist plot. Tafel plot of AZ31 alloy and AZ31-B_4C composites are shown in Figure 7.2(a). Tafel plot shows the relation between corrosion potential (E_{corr}) and corrosion current density (I_{corr}) for each material. Tafel plots mainly consist of cathodic and anodic regime. Hydrogen evolution is the main electrochemical reaction of cathodic regime whereas anodic part attributes dissolution of magnesium. Thus, study of anodic regime is more important to understand corrosion behaviour as well as corrosion morphology of AZ31 alloy and AZ31-B_4C composites in electrolytic solution. Figure 7.2(a) discloses that wt. %B_4C and corrosion performance is not showing a linear trend. Literature reveals that such a trend is mainly because of variation in scanning responses of cathodic as well as anodic regime for different amount of reinforcement. Hence, proper evaluation of E_{corr} and I_{corr} values is highly essential for each Tafel curve. Corrosion current density and potential values can be obtained from extrapolation of Tafel plots. Results obtained are presented in Table 7.1.

Table 7.1: Electrochemical corrosion parameters of base alloy and composites

Samples	Material	I_{corr} (mA/cm^2)	E_{corr} (V)
A	AZ31 Alloy	0.0007915	-1.5745
B	AZ31-0.5 B_4C	0.0004996	-1.6251
C	AZ31-1.0 B_4C	0.0004067	-1.5043
D	AZ31-1.5 B_4C	0.0004896	-1.6499
E	AZ31-2.0 B_4C	0.0004944	-1.5683

It is observed in literature for obtaining better corrosion characteristics, lowest value of I_{corr} and highest value of E_{corr} is desirable [Banerjee et al., 2019b; Banerjee et al., 2021a]. Table 7.1 discloses that AZ31- 1.0 B_4C is most corrosion resistant material followed by AZ31-2.0B_4C, AZ31, AZ31-0.5B_4C and AZ31-1.5B_4C. Table 7.1 also shows that corrosion potential of AZ31 is -1.5745 V in electrolytic solution (3.5% NaCl) whereas the same for AZ31-1B_4C is -1.5043 V. Values of corrosion potential yields that incorporation of 1 wt.% of B_4C significantly enhances corrosion resistance of AZ31 alloy. Moreover, E_{corr} values of AZ31-0.5B_4C, AZ31-

1.5B_4C and AZ31-2.0B_4C are -1.6251 V, -1.6499 V and -1.5683 V respectively. This result attributes that corrosion resistance decreases when 0.5% and 1.5 wt.% of B_4C are fortified in AZ31 alloy. Figure 7.2(a) also discloses an abrupt increase in current density values after a transition point for every sample. This nature is mainly due to initiation of pitting and severe corrosion. But slope of that sudden increment is comparatively slower for AZ31-1B_4C and AZ31-2B_4C than AZ31, AZ31-0.5B_4C and AZ31-1.5B_4C.

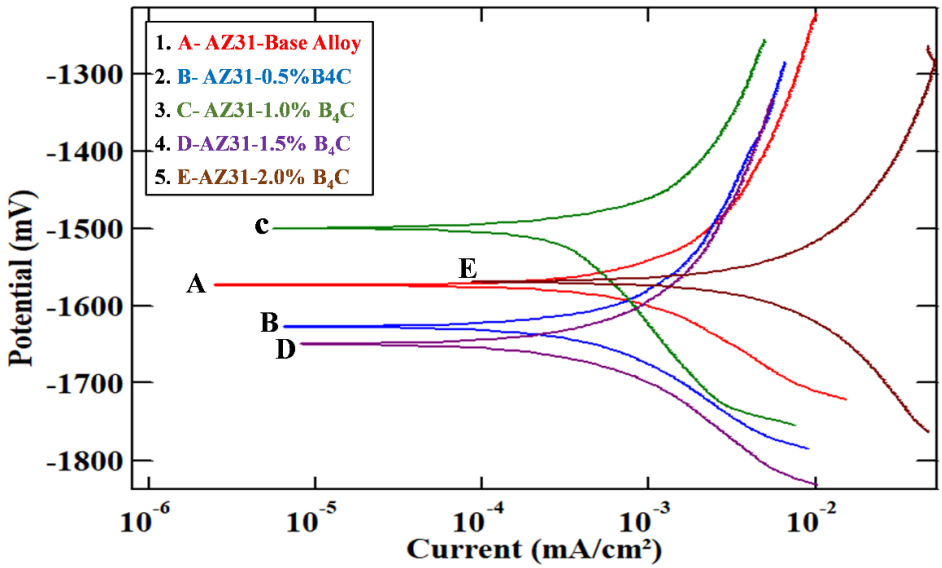

(a)

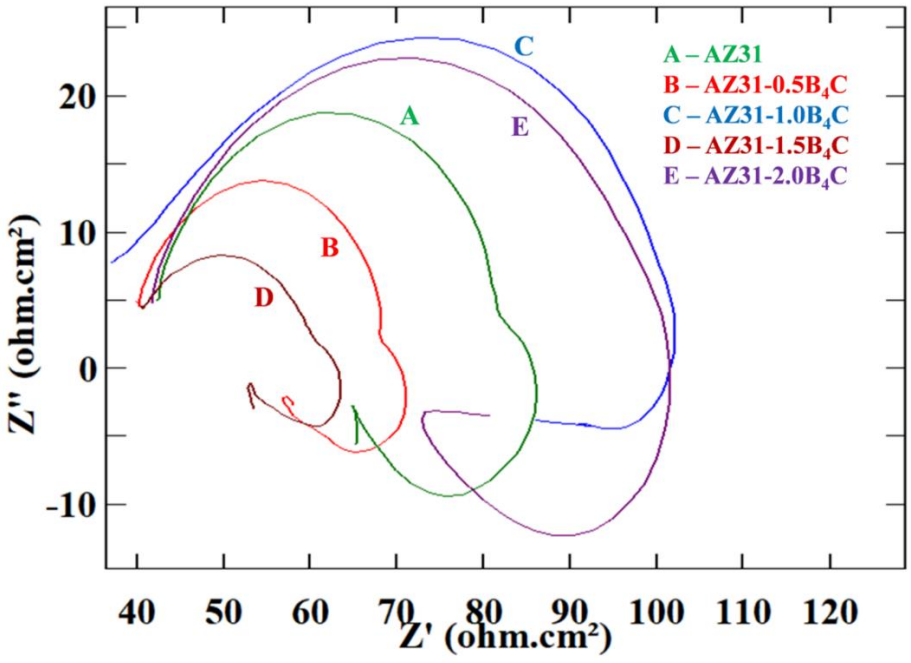

(b)

Figure 7.2: (a) Tafel plot, (b) Nyquist plot

7.3.1.2 Electrochemical Impedance Spectroscopy Study

Figure 7.2(b) depicts Nyquist plot of EIS study of AZ31 and AZ31- B_4C composites in 3.5% NaCl solution. EIS study is conducted with ±250 mV potential in both directions. All the obtained EIS plots consist of one high and one medium frequency capacitive semicircle along with one low frequency inductive loop. It is also observed in Figure 7.2(b) that nature of EIS plots is almost same for all materials except diameter. Similar nature is also observed by Turhan et al. (2011) and Falcon et al. (2011). The literature reveals that polarization resistance is directly related to diameter of capacitance loop and higher value yields greater corrosion resistance. [Turhan et al., 2011; Pathak et al., 2010; Song et al. 2016; Thirumalaikumarasamy et al., 2014; Wang et al., 2008]. Accordingly, it can be inferred from Figure 7.2(b) that AZ31-1.0B_4C exhibit higher corrosion resistance followed AZ31-2.0B_4C, AZ31 alloy, AZ31-0.5B_4C and lastly AZ31-1.5B_4C. Literature reveals that capacitive loop having higher frequency explains interfacial condition between surface and electrolyte whereas medium frequency capacitive loop signifies ion diffusion between produced film and material interfaces. Low frequency inductive loop signifies the presence of electrolyte diffusion at material–film interfaces resulting localized corrosion [Bakhsheshi et al., 2017; Kavimani et al., 2017]. Moreover, Nyquist plot depicted in Figure 7.2(b) implies that the incorporation of 1.0 and 2.0 wt. % B_4C particles increases the diameter of capacitive semicircle significantly compared to AZ31 alloy. Thus, it can be interpreted that more protective surface film has formed at materials – electrolyte interface with increasing value of impedance which helps to protect the material surface from corrosive attack. On the other hand, incorporation of 0.5 and 1.5 wt.% B_4C results in decrease in diameter of capacitive arc and produces prominent inductive loop due dominance of anodic potential. It is also found that size of capacitive arcs getting diminished with increased anodic potential which is an indication of electrolyte diffusion resulting attack of corrosive ions on sample surface. EIS plot is analysed through best fit semicircle method using Gill software. Finally, the order of corrosion potential for materials can be summarized as AZ31-1.0B_4C, AZ31- 2.0B_4C, AZ31, AZ31-0.5B_4C and AZ31-1.5B_4C. Thus, it can be attributed that AZ31-1.0B_4C is most corrosion resistance material among tested materials.

7.3.2 Corrosion Morphology

SEM micrographs of corroded surfaces of AZ31 alloy and AZ31-B_4C composites are presented in Figure 7.3. Visual inspection of SEM micrographs of corroded surfaces shows non uniform corrosion products. SEM micrographs depict presence of voluminous volcano like

deposits on corroded surface. Similar observations are also reported in literature [Kavimani et al., 2017; Ascencio et al., 2014]. Figure 7.3 also depicts cracks at corroded surface. Literature reveals that these cracks are mainly formed due to dehydration of deposited layers at atmospheric condition [Bakhsheshi et al., 2017]. Typically, these cracks provide safe passage to electrolyte solution to reach the matrix surface and expedite the corrosive attack. Accordingly, corrosion behaviour of AZ31 and AZ31-B_4C composites can be directly correlated with the nature and number of cracks [Turan et al., 2017; Banerjee et al., 2019b]. It is obvious from Figure 7.3 that surfaces of AZ31-1B_4C and AZ31-2B_4C contains smaller number of cracks compared to AZ31 alloy). Moreover, addition of 0.5wt.% and 1.5wt.% of B_4C forms pits and larger cracks. This observation is correlated with corrosion rate of base alloy and composites. Similar observations are noted by Ganguly et al. (2020) and Wang et al. (2008). Corrosion morphology of AZ31 alloy and AZ31-B_4C composites are further analysed by performing energy dispersive x-ray spectroscopy (EDS) study of corroded surfaces. SEM micrographs of corroded surfaces are mainly comprised of porous inside layer along with loosely bonded outside layers. EDS spectra of corroded surface of AZ31 and AZ31-B_4C composites are presented in Figure 7.4 depicts main elements of corroded surfaces as Mg and O. Percentages of Mg and O are maintaining atomic ratio around 2:1 which yields formation of either magnesium oxide (MgO) or magnesium hydroxide [Mg $(OH)_2$]. Literature also supports the formation of MgO and Mg $(OH)_2$ in corroded layers. The magnesium di-hydroxide layer acts as filter/barrier to electrolyte solution trying to percolate the surface of matrix material. Thus, Mg $(OH)_2$ prolongs the serious effect of corrosion [Song et al., 2016; Banerjee et al., 2021a]. Banerjee et al. (2019b) elucidated electrochemical reaction of magnesium alloy and its composites under corrosive environment. The dissolution mechanism in NaCl expressed through following reactions as:

$$Mg + 2H_2O \rightarrow Mg(OH)_2 + H_2 \quad (7.1)$$

$$Mg(OH)_2 + 2Cl^- \rightarrow MgCl_2 + 2OH^- \quad (7.2)$$

In Figure 7.4, presence of peak of chlorine is also noticed and noticeable change in percentage of chlorine is also present. Literature yields that chlorine peak in EDS spectra signifies formation of $MgCl_2$ in corroded layers. EDS spectra of AZ31, AZ31-1B_4C and AZ31-2B_4C shows reduced intensity of chlorine peak whereas larger intensity of chlorine is present for AZ31-0.5B_4C and AZ31-1B_4C. The presence of high amount of chlorine may speed up corrosion process as chlorine ion has tendency to percolate through the cracks on corroded layer

and spoil the surface of matrix metal. Percentage of chlorine remains in the order of AZ31-1B_4C < AZ31-2B_4C < AZ31 < AZ31-0.5B_4C < AZ31-1.5B_4C. Same order is also observed in crack generation in SEM micrographs. Thus, it is obvious that aggressive Cl^- ion infiltrates through those cracks and disturbs the sample surface. Similar observations are also reported in literature [Banerjee et al. (2019b); Thirumalaikumarasamy et al. (2014)].

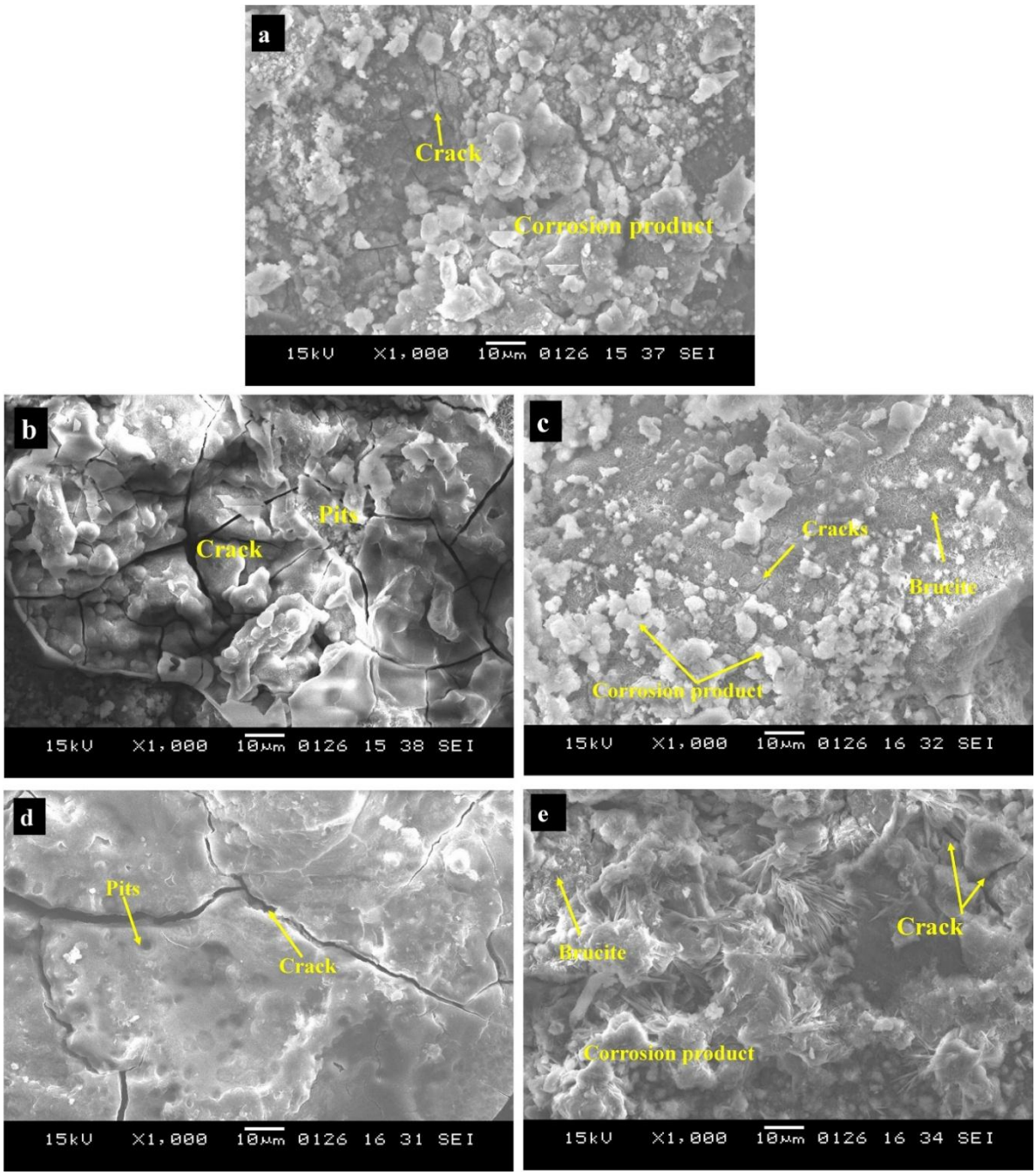

Figure 7.3: SEM images of corroded surface (a) AZ31, (b) AZ31-0.5B_4C, (c) AZ31-1B_4C, (d) AZ31-1.5B_4C, (e) AZ31-2B_4C

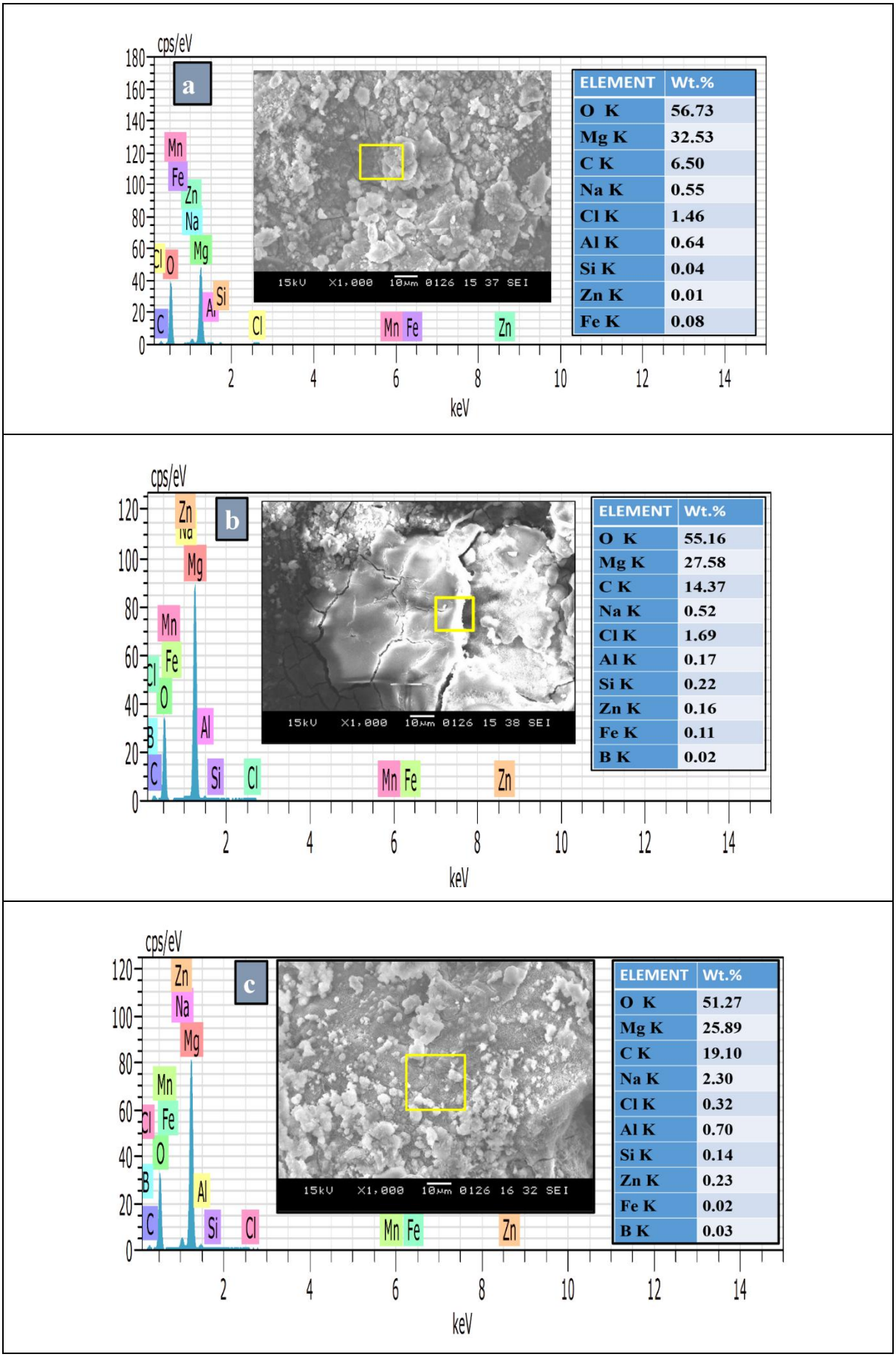
a
cps/eV
keV
Mn
Fe
Zn
Na
Mg
Cl
O
Si
Al
C
15kV X1,000 10µm 0126 15 37 SEI
ELEMENT | Wt.%
O K | 56.73
Mg K | 32.53
C K | 6.50
Na K | 0.55
Cl K | 1.46
Al K | 0.64
Si K | 0.04
Zn K | 0.01
Fe K | 0.08
b
15kV X1,000 10µm 0126 15 38 SEI
O K | 55.16
Mg K | 27.58
C K | 14.37
Na K | 0.52
Cl K | 1.69
Al K | 0.17
Si K | 0.22
Zn K | 0.16
Fe K | 0.11
B K | 0.02
B
c
15kV X1,000 10µm 0126 16 32 SEI
O K | 51.27
Mg K | 25.89
C K | 19.10
Na K | 2.30
Cl K | 0.32
Al K | 0.70
Si K | 0.14
Zn K | 0.23
Fe K | 0.02
B K | 0.03

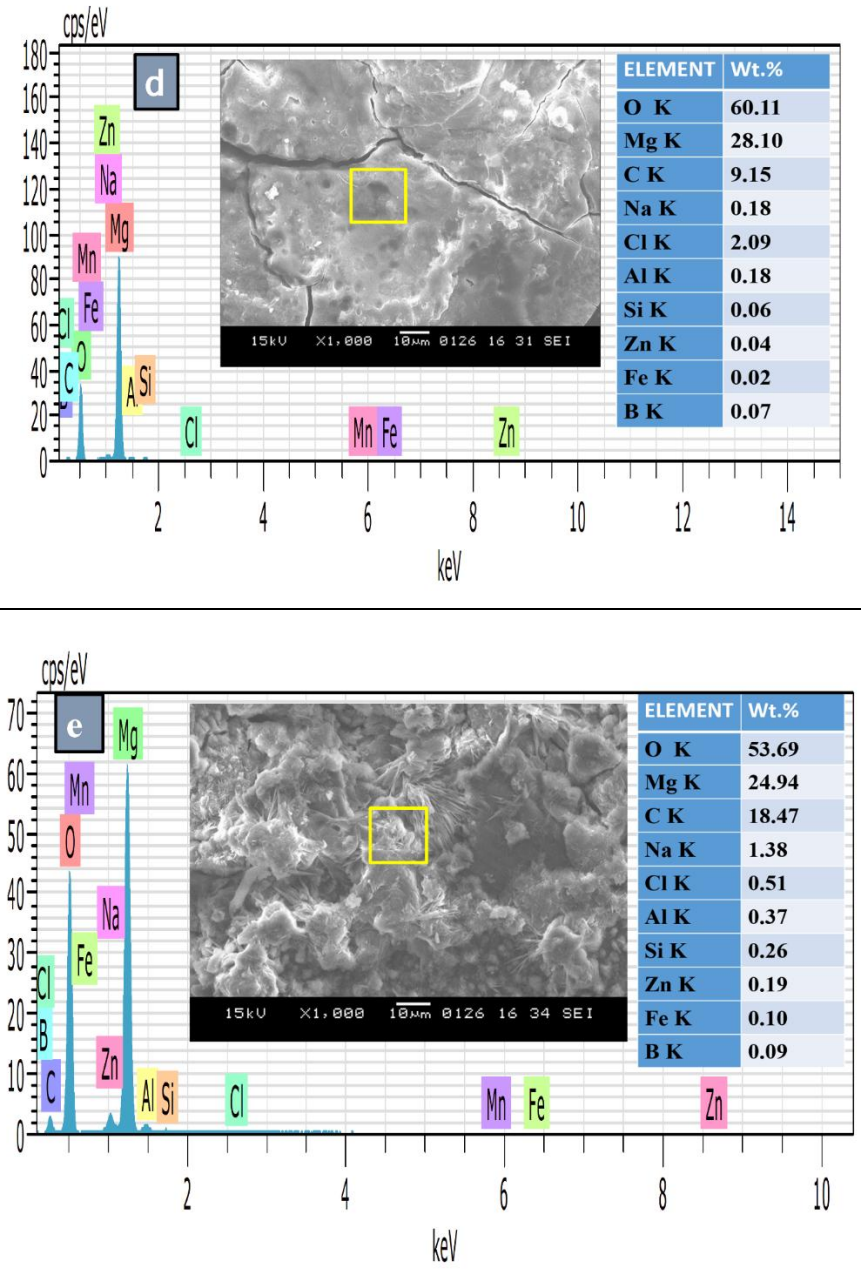

Figure 7.4: EDS spectra of corroded surface a) AZ31, b) AZ31-0.5B_4C, c) AZ31-1.0B_4C, d) AZ31-1.5B_4C, e) AZ31-2.0B_4C

7.4 Summary

In the current study, corrosion behaviour of base alloy and developed composites is investigated using potentiodynamic polarization test and electrochemical impedance spectroscopy (EIS). Tafel extrapolation analysis reveals that AZ31- 1.0 B_4C is most corrosion resistant material followed by AZ31-2.0B_4C, AZ31, AZ31-0.5B_4C and AZ31-1.5B_4C. The electrochemical impedance spectroscopy (EIS) also ascertains that AZ31-1.0 B_4C has higher value of impedance.

Chapter 8

Nanoindentation and Scratch Resistance Characteristics

8.1 Introduction

A broad range of applications of Mg based MMCs has raised the demand for typical analytical tools like nanoindentation test to understand the nature of deformation as well as failure by measuring elementary properties of matrix and reinforcement. Basically, nanoindentation test is a very useful technique to quantify elastic modulus and nanohardness. In this perspective, Oliver and Pharr method (1992) is widely accepted method among researchers. Banerjee et al. (2021a) have analysed the nanoindentation behaviour of magnesium matrix composite containing WC reinforcement. It was noticed that the incorporation of ceramic reinforcement significantly controls the elastic modulus and nano-hardness of composites.

Moreover, the scratch resistance of a material is of equal importance. Scratch test typically helps to achieve sufficient flexibility for various applications by changing tip characteristics (kinetics and material) in both single and multiple systems. In this context, the examination of the scratch resistance of Mg-MMC is of immense importance. But few literatures are available on the scratch resistance behaviour of Mg-MMCs. Recently, Banerjee et al. (2019d) have examined scratch resistance of AZ31-WC nanocomposites and concluded that Mg-MMC have highest scratch resistance under all loading conditions. Kumar et al. (2018) have evaluated wear and friction properties of Mg-0.4Ce-ZnO/Y_2O_3 nanocomposites using scratch tests at different loads. It was reported that mechanical and tribological performance of ZnO reinforced composites is quite satisfactory and better than Y_2O_3 reinforcement.

From comprehensive review of existing literature, it is comprehended that methodical study on nanoindentation test and scratch test of Mg-MMCs is scare. Power trains, pistons, steering shaft, housings, brake components and transmission cases are some applications, where MMCs can be utilized. Current investigation tries to remit that research gap by examining the mechanical and tribological performance of AZ31-B_4C composites by carrying out scratch and nanoindentation tests. Effect of addition of varying quantities of B_4C particles on nano-hardness and elastic modulus is computed by conducting nanoindentation tests following the constant indentation depth technique. Effects of varying ramp load and amount

of B_4C on scratch characteristics (COF and wear) are scrutinized. Finally, worn surface morphology of scratch tests is thoroughly examined through FESEM micrographs to identify possible mechanism of wear.

8.2 Experimental Details

8.2.1 Nanoindentation Test

Nanoindentation helps to examine mechanical properties of as-cast materials. In the current study, a nanoindentation tester (NHTX-55-0019, CSM) having Berkovic indenter is used. Berkovic indenter is selected because of its flexibility to quantify nano-hardness as well as elastic modulus. The pictorial view of nanoindentation set up is presented in Figure 8.1. The nanoindentation tester is attached with a computerized setup having preloaded Nanotest Platform software. This test is conducted by using CSM method (Continuous stiffness measurement) which assists to systematically collect load-displacement dataset. Constant depth (400 nm) technique is exercised to conduct tests. Constant loading-unloading rate of 10 mN/min is maintained while hold time is 2 s.

Figure 8.1: Pictorial view of Nanoindentation set up

8.2.2 Scratch Test

Scratch tester (TR-101-IAS) pictorial view presented in Figure 8.2. Scratch tests of as-cast samples are performed in a scratch tester (TR-101M4, DUCOM) following ASTM G171-03. During scratch tests, diamond tip indenter (Flank angle = 120°, R = 200 µm, Hemispherical) is used and force-controlled scratches are brought into existence by imposing progressive loading on stylus. A CCD camera is also attached to the experimental setup. The CCD camera helps to record the scratches for further review. For experimentation, starting load is considered as 20N and continued to three different loads 30N, 40N and 50N. Each experiment is performed five times in a sample maintaining an offset of 0.25 mm each and average of successive runs is considered. Snapshots of scratches are recorded with the help of Scarview software. Finally, scratch width is measured using SEM micrographs to evaluate wear depth and wear volume loss.

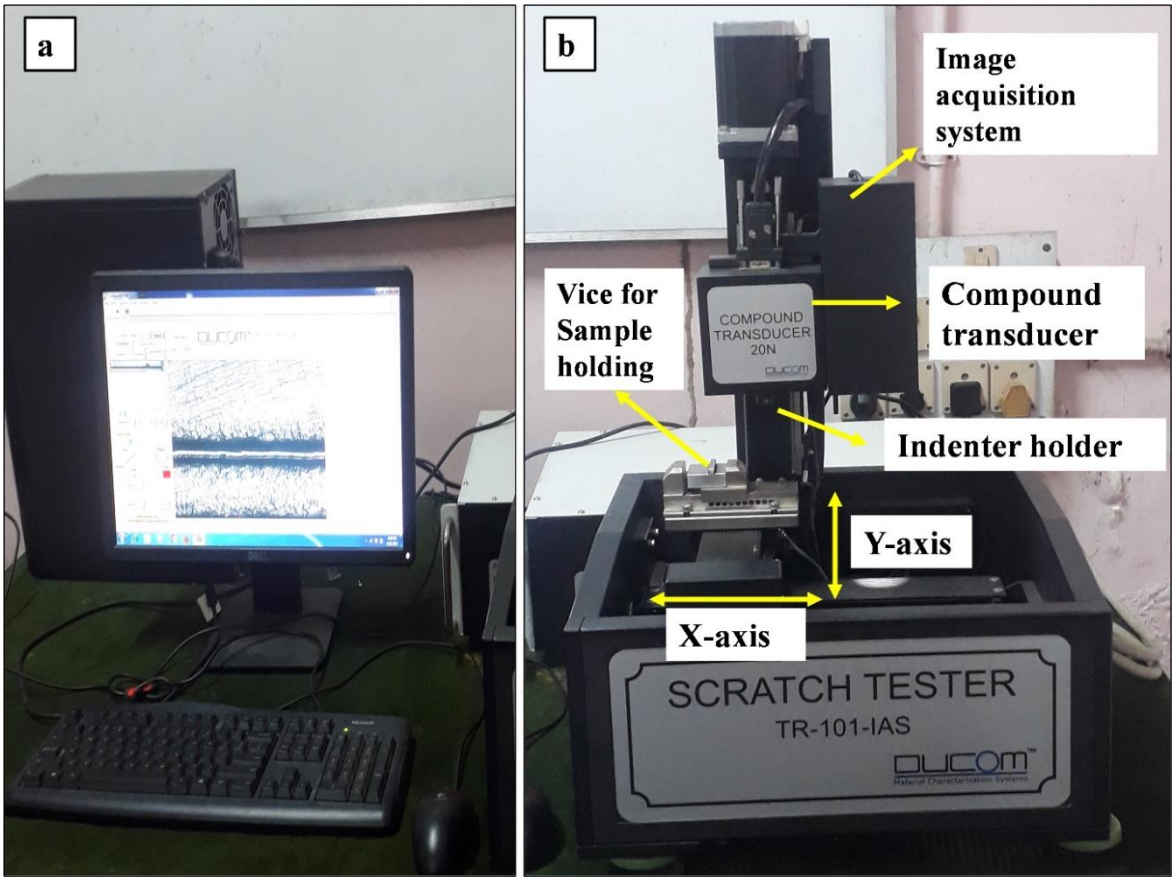

Figure 8.2: Pictorial view of scratch tester (TR-101-IAS)

8.3 Result and Discussion

8.3.1 Nanohardness and Elastic Modulus

Nanoindentation experiments of AZ31 alloy and AZ31-B_4C MMCs are conducted to evaluate elastic modulus and nano-hardness. Load-displacement plot acquired from nanoindentation tests of as-cast samples is presented as Figure 8.3. Mentioned figure depicts the nature of load-displacement curve as like elastic-plastic material without any pop-in effect.

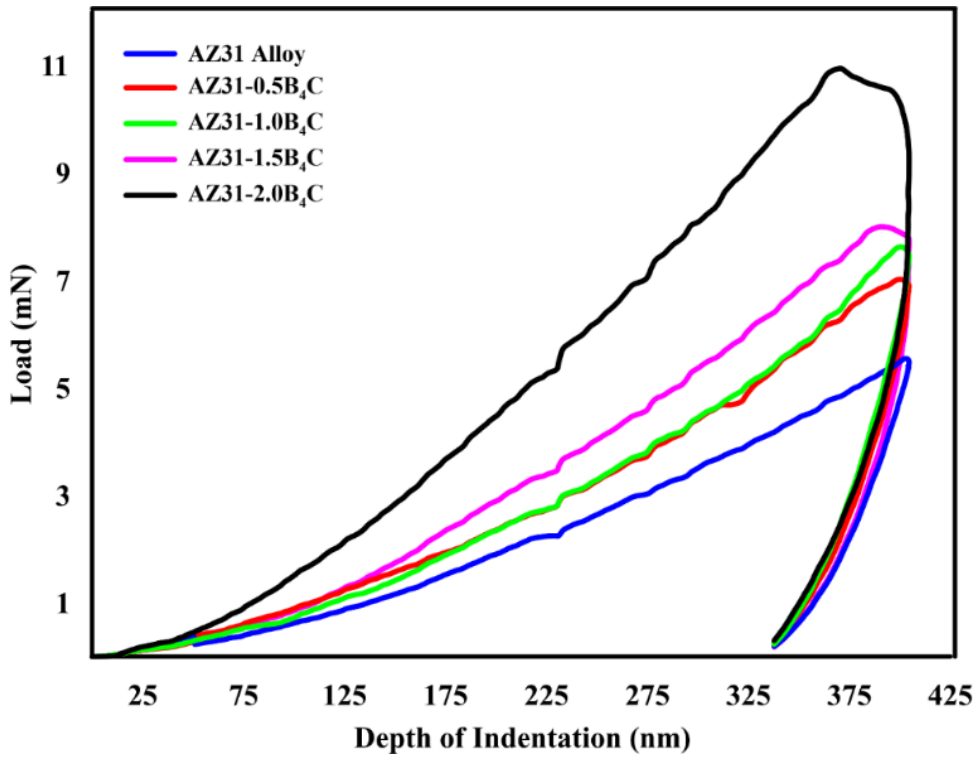

Figure 8.3: Load-displacement curve of Nanoindentation test

The force required for indentation enhanced significantly with increase in wt.% of B_4C particles. Meanwhile elastic modulus and nanohardness are found by inspecting load-displacement curve following Oliver-Pharr method [Oliver and Pharr, 1992]. Nanohardness values (H) are obtained from contact area (A_p) and applied load (F_{max}) considering equation (8.1) [Banerjee et al., 2021a; Lucca et al., 2010].

$$H = \frac{F_{max}}{A_p} \tag{8.1}$$

Reduced elastic modulus is computed using equation (8.2) given as:

$$E_r = \frac{\sqrt{\pi}}{2\beta}\frac{S}{\sqrt{A_P}} \quad (8.2)$$

Where, S = stiffness, for Berkovic indenter $\beta = 1.034$ (dimensionless correction factor) [Hu and Li, 2015; Lucca et al., 2010].

In the end, Elastic modulus (E) of as-cast material is calculated from indenter Poisson's ratio (ν_i= 0.07) and Young's modulus (E_i = 1411 GPa), and sample Poisson's ratio (ν_s = 0.3) following equation (8.3) [Hu and Li, 2015; Lucca et al., 2010; Shokrieh et al., 2013].

$$E = \frac{1-\nu_s^2}{\left(\frac{1}{E_r}\right)-\left(\frac{1-\nu_i^2}{E_i}\right)} \quad (8.3)$$

Table 8.1: Nanohardness and elastic modulus of AZ31 Alloy and AZ31-B_4C composites

Sl. No.	Nanohardness (GPa)	Elastic modulus (GPa)	F_{max} (mN)
AZ31 Alloy	1.775 ± 0.27	55.971 ± 3.14	6.83
AZ31-0.5B_4C	1.934 ± 0.21	63.009 ± 1.94	7.79
AZ31-1.0B_4C	2.037 ± 0.24	64.916 ± 2.15	7.87
AZ31-1.5B_4C	2.045 ± 0.43	66.857 ± 1.87	10.61
AZ31-2.0B_4C	3.519 ± 0.31	71.071 ± 2.21	11.15

Computed nano-hardness and elastic modulus of AZ31-B_4C MMNCs and AZ31 alloy are presented in Table 8.1. It discloses that nano-hardness and elastic modulus of AZ31 alloy enhanced by 98.25% and 27% respectively due to incorporation of 2 wt.% of B_4C. Noticeable improvement in these properties are primarily due to uniform scattering of B_4C particles in AZ31 alloy without any significant cluster formation. Similar phenomenon is reported in literature [Khandelwal et al. 2017; Aruna et al., 2025].

8.3.2 Scratch Analysis

Scratch behaviour of AZ31-B_4C composites and AZ31 alloy are experimentally evaluated under three ramp loads of 30N, 40N and 50N. Width of scratch after each successful tests are evaluated using SEM micrograph. Scratch width measurement procedure is shown in Figure 8.4(a). For brevity, stitched optical images for AZ31-1.0B4C is also shown in Figure 8.4(b) at ramp load. Variation of scratch width of as-cast samples w.r.to applied ramp load is presented in Figure 8.5, which clearly depicts the effect of ramp loading on scratch width. Scratch width

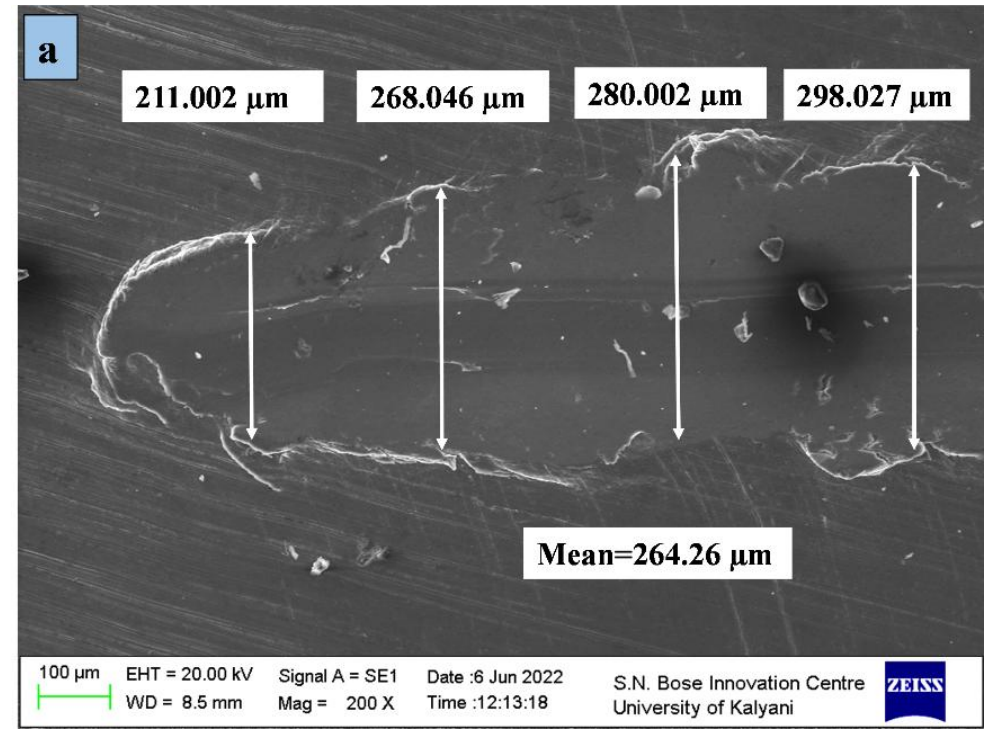

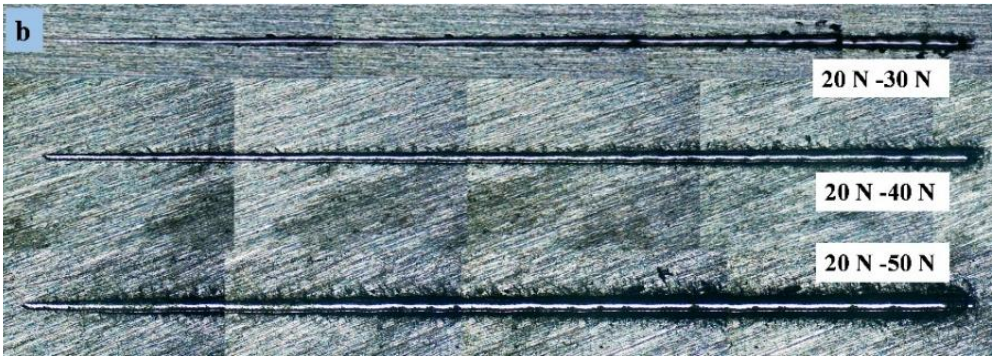

Figure 8.4: a) Scratch width measurement, b) Stitched optical images of the scratches on AZ31-1B_4C at ramp load (Left to right)

widens simultaneously with increase in enforced load. Figure 8.5 also discloses that AZ31 alloy has maximum scratch width and AZ31-2B_4C composite has minimum scratch among all as-cast materials. Typically, this behaviour is analogous with microhardness values of AZ31 alloy and AZ31-B_4C composites. Successful fortification of reinforcement in base matrix resists dislocation movement and reduce grain size which in turn increases microhardness values. This phenomenon enhances load carrying capacity and generates Orowan strengthening effect [Kumar et al. 2018]. Enhanced load-carrying capacity and improved hardness of composite samples provides protection against scratch which results in reduced scratch width of composite

samples. This finding is in accordance with existing document [Banerjee et al., 2019d; Banerjee et al., 2021c].

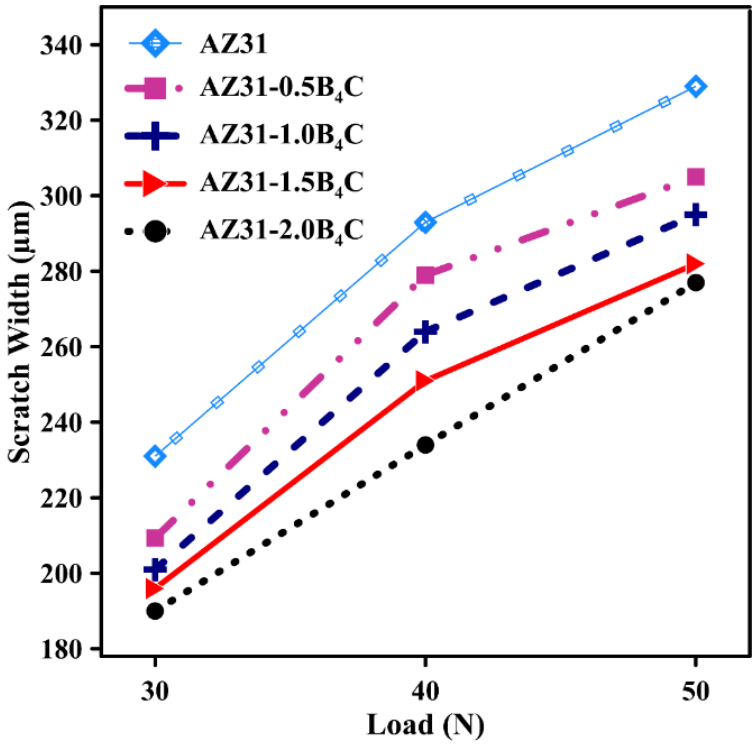

Figure 8.5: Effect of applied load on scratch width of AZ31 alloy and AZ31-B_4C composites

Figure 8.6(a) show the result of enforced load on COF of AZ31 alloy and AZ31-B_4C MMCs. Figure 8.6(a) depicts that COF of as-cast materials increases continuously w.r.to applied load. It is also found that COF increases with rise in wt.% of reinforcement. Enhancement in COF indicates that the scratch force increases with increase in B_4C content. In current investigation although width of scratch reduces with enhancement in wt.% of B_4C, scratch force enhances. As specification of indenter is same for all materials, it can be said that dissipated energy of scratch is more for AZ31-B_4C composites compared to AZ31 matrix. This can be justified by strengthening phenomenon attributed to the incorporation of B_4C particulates in AZ31 matrix. Higher dissipated energy leads towards higher COF value. Similar phenomenon is noticed previously [Banerjee et al., 2021a; Kumar et al., 2018]. Traction force of as-cast samples for 30N load at different time interval is presented in Figure 8.6(b). While Figure 8.6(c) shows the relation between frictional force and applied load on as-cast samples. Typically, traction coefficients are analogous to friction coefficients.

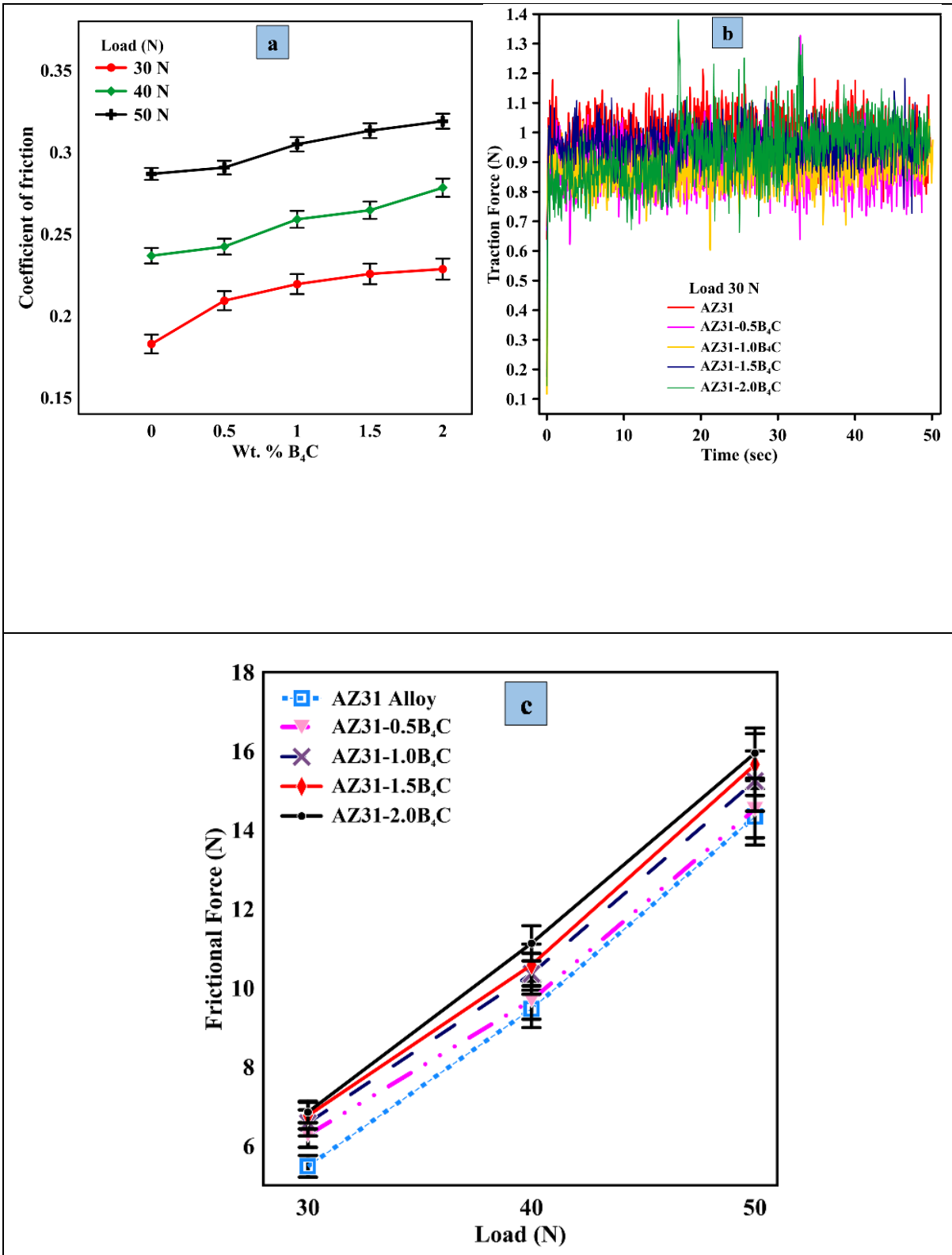

Figure 8.6: a) COF versus wt.% of B_4C at varying load, b) Traction force versus time (sec) for 30N load, (c) Frictional force versus applied load

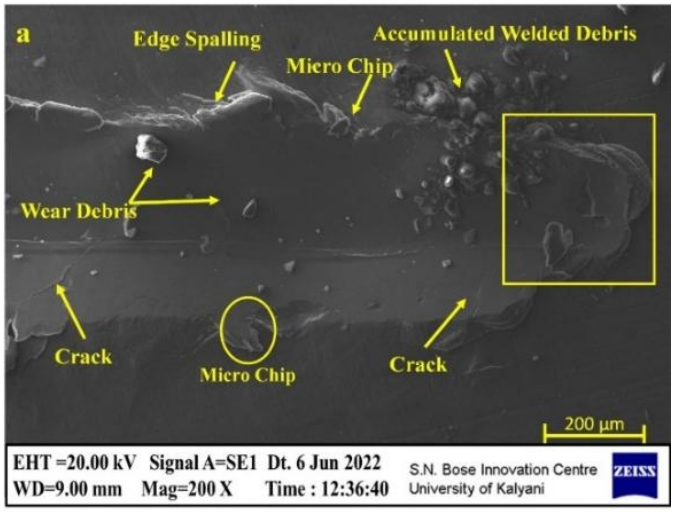

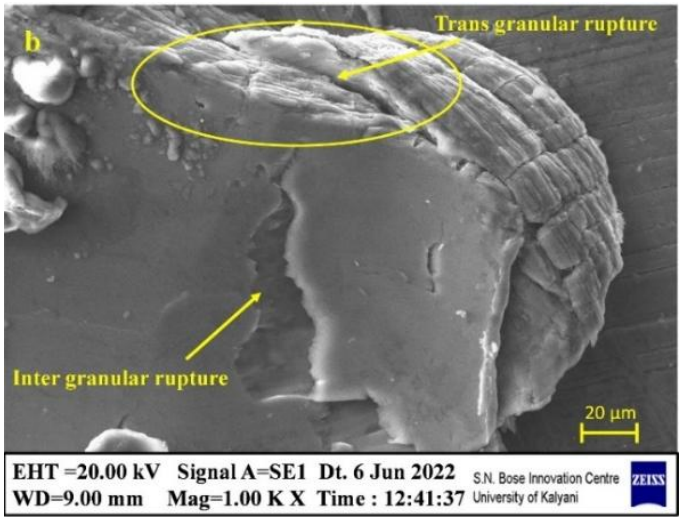

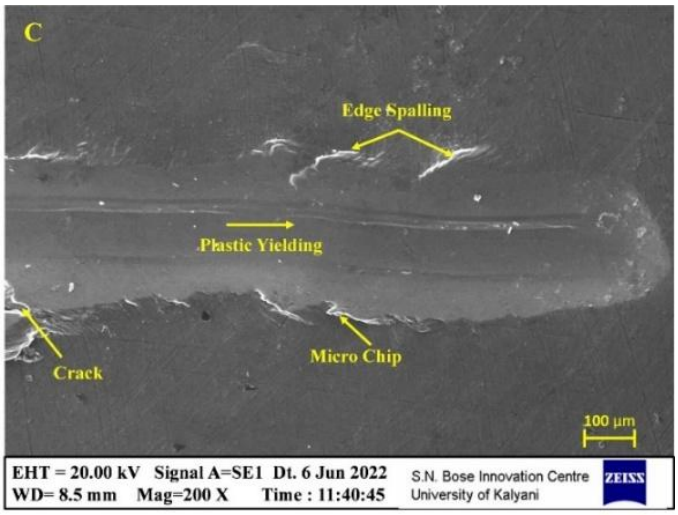

Figure 8.7 SEM micrograph of scratch surface (a) AZ31 alloy (low magnification), (b) AZ31 alloy (high magnification), and (c) AZ31-2B_4C composite

Scratch surfaces are further investigated under SEM to examine possible scratching mechanisms of AZ31 alloy and AZ31-B_4C MMNCs. For brevity, SEM micrographs of casted materials tested at 50N load are presented in Figure 8.7. Figure 8.7(a) displays the low magnification (200X) SEM micrograph of base alloy while Figure 8.7(b) shows the high magnification (1000X) SEM micrograph of AZ31 alloy (marked zone). Figure 8.7(a) depicts edge spalling, cracks, micro-cracks and welded chips on scratch track. Additionally, some quantities of welded debris are accumulated at the tip of scratch track which justifies the happening of ploughing. Banerjee et al. (2019d) reported similar observations for AZ31-WC composites. High magnification SEM micrograph depicts presence of trans granular rupture and intergranular rupture both. These phenomena are cataclysmic for any structural material. These ruptures are mainly generated due to thermal stress along with higher stress concentration. Presence of these ruptures signifies plasticity as dominant mechanism. Figure 8.7(c) shows SEM micrograph of scratch track of AZ31-2B_4C composite. Scratch track consists of sign of ploughing, edge spalling and micro-chip. These are typical sign of abrasive mechanism of wear. Such behaviour was observed by Banerjee et al. (2019d) for AZ31-WC composites.

8.4 Summary

Conforming to different practical applications, scrutiny of mechanical behaviour, nanoindentation and scratch characteristics is of immense importance. Consequently, varying wt.% of B_4C particles (0-2%) are fortified in AZ31 base alloy using USC technique. AZ31 alloy and AZ31-B_4C composites are subjected to scratch and nanoindentation tests. AZ31-2B_4C possesses 98.25% and 27% enhancement in nano-hardness and elastic modulus, respectively. Scratch width shows reducing trend with increase in quantity of reinforcement and incremental trend with intensifying applied load. AZ31 alloy concedes maximum wear while AZ31-2B_4C has minimum wear. COF during scratch operation increases moderately proportional to the increase in content of reinforcement and load both. SEM micrograph of scratch track depicts that delamination and abrasion controls wear of AZ31 alloy while abrasive wear is dominant for composites.

Chapter 9

Conclusion and Future Scope

9.1 Conclusion

The theme of the present thesis is to improve tribological behaviour of magnesium alloy with the addition of ceramic reinforced phase. In that context, extensive literature review is carried out to assess the research gap. Accordingly, judicious selection of magnesium alloy (AZ31) as matrix, sub-micron size boron carbide (B_4C) particles as reinforcement and ultrasonic vibration assisted stir casting as fabrication route is made.

AZ31-B_4C composites are successfully synthesized through ultrasonic assisted stir casting route. Fabricated composites reveal refinement in grain structure due to incorporation of B_4C particles. Optical microscopy confirms the microstructure of magnesium composites and depicts the presence of typical phases like α-Mg and β-$Mg_{17}Al_{12}$. Field emission scanning electron micrographs depict refined grain structure. Energy dispersive X-ray analysis and X-ray diffraction spectroscopy spectra confirms inclusion of B_4C particles in all composites. Elemental mapping results clearly justified the homogeneous distribution of B_4C particles in AZ31 matrix. The density of composites gets improved with the addition of wt.% of B_4C with minimal porosity. As expected, microhardness of composites increases with increase in wt.% of B_4C.

Wear resistance of AZ31-B_4C composites enhances due to addition of B_4C ceramic particles in AZ31 alloy in dry sliding condition and it monotonically increases with increase in wt.% of B_4C particles. For AZ31- B_4C composites, wear rate shows increasing trend with both applied load and sliding speed. AZ31-B_4C composites yield better friction behavior than magnesium alloy but coefficient of friction increases with increase in wt.% of B_4C in composites. Worn surface morphology depicts abrasion, plastic deformation and delamination are main wear mechanisms for magnesium alloy while oxidation and abrasion are the dominant wear mechanism for AZ31-B_4C composites. However, higher speed and sliding distances brings notable changes in wear rates in case of both the base alloy and composites.

In case of abrasive sliding, wear rate of AZ31 alloy is about 1.3-1.5 times more than AZ31-2.0B4C at all experimental conditions. Wear rate reduces with increase in abrasive grit size while the same increases with increase in sliding distance. Friction behavior of composite

is significantly enhanced due to incorporation of B_4C particles in AZ31 alloy. COF values decreased with the increase in wt.% of B_4C. Examination of worn surface morphology discloses that abrasion and oxidation are dominant for composite samples.

In regard to tribological behaviour at elevated temperatures, AZ31 alloy possesses around two times more wear rate than AZ31-2B_4C at high temperature zone. Enhancement in applied load and temperature results in higher rate of wear for all samples. Although, composite samples show enhanced wear resistance at all sliding conditions. COF reduces with elevation in temperature and reinforcement amount for all experimental conditions, resulting in improved tribological performance.

Corrosion performance of AZ31-B_4C composites are carried out utilising potentiodynamic polarisation test and electrochemical impedance spectroscopy in 3.5% NaCl solution. AZ31-1.0B_4C composite shows improved corrosion behaviour than AZ31 alloy. Tafel extrapolation analysis reveals that AZ31- 1.0 B_4C is most corrosion resistant material followed by AZ31-2.0B_4C, AZ31, AZ31-0.5B_4C and AZ31-1.5B_4C. The electrochemical impedance spectroscopy (EIS) also ascertains that AZ31-1.0 B_4C has higher value of impedance.

In regards to nanoindentation behaviour, AZ31-2.0B_4C possesses 98.25% and 27% enhancement in nanohardness and elastic modulus, respectively, compared to the AZ31 base alloy. Regarding scratch resistance behaviour, scratch width reduction is noticed with increase in quantity of reinforcement and it increases with rise in applied load. Composite samples exhibit better scratch resistance at all experimental conditions. Experimental results disclose that AZ31-2.0B_4C possesses around 24% decrease in scratch width compared to AZ31 alloy. It is also observed that wear rate decreases linearly with increase in wt.% of B_4C while COF increases moderately. SEM micrograph of scratch track depicts that delamination and abrasion controls wear of AZ31 alloy while abrasive wear is dominant for composites.

It my be noted that the above conclusions and findings are applicable within selected range of operating conditions.

9.2 Future Scope

Necessity of advanced materials are continuously raising due to change in societal and legislative concern. Accordingly, research fraternity is emphasizing towards development of newer materials. In the present investigation, Mg-MMC are synthesized though ultrasonic stir casting by incorporating B_4C particles in AZ31 alloy. Tribological behaviour is mostly

investigated are under different sliding conditions including dry sliding, abrasive siding, elevated temperature, scratch indentation and nanoindentation. Corrosion characteristics are also evaluated in 3.5% NaCl solution.

In futuristic approach, it is suggested following tasks that can be performed to improvise the research. Mg-MMC can be developed by different fabrication techniques such as friction stir processing, disintegrated melt deposition technique, powder metallurgy technique etc. Mechanical properties like tensile, bending and fatigue strength may be evaluated. Similarly, other ceramic reinforcements (like Ti, ZrO_2, Si_3N_4 etc.) may be explored. For corrosion studies, other medium like NaOH and HCl can be utilised and performance in different medium can be scrutinized to understand the corrosion behaviour of magnesium composites. Abrasive sliding behaviour can be conducted for different track diameter and different abrasive grit size paper. Tribological behaviour can also be determined with the addition of solid lubricants like graphite, molybdenum disulfide. Moreover, magnesium being a bio-compatible material has potential application in orthopaedic implants. Thus, research on magnesium composites in the field of bio-medical applications is a promising area of future study.

Bibliography

- Aatthisugan, I., Murugesan, R. and Rao, T.V.V.L.N., 2023. Influence of boron carbide content on dry sliding wear performances of AZ91D magnesium alloy. Proceedings of the Institution of Mechanical Engineers, Part J: Journal of Engineering Tribology, 237(4), pp.746-756.
- Aatthisugan, I., Rose, A.R. and Jebadurai, D.S., 2017. Mechanical and wear behaviour of AZ91D magnesium matrix hybrid composite reinforced with boron carbide and graphite. Journal of Magnesium and Alloys, 5(1), pp.20-25.
- Adaveesh, B., Halesh, G.M. and Kumar, V., 2017. Investigations on dry sliding wear behaviour of B4C reinforced ZA43 alloy composites. Materials Today: Proceedings, 4(10), pp.10957-10964.
- Archard, J.F., 1957. Elastic deformation and the laws of friction. Proceedings of the royal society of London. Series A. Mathematical and Physical Sciences, 243(1233), pp.190-205.
- Archard, J., 1953. Contact and rubbing of flat surfaces. Journal of Applied physics, 24(8), pp.981-988.
- Aronson, R.B., 1995. Why dry cutting. Manuf. Eng, 114(1), pp.33-36.
- Arora, H.S., Singh, H. and Dhindaw, B.K., 2013. Wear behaviour of a magnesium alloy subjected to friction stir processing. Wear, 303(1-2), pp.65-77.
- Aruna, M., Krishnan, A.M., Nagarajan, N., Prabagaran, S., Rathinavelu, V., Kavitha, N., Parthipan, N., Mohanavel, V., Soudagar, M.E.M., Al Obaid, S. and Alharbi, S.A., 2025. Integration of Magnesium Fluoride and Nano Alumina–Silicon Carbide Actions on Properties of AZ91 Alloy Hybrid Nanocomposites. International Journal of Metalcasting, pp.1-11.
- Ascencio, M., Pekguleryuz, M. and Omanovic, S.J.C.S., 2014. An investigation of the corrosion mechanisms of WE43 Mg alloy in a modified simulated body fluid solution: The influence of immersion time. Corrosion Science, 87, pp.489-503.

- Avedesian MM & Baker H., 1999. ASM speciality handbook: Magnesium and Magnesium alloys (Vol. 274). Materials Park, OH: ASM International (ISBN: 978-0-87170-657-7).
- Aydin, F., Sun, Y., Ahlatci, H. and Turen, Y., 2018. Investigation of microstructure, mechanical and wear behaviour of B_4C particulate reinforced magnesium matrix composites by powder metallurgy. Transactions of the Indian Institute of Metals, 71(4), pp.873-882.
- Aydin, M., Koç, R. and Akkoyunlu, A., 2015. Fabrication and characterisation of Mg-nano B_4C and B composites by powder metallurgy method. Advances in Materials and Processing Technologies, 1(1-2), pp.181-191.
- Bakhsheshi-Rad, H.R., Hamzah, E., Tok, H.Y., Kasiri-Asgarani, M., Jabbarzare, S. and Medraj, M., 2017. Microstructure, in vitro corrosion behavior and cytotoxicity of biodegradable Mg-Ca-Zn and Mg-Ca-Zn-Bi alloys. Journal of Materials Engineering and Performance, 26(2), pp.653-666.
- Bakkar, A. and Neubert, V., 2007. Corrosion characterisation of alumina–magnesium metal matrix composites. Corrosion Science, 49(3), pp.1110-1130.
- Balikai, A., Adarsha, H. and Keshavamurthy, R., 2022. Microstructure and nanoindentation response of Si3N4-reinforced magnesium-based composite synthesized by powder metallurgy route. Journal of The Institution of Engineers (India): Series D, 103(1), pp.235-247.
- Banerjee, S., Poria, S., Sutradhar, G. and Sahoo, P., 2019a. Dry sliding tribological behavior of AZ31-WC nano-composites. Journal of Magnesium and Alloys, 7(2), pp.315-327.
- Banerjee, S., Poria, S., Sutradhar, G. and Sahoo, P., 2019b. Corrosion behavior of AZ31-WC nano-composites. Journal of Magnesium and Alloys, 7(4), pp.681-695.
- Banerjee, S., Poria, S., Sutradhar, G. and Sahoo, P., 2019c. Tribological behavior of Mg-WC nano-composites at elevated temperature. Materials Research Express, 6(8), p.0865c6 (1-16).
- Banerjee, S., Poria, S., Sutradhar, G. and Sahoo, P., 2019d. Nanoindentation and scratch resistance characteristics of AZ31–WC nanocomposites. Journal of Molecular and Engineering Materials, 7(03 and 04), p.1950007(1-13).
- Banerjee, S., Poria, S., Sutradhar, G. and Sahoo, P., 2020. Abrasive wear behavior of WC nanoparticle reinforced magnesium metal matrix composites. Surface Topography: Metrology and Properties, 8(2), p.025001(1-18).

- Banerjee, S., Poria, S., Sutradhar, G. and Sahoo, P., 2021a. Nano-indentation and corrosion characteristics of ultrasonic vibration assisted stir-cast AZ31–WC–graphite nano-composites. International Journal of Metalcasting, 15(3), pp.1058-1072.
- Banerjee, S., Poria, S., Sutradhar, G. and Sahoo, P., 2021b. Mg-WC nanocomposites—recent advances and perspectives. Recent Advances in Layered Materials and Structures, pp.199-228.
- Banerjee, S., Sahoo, P. and Davim, J.P., 2021c. Tribological characterisation of magnesium matrix nanocomposites: a review. Advances in Mechanical Engineering, 13(4), pp.1-39.
- Banijamali, S.M., Najafi, S., Sheikhani, A. and Palizdar, Y., 2022. Dry tribological behavior of hot-rolled WE43 magnesium matrix composites reinforced by B_4C particles. Wear, 508, pp.204487 (1-14).
- Behnamian, Y., Serate, D., Aghaie, E., Zahiri, R., Tolentino, Z., Niazi, H. and Mostafaei, A., 2022. Tribological behavior of ZK60 magnesium matrix composite reinforced by hybrid MWCNTs/B_4C prepared by stir casting method. Tribology International, 165, p.107299 (1-13).
- Bharathi, P. and Sampath Kumar, T., 2023. Latest research and developments of ceramic reinforced magnesium matrix composites—A comprehensive review. Proceedings of the Institution of Mechanical Engineers, Part E: Journal of Process Mechanical Engineering, 237(3), pp.1014-1035.
- Blawert, C., Hort, N. and Kainer, K.U., 2004. Automotive applications of magnesium and its alloys. Trans. Indian Inst. Met, 57(4), pp.397-408.
- Canakci, A.Y.K.U.T., 2011. Microstructure and abrasive wear behaviour of B_4C particle reinforced 2014 Al matrix composites. Journal of Materials Science, 46(8), pp.2805-2813.
- Casati, R., Vedani, M. 2014. Metal matrix composites reinforced by nano-particles—a review. Metals, 4(1), pp.65-83.
- Chan, W.M., Cheng, F.T., Leung, L.K., Horylev, R.J. and Yue, T.M., 1997, March. Corrosion behavior of magnesium alloy AZ91 and its MMC in NaCl solution. In proceedings of Corrosion1997, pp. 1-5.
- Chinthamani, S., Kannan, G., George, G.D., Sreedharan, C.E.S. and Rajagopal, K.S., 2020. Effect of nano B4C on the tribological behaviour of magnesium alloy prepared through powder metallurgy. Materials Science, 26(4), pp.392-400.

- Cole, G.S. and Sherman, A.M., 1995. Light-weight materials for automotive applications. Materials Characterization, 35(1), pp.3-9.
- Contreras, A., Lopez, V.H. and Bedolla, E., 2004. Mg/TiC composites manufactured by pressureless melt infiltration. Scripta Materialia, 51(3), pp.249-253.
- Dalmis R, Cuvalci H, Canakci A, Guler O. 2016. Investigation of Graphite Nano Particle addition on the Physical and Mechanical Properties of ZA27 Composites. Advanced Composites Letters. 2016; 25(2), pp.37-42.
- Das, S., Morales, A.T. and Alpas, A.T., 2010. Microstructural evolution during high temperature sliding wear of Mg–3% Al–1% Zn (AZ31) alloy. Wear, *268*(1-2), pp.94-103.
- Deng, K.K., Wu, K., Wu, Y.W., Nie, K.B. and Zheng, M.Y., 2010. Effect of submicron size SiC particulates on microstructure and mechanical properties of AZ91 magnesium matrix composites. Journal of Alloys and Compounds, 504(2), pp.542-547.
- Dey, A., and Pandey, K. M., 2015. Magnesium Metal Matrix Composites-A Review. Reviews on Advanced Materials Science, 42(1), pp.58-67.
- Dieringa, H., 2018. Processing of magnesium-based metal matrix nano-composites by ultrasound-assisted particle dispersion: A review. Metals, 8(6), pp.431.
- Domnich, V., Reynaud, S., Haber, R.A. and Chhowalla, M., 2011. Boron carbide: structure, properties, and stability under stress. Journal of the American Ceramic Society, 94(11), pp.3605-3628.
- Eder, S.J., Grützmacher, P.G., Ripoll, M.R., Gachot, C. and Dini, D., 2022. Does speed kill or make friction better? - Designing materials for high velocity sliding. Applied Materials Today, 29, p.101588 (1-13).
- Endo, M., Hayashi, T., Itoh, I., Kim, Y.A., Shimamoto, D., Muramatsu, H., Shimizu, Y., Morimoto, S., Terrones, M., Iinou, S. and Koide, S., 2008. An anticorrosive magnesium/carbon nanotube composite. Applied Physics Letters, 92(6), pp. 063105 (1-3).
- Esmaily, M., Mortazavi, N., Svensson, J.E., Halvarsson, M., Jarfors, A.E., Wessén, M., Arrabal, R. and Johansson, L.G., 2016. On the microstructure and corrosion behavior of AZ91/SiC composites produced by rheocasting. Materials Chemistry and Physics, 180, pp.29-37.
- Esmaily, M., Svensson, J.E., Fajardo, S., Birbilis, N., Frankel, G.S., Virtanen, S., Arrabal, R., Thomas, S. and Johansson, L.G., 2017. Fundamentals and advances in magnesium alloy corrosion. Progress in Materials Science, 89, pp.92-193.

- Falcon, L.A., Bedolla B, E., Lemus, J., Leon, C., Rosales, I. and Gonzalez-Rodriguez, J.G., 2011. Corrosion Behavior of Mg-Al/TiC Composites in NaCl Solution. International Journal of Corrosion, 2011(1), p.896845 (1-7).
- Friedrich, H.E. and Mordike, B.L., 2006. Magnesium Technology (Vol. 212). Springer-Verlag Berlin Heidelberg, pp.499-632.
- Funatsu, K., Fukuda, H., Takei, R., Umeda, J., &Kondoh, K., 2013. Quantitative evaluation of initial galvanic corrosion behavior of CNTs reinforced Mg–Al alloy. Advanced Powder Technology, 24(5), pp. 833-837.
- Ganguly, S., Mondal, A.K., Sarkar, S., Basu, A., Kumar, S. and Blawert, C., 2020. Improved corrosion response of squeeze-cast SiC nanoparticles reinforced AZ91-2.0 Ca-0.3 Sb alloy. Corrosion Science, 166, p.108444 (1-15).
- Gnanavelbabu, A., Surendran, K.S., Loganathan, P. and Vinothkumar, E., 2022. Effect of ageing temperature on the corrosion behaviour of UHTC particulates reinforced magnesium composites fabricated through ultrasonic assisted squeeze casting process. Journal of Alloys and Compounds, 856, p.158173(1-15).
- García-Rodríguez, S., Torres, B., Maroto, A., López, A. J., Otero, E., and Rams, J., 2017. Dry sliding wear behavior of globular AZ91 magnesium alloy and AZ91/SiC_p composites. Wear, 390, pp.1-10.
- Ghasemi, A., Penther, D. and Kamrani, S., 2018. Microstructure and nanoindentation analysis of Mg-SiC nanocomposite powders synthesized by mechanical milling. Materials Characterization, 142, pp.137-143.
- Gobara, M., Shamekh, M., and Akid, R., 2015. Improving the corrosion resistance of AZ91D magnesium alloy through reinforcement with titanium carbides and borides. Journal of Magnesium and Alloys, 3(2), pp.112-120.
- Goh, C.S., Gupta, M., Wei, J. and Lee, L.C., 2007. Characterization of high-performance Mg/MgO nanocomposites. Journal of Composite Materials, 41(19) pp.2325-2335.
- Goh, C. S., Wei, J., Lee, L. C., and Gupta, M., 2008. Ductility improvement and fatigue studies in Mg-CNT nanocomposites. Composites Science and Technology, 68(6), pp.1432-1439.
- Gokalp, I. and Incesu, A., 2023. Effect of Ca addition to the elevated temperature mechanical properties of AZ series magnesium alloys. International Journal of Metalcasting, 17(2), pp.1402-1412.

- Gopal, P.M., Prakash, K.S., Nagaraja, S. and Aravinth, N.K., 2017. Effect of weight fraction and particle size of CRT glass on the tribological behaviour of Mg-CRT-BN hybrid composites. Tribology International, 116, pp.338-350.
- Gopal, P.M., Kavimani, V. and Sudhagar, S., 2025. Evolution and recent advancements of composite materials in industrial applications. In Applications of Composite Materials in Engineering, Eds. M. Puttegowda et al., Woodhead Publishing, pp. 317-334.
- Guan, H., Xiao, H., Ouyang, S., Tang, A., Chen, X., Tan, J., Feng, B., She, J., Zheng, K. and Pan, F., 2022. A review of the design, processes, and properties of Mg-based composites. Nanotechnology Reviews, 11(1), pp.712-730.
- Guleryuz, L.F., Ozan, S., Uzunsoy, D. and Ipek, R.A.S.İ.M., 2012. An investigation of the microstructure and mechanical properties of B_4C reinforced PM magnesium matrix composites. Powder Metallurgy and Metal Ceramics, 51(7-8), pp.456-462.
- Guleryuz, L.F., Ozan, S.E.R.T.A.N., Uzunsoy, D. and Ipek, R.A.S.İ.M., 2013. Investigation of dry sliding wear behaviour of B_4C particulate reinforced Mg matrix composites. Acta Physica Polonica A, 123(2), pp.488-489.
- Gupta, M. and Seetharaman, S., 2017. Magnesium based nanocomposites for cleaner transport. Nanotechnology for Energy Sustainability, (ISBN: 9783527696109), pp.809-830,
- Gupta, M., & Ling, S. N. M., 2011. Magnesium, Magnesium alloys, and Magnesium composites. John Wiley & Sons.
- Gupta, M., Lai, M.O. and Saravanaranganathan, D., 2000. Synthesis, microstructure and properties characterization of disintegrated melt deposited Mg/SiC composites. Journal of Materials Science, 35(9), pp.2155-2165.
- Gupta, M. and Wong, W.L.E., 2015. Magnesium-based nanocomposites: Lightweight materials of the future. Materials Characterization, 105, pp.30-46.
- Habibnejad-Korayem, M., Mahmudi, R., Ghasemi, H.M. and Poole, W.J., 2010. Tribological behavior of pure Mg and AZ31 magnesium alloy strengthened by Al_2O_3 nano-particles. Wear, 268(3-4), pp.405-412.
- Haghshenas, M., Song, X., Hasannaeimi, V., Mukherjee, S. and Gupta, M., 2020. Magnesium–samarium oxide nanocomposites: Room-temperature depth-sensing nanoindentation response. International Journal of Lightweight Materials and Manufacture, 3(3), pp.217-225.

- Hamid, Z.A., Abou El-khair, M.T. and Hassan, H.B., 2011. Synthesis and protection of AM50 magnesium alloy and its composites using environmentally pretreatment electrolyte. Surface and Coatings Technology, 206(6), pp.1041-1050.
- Hashim, J., Looney, L. and Hashmi, M.S.J., 1999. Metal matrix composites: production by the stir casting method. Journal of Materials Processing Technology, 92, pp.1-7.
- Hassan, S.F. and Gupta, M., 2002. Development of ductile magnesium composite materials using titanium as reinforcement. Journal of Alloys and Compounds, 345(1-2), pp.246-251.
- Hassan, S.F. and Gupta, M., 2006. Effect of particulate size of Al_2O_3 reinforcement on microstructure and mechanical behavior of solidification processed elemental Mg. Journal of Alloys and Compounds, 419(1-2), pp.84-90.
- He, R., Gahlawat, S., Guo, C., Chen, S., Dahal, T., Zhang, H., Liu, W., Zhang, Q., Chere, E., White, K. and Ren, Z., 2015. Studies on mechanical properties of thermoelectric materials by nanoindentation. Physica Status Solidi (a), 212(10), pp.2191-2195.
- Hihara, L.H. and Kondepudi, P.K., 1993. The galvanic corrosion of SiC monofilament/ZE41 Mg metal-matrix composite in 0.5 M NaNO3. Corrosion Science, 34(11), pp.1761-1772.
- Hu, C. and Li, Z., 2015. A review on the mechanical properties of cement-based materials measured by nanoindentation. Construction and Building Materials, 90, pp.80-90.
- Idrisi, A.H. and Mourad, A.H.I., 2019. Conventional stir casting versus ultrasonic assisted stir casting process: Mechanical and physical characteristics of AMCs. Journal of Alloys and Compounds, 805, pp.502-508.
- Jiang, Q.C., Wang, H.Y., Ma, B.X., Wang, Y. and Zhao, F., 2005. Fabrication of B_4C particulate reinforced magnesium matrix composite by powder metallurgy. Journal of Alloys and Compounds, 386(1-2), pp.177-181.
- Joost, W.J. and Krajewski, P.E., 2017. Towards magnesium alloys for high-volume automotive applications. Scripta Materialia, 128, pp.107-112.
- Joost, W.J., 2012. Reducing vehicle weight and improving US energy efficiency using integrated computational materials engineering. Journal of the Minerals, Metals and Materials Society, 64, pp.1032-1038.
- Jutanaiman, S.P.H. and Syahrial, A.Z., 2020, September. Characteristics of Magnesium/B4C Reinforced Composite Fabricated by Stir Casting Method. In IOP Conference Series: Materials Science and Engineering, 924,1, p. 012020 (1-9).

- Kainer, K.U. and Mordike, B.L. eds., 2000. Magnesium alloys and their applications. Weinheim: Wiley-VCH. (ISBN: 3883551848) pp. 119-124.
- Kim, J.J. and Do, S.H., 2008. Recent development and applications of magnesium alloys in the Hyundai and Kia Motors Corporation. Materials Transactions, 49(5), pp.894-897.
- Kavimani, V., Soorya Prakash, K. and Arun Pandian, M., 2017. Influence of r-GO addition on enhancement of corrosion and wear behaviour of AZ31 MMC. Applied Physics A, 123(8), pp.1-11.
- Kaviti, R.V.P., Jeyasimman, D., Parande, G., Gupta, M. and Narayanasamy, R., 2018. Investigation on dry sliding wear behavior of Mg/BN nanocomposites. Journal of Magnesium and Alloys, 6(3), pp.263-276.
- Kaviti, R. V. P., Jeyasimman, D., Parande, G., Gupta, M., Narayanasamy, R., and Koppad, P. G., 2019. Improving the friction and wear characteristics of AZ31 alloy with the addition of Al_2O_3 nanoparticles. Materials Research Express, 6(12), p.126505, pp.1-13
- Khan, F., Hossain, N., Mim, J.J., Rahman, S.M., Iqbal, M.J., Billah, M. and Chowdhury, M.A., 2025. Advances of composite materials in automobile applications–A review. Journal of Engineering Research, 13(2), pp.1001-1023.
- Khandelwal, A., Mani, K., Srivastava, N., Gupta, R. and Chaudhari, G.P., 2017. Mechanical behavior of AZ31/Al2O3 magnesium alloy nanocomposites prepared using ultrasound assisted stir casting. Composites Part B: Engineering, 123, pp.64-73.
- Kulekci, M.K., 2008. Magnesium and its alloys applications in automotive industry. The International Journal of Advanced Manufacturing Technology, 39(9), pp.851-865.
- Kumar, A., Keerti, S., Jain, J., Sinha, S., Tekumalla, S. and Gupta, M., 2018, "Investigations of wear response of pure Mg and Mg-0.4 Ce-Y_2O_3/ZnO nano-composites using a single and repeated scratch tests," Tribology Transactions, 61(5), pp. 951-959.
- Kumar, D. and Thakur, L., 2023. Investigation on mechanical and wear performance of ultrasonic-assisted stir cast AZ91D/Al_2O_3 magnesium matrix composites. Metals and Materials International, 29(9), pp. 2767-2781.

- Kumar, D. S., Sasanka, C. T., Ravindra, K., and Suman, K. N. S., 2015. Magnesium and its alloys in automotive applications–a review. American Journal of Material Science and Technology, 4(1), pp. 12-30.
- Kumar, D., Phanden, R. K., and Thakur, L., 2021. A review on environment-friendly and lightweight magnesium-based metal matrix composites and alloys. Materials Today: Proceedings, 38, pp. 359-364.
- Kumar, K. C., Kumar, B. R., and Rao, N. M., 2022. Microstructural, mechanical characterization, and fractography of AZ31/SiC reinforced composites by stir casting method. Silicon, 14(9), pp. 5017-5027.
- Kumar, T.S., Shalini, S., Ramu, M. and Govindaraju, M., 2019. Characterisation of AZ31/ZrO_2 composites produced via stir casting. Materials Research Express, 6(11), pp.1165d1.
- Labib, F., Ghasemi, H.M. and Mahmudi, R., 2016. Dry tribological behavior of Mg/SiC_p composites at room and elevated temperatures," Wear, 348, pp. 69-79.
- Lan, J., Yang, Y. and Li, X., 2004. Microstructure and microhardness of SiC nanoparticles reinforced magnesium composites fabricated by ultrasonic method. Materials Science and Engineering: A, 386(1-2), pp.284-290.
- Lei, T., Tang, W., Cai, S. H., Feng, F. F., and Li, N. F. 2012. On the corrosion behaviour of newly developed biodegradable Mg-based metal matrix composites produced by in situ reaction. Corrosion Science, 54, pp.270-277.
- Li, N. and Zheng, Y., 2013. Novel magnesium alloys developed for biomedical application: review. Journal of Materials Science and Technology, 29(6), pp.489-502.
- Liang, C., Han, X., Su, T.F., Li, C. and An, J., 2014. Sliding wear map for AZ31 magnesium alloy. Tribology Transactions, 57(6), pp.1077-1085.
- Lim, S.C., Ashby, M.F. and Brunton, J.H., 1989. The effects of sliding conditions on the dry friction of metals. Acta Metallurgica, 37(3), pp.767-772.
- Lim, C. Y. H., Leo, D. K., Ang, J. J. S., and Gupta, M. 2005. Wear of magnesium composites reinforced with nano-sized alumina particulates. Wear, 259(1-6), pp.620-625.
- Lim, C. Y. H., Lim, S. C., and Gupta, M., 2003. Wear behaviour of SiCp-reinforced magnesium matrix composites. Wear, 255(1-6), pp. 629-637.
- Lin, R.J., Chen, R.H. and Huang, F.H., 2014. Green innovation in the automobile industry. Industrial Management & Data Systems, 114(6), pp.886-903.

- Liu, X., Jia, S. and Nastac, L., 2014. Ultrasonic cavitation-assisted molten metal processing of cast A356-nano-composites. International Journal of Metalcasting, 8(3), pp.51-58.
- Lucca, D.A., Herrmann, A.K. and Klopfstein, M.J., 2010. Nanoindentation: Measuring methods and applications. CIRP Annals, 59(2), pp.803-819.
- Lv, X., Deng, K.K., Wang, C.J., Nie, K.B., Shi, Q.X. and Liang, W., 2022. The corrosion properties of AZ91 alloy improved by the addition of trace submicron SiCp. Materials Chemistry and Physics, 286, pp.126143.
- Ma, X.L., Dong, L.H. and Wang, X., 2014. Microstructure, mechanical property and corrosion behavior of co-continuous β-TCP/MgCa composite manufactured by suction casting. Materials and Design, 56, (1980-2015), pp.305-312.
- Majzoobi, G.H. and Rahmani, K., 2020. Mechanical characterization of Mg-B_4C nanocomposite fabricated at different strain rates. International Journal of Minerals, Metallurgy and Materials, 27(2), pp.252-263.
- Mallick, P.K. ed., 2020. Materials, design and manufacturing for lightweight vehicles. Woodhead Publishing (ISBN:978-0-12-819029-6).
- Mansouri, A., Ghasemi, H.M., Yazdi, R., Mahmudi, R. and Sohi, M.H., 2022, Dry tribological behaviour of a cast Mg-Gd-Zr-Ag alloy at room and elevated temperatures. Journal of Materials Research and Technology, 18, pp.5126-5143.
- Meenashisundaram, G.K., Nai, M.H., Almajid, A. and Gupta, M., 2015. Development of high-performance Mg–TiO_2 nanocomposites targeting for biomedical/structural applications. Materials & Design 65, (1980-2015), pp.104-114.
- Meenashisundaram, G.K., Seetharaman, S. and Gupta, M., 2014. Enhancing overall tensile and compressive response of pure Mg using nano-TiB_2 particulates. Materials Characterization, 94, pp.178-188.
- Meher, A., Mahapatra, M.M., Samal, P., Vundavilli, P.R. and Madavan, S.P., 2019. Synthesis, microstructure and mechanical properties of magnesium matrix composites fabricated by stir casting. Materials Today: Proceedings, 18, pp.4034-4041.
- Mindivan, H., Efe, A., Kosatepe, A.H. and Kayali, E.S., 2014. Fabrication and characterization of carbon nanotube reinforced magnesium matrix composites, Applied surface science, 318, pp.234-243.
- Miracle, D.B., 2005. Metal matrix composites–from science to technological significance. Composites Science and Technology, 65(15-16), pp.2526-2540.

- Mohanty, P., Mahapatra, R., Padhi, P., Ramana, C.V. and Mishra, D.K., 2020. Ultrasonic cavitation: An approach to synthesize uniformly dispersed metal matrix nanocomposites—A review. Nano-Structures & Nano-Objects, 23, p.100475 (1-14).
- Moheimani, S.K., Keshtgar, A., Khademzadeh, S., Tayebi, M., Rajaee, A. and Saboori, A., 2022. Tribological behaviour of AZ31 magnesium alloy reinforced by bimodal size B_4C after precipitation hardening. Journal of Magnesium and Alloys, 10(11), pp.3267-3280.
- Molinari, A., Estrin, Y. and Mercier, S., 1999. Dependence of the coefficient of friction on the sliding conditions in the high velocity range. Journal of Tribology,121(1), pp.35-41
- Mondal, A.K. and Kumar, S., 2009. Dry sliding wear behaviour of magnesium alloy-based hybrid composites in the longitudinal direction. Wear, 267(1-4), pp.458-466.
- Monish, P., Hari, K.K. and Rajkumar, K., 2023. Manufacturing and characterisation of magnesium composites reinforced by nanoparticles: a review. Materials Science and Technology, 39(15), pp.1858-1876.
- Mordike, B.L. and Ebert, T.J.M.S., 2001. Magnesium: properties—applications—potential. Materials Science and Engineering: A, 302(1), pp.37-45.
- Mussatto, A., Ahad, I.U., Mousavian, R.T., Delaure, Y. and Brabazon, D., 2021. Advanced production routes for metal matrix composites. Engineering Reports, 3(5), pp.1-25.
- Narayanasamy, P., Selvakumar, N. and Balasundar, P., 2018. Effect of weight percentage of TiC on their tribological properties of magnesium composites. Materials Today: Proceedings, 5(2), pp.6570-6578.
- Nautiyal, P., Jain, J. and Agarwal, A., 2016. Influence of microstructure on scratch-induced deformation mechanisms in AZ80 magnesium alloy. Tribology Letters, 61(3), pp.1-29.
- Nguyen, Q.B., Sim, Y.H.M., Gupta, M. and Lim, C.Y.H., 2015. Tribology characteristics of magnesium alloy AZ31B and its composites. Tribology International, 82, pp.464-471.
- Nie, K. B., Wang, X. J., Hu, X. S., Xu, L., Wu, K., & Zheng, M. Y., 2011a. Microstructure and mechanical properties of SiC nanoparticles reinforced magnesium matrix composites fabricated by ultrasonic vibration. Materials Science and Engineering: A, 528(15), pp.5278-5282.

- Nie, K.B., Wang, X.J., Wu, K., Xu, L., Zheng, M.Y. and Hu, X.S., 2011b. Processing, microstructure, and mechanical properties of magnesium matrix nanocomposites fabricated by semisolid stirring-assisted ultrasonic vibration. Journal of Alloys and Compounds, 509(35), pp.8664-8669.
- Nie, K.B., Wang, X.J., Deng, K.K., Hu, X.S. and Wu, K., 2021. Magnesium matrix composite reinforced by nanoparticles–a review. Journal of Magnesium and Alloy. 9(1), pp.57-77.
- Nie, K.B., Wang, X.J., Wu, K., Hu, X.S. and Zheng, M.Y., 2012. Development of SiCp/AZ91 magnesium matrix nanocomposites using ultrasonic vibration. Materials Science and Engineering: A, 540, pp.123-129.
- Nirala, A., Soren, S., Kumar, N. and Kaushal, D.R., 2020. A comprehensive review on mechanical properties of Al-B_4C stir casting fabricated composite. Materials Today: Proceedings, 21, pp.1432-1435.
- Nunez-Lopez, C.A., Skeldon, P., Thompson, G.E., Lyon, P., Karimzadeh, H. and Wilks, T.E., 1995. The corrosion behaviour of Mg alloy ZC71/SiCp metal matrix composite. Corrosion Science, 37(5), pp.689-708.
- Nunez-Lopez, C.A., Habazaki, H., Skeldon, P., Thompson, G.E., Karimzadeh, H., Lyon, P. and Wilks, T.E., 1996. An investigation of microgalvanic corrosion using a model magnesium-silicon carbide metal matrix composite. Corrosion Science, 38(10), pp.1721-1729.
- Oge, T.O., Oge, M., Yilmaz, V.M. and Ozdemir, F.B., 2019. Effect of B_4C addition on the microstructure, hardness and dry-sliding-wear performance of AZ91 composites produced with hot pressing. Materials and Technology, 53(3), pp.433-442
- Oliver, W.C. and Pharr, G.M., 1992. An improved technique for determining hardness and elastic modulus using load and displacement sensing indentation experiments. Journal of Materials Research, 7(6), pp.1564-1583.
- Paidar, M., Bokov, D., Mehrez, S., Ojo, O.O., Ramalingam, V.V. and Memon, S., 2021. Improvement of mechanical and wear behavior by the development of a new tool for the friction stir processing of Mg/B_4C composite. Surface and Coatings Technology, 426, p.127797 (1-13).
- Paramsothy, M., Chan, J., Kwok, R. and Gupta, M., 2012. Al_2O_3 nanoparticle addition to commercial magnesium alloys: multiple beneficial effects. Nanomaterials, 2(2), pp.147-162.

- Pardo, A., Merino, M.C., Coy, A.E., Viejo, F., Arrabal, R. and Feliú Jr, S., 2008. Influence of microstructure and composition on the corrosion behaviour of Mg/Al alloys in chloride media. Electrochimica Acta, 53(27), pp.7890-7902.
- Pardo, A., Merino, S., Merino, M.C., Barroso, I., Mohedano, M., Arrabal, R. and Viejo, F., 2009. Corrosion behaviour of silicon–carbide-particle reinforced AZ92 magnesium alloy. Corrosion Science, 51(4), pp.841-849.
- Pathak, S.S., Blanton, M.D., Mendon, S.K. and Rawlins, J.W., 2010. Investigation on dual corrosion performance of magnesium-rich primer for aluminum alloys under salt spray test (ASTM B117) and natural exposure. Corrosion Science, 52(4), pp.1453-1463.
- Ponappa, K., Aravindan, S. and Rao, P.V., 2013. Influence of Y_2O_3 particles on mechanical properties of magnesium and magnesium alloy (AZ91D). Journal of Composite Materials, 47(10), pp.1231-1239.
- Prabhu, R.T., 2016. Effect of synthetic graphite and activated charcoal addition on the mechanical, microstructure and wear properties of AZ 81 Mg alloys. Journal of Materials Research and Technology, 5(3), pp.259-267.
- Prakash, K.S., Balasundar, P., Nagaraja, S., Gopal, P.M. and Kavimani, V., 2016. Mechanical and wear behaviour of Mg–SiC–Gr hybrid composites. Journal of Magnesium and Alloys, 4(3), pp.197-206.
- Praveenkumar, R., Periyasamy, P., Mohanavel, V. and Ravikumar, M.M., 2020. Mechanical and Tribological Behavior of Mg-Matrix Composites Manufactured by Stir Casting. International Journal of Vehicle Structures & Systems (IJVSS), 12(1) pp. 117-120.
- Qi, Q. J., 2006. Evaluation of sliding wear behavior of graphite particle-containing magnesium alloy composites. Transactions of Nonferrous Metals Society of China, 16(5), pp.1135-1140.
- Raghav, G.R., Balaji, A.N., Muthukrishnan, D., Sruthi, V. and Sajith, E., 2018. An experimental investigation on wear and corrosion characteristics of Mg-Co nanocomposites. Materials Research Express, 5(6), p.066523.
- Rahmani, K. and Majzoobi, G.H., 2019. The effect of compaction loading rate on hardness and wear resistance of Mg–B4C nanocomposite. Materials Research Express, 6(12), p.125081.
- Rajkumar, P.R., Kailasanathan, C., Senthilkumar, A., Selvakumar, N. and JohnRajan, A., 2020. Study on formability and strain hardening index: influence of particle size of

boron carbide (B4C) in magnesium matrix composites fabricated by powder metallurgy technique. Materials Research Express, 7(1), p.016597 (1-17).

- Ravichandran, M., Veerappan, G., Dhinakaran, V. and Katiyar, J.K., 2022. Optimization of tribo-mechanical properties of boron carbide reinforced magnesium metal matrix composite. Proceedings of the Institution of Mechanical Engineers, Part J: Journal of Engineering Tribology, 236(9), pp.1814-1826.
- Sankaranarayanan, S., Sabat, R.K., Jayalakshmi, S., Suwas, S., Almajid, A. and Gupta, M., 2015. Mg/BN nanocomposites: nano-BN addition for enhanced room temperature tensile and compressive response. Journal of Composite Materials, 49(24), pp.3045-3055.
- Sankaranarayanan, S., Sabat, R.K., Jayalakshmi, S., Suwas, S. and Gupta, M., 2014. Effect of nanoscale boron carbide particle addition on the microstructural evolution and mechanical response of pure magnesium. Materials & Design (1980-2015), 56, pp.428-436.
- Saravanan, R.A. and Surappa, M.K., 2000. Fabrication and characterisation of pure magnesium-30 vol.% SiCP particle composite. Materials Science and Engineering: A, 276 (1-2), pp.108-116.
- Sardar, S., Karmakar, S.K. and Das, D., 2017. Ultrasonic assisted fabrication of magnesium matrix composites: a review. Materials Today: Proceedings, 4(2), pp.3280-3289.
- Satish, J. and Satish, K.G., 2018, February. Preparation of magnesium metal matrix composites by powder metallurgy process. In IOP Conference Series: Materials Science and Engineering, 310, (1), p. 012130 (1-8).
- Seenuvasaperumal, P., Elayaperumal, A. and Jayavel, R., 2017. Influence of calcium hexaboride reinforced magnesium composite for the mechanical and tribological behaviour. Tribology International, 111, pp.18-25.
- Selvam, B., Marimuthu, P., Narayanasamy, R., Anandakrishnan, V., Tun, K.S., Gupta, M. and Kamaraj, M., 2014. Dry sliding wear behaviour of zinc oxide reinforced magnesium matrix nano-composites. Materials & Design, 58, pp.475-481.
- Shanthi, M., Nguyen, Q.B. and Gupta, M., 2010. Sliding wear behaviour of calcium containing AZ31B/Al2O3 nanocomposites. Wear, 269(5-6), pp.473-479.
- Shanthi, M., Xia, G.L.X. and Gupta, M., 2011. Effect of Mg/nano-Al_2O_3 interaction time during stirring on microstructure and mechanical properties of Mg–Al_2O_3 composite. Materials Science and Technology, 27(8), pp.1341-1346.

- Sharma, S.C., Anand, B. and Krishna, M., 2000. Evaluation of sliding wear behaviour of feldspar particle-reinforced magnesium alloy composites. Wear, 241(1), pp.33-40.
- Shen, M., Zhu, X., Han, B., Ying, T. and Jia, J., 2022. Dry sliding wear behaviour of AZ31 magnesium alloy strengthened by nanoscale SiCp. Journal of Materials Research and Technology, 16, pp.814-823.
- Shinde, D.M. and Sahoo, P., 2022. Influence of speed and sliding distance on the tribological performance of submicron particulate reinforced Al-12Si/1.5 Wt% B4C composite. International Journal of Metalcasting, 16(2), pp.739-758.
- Shokrieh, M.M., Hosseinkhani, M.R., Naimi-Jamal, M.R. and Tourani, H.J.P.T., 2013. Nanoindentation and nanoscratch investigations on graphene-based nanocomposites. Polymer Testing, 32(1), pp.45-51.
- Sinha, S.K., Reddy, S.U. and Gupta, M., 2006. Scratch hardness and mechanical property correlation for Mg/SiC and Mg/SiC/Ti metal–matrix composites. Tribology International, 39(2), pp.184-189.
- Song, G.L. and Gannon, P.E., 2016. The surface films and their possible roles in Mg corrosion. Magnesium Technology 2016, pp.285-290.
- Song, J., She, J., Chen, D. and Pan, F., 2020. Latest research advances on magnesium and magnesium alloys worldwide. Journal of Magnesium and Alloys, 8(1), pp.1-41.
- Srinivasan, M., Loganathan, C., Kamaraj, M., Nguyen, Q.B., Gupta, M. and, Narayanasamy, R., 2012. Sliding wear behaviour of AZ31B magnesium alloy and nano-composite. Transactions of Nonferrous Metals Society of China, 22(1), pp.60-65.
- Subramani, M., Huang, S.J. and Borodianskiy, K., 2022. Effect of SiC nanoparticles on AZ31 magnesium alloy. Materials, 15(3), p.1004.
- Subramanian, C., 1991. Effects of sliding speed on the unlubricated wear behavior of Al-12.3 wt.% Si alloy. Wear, 1991, 151(1), pp.97-110.
- Suh, N. P., 1977. An overview of the delamination theory of wear. Wear, 44(1), pp.1-16.
- Suh, N.P., 1973. The delamination theory of wear. Wear, *25*(1), pp.111-124.
- Sunu Surendran, K.T. and Gnanavelbabu, A., 2022. Tribological behaviour of AZ91D/ultra-high-temperature ceramic composites at room and elevated temperatures. Proceedings of the Institution of Mechanical Engineers, Part J: Journal of Engineering Tribology, 236 (9), pp.1855-1870.

- Thakur, S.K. and Dhindaw, B.K., 2001. The influence of interfacial characteristics between SiCp and Mg/Al metal matrix on wear, coefficient of friction and microhardness. Wear, 247(2), pp.191-201.
- Thakur, S.K., Kwee, G.T. and Gupta, M., 2007. Development and characterization of magnesium composites containing nano-sized silicon carbide and carbon nanotubes as hybrid reinforcements. Journal of Materials Science, 42 (24), pp.10040-10046.
- Thevenot, F., 1990. Boron carbide—a comprehensive review. Journal of the European Ceramic Society, 6(4), pp. 205-225.
- Thirugnanasambandham, T., Chandradass, J. and Kannan, T.T.M., 2021. Influence of load and sliding speed on wear behavior of AZ91E magnesium alloy nanocomposite by dry sliding. Materials Today: Proceedings, 45, pp.6553-6557.
- Thirugnanasambandham, T., Chandradass, J., Sethupathi, P.B. and Martin, M.L.J., 2019. Experimental study of wear characteristics of Al_2O_3 reinforced magnesium-based metal matrix composites. Materials Today: Proceedings, 14, pp.211-218.
- Thirumalaikumarasamy, D., Shanmugam, K. and Balasubramanian, V., 2014. Comparison of the corrosion behaviour of AZ31B magnesium alloy under immersion test and potentiodynamic polarization test in NaCl solution. Journal of Magnesium and Alloys, 2(1), pp.36-49.
- Tiwari, S., Balasubramaniam, R. and Gupta, M., 2007. Corrosion behavior of SiC reinforced magnesium composites. Corrosion science, 49(2), pp.711-725.
- Tomar, V., Kumar, B., Singh, T., Tyagi, P. and Kumar, A., 2023. Investigation of mechanical and tribological behaviors of MMC fabricated through FSP. International Journal of Energy Resources Applications, 2(1), pp.1-15.
- Toptan, F., Rego, A., Alves, A.C. and Guedes, A., 2016. Corrosion and tribocorrosion behavior of Ti–B_4C composite intended for orthopaedic implants. Journal of the Mechanical Behavior of Biomedical Materials, 61, pp.152-163.
- Tun, K. S., and Gupta, M., 2007. Improving mechanical properties of magnesium using nano-yttria reinforcement and microwave assisted powder metallurgy method. Composites Science and Technology, 67(13), pp.2657-2664.
- Tun, K. S., Jayaramanavar, P., Nguyen, Q. B., Chan, J., Kwok, R., and Gupta, M., 2012. Investigation into tensile and compressive responses of Mg–ZnO composites. Materials Science and Technology, 28(5), pp.582-588.

- Turan, M.E., Sun, Y., Akgul, Y., Turen, Y. and Ahlatci, H., 2017. The effect of GNPs on wear and corrosion behaviors of pure magnesium. Journal of Alloys and Compounds, 724, pp.14-23.
- Turhan, M.C., Li, Q., Jha, H., Singer, R.F. and Virtanen, S., 2011. Corrosion behaviour of multiwall carbon nanotube/magnesium composites in 3.5% NaCl. Electrochimica Acta, 56(20), pp.7141-7148.
- Veeranjaneyulu, I., Chittaranjan Das, V. and Karumuri, S., 2023. Investigation of Mechanical Properties and Microstructure of AZ31-SiC-Graphite Hybrid Nanocomposites Fabricated by Bottom Pouring-Type Stir Casting Machines. Advances in Materials Science and Engineering, 2023(1), p.3402348.
- Wang, H. Y., Jiang, Q. C., Li, X. L., and Wang, J. G., 2003. In situ synthesis of TiC/Mg composites in molten magnesium. Scripta Materialia, 48(9), pp.1349-1354.
- Wang, S.Q., Yang, Z.R., Zhao, Y.T. and Wei, M.X., 2010. Sliding wear characteristics of AZ91D alloy at ambient temperatures of 25–200 C. Tribology Letters, 38(1), pp.39-45.
- Wang, X.J., Wang, N.Z., Wang, L.Y., Hu, X.S., Wu, K., Wang, Y.Q. and Huang, Y.D., 2014. Processing, microstructure and mechanical properties of micro-SiC particles reinforced magnesium matrix composites fabricated by stir casting assisted by ultrasonic treatment processing. Materials & Design, 57, pp.638-645.
- Wang, Y., Wei, M., Gao, J., Hu, J., & Zhang, Y., 2008. Corrosion process of pure magnesium in simulated body fluid. Materials letters, 62 (14), pp.2181-2184.
- Wei, T.Z., Shamsuri, S.R.B., Yee, C.S., Abd Rashid, M.W. and Ahsan, Q., 2013. Effect of sliding velocity on wear behavior of magnesium composite reinforced with SiC and MWCNT. Procedia Engineering, 68, pp.703-709.
- Xiao, P., Gao, Y., Yang, X., Xu, F., Yang, C., Li, B., Li, Y., Liu, Z. and Zheng, Q., 2018. Processing, microstructure and ageing behavior of in-situ submicron TiB2 particles reinforced AZ91 Mg matrix composites. Journal of Alloys and Compounds, 764, pp.96-106.
- Yao, Y. and Chen, L., 2014. Processing of B_4C particulate-reinforced magnesium-matrix composites by metal-assisted melt infiltration technique. Journal of Materials Science & Technology, 30(7), pp.661-665.
- Zafari, A., Ghasemi, H.M. and Mahmudi, R., 2012. Tribological behavior of AZ91D magnesium alloy at elevated temperatures. Wear, 292, pp.33-40.

- Zafari, A., Ghasemi, H.M. and Mahmudi, R., 2014. An investigation on the tribological behavior of AZ91 and AZ91+ 3 wt% RE magnesium alloys at elevated temperatures. Materials & Design (1980-2015), 54, pp.544-552.
- Zhang, C., Zhang, T., Wang, Y., Wei, F., Shao, Y., Meng, G., Wang, F. and Wu, K., 2015. Effect of SiC particulates on the corrosion behavior of extruded AZ91/SiCp composites during the early stage of exposure. Journal of The Electrochemical Society, 162(14), p.C754.
- Zhang, L., Luo, X., Liu, J., Leng, Y. and An, L., 2018. Dry sliding wear behavior of Mg-SiC nanocomposites with high volume fractions of reinforcement. Materials Letters, 228, pp.112-115.
- Zhang, W., 2021. A review of tribological properties for boron carbide ceramics. Progress in Materials Science, 116, p.100718.
- Zhang, W., 2022. A novel ceramic with low friction and wear toward tribological applications: Boron carbide-silicon carbide. Advances in Colloid and Interface Science, 301, p.102604.
- Zhang, Y., Zhang, G. and Wei, M., 2009. Controlling the biodegradation rate of magnesium using biomimetic apatite coating. Journal of Biomedical Materials Research Part B: Applied Biomaterials: An Official Journal of The Society for Biomaterials, The Japanese Society for Biomaterials, and The Australian Society for Biomaterials and the Korean Society for Biomaterials, 89(2), pp.408-414.
- Zhao, Y.X., Irving, P.E. and Cini, A., 2009. Hardness environments around fatigued scratches in clad and unclad 2024 T351 aluminium alloy. Materials Science and Engineering: A, 500 (1-2), pp.16-24.
- Zhou, D., Qiu, F., Wang, H. and Jiang, Q., 2014. Manufacture of nano-sized particle-reinforced metal matrix composites: a review. Acta Metallurgica Sinica (English Letters), 27(5), pp.798-805.
- Zhou, W. and Xu, Z.M., 1997. Casting of SiC reinforced metal matrix composites. Journal of Materials Processing Technology, 63(1-3), pp.358-363.
- Zucchi, F., Trabanelli, G., Grassi, V. and Frignani, A., 2004. Corrosion behavior in sodium sulfate and sodium chloride solutions of SiCp reinforced magnesium alloy metal matrix composites. Corrosion, 60(4), pp.362-368.

List of Publications from the Thesis

ASME Journal of Tribology
Online journal at:
https://asmedigitalcollection.asme.org/tribology

Nanoindentation, Scratch Resistance, and Elevated Temperature Tribological Behavior of AZ31-B C Composites

Vikram Titarmare
Department of Mechanical Engineering,
Jadavpur University,
Kolkata 700032, India
e-mail: vptitarmare@gcoen.ac.in

Sudip Banerjee
Department of Mechanical Engineering,
National Institute of Technology Mizoram,
Aizawl 796012, Mizoram, India
e-mail: banerjee.sudip71@gmail.com

Prasanta Sahoo[1]
Department of Mechanical Engineering,
Jadavpur University,
Kolkata 700032, India
e-mail: prasanta.sahoo@jadavpuruniversity.in

The present study investigates the outcome of the incorporation of different amounts of B_4C particles (0–2 wt%) in AZ31 alloy on nanohardness, elastic modulus, scratch resistance, and elevated temperature tribological behavior. AZ31-B_4C composites are produced by an ultrasonic stir casting technique. Mechanical properties of synthesized materials are evaluated by conducting nanoindentation tests following a constant depth method for a loading–unloading rate of 10 mN/min. The nanoindentation test reveals that the AZ31-2B_4C composite possesses 98.25% and 27% enhancement in nanohardness and elastic modulus, respectively, compared to the AZ31 matrix. Scratch behavior (scratch hardness, wear loss, and friction coefficient (COF)) is studied under ramp loading conditions (20–30 N, 20–40 N, and 20–50 N) using a diamond indenter. Composite samples exhibit better scratch resistance at all experimental conditions. Experimental results disclose that AZ31-2B_4C possesses around a 24% decrement in scratch width compared to AZ31 alloy. It is also observed that the wear-rate decreases linearly with an increase in wt% of B_4C while COF increases moderately. The pin-on-disc type tribo-meter is utilized to study the tribological behavior of AZ31 alloy and AZ31-B_4C composites at elevated temperatures (50–250 °C) under varying loads (20–40 N). The wear-rate of the base alloy increases continuously following a steep slope with respect to an increase in temperature while wear-rate composite samples do not possess any significant change up to a transition temperature after which the wear-rate increases significantly. Finally, scratch track and worn surfaces of samples tested under elevated temperature conditions are examined under SEM to evaluate dominant wear mechanisms. [DOI: 10.1115/1.4068913]

Keywords: composites, dry friction, indentation, scratching

Introduction

Metal matrix composite (MMC) has gained prominence as a critical material in the evolution of progressive decades in terms of trade as well as technology. MMCs offer higher strength, enhanced wear resistance, fracture toughness, stiffness, and withstand elevated temperatures. As a result, the utilization of MMC has gained wide acceptance from transportation industries like automobiles, railways, aerospace, etc. [1,2]. Nowadays, magnesium (Mg), Titanium (Ti), aluminum (Al), and nickel (Ni) alloys are widely used as matrix materials because of their specific applications in aircraft, missiles, automotive, and electronics applications. In this context, magnesium (Mg)-based composites have emerged as a better alternative. Nowadays, Mg composites are quickly displacing aluminum and other metals as structural materials in automotive and transportation industries owing to their elevated stiffness, specific strength, etc. [3,4]. Typically, the development of MMCs mainly depends on the selection of three parameters: (a) matrix material, (b) reinforcement, and (c) fabrication method [5,6]. With the addition of suitable ceramic reinforcement particles, Mg composites are produced as a unique aspirant for wear-friction applications even in strident environments like dry friction clutch, brake disc applications, etc. Thus, improving other properties of Mg-MMCs in addition to their outstanding lightweight feature can make them a possible choice for challenging tribological applications [7]. The main efficacy of the wear-resistant material depends on intrinsic and extrinsic parameters. Intrinsic parameters include the type of material, microstructure, and counterpart material. At the same time, extrinsic parameters are difficult to replace as they depend on equipment design. It includes applied load, wear environment, sliding speed, and distance. As a result, selecting a suitable matrix and reinforcement material is a crucial task. Till now, researchers have used different Mg alloys like AZ31, AZ61, AZ91, etc. [8–10]. These alloys have a wide range of mechanical properties (with 300 MPa tensile strength and 40% ductility). Accordingly, AZ31 alloy is chosen in the current study as it exhibits modest mechanical properties without significant changes in ductility.

Till date, different micron-sized reinforcements like SiC [11–13], Al_2O_3 [14,15], Boron Nitride (BN) [16,17], and Tungsten Carbide

[1]Corresponding author.

Contributed by the Tribology Division of ASME for publication in the JOURNAL OF TRIBOLOGY. Manuscript received March 21, 2025; final manuscript received June 7, 2025; published online July 3, 2025. Assoc. Editor: Maria Faga.

Physica Scripta

PAPER

Effect of sliding speed and sliding distance on wear behavior of AZ31-B C composite

RECEIVED
3 May 2024

REVISED
19 June 2024

ACCEPTED FOR PUBLICATION
2 July 2024

PUBLISHED
11 July 2024

Vikram Titarmare[1,2], **Sudip Banerjee**[1,3] **and Prasanta Sahoo**[1,*]

[1] Department of Mechanical Engineering, Jadavpur University, Kolkata, India
[2] Department of Mechanical Engineering, Government College of Engineering, Nagpur, India
[3] Department of Mechanical Engineering, National Institute of Technology Sikkim, Sikkim, India
[*] Author to whom any correspondence should be addressed.

E-mail: psjume@gmail.com **and** prasanta.sahoo@jadavpuruniversity.in

Keywords: AZ31-B_4C composites, wear, friction, sliding speed, sliding distance

Abstract

Emphasis of current research is to investigate the dry sliding behavior of AZ31 magnesium alloy and AZ31–1.5B_4C magnesium metal matrix composites (MMCs) at varying sliding speeds and sliding distances. Magnesium alloy and composite are fabricated through ultrasonic assisted stir casting method. Optical microscope (OM), scanning electron microscopy (SEM), and energy dispersive x-ray analysis (EDAX) are used to characterize developed materials. Microhardness of all materials is measured using a Vickers microhardness tester. Wear-friction behavior is investigated in dry sliding mode using pin-on-disc tribometer at room temperature. Magnesium alloy and composite are tested over a range of sliding speeds (0.25–1.25 m s^{-1}) and distances at a moderate normal load (20N). Wear morphology is finally investigated for composites and alloy under SEM and EDAX. SEM micrographs of as-cast AZ31-1.5B_4C composite reveals uniform distribution of B_4C particles with noticeable refinement in grain structure. EDAX spectra of AZ31-1.5B_4C composite depict the presence of boron and carbon along with existing elements of AZ31 alloy. Microhardness has enhanced around 30% for Mg-MMC by incorporating 1.5 wt% B_4C in AZ31 alloy. Furthermore, the use of B_4C as reinforcement increases the density of the composite. Wear rate is reduced by around 20% and COF is reduced by around 25% for AZ31-1.5B_4C composite compared to AZ31 alloy for all experimental conditions. Abrasion, oxidation, adhesion and delamination wear mechanisms are observed as dominant mechanism for varying sliding speeds and distances.

1. Introduction

Nowadays, transport sectors have focused mainly on lightweight materials for the automobile and aerospace industries [1–3]. In this regard, magnesium (Mg) alloys are in demand owing to their low density and different specific properties [2–5]. However, mediocre tribological properties, low ductility, and thermal stability issues limit their use in industrial applications. In this context, incorporation of ceramic based reinforcements is the first choice among researchers. Existing literature has demonstrated that addition of ceramic reinforcement in the magnesium matrix results in significant improvement in the tribological and mechanical properties [6]. It is observed in literature that incorporation of only 2 wt% of nano-particles has significantly enhanced mechanical as well as tribological properties [7–12]. Till date, a variety of micro /nano-sized ceramic particulates such as TiC, Al_2O_3, SiC, BN, WC and B_4C are fortified in Mg matrix through different processing techniques [13–22]. Shen *et al* [23] fortified micro SiC particles in AZ31B alloy through an ultrasonic stir casting route and investigated enhanced elastic modulus, ultimate tensile strength and yield strength of the composite. Similarly, Ravichandran *et al* [24] developed Mg-B_4C composite through powder metallurgy route. It has been discovered that Mg-B_4C composite possesses high hardness, excellent tribological properties and high compressive strength. Recently, Narayanasamy *et al* [25] have produced magnesium composite by reinforcing TiC (25–35 μ) through powder metallurgy technique. Superior microhardness, lower wear loss and better friction property

Tribology International 194 (2024) 109455

Contents lists available at ScienceDirect

Tribology International

journal homepage: www.elsevier.com/locate/triboint

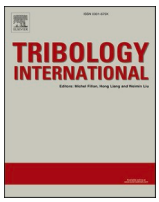

Abrasive wear behavior of AZ31 −B_4C composites

Vikram Titarmare [a,b], Sudip Banerjee [c], Prasanta Sahoo [a,*]

[a] Department of Mechanical Engineering, Jadavpur University, Kolkata, India
[b] Department of Mechanical Engineering, Government College of Engineering, Nagpur, India
[c] Department of Mechanical Engineering, National Institute of Technology Sikkim, Sikkim, India

ARTICLE INFO

Keywords:
AZ31 −B_4C composites
Abrasive Wear
Abrasive grit
Coefficient of friction

ABSTRACT

Abrasive wear behavior of AZ31 −B_4C composites having varying amount of B_4C particles (0 −2 wt%) is investigated. AZ31 −B_4C composites are synthesized through ultrasonic assisted stir casting method. Characterizations of as-cast composites are performed through optical microscopy and field emission scanning electron microscopy. Compositional analyses are performed using energy dispersive X-ray analysis (EDS). Microstructural analyses disclose uniform distribution of B_4C ceramic particles in AZ31 matrix. Compositional analyses confirm incorporation of B_4C particles in AZ31 matrix. Both microhardness testing and density measurements are performed. Microhardness value is enhanced by 54.9% compared to base alloy by incorporating 2 wt% of B_4C particles. Pin-on-disk tribotester is employed to scrutinize abrasive wear and friction characteristics of developed materials at varying sliding distance (40, 50 and 60 mm track dia.) and different abrasive grits (400, 500 and 600 grit). Wear rate of AZ31 alloy is about 1.3 − 1.5 times more than AZ31 − 2.0B_4C composite for all experimental conditions. Wear rate reduces with increase in abrasive grit size while the same increases with increase in sliding distance. Finally, worn surface morphology of developed materials is also analyzed through FESEM and EDAX spectra. Examination of worn surface morphology discloses that abrasion and oxidation are dominant for composite samples.

1. Introduction

In recent years, societal and environmental needs as well as legislative restrictions are changing quite often with respect to different vehicle standards and traffic norms. In this regard, industries and researchers are giving thoughtful attention towards light weight and high performing materials. Recently researchers are considering Mg/Mg alloys as favourable choice in aerospace, automotive and electronics industries because of their lower density, excellent cast-ability, damping capacity, superior machinability and recyclability [1]. Magnesium also possesses better specific strength and stiffness. Due to this, design engineers are fascinated towards Mg/Mg alloys as an energy efficient material. However, magnesium still has few bottlenecks like poor ductility, inferior abrasion resistance, lower corrosion resistance etc. [2,3]. To overcome such limitations, researchers are reinforcing ceramic based reinforcements in Mg matrix to develop magnesium metal matrix composite (Mg−MMC). Properties of MMCs are primarily dependent on the reinforcement size, type and amount. Normally particulate reinforcement is preferred over whiskers and fibers owing to its economical aspect, ease of fabrication and isotropic properties. The particulate reinforcement utilised so far in Mg matrix are preferably oxides, carbides and nitrides. In this regard, widely employed reinforced particles are Al_2O_3, SiC, TiC, B_4C, WC, BN, TiB_2, ZrO_2, TiO_2, Si_3N_4 etc. [4]. Recent literature also reported that particle size is an important aspect to achieve desirable properties. Dey and Pandey [5] reveals that reinforcement having lower particle size helps to achieve better specific properties. Gopal et al. [6] investigated the role of amount and size of reinforcement on mechanical and tribological characteristics. It was observed that reinforcement having lower particle size possesses better result. Accordingly, in this investigation, submicron sized boron carbide (B_4C) particulate is selected as reinforcement phase. B_4C is chosen here because of its non-reactivity with molten magnesium, low density (2.52 g/cc), excellent hardness (3500 kg.mm^{-2}), good elastic modulus (460 Gpa), high melting point (upto 2450 °C), excellent wear resistance, good wettability and high thermo- chemical stability [7,8]. Aatthisugan et al. [9] have incorporated B_4C particles in Mg matrix and observed enhanced specific properties. Aydin et al. [10] have fortified B_4C particles in Mg matrix and obtained excellent mechanical, microstructural and tribological properties. Titarmare et al. [7,11,12] have incorporated sub-micron sized B_4C particles in AZ31 matrix and achieved superior

* Corresponding author.
E-mail addresses: psjume@gmail.com, prasanta.sahoo@jadavpuruniversity.in (P. Sahoo).

https://doi.org/10.1016/j.triboint.2024.109455
Received 4 October 2023; Received in revised form 15 November 2023; Accepted 20 February 2024
Available online 21 February 2024

Special Issue: ITRS2021

Institution of MECHANICAL ENGINEERS
Journal of ENGINEERING TRIBOLOGY

Proc IMechE Part J:
J Engineering Tribology
2023, Vol. 237(4) 824–842

DOI: 10.1177/13506501221113661
journals.sagepub.com/home/pij
SAGE

Dry sliding tribological behavior of ultrasonic stir cast AZ31-B_4C composites

Vikram P Titarmare[1], Sudip Banerjee[1] and Prasanta Sahoo[1]

Abstract

The current study deals with the tribological characterization of AZ31-B_4C composites synthesized through ultrasonic vibration associated stir casting route. B_4C particles with varying weight percentage (0.5–2.0 wt. %) are reinforced in magnesium alloy to produce the composites. Optical microscope (OM), scanning electron microscope (SEM) and energy dispersive x-ray analysis (EDX) are utilized to characterize AZ31 alloy and composites so fabricated. Characterization illustrates the presence of boron carbide (B_4C) and its effect on the grain refinement of composites. Micro hardness of composites is measured through Vickers's micro hardness tester. AZ31-B_4C composites exhibit better hardness compared to AZ31 magnesium alloy. Micro hardness of AZ31- $2B_4C$ composite is increased by about 49% compared to AZ31 alloy. Dry sliding tribological behavior is investigated using a pin-on-disc tribo-tester. Wear behavior of AZ31 alloy and AZ31-B_4C composites is investigated under applied load of 10–40N and sliding speed of 0.1 to 0.4 m/s. The composites show better wear and friction behavior. Wear resistance of AZ31-$2B_4C$ composite is improved around 30% compared to base alloy when tested at 0.2 m/s sliding speed and 40N load. SEM and EDX analysis of worn-out surfaces reveal the wear mechanisms based on different sliding parameters. The wear morphology of pin samples reveals the presence of abrasion, oxidation, adhesion and delamination mechanism either occurring individually or in mixed mode on the pin surface.

Keywords

AZ31-B_4C composites, ultrasonic assisted stir casting, wear, friction, dry sliding

Date received: 24 April 2022; accepted: 27 June 2022

Introduction

Among commonly utilized structural metals and alloys, magnesium is the lightest. Magnesium is preferred as structural material in automobile industries because of its light weight, good specific strength and stiffness. These factors are vital in design of weight saving components in automobile and aerospace applications.[1] Use of magnesium in transport vehicles may reduce the legislative and environmental concerns to some extent. In aerospace industries most vital objective is weight reduction which would aid to bring down operational cost by lowering fuel consumption. Magnesium finds applications in civil and military aircraft, electronic, sports as well as medical fields.[2] Magnesium alloy has got excellent castability, high thermal conductivity and good mechanical properties. Accordingly magnesium alloys are utilized in automobiles as engine components, castings of gear boxes, transmission casings etc. However, these alloys exhibit low ductility and poor tribological properties. Mechanical properties of pure magnesium or its alloys can be effectively improved by adding ceramic reinforcement, e.g., oxides, nitrides and carbides. Magnesium based metal matrix composite has the advantage of light weight and good specific strength. At the same time, it compensates disadvantages like low strength and poor corrosion resistance observed in pure magnesium.[3,4] Moreover, size of reinforcements can also play big role in controlling the properties of the composite. Micron sized reinforcement in magnesium alloy possesses different limitations as wettability, agglomeration, porosity and non- uniform dispersion.[5] Thus, research studies are focused on sub-micron sized reinforcement.[6–8]

Metal matrix composites with sub-micron reinforcements are able to provide better combination of mechanical properties like high ductility, enhanced toughness, and increased strength, better thermal and excellent

[1]Department of Mechanical Engineering, Jadavpur University, Kolkata-700032, India

Corresponding author:
Prasanta Sahoo, Department of Mechanical Engineering, Jadavpur University, Kolkata-700032, India
Emails: psjume@gmail.com; prasanta.sahoo@jadavpuruniversity.in

Trans Indian Inst Met (2023) 76(9):2445–2461
https://doi.org/10.1007/s12666-022-02709-z

ORIGINAL ARTICLE

Corrosion Characteristics of AZ31-B_4C Composites

Vikram P. Titarmare[1] · Sudip Banerjee[1] · Prasanta Sahoo[1]

Received: 22 May 2022 / Accepted: 18 July 2022 / Published online: 13 August 2022

Abstract In this research, influence of boron carbide (B_4C) particles on the corrosion behavior of magnesium metal matrix composite is examined. AZ31-B_4C composites are fabricated through ultrasonic vibration-assisted stir casting process by reinforcing varying amount of boron carbide (0.5–2 wt.%) in AZ31 alloy. Characterizations of the composites are carried out using optical microscope , scanning electron microscope (SEM) and energy-dispersive spectroscope (EDS). The optical images show equiaxed orientation of grains in fabricated composites. SEM analysis confirms uniform distribution of reinforcement particles in composites. EDAX result confirms the inclusion of B_4C particles in the Mg matrix. The microhardness of all composites and base alloy is measured using Vickers's microhardness tester. Microhardness values are found to be increased with increase in wt.% of B_4C nanoparticles. Electrochemical corrosion tests are carried out on AZ31-B_4C metal matrix composites in 3.5% NaCl solution. AZ31-1B_4C composite is found to be the most corrosion-resistant material among tested materials. Furthermore, corrosion morphology of samples is scrutinized under SEM and EDS.

Keywords AZ31-B_4C · Nanocomposites · Corrosion potential · NaCl · Electrochemical test

1 Introduction

Material selection of any component depends on strength, corrosion resistance, density and stiffness of the material. Strength and stiffness furnish requisite functions and safety, higher strength to weight ratio helps to achieve higher payload while durability is dependent on corrosion characteristics [1]. Being lightweight structural material (75% lighter than steel and 33% lightweight than aluminum), magnesium/magnesium alloys extend distinctive and unique properties. Magnesium also offers excellent machinability, noticeable damping capability, better stiffness and good castability [2, 3]. Consequently, magnesium-based materials are drawing attention of scientific community. In automotive and aerospace industry, Mg/Mg alloys are found to be a possible potential replacement of aluminum due to density difference (~25%) and comparatively lesser specific gravity (~35%) [4]. Still application of magnesium is hindered by high corrosion rate of Mg/Mg alloys. Basically, Mg/Mg alloys are highly susceptive to galvanic corrosion which disturbs the steadiness of the setup. Accordingly, researchers are trying to improve the corrosion behavior of Mg/Mg alloys by either incorporating ceramic-based reinforcements or using high-purity alloying components [5]. Use of high-purity alloying element may enhance corrosion behavior of C_p-Mg but that much enhancement is inadequate to resolve galvanic corrosion related issues of Mg alloys [6]. Accordingly, magnesium metal matrix composites are considered to attain better corrosion property. The role of ceramic reinforcement is one of the deciding factors to improve corrosion resistance of magnesium alloy in electrochemical environment. Last two decades have witnessed increasing attention from scientific community toward magnesium metal matrix composites having sub-micron sized reinforcements. Accordingly,

✉ Prasanta Sahoo
psjume@gmail.com; prasanta.sahoo@jadavpuruniversity.in

[1] Department of Mechanical Engineering, Jadavpur University, Kolkata 700032, India

Materials Today: Proceedings 59 (2022) 153–160

Contents lists available at ScienceDirect

journal homepage: www.elsevier.com/locate/matpr

Fabrication and characterization of AZ31-B_4C composites

Vikram Titarmare *, Sudip Banerjee, Prasanta Sahoo

Department of Mechanical Engineering, Jadavpur University, Kolkata 700032, India

ARTICLE INFO

Article history:
Available online 20 November 2021

Keywords:
Magnesium
Boron carbide
Nanocomposite
Ultrasonic stir casting
Fabrication

ABSTRACT

In the present study, Magnesium Alloy (AZ31) and AZ31-B_4C composites reinforced with the varying amount (0–2 wt%) of nano-sized B_4C in particulate form are fabricated through an Ultrasonic stir casting process. The mechanical properties and microstructure characterization are mainly investigated. The microstructural characterization is done through an optical microscope (OM) and scanning electron microscope (SEM) to examine the dispersion and homogeneity of B_4C particulates in the Magnesium matrix. Elemental analysis is carried using an energy dispersive X-ray Spectrometer (EDAX). EDAX results indicate the presence of different elements such as Mg, B, C, Al, Zn etc. in base alloy and composites. Mechanical properties such as microhardness and density of base alloy and composites are also determined. Hardness and Density are found to increase with the increasing weight percentage of reinforcement. Microstructure examination found equiaxed grains in fabricated Alloy and Nano Composites. The mechanical characterization shows good interfacial bonding between the Mg matrix and B_4C reinforcement material.

Selection and peer-review under responsibility of the scientific committee of the Third International Conference on Recent Advances in Materials and Manufacturing 2021

1. Introduction

Magnesium or its alloy is one of the lightest materials among all structural materials. It has a density of 1.74 g/cm^3 which is very close to structural plastic (1.7 g/cm^3) and 2/3rd, 1/5th and 1/2nd compared to metallic materials like steel, aluminum, and titanium respectively. Along with this, it has very good damping and vibrational characteristic. Owing to this, many researchers, scientists and industries are in search of advanced material that helps to reduce the weight of the vehicles well as emissions. Thus, The vehicle will be more energy-efficient. Economical use of scarce energy resources is the need of the hour due to various factors such as

- Depletion of energy resources,
- Skyrocketing prices of oil,
- Strict restrictions on emission to protect the environment,
- Increasing Demand for oil or energy.

Advanced Lightweight material is the most needed solution among multiple research aspects. Which will avoid energy crises for future generations and environmental impacts. Already in 2007, Kia motors started to use magnesium alloy in their vehicles' seat frame which causes weight reduction of about 6 kg and approx. 40 kg in comparison to steel material [1]. Nowadays, Demand for magnesium is increased multiple folds, Proper selection of material for the transportation sector may reduce global emission by approximately by1400 million tons of CO or CO_2 [1,2]. However, monolithic Mg and its alloys have got limitations in properties such as low elastic modulus and ductility, loss of strength with temperature and poor creep resistance. These limitations are circumvented by the addition of different types of reinforcement to produce magnesium metal matrix composite (MMC). The reinforcements typically used are hard ceramic particles to have crack resistance and effective load transfer of MMCs. Ceramic particulates are preferred compared to metallic particles and fibers, due to better high-temperature capabilities and corrosion resistance [1,2]. Commonly used reinforcements in particulate form are carbides (WC, B_4C SiC), Nitrides (BN, TiN), Oxides (Al_2O_3, ZrO_2), etc. [3–9]. Particulate ceramic reinforcements used till now in magnesium and aluminum alloys as ceramic reinforcement are Al_2O_3, Y_2O_3, SiC, WC, BN [10–25].

Metal matrix composites are used increasingly at the commercial level due to tailored property combinations such as high specific strength, high thermal stability, and structural ductility in the transportation industry. Last decade witnessed extensive use of ceramic nano reinforcement in metal alloys due to a significant

* Corresponding author.
E-mail address: vikramtitarmare@rediffmail.com (V. Titarmare).

https://doi.org/10.1016/j.matpr.2021.10.373

Selection and peer-review under responsibility of the scientific committee of the Third International Conference on Recent Advances in Materials and Manufacturing 2021

Ultrasonic-Assisted Stir Casting Synthesis and Characterization of Magnesium Metal Matrix Composites

Vikram P. Titarmare, Sudip Banerjee, and Prasanta Sahoo

Abstract The present study considers synthesis and characterization of magnesium-based composites. The ultrasonic-assisted stir cast route is utilized to incorporate nano B_4C particles at different weight % such as 0.5, 1.0, 1.5 and 2.0. in AZ31 matrix. The morphologies of base alloy and composites are investigated under optical microscope and field emission scanning electron microscope (FESEM). Optical microscopy reveals α-Mg and β-$Mg_{17}Al_{12}$ while field emission scanning electron microscopy exhibits the uniform distribution of ceramic B_4C particles in magnesium matrix. Vicker's micro hardness tester is utilized to measure the hardness of composites and base alloy. Prepared composites depict improved micro hardness over AZ31 alloy. Density of composites and alloys is determined with the help of Archimedes principle. The density of composite is significantly enhanced compared to base alloy.

Keywords Ultrasonic-assisted stir cast · AZ31 alloy · Boron carbide · Micro hardness · Archimedes principle

1 Introduction

Magnesium and its alloys offer a significant alternative for weight critical applications in transport industries due to their low density and high specific strength. Global competition and legislative regulatory norms have witnessed the frequent modification and incorporation of new technologies in modern automobiles (like cars, buses and trucks). Lightweight vehicles enhance fuel economy around 7% for each 10%

V. P. Titarmare · P. Sahoo
Jadavpur University, Kolkata, India

V. P. Titarmare
Government College of Engineering Nagpur, Nagpur, India

S. Banerjee (✉)
National Institute of Technology Sikkim, Ravangla, Sikkim, India
e-mail: banerjee.sudip71@gmail.com

P. Sahoo and T. K. Barman (eds.), *Advances in Materials, Manufacturing and Design*,
Lecture Notes in Mechanical Engineering,
https://doi.org/10.1007/978-981-97-6667-3_5